



Durham E-Theses

Modern approaches to the exchange-correlation problem

Peach, Michael Joseph George

How to cite:

Peach, Michael Joseph George (2009) *Modern approaches to the exchange-correlation problem*, Durham theses, Durham University. Available at Durham E-Theses Online: <http://etheses.dur.ac.uk/2043/>

Use policy

The full-text may be used and/or reproduced, and given to third parties in any format or medium, without prior permission or charge, for personal research or study, educational, or not-for-profit purposes provided that:

- a full bibliographic reference is made to the original source
- a [link](#) is made to the metadata record in Durham E-Theses
- the full-text is not changed in any way

The full-text must not be sold in any format or medium without the formal permission of the copyright holders.

Please consult the [full Durham E-Theses policy](#) for further details.

MODERN APPROACHES
TO THE
EXCHANGE-CORRELATION
PROBLEM

MICHAEL JOSEPH GEORGE PEACH

2009

The copyright of this thesis rests with the author or the university to which it was submitted. No quotation from it, or information derived from it may be published without the prior written consent of the author or university, and any information derived from it should be acknowledged.



SUBMITTED IN CONFORMITY WITH THE REQUIREMENTS FOR
THE DEGREE OF DOCTOR OF PHILOSOPHY



25 MAR 2009

Abstract

MODERN APPROACHES TO THE EXCHANGE-CORRELATION PROBLEM

Kohn-Sham density functional theory (DFT) is the most prevalent electronic structure method in chemistry. Whilst formally exact, in practice it affords reasonable accuracy with reasonable computational cost and is the method of choice when considering molecules of non-trivial size. The key quantity is the exchange-correlation energy functional, the exact form of which is unknown. Approximate exchange-correlation functionals, particularly B3LYP and PBE, are routinely applied to chemical problems. However, it is not possible to guarantee a given accuracy in advance, nor is there a systematic means of obtaining a more accurate answer. Existing functionals are applied to ever more challenging problems and the accuracy required of them is continually increasing—the need for more accurate functionals is one of the major challenges in electronic structure theory. This thesis focuses on several approaches that attempt to address this issue.

In chapter 1 the electronic structure problem is outlined and discussed in terms of the Schrödinger equation and solutions involving wavefunctions. In chapter 2, the formal foundations of DFT are presented and methods of approximating the exchange-correlation functional are introduced.

A promising new direction for developing exchange-correlation functionals, through attenuation of the exchange term, is introduced and discussed in detail in chapter 3. The accuracy of such functionals is investigated and compared to that obtained from conventional approaches, with a particular emphasis on the dependence on the attenuation parameters. It is then demonstrated that attenuated functionals offer the prospect of significantly improved descriptions of excitation energies, particularly for those of charge-transfer character.

Application of attenuated functionals to excitation energies that are problematic for conventional functionals is undertaken in chapter 4. Insight into the conflicting performance of conventional methods for different charge-transfer excitations is provided through a consideration of the orbital overlap between the orbitals involved in an excitation. Through this overlap quantity, a diagnostic test is proposed that enables a user to judge in advance the reliability of excitation energies from conventional functionals.

Attenuated functionals are then applied to other difficult properties in chapter 5. Firstly they are used to study the bond length alternation and band gap in polyacetylene and polyyne oligomers and infinite chains. Then they are used to calculate nuclear magnetic resonance parameters in both main-group and first-row transition metal systems, through the theoretically rigorous optimised effective potential method.

An entirely different approach to functional development is considered in chapter 6, where the adiabatic connection formalism is introduced as an alternative method of obtaining the exchange-correlation functional. For a series of two-electron systems, exact input data is used to determine the applicability of a number of simple mathematical forms in modelling the exact adiabatic connection. The conclusions from these simple systems are then used to provide insight into the possibility of using this approach in functional development.

Contents

Contents	iv
List of Figures	vi
List of Tables	ix
Definitions	xv
1 Quantum mechanics	1
1.1 Quantisation and the Schrödinger equation	1
1.2 Simplifying the Schrödinger equation	3
1.3 Modelling the wavefunction	7
1.4 Hartree–Fock theory	8
1.5 Introducing correlation	13
2 Density functional theory	22
2.1 The Hohenberg–Kohn theorems	23
2.2 Kohn–Sham theory	27
2.3 Exchange–correlation functionals	30
3 Exchange-attenuation	37
3.1 Assessment of a hybrid functional	38
3.2 Attenuated exchange	42
3.3 Parameter dependence of attenuated functionals	49
3.4 Excited states	55
4 Electronic excitations	61
4.1 Linear response formulation of TDDFT	62
4.2 Failings of standard functionals	66
4.3 Assessment of exchange–correlation functionals	69
4.4 Correlation between error and orbital overlap	76
4.5 Application of TDDFT to triazene chromophores	86

5	Further applications of attenuated functionals	95
	<i>I. Polyacetylene and polyynes</i>	
5.1	Bond length alternation and band gap	95
5.2	Polyacetylene (PA)	98
5.3	Polyynes (PY)	103
	<i>II. Nuclear magnetic resonance</i>	
5.4	Evaluating magnetic response	108
5.5	Functional performance	111
6	Adiabatic connection	118
6.1	Computational approach	125
6.2	Ground state H ₂ potential energy curves	130
6.3	Helium isoelectronic series	145
6.4	Toward a practical functional	150
7	Conclusions	159
A	Supplementary information for chapter 6	163
B	Publications	166
C	Conferences attended	168
	References	169
	Index	189

List of Figures

3.1	The mean absolute error $ d $ for the subset atomisation energy assessment, as a function of the attenuation parameters α and μ , with $\beta = 1 - \alpha$	50
3.2	The shape of the attenuation curves for the exact exchange contribution to the exchange–correlation energy with different functionals. . .	53
3.3	The mean absolute error $ d $ for the subset atomisation energy assessment, as a function of the attenuation parameters α and μ , with $\beta = 0.65 - \alpha$	53
4.1	Schematic structures of the molecules for which excitation energies have been considered.	70
4.2	PBE excitation energy errors plotted against various definitions of Λ	79
4.3	Excitation energy errors plotted against Λ [eq. (4.36)] using (a) PBE, (b) B3LYP, and (c) CAM-B3LYP, for local excitations (Δ), Rydberg excitations (\times), and CT excitations (\bullet).	80
4.4	Charge-transfer dominant orbital transitions in DMABN and the model tripeptide, exemplifying large and small Λ , determined using the PBE GGA. All orbital plots in this work use a contour of 0.023 a.u.	82
4.5	Schematic structures of the triazene molecules considered.	87
4.6	Dominant orbital transition for the predicted problematic excitation in triazene II, determined using the PBE GGA	88
4.7	Gas phase excitation energies of triazene II. The value on the left hand side of each TDDFT level is the error in eV relative to RI-CC2. The value on the right hand side is Λ	90
4.8	Gas phase dominant PBE orbital transitions for triazene II. Errors and Λ values are given in figure 4.7.	92
5.1	BLA in polyacetylene oligomers, as a function of $1/N$	99
5.2	HO–LU gap in polyacetylene oligomers, as a function of $1/N$	101
5.3	CAM-B3LYP extrapolation of TDDFT excitation energy for polyacetylene.	102

5.4	TDDFT excitation energy in polyacetylene oligomers, as a function of $1/N$	103
5.5	BLA in polyacetylene oligomers, as a function of $1/N$	105
5.6	HO–LU gap in polyacetylene oligomers, as a function of $1/N$	106
5.7	CAM-B3LYP extrapolation of TDDFT excitation energy for polyynes.	106
5.8	TDDFT excitation energy in polyacetylene oligomers, as a function of $1/N$	107
5.9	The N_2 exchange–correlation potential v_{xc} obtained from an O-CAM-B3LYP calculation, with the nuclei at ± 1.0375 bohr.	113
5.10	The CrO_4^{2-} exchange–correlation potential v_{xc} obtained from an O-CAM-B3LYP calculation, plotted along a Cr–O bond with the Cr nucleus at the origin and the O nucleus at 3.118 bohr.	116
6.1	Schematic representation of the adiabatic connection; E_{xc} and $-T_c$ are given by the integrals as indicated.	122
6.2	Potential energy curve of H_2 determined using FCI, compared with those from self-consistent HF, MCY1 and B3LYP.	131
6.3	Potential energy curve of H_2 determined using FCI, compared with the AC1 curve.	131
6.4	Comparison of W_λ from MCY1, AC1 and AC6, evaluated at internuclear separations of (a) 1.4 bohr, (b) 5 bohr, and (c) 10 bohr.	135
6.5	$\partial^2 W_\lambda / \partial \lambda^2$, as a function of R for various values of λ	136
6.6	Potential energy curve of H_2 determined using FCI, compared with those from AC2 and AC4.	139
6.7	Potential energy curve of H_2 determined using FCI, compared with those from AC2(H&H) and AC4(H&H).	139
6.8	Potential energy curve of H_2 determined using FCI, compared with those from AC3 and AC5.	140
6.9	Potential energy curve of H_2 determined using FCI, compared with that obtained from AC6.	141
6.10	Potential energy curve of H_2 determined using FCI, compared with those obtained from AC7, AC8 and AC9	142
6.11	The error in total electronic energy $\Delta E = E - E^{FCI}$ for self-consistent B3LYP and the AC approximations of table 6.3 for the H_2 molecule as a function of R . The shaded area of part (a) denotes the scale of part (b).	144
6.12	The error in total electronic energy $\Delta E = E - E^{FCI}$ for self-consistent B3LYP and the AC approximations of table 6.3 for the helium isoelectronic series as a function of Z . The shaded area of part (a) denotes the scale of part (b).	147
6.13	W_λ^{AC1} curves for the helium isoelectronic series.	150

5.4	TDDFT excitation energy in polyacetylene oligomers, as a function of $1/N$	103
5.5	BLA in polyacetylene oligomers, as a function of $1/N$	105
5.6	HO–LU gap in polyacetylene oligomers, as a function of $1/N$	106
5.7	CAM-B3LYP extrapolation of TDDFT excitation energy for polyynes.	106
5.8	TDDFT excitation energy in polyacetylene oligomers, as a function of $1/N$	107
5.9	The N_2 exchange–correlation potential v_{xc} obtained from an O-CAM-B3LYP calculation, with the nuclei at ± 1.0375 bohr.	113
5.10	The CrO_4^{2-} exchange–correlation potential v_{xc} obtained from an O-CAM-B3LYP calculation, plotted along a Cr–O bond with the Cr nucleus at the origin and the O nucleus at 3.118 bohr.	116
6.1	Schematic representation of the adiabatic connection; E_{xc} and $-T_c$ are given by the integrals as indicated.	122
6.2	Potential energy curve of H_2 determined using FCI, compared with those from self-consistent HF, MCY1 and B3LYP.	131
6.3	Potential energy curve of H_2 determined using FCI, compared with the AC1 curve.	131
6.4	Comparison of W_λ from MCY1, AC1 and AC6, evaluated at internuclear separations of (a) 1.4 bohr, (b) 5 bohr, and (c) 10 bohr.	135
6.5	$\partial^2 W_\lambda / \partial \lambda^2$, as a function of R for various values of λ	136
6.6	Potential energy curve of H_2 determined using FCI, compared with those from AC2 and AC4.	139
6.7	Potential energy curve of H_2 determined using FCI, compared with those from AC2(H&H) and AC4(H&H).	139
6.8	Potential energy curve of H_2 determined using FCI, compared with those from AC3 and AC5.	140
6.9	Potential energy curve of H_2 determined using FCI, compared with that obtained from AC6.	141
6.10	Potential energy curve of H_2 determined using FCI, compared with those obtained from AC7, AC8 and AC9	142
6.11	The error in total electronic energy $\Delta E = E - E^{FCI}$ for self-consistent B3LYP and the AC approximations of table 6.3 for the H_2 molecule as a function of R . The shaded area of part (a) denotes the scale of part (b).	144
6.12	The error in total electronic energy $\Delta E = E - E^{FCI}$ for self-consistent B3LYP and the AC approximations of table 6.3 for the helium isoelectronic series as a function of Z . The shaded area of part (a) denotes the scale of part (b).	147
6.13	W_λ^{AC1} curves for the helium isoelectronic series.	150

6.14	The H_2 potential energy curve obtained with standard adiabatic connection approaches and with those that use the additional $W_{\infty}^{PC,FCI}$ as input.	153
6.15	The error in total electronic energy $\Delta E = E - E^{FCI}$, as obtained with standard adiabatic connection approaches and with those that use the additional $W_{\infty}^{PC,FCI}$ as input.	154
6.16	Potential energy curve of CO determined using CCSD(T), compared with those from various AC approximations.	155
6.17	Potential energy curve of CO determined using CCSD(T) compared with curves, shifted to a common reference at 0.9 bohr, from various AC approximations.	156

List of Tables

1.1	The basis set dependence of the total energy of H^- with Hartree-Fock theory, MP2 and CCSD; all energies are in Hartree.	21
3.1	The species included in the assessments set; see the text for original references.	39
3.2	Mean error d and mean absolute error $ d $, relative to reference values, for the assessments in table 3.1, with the B3LYP exchange-correlation functional in the unrestricted (UKS) and restricted open-shell (ROKS) formalisms.	41
3.3	Mean error d and mean absolute error $ d $, relative to reference values, comparing B3LYP and CAM-B3LYP for the assessments of table 3.1. Open-shell calculations use the unrestricted formalism.	48
3.4	Mean error d and mean absolute error $ d $, relative to reference values, comparing three optimised attenuated forms with CAM-B3LYP, for the assessments of table 3.1. Open-shell calculations use the unrestricted formalism.	52
3.5	Vertical excitation energy errors for CO, N_2 , H_2CO , and C_2H_4 , and combined errors for valence and Rydberg excitations, in eV.	56
3.6	Vertical excitation energies of the model dipeptide, in eV.	57
3.7	Vertical excitation energies of DMABN, in eV.	58
4.1	TDDFT excitation energies and reference values, in eV.	73
4.1	Continuation of: TDDFT excitation energies and reference values, in eV.	74
4.2	Error analysis for the excitations considered in table 4.1 (mean error d , mean absolute error $ d $, standard deviation (SD), and maximum positive and negative deviations) in eV.	76
4.3	Values of the overlap quantity Λ of eq. (4.36)	84
4.3	Continuation of: Values of the overlap quantity Λ of eq. (4.36)	85
5.1	TDDFT excitation energies and HO-LU gaps (in eV) in polyacetylene oligomers, as a function of the number of carbon atoms, N	100

5.2	TDDFT excitation energies and HO-LU gaps (in eV) in polyene oligomers, as a function of the number of carbon atoms, N	104
5.3	NMR isotropic shielding constants (in ppm) for main-group molecules compared to experimental values.	112
5.4	NMR isotropic shielding constants and chemical shifts (in ppm) of complexed formaldehyde and formaldehyde compared with reference CCSD(T) values	113
5.5	Transition metal NMR isotropic shielding constants and chemical shifts δ (in ppm) compared with experimental chemical shifts δ_{Expt}	115
6.1	H ₂ FCI total electronic and exchange-correlation energies (in Hartree) as a function of bond distance R (in bohr), compared to reference total electronic energies.	130
6.2	Equilibrium bond lengths R_e in bohr, and zero point (ZP), fundamental ($v=0 \rightarrow v=1$) and first overtone ($v=0 \rightarrow v=1$) vibrational wavenumbers in cm ⁻¹ , compared to reference total electronic energies.	133
6.3	Approximate AC forms considered in this study. For the definitions of a , b and c , see appendix A.	138
6.4	Helium isoelectronic series basis set scaling factors.	146
6.5	Helium isoelectronic series FCI and exchange-correlation energies (in Hartree) compared to reference values	146

For my father, Kenneth James Peach (1938–2008)

This work is dedicated to those who believed that I could do it. . .

Author's Declaration

The material contained within this thesis has not previously been submitted for a degree at the University of Durham or any other university. The research reported within this thesis has been conducted by the author unless otherwise indicated.

Copyright Notice

The copyright of this thesis rests with the author. No quotation from it should be published without their prior written consent and information derived from it should be acknowledged.

Acknowledgements

Over the past three years I have had the pleasure of working with some very talented individuals, who have provided me with intellectual stimulation, good company and some humorous anecdotes. Firstly my sincere thanks and gratitude goes to David Tozer, for his unwavering enthusiasm, for his tireless quest for perfection and for giving me the opportunity to learn and discover. Special thanks also goes to Andy Teale, Austin Dwyer, Ruth Le Sueur and Tom Keal, for always sparing time for me when I needed advice or assistance. I would like to thank Will Ng, Peter Benfield and John Kattirtzi for making me think hard when answering their questions.

I had the good fortune to work with Trygve Helgaker and Erik Tellgren during their year spent in Durham; I thank them for their entertaining company and for the successful projects that arose from their visit. For kind provision of the codes used in this project, and for valuable collaborations, I thank Trygve Helgaker, Paweł Salek, Aron Cohen, Kenneth Ruud and Andy Teale. Also I thank Gareth Williams, Frank de Proft and David O'Hagan for providing me with the opportunity to consider some chemically relevant applications, Nicholas Handy for the opportunity to work on some interesting ideas and the EPSRC for financial support.

During my time in Durham I have made many friends; my thanks goes to all of them. There are a few people I would specifically like to thank however—Tracy Hyman, Alex Jefferson and Helen McPhee. Thanks also goes to those people who I have taught, specifically the members of my first tutorial group. A special mention should go to my extended family, particularly my Mum and Dad, who have always supported my endeavours and who always believed in me. Finally I wish to thank Bridgette Cooper, who helped me through a difficult time in my life, for her understanding, company, patience and friendship.

DEFINITIONS

<i>A</i>	Electron affinity
A	Electron acceptor
aug-cc-pVNZ	Dunning style correlation consistent N - ζ basis set with one additional level of diffuse functions (d-aug includes a further additional level)
AC	Adiabatic connection
AC i	Approximate adiabatic connection form ($i = 1, \dots, 9$)
B88	Becke 1988 exchange gradient correction
B3LYP	Becke-3-Lee-Yang-Parr hybrid exchange-correlation functional containing a fixed 20% exact orbital exchange
BHLYP	Becke half-and-half hybrid exchange-correlation functional containing a fixed 50% exact orbital exchange
BLA	Bond-length alternation
CAM-B3LYP	Coulomb-attenuation method exchange-correlation functional of Yanai <i>et al.</i> , attenuating from 19% to 65% exact orbital exchange
CAM(α, β, μ)	Attenuated exchange-correlation functional of the form of eqs. (3.12), (3.17) and (3.18) with attenuation parameters α , β and μ
CASPT2	Complete active space SCF with second-order perturbation theory; CI based method of including multireference character in the ground state wavefunction, with additional correlation effects treated through second-order perturbation theory
CC	Coupled cluster method
CC2	Coupled cluster method with approximate treatment of double excitations
cc-pCVNZ	Dunning style correlation consistent N - ζ basis set with additional optimised core functions (high exponents)
cc-pVNZ	Dunning style correlation consistent N - ζ basis set
CI	Configuration interaction method
CT	Charge-transfer character excitation
D	Electron donor
DFT	Density functional theory
DMABN	4-(N,N -dimethylamino)benzonitrile
ee	Electron-electron interaction
ESE	Electronic Schrödinger equation (within the Born-Oppenheimer approximation)

FCI	Full configuration interaction—all possible excited state determinants are allowed to contribute to the wavefunction, corresponding to the exact solution of the electronic Schrödinger equation within a finite basis set
GGA	Generalised gradient approximation, referring to exchange–correlation functionals that are functionals of the density gradient in addition to the density
GL2	Görling–Levy second-order density functional perturbation theory
GTO	Gaussian type orbital, used in atomic-centred basis sets
hybrid	Exchange–correlation functional that mixes a fixed portion of orbital-dependent exact exchange into a density functional
HO	Highest occupied orbital
HF	Hartree–Fock theory where the wavefunction is represented by a single determinant
<i>I</i>	Ionisation potential
KS	Kohn–Sham formulation of density functional theory
KT2	Keal–Tozer GGA exchange–correlation functional designed for evaluation of magnetic response parameters
LSDA	Local spin density approximation, referring to exchange–correlation functionals that are solely functionals of the electron density
LU	Lowest unoccupied orbital
LYP	Lee–Yang–Parr GGA correlation functional based on data for the helium atom
MP2	Møller–Plesset second-order perturbation theory
ne	Nuclear–electron interaction
nn	Nuclear–nuclear interaction
O-	Prefix; indicates evaluation using the optimised effective potential method
OEP	Optimised effective potential; referring either to a multiplicative exchange–correlation potential obtained from the Wu–Yang method, or to the method itself
PA	Polyacetylene
PP	<i>N</i> -phenylpyrrole
PCM	Polarisable continuum model method for modelling solvent effects
PBE	Perdew–Burke–Ernzerhof GGA exchange–correlation functional
PBE0	Hybrid exchange–correlation functional based on PBE containing a fixed 25% exact orbital exchange

PY	Polyyne
ROHF/ROKS	Restricted open-shell treatment where all paired electrons occupy orbitals that have identical spatial parts
RI-	Prefix; resolution of the identity approximation, simplifying the evaluation of computationally expensive two-electron integrals
SD	Single and double excitations, referring to the level of excitations included in a truncated CI or CC expansion.
SDT	Single, double and triple excitations, referring to the level of excitations included in a truncated CI or CC expansion.
SD(T)	Full single and double (and approximate perturbative treatment of triple) excitations, referring to the level of excitations included in a truncated CI or CC expansion.
TDDFT	Time-dependent density functional theory, where excited state properties are computed via the linear response of the ground state to a time-dependent electromagnetic field
TPSS	Tao-Perdew-Staroverov-Scuseria meta-GGA exchange-correlation functional
UHF/UKS	Unrestricted open-shell treatment where all electrons are allowed to occupy orbitals with differing spatial parts
VWN	Vosko-Wilk-Nusair LSDA correlation functional based on quantum Monte-Carlo data for the homogeneous electron gas
WY	Wu-Yang procedure for evaluation of a multiplicative exchange-correlation potential associated with a given input density
XC	Exchange-correlation, referring to the unknown component of the energy partitioning in Kohn-Sham DFT

MODERN APPROACHES
TO THE
EXCHANGE CORRELATION
PROBLEM

Quantum mechanics

Quantum mechanics is introduced as a solution to the failure of classical Newtonian mechanics in describing atomic-scale interactions, through the Schrödinger equation. The wavefunction arises naturally from this. The wavefunction's importance is then highlighted as the basis of a hierarchy of methods used for solving problems in theoretical chemistry, and some of the techniques used to solve these equations in practice are presented. The benefits and pitfalls of such methods are discussed to justify the consideration of methods which dispense with the wavefunction entirely.

I think I can safely say that no one understands quantum mechanics

Richard Feynman

1.1 QUANTISATION AND THE SCHRÖDINGER EQUATION

Newtonian mechanics allowed the universe to be described by a series of equations. Physicists became complacent in the 200 years following Newton's publication of *Principia*, believing that it could describe everything in the universe; Laplace went so far as to claim that given appropriate information of all the particles in the universe at an instant in time, he could predict both the entirety of history and the future. The universe had other ideas.



Modelling reality: quantisation

There are physical phenomena associated with electromagnetic (EM) radiation and atoms that cannot be adequately explained through Newtonian (classical) mechanics. Light demonstrates many wave-like properties. However, when Rayleigh applied statistical mechanics to the energy distribution of black-body radiation, he found that not only was the result counter to what is experimentally observed, an infinite amount of energy would be concentrated at the highest frequencies of EM radiation. Planck, in 1901,¹ proposed that EM radiation is absorbed and emitted only in discrete amounts of definite size, or quanta. Application of the same statistical mechanics to this model gave results in remarkable agreement with experiment.

Einstein later elaborated on this quantisation of light² by suggesting it consisted of discrete packets of energy, to demonstrate that the transfer of energy between light and metals occurred in packeted, quantised amounts, hence explaining the photoelectric effect. Bohr³ proposed the quantisation of orbital angular momentum in atoms, explaining atomic spectra and the stability of atoms. Although their work could be considered as merely patching Newtonian mechanics, it paved the way for the ‘New Quantum Theory’, and it highlights the importance of the symbiotic relationship between theory and experiment.

1924 saw de Broglie⁴ hypothesise that all particles possessed a wavelength, but that only those with sufficiently small momenta (such as electrons) have observable wave-like properties. This suggested that it would be possible to describe particulate motion using a wave equation. In 1925 Heisenberg⁵ developed what later became known as matrix mechanics, which would prove equivalent to Schrödinger’s wave equation, and later Feynman’s path integral⁶ formulation. For brevity we shall focus on the Schrödinger formulation. 1926 saw Schrödinger^{7–12} produce a wave equation from which quantisation arises naturally, and that describes the full dynamical motion of quantised systems, in the non-relativistic limit. It was obtained by considering Hamilton’s observation of a link between mechanics and optics—that the zero-wavelength limit of an optics problem corresponded to a mechanical system. Using Hamilton’s observation, coupled with de Broglie’s relations and by ensuring that the

zero-wavelength limit of the equation satisfied the motion as determined by Newtonian mechanics for a plane wave, the time-dependent Schrödinger equation was obtained. It provides a coherent method of describing the interactions of non-relativistic fundamental particles. The interested reader is referred to refs. 13 and 14 for general discussion.

Relativistic consequences

From this point, we concern ourselves primarily with the interactions of electrons and nuclei. Spin is essential in a description of such interactions since electrons are fermions of spin 1/2. Schrödinger's equation does not predict fundamental particle spin—this arises mathematically from special relativity, which is not accounted for in the Schrödinger Equation. Spin is necessarily added as a variable by allowing an additional degree of freedom which takes discrete values. The resultant equation is consistent with the non-relativistic limit of the Dirac equation^{15,16} (which does satisfy the requirements of special relativity, hence spin naturally arises).

Since the Schrödinger equation does not account for special-relativistic effects, it is itself an approximation. Such effects however are important generally only for species which have a high nuclear charge. Whilst it is possible to add on relativistic effects through various methods,¹⁷ in the context of this thesis such approaches are an unnecessary complication. From this point we shall be content with simplifying the equation we need to solve.

1.2 SIMPLIFYING THE SCHRÖDINGER EQUATION

We begin with the time-dependent Schrödinger equation,

$$-i\hbar\frac{\partial\psi}{\partial t} = \hat{H}_{\text{gen}}\psi(\mathbf{x}^p, t), \quad (1.1)$$

where ψ is the wavefunction, \mathbf{x} is a co-ordinate accounting for position \mathbf{r} and particle spin s , t is time, and p a particle index such that $\mathbf{x}^p = \mathbf{x}_1, \dots, \mathbf{x}_p$. If we consider this with a generic many body Hamiltonian,

$$\hat{H}_{\text{gen}} = -\sum_p \frac{\hbar^2}{2m_p} \nabla_p^2 + V(\mathbf{x}^p, t), \quad (1.2)$$

with V a potential, \hbar Planck's constant, and m_p the particle mass, it is not in general soluble, at least analytically. Approximations are required. Here we present these approximations and justify them in terms of arriving at a (more) soluble problem which still includes the required physical content.

Removing time-dependence

The first approximation is the removal of time-dependence. If the system does not have any contributions to the external potential except those from the nuclei of the constituent atoms, the Hamiltonian will not depend on time. In such a case the time-dependence may be separated into a multiplicative term which takes the form of a complex-valued exponential phase factor. According to the Born interpretation¹⁸ of the wavefunction, the wavefunction itself does not have a physical meaning; the square of the wavefunction in position space is proportional to the probability of finding a particle at that point in space, and is interpreted as a probability density. Consequently the phase factor has no effect upon the interpretation of the wavefunction. For applications with time-independent potentials it is therefore possible to remove the direct time-dependence, resulting in the time-independent (TI) Schrödinger equation (SE), given here in atomic units—the unit of length is the Bohr radius (0.5292Å), charge is the charge of the electron e and mass the mass of the electron m_e (which are then used throughout the remainder of this thesis);

$$\hat{H}_{\text{TI}}\psi(\mathbf{x}^i, \mathbf{R}^I) = E\psi(\mathbf{x}^i, \mathbf{R}^I), \quad (1.3)$$

$$\hat{H}_{\text{TI}} = -\frac{1}{2} \sum_i \nabla_i^2 - \sum_I \frac{1}{2\bar{m}_I} \nabla_I^2 - \sum_{i,I} \frac{Z_I}{r_{iI}} + \sum_{i,j>i} \frac{1}{r_{ij}} + \sum_{I,J>I} \frac{Z_I Z_J}{r_{IJ}}. \quad (1.4)$$

In eqs. (1.3) and (1.4) E is the energy associated with ψ , i and j are indices over electrons, I and J are indices over nuclei, \bar{m}_I is the mass in atomic units associated with nuclei I , and the \mathbf{R} represent the spatial co-ordinates of the nuclei. The r refer to distances between particles. The terms involving the differential ∇^2 operator are the kinetic energy terms of the electrons and nuclei, and the remaining terms account for the Coulomb interactions of the electrons with the nuclei, the electrons with each other, and the nuclei with each other.

Separation of nuclear-dependence

For systems containing more than two independent particles, where the motions of electrons and nuclei interact solely through a Coulomb operator, the time-independent SE is too complex to solve to arbitrary accuracy. However, by exploiting the significant difference in mass between an electron and a nucleus, it is a reasonable physical assumption to treat nuclei as fixed. The electrons react essentially instantaneously to any movement of the nuclei, thus are considered to move in a potential defined by the nuclei. This approximation, due to Born and Oppenheimer,¹⁹ allows the separation of the SE by de-coupling into two parts: An electronic part which describes the electrons in a field due to the nuclei, and a nuclear part which describes the nuclei in a field due to the electrons. This is a great simplification over the full SE as it removes the kinetic energy of the nuclei, and the potential energy from the nuclear–nuclear repulsion becomes constant for a given set of nuclear co-ordinates. The electrons therefore interact with a potential consisting of stationary point charges.

$$\hat{H}_{\text{elec}}\psi(\mathbf{x}^i; \mathbf{R}) = E\psi(\mathbf{x}^i; \mathbf{R}), \quad (1.5)$$

$$\hat{H}_{\text{elec}} = -\frac{1}{2} \sum_i \nabla_i^2 - \sum_{i,I} \frac{Z_I}{r_{iI}} + \sum_{i,j>i} \frac{1}{r_{ij}} \quad (1.6)$$

where we now indicate a parametric dependence on \mathbf{R} . In general we will omit this co-ordinate for clarity in the notation. We denote the simplified SE as the electronic Schrödinger equation (ESE), and note that \hat{H}_{elec} is Hermitian. The eigenvalues E and eigenvectors ψ obtained from solving this equation form the spectrum of the Hamiltonian. The spectrum consists of a countable (but possibly infinite) set of bound, discrete states, and continuous states. They form a complete basis in terms of which an observable state ψ may be written, from which it follows that the expectation value (the mean of the energies obtained from many measurements), given by

$$\langle \hat{H} \rangle = \frac{\langle \psi | \hat{H} | \psi \rangle}{\langle \psi | \psi \rangle}, \quad (1.7)$$

is an upper bound on the exact ground state energy E_0 . E_0 is only obtained if eq. (1.7) is evaluated with the exact ground state wavefunction ψ_0 .

Chemical applications are primarily concerned with the evaluation of the total energy and properties of a system associated with the expectation value $\langle \psi | \hat{H}_{\text{elec}} | \psi \rangle$, particularly for the (approximate) ground state wavefunction ψ_0 . Therefore in general the term

$$E_{\text{nn}} = \sum_{I, J > I} \frac{Z_I Z_J}{r_{IJ}} \quad (1.8)$$

is added to the energy in eq. (1.5) to obtain the total electronic energy of a system. In order to model the dependence of the electrons on the nuclear framework within the ESE, the equation is solved at a variety of different nuclear positions, mapping out a potential energy surface.

This approach is valid in cases where the electrons do not change state as the positions of the nuclei change. For cases where two or more electronic states become close in energy, the Born–Oppenheimer approximation becomes invalid and it becomes necessary to account for possible coupling between electronic states. In this thesis we do not consider such ‘non-adiabatic’ scenarios.

The ESE can be solved analytically for a variety of model systems involving one or two particles in some (generally unphysical) external potential, such as a particle in a harmonic potential well. These give insight into more complex systems. However, solutions for many-particle systems are complicated. It is possible by changing to centre of mass co-ordinates, and separating the radial and angular motion, to solve the ESE exactly for hydrogenic atoms. It is also possible, by changing to elliptical co-ordinates, to solve for the solutions in simple systems such as H_2^+ where the electron motion is confined to an ellipse around the two nuclei.²⁰ More complex systems, such as the He atom, or H_2 , cannot be solved in closed form.

All methods used to solve the ESE for many particle systems involve further approximation. The extent to which these additional approximations affect the accuracy of the results depends upon the severity of the approximation. The next step involves attempting to approximate the electronic wavefunction based on properties that the exact wavefunction must satisfy.

1.3 MODELLING THE WAVEFUNCTION

There are several conditions a model wavefunction should satisfy in order that it incorporate as much of the underlying physics as possible. As mentioned above, the wavefunction has no direct physical interpretation. Since only the square of the position representation wavefunction has physical meaning, the wavefunction need not be real-valued. Whilst in general a real-valued wavefunction is sufficient, in the presence of magnetic fields for example it may become complex-valued.

Equally, since the ESE is a second-order differential equation, the n -electron wavefunction needs to be analytic to second-order with respect to spatial coordinates. If the system under consideration is comprised of a finite number of particles (as is the case for the majority of systems in this thesis), the wavefunction must be finite in order that it is square normalisable;

$$\|\psi(\mathbf{x}^n)\| = \int_{-\infty}^{\infty} d\mathbf{x}^n |\psi(\mathbf{x}^n)|^2 < \infty. \quad (1.9)$$

This is also a requirement if it is to satisfy the Born interpretation. Furthermore it should be a one-to-one function; it must take exactly one value at every value of each co-ordinate.

The simplest wavefunction that satisfies these properties is a Hartree product.²¹⁻²³ It is derived by considering a Hamiltonian in which there is no interaction between electron pairs (a ‘one-electron’ Hamiltonian), and takes the form of a product of one-electron orbitals;

$$\psi(\mathbf{x}^n) = \prod_i \chi_i(\mathbf{x}_i). \quad (1.10)$$

Such a wavefunction is for bosonic systems a reasonable approximation to the exact wavefunction. However, a wavefunction of this form does not satisfy the Pauli principle²⁴ for fermionic particles, which states that the wavefunction must be antisymmetric with respect to the exchange of identical particles [for instance $\psi(\mathbf{x}_1, \mathbf{x}_2) = -\psi(\mathbf{x}_2, \mathbf{x}_1)$]. The simplest model wavefunction which satisfies this additional constraint is obtained by antisymmetrising a Hartree product. The antisymmetrised Hartree product is a determinant of

one-electron orbitals (a Slater determinant)^{25,26}

$$\psi(\mathbf{x}^n) = \frac{1}{\sqrt{n!}} \det|\chi_1(\mathbf{x}_1)\chi_2(\mathbf{x}_2)\cdots\chi_n(\mathbf{x}_n)|. \quad (1.11)$$

A wavefunction of this form is invariant to unitary rotations of the orbitals.

1.4 HARTREE–FOCK THEORY

Hartree–Fock theory^{21–23,27,28} approximates the wavefunction as a single Slater determinant comprised of orthonormal one-electron spin orbitals $\chi_k(\mathbf{x}_k)$, defined as $\varphi_k(\mathbf{r}_k)\sigma(s)$ where σ accounts for the possibility of α and β spin states, and in which we assume the φ_k to be real-valued. The electronic energy associated with a wavefunction of this form is given by its expectation value with the full \hat{H}_{elec} , and takes the form

$$E_{\text{HF}} = \sum_i (i|\hat{h}|i) + \frac{1}{2} \sum_{i,j} [(ii|jj) - (ij|ji)] + \sum_{I,J>I} \frac{Z_I Z_J}{r_{IJ}} \quad (1.12)$$

where the first term is the expectation value of the one-electron Hamiltonian

$$(i|\hat{h}|j) = \int d\mathbf{x} \chi_i(\mathbf{x})\hat{h}(\mathbf{x})\chi_j(\mathbf{x}), \quad (1.13)$$

which consists of kinetic and nuclear–electron attraction components such that

$$\hat{h}(\mathbf{x}_1) = -\frac{1}{2}\nabla_1^2 - \sum_I \frac{Z_I}{|\mathbf{r}_1 - \mathbf{R}_I|}. \quad (1.14)$$

The second term in eq. (1.12) is the two-electron term and consists of integrals of the form

$$(ij|kl) = \iint d\mathbf{x}_1 d\mathbf{x}_2 \chi_i(\mathbf{x}_1)\chi_j(\mathbf{x}_1)\frac{1}{r_{12}}\chi_k(\mathbf{x}_2)\chi_l(\mathbf{x}_2). \quad (1.15)$$

The first part $[(ii|jj)]$ is the classical Coulomb repulsion of a charge distribution with itself. The second part $[(ij|ji)]$ is the exchange energy, which arises due to the wavefunction satisfying the antisymmetry of the Pauli principle for fermions. Physically the exchange term corresponds to like-spin electrons avoiding one another, lowering the electron–electron repulsion. The final term in eq. (1.12) is due to the nuclear–nuclear repulsion.

Since in Hartree-Fock theory the energy is defined as the expectation value of a Hamiltonian, it satisfies the variational principle; the value of E_{HF} evaluated with a trial wavefunction ψ_{trial} is always above the value of $E_{\text{HF}}[\psi_{\text{HF}}]$. This provides a method of computing the Hartree-Fock wavefunction for a system through minimisation of the energy with respect to changes in the orbitals. Under the constraint that the orbitals remain orthonormal through the minimisation procedure, the Hartree-Fock equations are obtained:

$$\hat{F}(\mathbf{x}_1)\chi_i(\mathbf{x}_1) = \sum_j \varepsilon_{ji}\chi_j(\mathbf{x}_1), \quad (1.16)$$

where ε is a matrix of Lagrange multipliers, and $\hat{F}(\mathbf{x})$ is the effective Hamiltonian for the one-electron Schrödinger Equation,

$$\hat{F}(\mathbf{x}_1) = \hat{h}(\mathbf{x}_1) + \hat{J}(\mathbf{x}_1) + \hat{K}(\mathbf{x}_1), \quad (1.17)$$

with $\hat{h}(\mathbf{x})$ defined as in eq. (1.14). $\hat{J}(\mathbf{x})$ and $\hat{K}(\mathbf{x})$ are defined as

$$\hat{J}(\mathbf{x}_1) = \sum_j \int d\mathbf{x}_2 \frac{\chi_j(\mathbf{x}_2)\chi_j(\mathbf{x}_2)}{r_{12}} \quad (1.18)$$

$$\hat{K}(\mathbf{x}_1)\chi_i(\mathbf{x}_1) = - \sum_j \int d\mathbf{x}_2 \frac{\chi_i(\mathbf{x}_2)\chi_j(\mathbf{x}_2)}{r_{12}} \chi_j(\mathbf{x}_1). \quad (1.19)$$

The Coulomb operator \hat{J} , modelling a classical charge interaction, is a local operator. The exchange operator \hat{K} however is non-local, and requires information on all of the χ at all points in space. Note that \hat{F} , as \hat{H}_{elec} , is Hermitian, and invariant to unitary orbital transformations, so it is possible to transform the orbitals such that the matrix ε is diagonal. Hence the standard canonical form,

$$\hat{F}(\mathbf{x})\chi_i(\mathbf{x}) = \varepsilon_i\chi_i(\mathbf{x}), \quad (1.20)$$

is obtained. These equations require the solution be found iteratively due to the form of the electron-electron interaction; the field experienced by an electron in orbital χ_i depends on the remaining orbitals. There is a substantial literature devoted to the efficient solution of such self-consistent field (SCF) equations (see for instance ref. 14). In this thesis we assume that the solution

can be found. It is important to note that there are in general many solutions to such a set of non-linear equations. This is due in part to the existence of various stationary points in addition to the global minimum corresponding to the ground state (which we are primarily interested in), and also due to the invariance to unitary transformations which implies that each stationary point may be represented in infinitely many ways.

From the solution of the Hartree-Fock equations, we obtain from the SCF procedure a set of orthonormal eigenfunctions (spin orbitals) $\{\chi_k\}$, and eigenvalues (orbital energies) $\{\varepsilon_k\}$. For an n -electron system, the n -lowest correspond to the occupied orbitals, and the remaining are termed unoccupied or virtual orbitals. In principle the spectrum of the Hartree-Fock Hamiltonian is infinite. In practice we introduce a finite set (of size B) of known one-electron functions η in which we expand the orbitals,

$$\chi_i(\mathbf{x}) = \sum_b^B c_{bi} \eta_b(\mathbf{x}) \quad (1.21)$$

where the \mathbf{c} are expansion coefficients to be determined.

Basis sets

There are two types of basis set in common use; the first involves using plane-waves. The second, which we use exclusively in this thesis, involves atom-centred basis functions. Consider a one-electron system in a central field (in which we use angular co-ordinates r , θ and ϕ), for which it is possible to separate the solution into radial and angular parts. For such systems it can be shown¹⁴ that a complete basis may be written in terms of a system-independent angular part, and a system-dependent radial part

$$\eta_{b,nlm} = \eta_{b,nl}(r) Y_{lm}(\theta, \phi) \quad (1.22)$$

where the indices n , l and m refer to the quantum numbers of the basis function in question. For the angular part, the spherical harmonics $Y_{lm}(\theta, \phi)$ form a complete orthonormal set, and hence these are used as the angular basis set in all electronic structure calculations.

A natural approach for a radial basis set $\eta_{b,nl}(r)$ is the radial part of hydrogenic orbitals which arise from the solution of the ESE for the H atom.

They take the form of Laguerre polynomials and terms involving the quantum number n multiplying an exponential. However they are only complete for bound states, and their form requires a large number of terms to obtain accuracy in arbitrary systems.

If we replace the complex dependence on n and take a form consisting of Laguerre polynomials and an exponential, we obtain a complete orthogonal set. However, it is not possible to obtain accurate descriptions of different orbitals with an exponential of fixed exponent. By varying exponents it is possible to produce much more tractable approximations to orbitals, but this destroys the orthogonality of the functions. Therefore, replacing the complex nodal structure of the Laguerre polynomials with a simpler polynomial, we obtain Slater-type orbitals, consisting of simple atomic-centred polynomials multiplying an exponential;

$$\eta_b = Nx_1^f x_2^g x_3^h \exp(-\alpha r_b) \quad (1.23)$$

where the x_i are the relative co-ordinates in the three Cartesian directions, $f + g + h = l$, and N a normalisation constant.

Such basis sets allow high accuracy to be achieved, but the difficulty in the manipulation of such functions makes using a large number prohibitive in extended systems. The most widely used basis set is therefore a Gaussian-type orbital (GTO), proposed by Boys.²⁹ Such an approach takes a Gaussian function, multiplied by a simple polynomial:

$$\eta_b = Nx_1^f x_2^g x_3^h \exp(-\alpha r_b^2). \quad (1.24)$$

Whilst the form of a Gaussian function is such that several are required to achieve the same level of accuracy obtained from a single Slater-type orbital, the significant difference in the speed of integral evaluation allows many more GTO's to be used for equivalent computational cost. Perhaps the most appealing feature is that all GTO integrations may be performed through recurrence relations. The form of GTO presented here are Cartesian GTOs. These allow for efficient integral calculation due to their separability into the three Cartesian directions, but for calculations with $l \geq 2$ additional functions are introduced over the corresponding spherical harmonic GTOs. Given that the spherical harmonic GTOs can be obtained as linear combinations of the

Cartesian GTOs it usually proves more efficient to perform a transformation into the spherical harmonic basis and reduce the number of basis functions in a calculation. Their use also helps to limit problems of linear-dependency in basis sets.

If we substitute eq. (1.21) into eq. (1.20), and ‘project’ onto the space spanned by the basis functions η (by multiplying on the left and integrating), we obtain the Roothaan–Hall^{30,31} equations,

$$\sum_b c_{bi} \int d\mathbf{x} \eta_a F_i \eta_b = \epsilon_i \sum_b c_{bi} \int d\mathbf{x} \eta_a \eta_b, \quad (1.25)$$

$$\mathbf{F}\mathbf{c} = \mathbf{S}\mathbf{c}\epsilon, \quad (1.26)$$

which are a set of matrix equations used for solving a Hartree–Fock calculation, and in which \mathbf{S} is the overlap matrix

$$S_{ab} = \int d\mathbf{x} \eta_a \eta_b, \quad (1.27)$$

which arises due to the non-orthogonality of GTO basis sets.

If we consider atomic calculations, we need to provide a basis consisting of sufficient functions to describe each individual orbital, for example in the carbon atom as a minimal basis we would have a set of GTO’s representing 1s, 2s and 2p functions. The addition of more functions will improve the accuracy as the flexibility of the basis set increases. It should be pointed out however that in general it is necessary to include functions of higher angular momenta than those required by a minimal basis. The reasoning for which is twofold. Firstly, a basis set must contain the flexibility to describe the distortion of the atomic orbitals due to other atoms in molecules, and secondly to allow a description of electron correlation (the subject of the next section).

Open-shell calculations

So far we have formulated a series of equations to solve the ESE under the constraint that the wavefunction take the form of a single determinant. We now consider the form of the spin orbitals. Consider a one-electron system; we have (by convention) a single occupied α -spin orbital. If we add another electron to this system (and we assume that the spins pair), we could occupy

an orbital with an identical spatial part but with β -spin. On addition of a third electron we could then take an additional α -spin orbital with a different spatial part to the first. This approach, whereby all paired electrons occupy orbitals constrained to have identical spatial parts, is known as the restricted formalism.

Equally we could take our second electron and occupy an orbital of β -spin where the spatial part differed from that of the first orbital, and in which the spatial part of the orbitals, for all subsequent electrons added to the system, is unconstrained. This corresponds to an unrestricted formalism.

In general the two approaches give equivalent results for systems where there are no unpaired electrons; however, this is not necessarily the case for dissociation into open-shell fragments where the spin-symmetry may be broken. The treatment of systems with unpaired electrons however will be different.

1.5 INTRODUCING CORRELATION

The Hartree–Fock energy is always above that of the exact energy for a many-electron system. For one-electron systems it is exact, because the mean-field approximation of the interaction of an electron with others has no effect. The amount by which the Hartree–Fock energy differs from the exact energy is defined as the correlation energy of a system;

$$E_c = E_{\text{Exact}} - E_{\text{HF}} \quad (1.28)$$

and since the Hartree–Fock energy is an upper bound on the exact energy, $E_c \leq 0$. The correlation energy arises physically from an electron having knowledge of the location of the remaining electrons. In practice it is missed in Hartree–Fock theory due to approximating the wavefunction as a single determinant. The single-determinantal picture fails for two reasons: Firstly the mean-field electron–electron interaction fails to model the electron–electron cusp for unlike-spin electrons, resulting in electrons becoming too close to one another and an artificially high energy; secondly a single determinant is fundamentally unable to describe the physical reality under certain circumstances. For instance, in the case of H_2 approaching dissociation, we have a single-determinantal wavefunction with a contribution from both two neutral H atoms and from an unphysical H^+ and H^- arrangement. The simplest

method of correcting this involves somehow removing the ionic configuration from the wavefunction leaving correctly occupied orbitals. In the case of H_2 we can do this by adding in some quantity of an excited state single-determinant to cancel out the unwanted term. Such an approach is an illustration of configuration interaction (CI).

Configuration interaction theory

Configuration interaction wavefunctions are obtained by writing the wavefunction as a linear combination of Slater determinants in which electrons occupy orbital configurations different to a reference ground state (so called excited state determinants).

$$|\psi_{\text{CI}}\rangle = (1 + \sum_{\mu} c_{\mu} \hat{\tau}_{\mu}) |\psi_{\text{HF}}\rangle \quad (1.29)$$

$$|\psi_{\text{CI}}\rangle = (1 + \hat{T}_1 + \hat{T}_2 + \dots) |\psi_{\text{HF}}\rangle, \quad (1.30)$$

$$\hat{T}_1 = \sum_{i,\alpha} c_{\alpha}^i \hat{\tau}_i^{\alpha} \quad (1.31)$$

$$\hat{T}_2 = \sum_{i < j, \alpha < \beta} c_{\alpha\beta}^{ij} \hat{\tau}_{ij}^{\alpha\beta} \quad (1.32)$$

with $\hat{\tau}$ excitation operators which provide a convenient notation of occupying non-ground state configurations. The coefficients c in such an expansion are then optimised to minimise the electronic energy. In full configuration interaction (FCI), all possible excited state determinants are included, and the exact electronic energy for a system is obtained, but necessarily within a finite basis set. This may be viewed as removing the single-determinant approximation and improving flexibility in the wavefunction by allowing all possible orbital occupations to contribute to the energy.

In practice it is almost always necessary to truncate the expansion at some finite order. CIS (CI singles) is actually equivalent to Hartree–Fock theory since singly excited determinants do not interact with the ground state determinant as there is no coupling between the occupied and virtual orbitals in the Fock operator. CIS does contain information about excited states as singly excited determinants do interact with one another. Usually therefore the CISD method (CI with single and double excitations) is used.

There are cases where a CI expansion necessarily involves large contributions from excited state determinants, such as the case of stretched H_2 mentioned earlier and ozone (when there are degeneracies), where the Hartree–Fock wavefunction is a poor representation. An alternative approach involves the truncation of the CI expansion to include a relatively small number of configurations, and the optimisation of both the expansion coefficients and the orbitals themselves, giving multi-configurational SCF theory (MCSCF). The aim is to provide as compact a representation of the wavefunction as possible while including the relevant physics. In the case of H_2 , the MCSCF energy is below the Hartree–Fock energy, but above the FCI energy, although it will lead to a correct description of dissociation.

A method is size-extensive if, for N infinitely separated non-interacting fragments X ,

$$E(X \cdots X) = NE(X); \quad (1.33)$$

the energy of a fragment is independent of the system in which it is computed. Truncated CI expansions are not size-extensive, although FCI is. If we consider H_2 with the CISD model, it will give rise to all of the single and double excitations, and is thus FCI. If instead we have two infinitely separated H_2 molecules, some of these excitation processes will correspond to quadruple excitations, hence will not be included at the CISD level (CISDTQ would be required for FCI). This is an important measure of the consistency of accuracy for molecules with differing numbers of electrons. This failure of truncated CI expansions to satisfy the size-extensivity condition severely limits their applicability as successful correlated methods. Davidson introduced a correction which approximately accounts for the error in size-extensivity due to truncating CI.³² In general better results are obtained with the more widely used coupled cluster methods.

Coupled cluster theory

There are properties of the FCI wavefunction that are lost in truncating the level of included excitations. An alternative approach arises through considering the FCI wavefunction and its relation to Hartree–Fock theory, and whether it can be approximated differently.

The simplest approximation of correlating electrons is to assume that they correlate in pairs; for instance two electrons in orbitals i and j disturb each other's movement and excite themselves into different orbitals α and β , a process with which we associate an amplitude t ; if the wavefunction is expanded as a sum over all such pairwise processes that may occur in a system the pair-cluster approximation is obtained, which corresponds to CCD (coupled cluster doubles). The wavefunction importantly takes the form of a product of excitation operators³³⁻³⁵ acting on the Hartree–Fock reference determinant (in contrast to the sum form in CI theory), and is usually written as

$$|\psi_{\text{CC}}\rangle = \prod_{\mu} (1 + t_{\mu} \hat{\tau}_{\mu}) |\psi_{\text{HF}}\rangle. \quad (1.34)$$

$$\prod_{\mu} (1 + t_{\mu} \hat{\tau}_{\mu}) = \exp(t_{\mu} \hat{\tau}_{\mu}), \quad (1.35)$$

$$\hat{T} = t_{\mu} \hat{\tau}_{\mu} \quad (1.36)$$

$$\hat{T} = \hat{T}_1 + \hat{T}_2 + \dots + \hat{T}_n \quad (1.37)$$

$$|\psi_{\text{CC}}\rangle = \exp(\hat{T}) |\psi_{\text{HF}}\rangle. \quad (1.38)$$

This equation must be solved iteratively for the amplitudes \mathbf{t} , and the energy then minimised with respect to these amplitudes. Equation (1.35) holds due to the property of the excitation operators that $\hat{\tau}_{\mu}^2 = 0$, giving rise to the exponential ansatz of the coupled cluster wavefunction. In practice the amplitudes and energy are obtained from more practicable expressions derived through the use of the Campbell–Baker–Hausdorff formula³⁶ of $e^{-\hat{T}} \hat{H} e^{\hat{T}}$; if the Hamiltonian is pre-multiplied by the inverse of the exponential operator, the resulting series naturally truncates.

Although the doubles term provides the dominant contribution to electron correlation for electrons close together in space, in general the singles terms should also be included to give CCSD; it represents relaxing the orbitals due to the mean-field of Hartree–Fock changing depending on the orbital occupations. The CCSD method is widely used as a benchmark method for molecules of reasonable size. It is not possible in general to obtain a truly quantitative accurate description however without the additional inclusion of (at least) the triples contribution (CCSDT).³⁷ However this method is far too computationally expensive for all except the simplest systems.

It is possible to simplify CCSD and CCSDT by observing that at each level of theory the terms of highest cost correspond to corrections to the top level of excitation; hence the cost of the methods may be reduced if we only want to treat the top level excitations approximately. This gives rise to the iterative CC2^{38,39} and CC3^{40,41} methods, which are approximations to the CCSD and CCSDT methods respectively, and which importantly may be applied to the calculation of excited state properties as a wavefunction exists for each of these methods. The connection of these methods is described in ref. 41.

Owing to the product nature of the wavefunction in CC, each determinant may be reached through several processes; for instance a doubly excited determinant may be reached through either a single, connected process of exciting two electrons, or through a combination of two independent, disconnected processes each exciting one electron. Therefore compared to CI, excitations of higher order than those explicitly included in the theory may contribute to the wavefunction through these disconnected processes.

If we consider the two truncated methods CISD and CCSD, we can compare the excitations that are included in each wavefunction:

$$|\psi_{\text{CI}}\rangle = (1 + \hat{T}_1 + \hat{T}_2)|\psi_{\text{HF}}\rangle \quad (1.39)$$

$$|\psi_{\text{CC}}\rangle = (1 + \hat{T}_1 + [\hat{T}_2 + \frac{1}{2}\hat{T}_1^2] + [\hat{T}_1\hat{T}_2 + \frac{1}{6}\hat{T}_1^3] + [\frac{1}{2}\hat{T}_2^2 + \frac{1}{2}\hat{T}_1^2\hat{T}_2 + \frac{1}{24}\hat{T}_1^4] + \dots)|\psi_{\text{HF}}\rangle; \quad (1.40)$$

from this it can be seen that in our case of two H₂ molecules, some quadruple excitations are included as products of the single and double excitations in CCSD. In the case that the two H₂'s are non-interacting this accounts for all of the possible quadruple excitations, hence the method is size-extensive. A size-extensive variation of configuration interaction, quadratic CISD (QCISD),⁴² also exists, but it can be demonstrated that it is actually equivalent to an approximate Coupled cluster theory.^{43,44}

CC theory however is not variational (although the error due to this is in general much smaller than the error experienced in CI theory due to the lack of size-extensivity). Another treatment, which allows the restoration of size-extensivity whilst again losing the variationality of the wavefunction, can

be achieved from perturbation theory, which offers a potentially less computationally demanding solution.

Perturbation theory

Consider a general Hamiltonian that may be split into two parts; a large reference part \hat{H}_0 whose eigenfunctions are known exactly and a small correction \hat{H}_1 which makes the solution of the full Hamiltonian problematic. We term the small correction \hat{H}_1 the perturbation. In order to approximate the exact energy and wavefunction for the full Hamiltonian, a parameter λ is introduced to turn on the perturbation; the zeroth-order approximation therefore corresponds to $\lambda = 0$ and the physical system corresponds to $\lambda = 1$. Assuming that both the wavefunction and energy vary smoothly with λ , we may write a Taylor series for them in terms of λ . Analysis of the resultant equation allows (by collecting terms of equivalent powers in λ) various orders of approximation to the exact problem to be formulated. It can be shown that the first-order correction to the energy may be calculated in terms of the ground state wavefunction as

$$E_1 = \langle \psi_0 | \hat{H}_1 | \psi_0 \rangle, \quad (1.41)$$

This is widely used to describe the response of a system to small electric fields, to account for corrections to the Born–Oppenheimer approximation and to correct for the absence of certain special relativistic effects.

Of relevance to our discussion on electron correlation however is when \hat{H}_0 is defined to be a sum over the one-electron Hamiltonians of eq. (1.17) and \hat{H}_1 is the difference between the exact Hamiltonian and this Hamiltonian; in this case we obtain Møller–Plesset⁴⁵ perturbation theory, which is size-extensive regardless of truncation level.

It can be shown that the Hartree–Fock energy is actually the first-order correction; it includes both E_0 and E_1 . The second-order correction E_2 is given by

$$E_2 = -\frac{1}{4} \sum_{i,j,\alpha,\beta} \frac{|(ij|\alpha\beta) - (ij|\beta\alpha)|^2}{\varepsilon_\alpha + \varepsilon_\beta - \varepsilon_i - \varepsilon_j}, \quad (1.42)$$

which is the widely used second-order Møller–Plesset theory (MP2) correlation energy; in this expression α and β represent virtual orbitals.

Unfortunately whilst this method has a lower computational cost than the CCSD method since it both scales more favourably with system size and its computation is non-iterative, it suffers from several notable deficiencies. Whilst it is able to model dispersion interactions, and in many cases offers an improved description over the Hartree–Fock method, it can give rise to completely unphysical solutions. Again consider stretched H_2 ; due to the nature of the reference wavefunction, as the bond is stretched the eigenvalue differences on the denominator of the E_2 expression will tend to zero, giving rise to an infinitely negative correlation energy at infinite bond distance. Adding additional correction terms (for instance E_3 and E_4) do not in general provide systematic improvement.

The application of perturbation theory is not limited to the Hartree–Fock Hamiltonian however. Another important method is the complete active space self-consistent field method with second-order perturbation theory (CASPT2), which applies perturbation theory to a multi-configurational wavefunction in which all configurations are included that arise from the distribution of, for instance, the valence electrons amongst a set number of orbitals. Typically orbitals are chosen to be active based on their relevance to the problem under consideration. This method has been applied quite successfully to the accurate calculation of excited states, for instance see refs. 46–48.

Recall the CC methods of the previous subsection; we noted that CCSD is in general an excellent approximation to the exact wavefunction, but that CCSDT is required to achieve the desired accuracy in many cases. The triples correction is small compared to the doubles: Therefore consider including the main effect of the triples contribution perturbatively, giving CCSD(T) theory;⁴⁹ this approach is essentially the application of Møller–Plesset perturbation theory to the CCSD wavefunction. CCSD(T) is less computationally demanding than the CCSDT method, and the most expensive step is not iterative, although it is still only routinely applied to modestly sized systems. Whilst significant accuracy may be achieved from this method, there is no associated wavefunction.

There have recently been a number of significant technical developments

in wavefunction theory which allow the treatment of larger systems; the interested reader is referred to for instance refs. 50–52. Despite these developments, wavefunction methods in general remain computationally difficult to apply to large systems. One factor that has not yet been discussed, but which was alluded to earlier, is the basis set dependence of correlated wavefunction methods.

Basis set dependence of correlated methods

One of the major drawbacks of wavefunction theory-based correlated methods is that in order to correctly model the electron–electron cusp, a large basis set is required. The requirement of a basis set capable not just of describing the occupied orbitals, but the unoccupied orbitals as well, coupled with the need to include higher order excitations as the system-size increases, generally means that an accurate calculation on an arbitrary system can easily be intractable. As a simple illustration we consider the spherically symmetric H^- ion. Due to symmetry, only s-angular momenta functions can contribute to the Hartree–Fock energy. Even in an extensive s-basis set we get an energy of -0.4879 Hartree, which is significantly above the exact energy of -0.52775 Hartree, and actually above that of the H atom; correlation plays a significant role.

Presented in table 1.1 are the energies obtained with Hartree–Fock, MP2 and CCSD as a function of basis set size, as higher angular momenta functions are added. The time column gives an indication of the relative cost of the CCSD. MP2 theory recovers a significant portion of the correlation energy. CCSD is equivalent to FCI in the case of a two-electron system, so we do approach the exact answer as the basis set increases, although we still do not reach that point even with the largest basis set used.

The preceding discussion has illustrated the complexities associated with obtaining accurate wavefunctions; Hartree–Fock theory provides a qualitative description in many cases, but electron correlation is important in achieving chemical accuracy. Methods that incorporate correlation based on excited state determinants present individual problems and do so at a high computa-

Table 1.1: The basis set dependence of the total energy of H^- with Hartree-Fock theory, MP2 and CCSD; all energies are in Hartree.

Basis components and total functions		HF	MP2	CCSD	Rel. time (CCSD)
7s	7	-0.4879097	-0.5017765	-0.5139288	1
7s6p	25	-0.4879097	-0.5145345	-0.5264218	5
7s6p5d	50	-0.4879097	-0.5168917	-0.5272851	24
7s6p5d4f	78	-0.4879097	-0.5175700	-0.5274687	156
7s6p5d4f3g	105	-0.4879097	-0.5178061	-0.5275256	550
7s6p5d4f3g2h	127	-0.4879097	-0.5178898	-0.5275452	1400
32s	32	-0.4879296	-0.5018341	-0.5144958	327

tional cost. In the next chapter we go on to consider a theory based around a much less complex, and more physically intuitive quantity—the electron density.

Density functional theory

The electron density is introduced as a quantity that in principle contains sufficient information to replace the wavefunction, through the theorems of Hohenberg and Kohn. It is then shown how this may be used to solve electronic structure problems in formally exact Kohn–Sham theory with the introduction of the exchange–correlation functional. The practical approximation of this unknown functional is then considered.

In chapter 1 the solution of the Schrödinger equation was discussed, primarily in terms of the various approaches to finding good approximations to the exact ground state wavefunction ψ_0 . It was shown that obtaining good approximations to ψ_0 is difficult in practice, particularly as the system-size increases.

Consider a water molecule; the wavefunction depends explicitly on the position and spin of the ten electrons, and parametrically on the positions of the three nuclei, giving a wavefunction which depends explicitly on forty co-ordinates and implicitly on another nine—the wavefunction is exceedingly complicated. Let us consider whether it is excessively so; can the information in the wavefunction be contained in some simpler quantity?

Eliminating the wavefunction

In order to simplify a many-electron wavefunction ψ , which depends on many co-ordinates, we consider the multiple integration

$$n \int \cdots \int d\mathbf{x}_2 \cdots d\mathbf{x}_n d\mathbf{s}_1 |\psi(\mathbf{x}^n)|^2 = \rho(\mathbf{r}_1). \quad (2.1)$$

Here we omit the integration over the spatial co-ordinate of one electron, obtaining the one-electron density $\rho(\mathbf{r}_1)$. This is a non-negative function of three spatial co-ordinates, and as such is a much simpler quantity than the wavefunction. The quantity $d\mathbf{r}_1 \rho(\mathbf{r}_1)$ corresponds to the probability of finding an electron in the volume element $d\mathbf{r}_1$. The density integrates to the total number of electrons;

$$\int d\mathbf{r}_1 \rho(\mathbf{r}_1) = n, \quad (2.2)$$

which follows from the orthonormality of the wavefunction. There are cusps in the density at the positions of the nuclei to prevent divergence of the nuclear-electron term in the one-electron Hamiltonian [eq. (1.14)]. Further, the slope of the cusp is related to the charge of the nucleus. It seems therefore that the density contains all of the information needed to specify the Hamiltonian—the charge and location of the nuclei, and the number of electrons. Given its comparatively simple form, the density seems attractive as an alternative to the wavefunction.

2.1 THE HOHENBERG–KOHNS THEOREMS

In 1964 Hohenberg and Kohn⁵³ established the soundness of using the density as the fundamental variable for solving the Schrödinger equation by proving that the density uniquely determines the external potential

$$v(\mathbf{r}_1) = - \sum_I \frac{Z_I}{|\mathbf{r}_1 - \mathbf{R}_I|} \quad (2.3)$$

and hence the wavefunction of a system. They also established a variational principle based on the density. We now consider their proofs.

The first Hohenberg–Kohn theorem

In order to prove the relationship between the density and an external potential, consider two external potentials v^1 and v^2 that give rise to the same ground state density $\rho_0(\mathbf{r})$. With each of these external potentials we associate a Hamiltonian (\hat{H}^1 and \hat{H}^2), for which there exists associated wavefunctions and total electronic energies ψ_0^1 , E_0^1 , ψ_0^2 and E_0^2 . If the two potentials differ

by at most an additive constant, then the Hamiltonians will also differ only by such a constant, and the wavefunctions will be identical.

If instead the potentials differ by more than an additive constant the two wavefunctions will not be equal. From the variational principle, the lowest possible energy of $\langle \psi | \hat{H}^1 | \psi \rangle$, E_0^1 , arises from its evaluation with ψ_0^1 . If $\langle \psi | \hat{H}^1 | \psi \rangle$ is instead evaluated with ψ_0^2 , then the resultant energy will be above E_0^1 ,

$$E_0^1 < \langle \psi_0^2 | \hat{H}^1 | \psi_0^2 \rangle = \langle \psi_0^2 | \hat{H}^2 | \psi_0^2 \rangle + \langle \psi_0^2 | \hat{H}^1 | \psi_0^2 \rangle - \langle \psi_0^2 | \hat{H}^2 | \psi_0^2 \rangle \quad (2.4)$$

$$= \langle \psi_0^2 | \hat{H}^2 | \psi_0^2 \rangle + \langle \psi_0^2 | \hat{H}^1 - \hat{H}^2 | \psi_0^2 \rangle \quad (2.5)$$

$$= E_0^2 + \int d\mathbf{r} \rho_0(\mathbf{r}) [v^1(\mathbf{r}) - v^2(\mathbf{r})]. \quad (2.6)$$

Equation (2.6) follows since it was assumed the Hamiltonians only differ in the external potential. By permuting the indices 1 and 2, a second inequality can be obtained that is incompatible with the first since they give rise to $E_0^1 + E_0^2 < E_0^1 + E_0^2$. Therefore two external potentials giving rise to the same density can differ by no more than an additive constant. It follows the external potential is uniquely determined by $\rho(\mathbf{r})$ to within a constant. Since $\rho(\mathbf{r})$ also determines n [through eq. (2.2)] it follows that the density will determine the Hamiltonian up to a constant. From the Hamiltonian we obtain the wavefunction, and from that all the properties associated with a system.

The density therefore allows us to completely specify the Schrödinger equation. Each component of the total energy E (associated with a given operator in the Hamiltonian) may be obtained from the density. Therefore we may write an energy expression in terms of functionals of the density,

$$E[\rho(\mathbf{r})] = T[\rho(\mathbf{r})] + V_{\text{ne}}[\rho(\mathbf{r})] + V_{\text{ee}}[\rho(\mathbf{r})], \quad (2.7)$$

in which T represents the kinetic energy, V_{ne} the energy of interaction between the electrons and nuclei, V_{ee} the electron–electron interaction energy and where $[\]$ is notation for a functional. Here the nuclear–nuclear repulsion term, which is not dependent on the density, is omitted for clarity. Note however that the arguments presented do not preclude the possibility of a potential giving rise to more than one ground state density for systems with degenerate ground states.

The second Hohenberg–Kohn theorem

We now consider developing a variational principle in terms of the density. Equation (2.7) can be written as the sum of two terms; the first term is V_{ne} , given by

$$V_{\text{ne}}[\rho(\mathbf{r})] = \int d\mathbf{r} \rho(\mathbf{r})v(\mathbf{r}). \quad (2.8)$$

The second is $F_{\text{HK}}[\rho(\mathbf{r})]$, which we define as

$$F_{\text{HK}}[\rho(\mathbf{r})] = T[\rho(\mathbf{r})] + V_{\text{ee}}[\rho(\mathbf{r})] = \langle \psi | \hat{T} + \hat{V}_{\text{ee}} | \psi \rangle. \quad (2.9)$$

For a given approximate density $\tilde{\rho}$, from the first HK theorem we have an associated external potential \tilde{v} and hence an associated $\tilde{\psi}$. By applying the wavefunction variational principle to $\tilde{\psi}$, we obtain

$$\langle \tilde{\psi} | \hat{H} | \tilde{\psi} \rangle = \int d\mathbf{r} \tilde{\rho}(\mathbf{r})v(\mathbf{r}) + F_{\text{HK}}[\tilde{\rho}(\mathbf{r})] \quad (2.10)$$

$$= E[\tilde{\rho}(\mathbf{r})] \geq E[\rho(\mathbf{r})], \quad (2.11)$$

thus establishing a variational principle in terms of the density. It is therefore necessary to minimise the energy with respect to changes in the density, subject to the constraint that the number of electrons is conserved ($C[\rho(\mathbf{r})] = \int d\mathbf{r} \rho(\mathbf{r}) = n$). In practice this is achieved through the use of the Lagrange undetermined multiplier approach. The quantity

$$E[\rho(\mathbf{r})] - \mu(C[\rho(\mathbf{r})]) \quad (2.12)$$

is extremised via solving for μ in

$$\frac{\delta E[\rho(\mathbf{r})]}{\delta \rho(\mathbf{r})} - \mu \frac{\delta C[\rho(\mathbf{r})]}{\delta \rho(\mathbf{r})} = 0 \quad (2.13)$$

where we introduce the δ notation for the derivative of a functional with respect to a function. The associated Euler–Lagrange equation is therefore

$$\mu = \frac{\delta T[\rho(\mathbf{r})]}{\delta \rho(\mathbf{r})} + v(\mathbf{r}) + \frac{\delta V_{\text{ee}}[\rho(\mathbf{r})]}{\delta \rho(\mathbf{r})}. \quad (2.14)$$

By necessity the densities considered thus far are v -representable; meaning they are derived from some associated external potential. This presents a problem as whilst we know the exact density for a system will be v -representable,

the conditions which constitute such a density are not known. Hence obtaining a v -representable density for use as a trial density is difficult since certain reasonable trial densities are not v -representable.^{54,55}

Further, we have established the existence of $F[\rho(\mathbf{r})]$, but as yet no clue as to its evaluation except in terms of its associated wavefunction.

The Levy constrained search approach

An n -representable electron density is one that can be derived from an anti-symmetric n -electron wavefunction. The conditions constituting n -representability are known, and perhaps more importantly for our purposes, these conditions are met by any normalised wavefunction from orbitals expanded in GTO basis sets.

In order to solve the issue of v -representable trial densities, Levy introduced the constrained search approach^{54,56} that instead allows minimisation over n -representable densities. It can be demonstrated that the v -representable densities form a subset of the n -representable ones, so the exact solution is both v - and n -representable.

The Levy approach works simply by partitioning the minimisation into two stages; firstly the energy is minimised over all wavefunctions ψ_n giving rise to a given n -representable density ρ_n , and then minimised over all possible n -representable densities to obtain E_0 ;

$$E_0 = \min_{\rho_n} \left(\min_{\psi_n \rightarrow \rho_n} \langle \psi_n | \hat{T} + \hat{V}_{ee} + \hat{V}_{ne} | \psi_n \rangle \right) \quad (2.15)$$

$$E_0 = \min_{\rho_n} \left(\min_{\psi_n \rightarrow \rho_n} \langle \psi_n | \hat{T} + \hat{V}_{ee} | \psi_n \rangle + \int d\mathbf{r} \rho_n(\mathbf{r}) v(\mathbf{r}) \right) \quad (2.16)$$

$$= \min_{\rho_n} \left(F_L[\rho_n(\mathbf{r})] + \int d\mathbf{r} \rho_n(\mathbf{r}) v(\mathbf{r}) \right). \quad (2.17)$$

In this expression the external potential has been excluded from the first minimisation since its contribution is identical for each wavefunction. The first minimisation is defined as

$$F_L[\rho_n(\mathbf{r})] = \min_{\psi_n \rightarrow \rho_n} \langle \psi_n | \hat{T} + \hat{V}_{ee} | \psi_n \rangle, \quad (2.18)$$

the Levy universal functional F_L . It is now practicable to perform a minimisation in terms of the density. However we still need some tractable approach for obtaining F_L without the associated wavefunction.

2.2 KOHN–SHAM THEORY

From the previous section we now recognise that the ground state density $\rho(\mathbf{r})$ determines the external potential $v(\mathbf{r})$, n and in turn the energy of a system. Further we have established a procedure through which we may find the exact density and energy of the ground state. We have succeeded in replacing the wavefunction with a much simpler quantity.

However, whilst we have a formally exact theory, the form of $F_L[\rho(\mathbf{r})]$ is unknown. Progress can be made in this area by considering the properties of known systems, analogously to the use of known conditions in the derivation of approximate forms for the wavefunction in chapter 1. Specifically we consider F_L for the homogeneous electron gas, and a general non-interacting system. Since F_L has contributions from T and from V_{ee} , we consider the two components separately.

Explicit functionals of the density

T can be expressed exactly as a functional of the first-order density matrix, but may be expressed as an explicit functional of the density if we limit the system to be a homogeneous electron gas. In that case it takes the simple form of

$$T_{\text{TF}}[\rho(\mathbf{r})] = \frac{3}{10}(3\pi^2)^{\frac{2}{3}} \int d\mathbf{r} \rho^{\frac{5}{3}}(\mathbf{r}). \quad (2.19)$$

This proves to be a very poor approximation to the kinetic energy, and Thomas–Fermi^{57,58} theory (whereby this approximate T_{TF} is applied to interacting systems) is unrealistic, failing even to bind any molecular system. A correction term due to von Weizsäcker,⁵⁹ denoted T_{W} , may be added to T_{TF} , which involves the gradient of the density:

$$T_{\text{W}}[\rho(\mathbf{r}), \nabla\rho(\mathbf{r})] = \frac{1}{8} \int d\mathbf{r} \frac{|\nabla\rho(\mathbf{r})|^2}{\rho(\mathbf{r})}. \quad (2.20)$$

Note that T_W is equivalent to the exact T_s [defined below in eq. (2.23)] for a one or two-electron system. This gradient correction helps, but it still precludes a theory competitive even with Hartree–Fock.

If as in Hartree–Fock theory we neglect correlation, V_{ee} may be expressed as the sum of a Coulomb contribution J and an exchange contribution K . For any system J is an explicit functional of the density, given by

$$J[\rho(\mathbf{r})] = \iint d\mathbf{r}_1 d\mathbf{r}_2 \frac{\rho(\mathbf{r}_1)\rho(\mathbf{r}_2)}{|\mathbf{r}_1 - \mathbf{r}_2|}. \quad (2.21)$$

The value of K may be obtained, as with T in the general case, from a knowledge of the first-order density matrix. As shown by Dirac,⁶⁰ in the case of the homogeneous electron gas it is possible to obtain an exchange energy as a functional of only the density;

$$E_x[\rho(\mathbf{r})] = -\frac{3}{4}(3\pi)^{\frac{1}{3}} \int d\mathbf{r} \rho^{\frac{4}{3}}(\mathbf{r}). \quad (2.22)$$

This proves to be of significant use, although not in the context of Thomas–Fermi theory.

The Kohn–Sham system

For an arbitrary non-interacting system with external potential $v(\mathbf{r})$, the analysis of section 1.3 demonstrates that the exact wavefunction takes the form of a single Slater determinant. It is therefore possible to obtain the exact kinetic energy for a non-interacting system by evaluating it according to

$$T_s[\rho(\mathbf{r})] = \sum_i^n \langle \chi_i(\mathbf{x}) | -\frac{1}{2}\nabla^2 | \chi_i(\mathbf{x}) \rangle. \quad (2.23)$$

Equally we may obtain the exact density for a non-interacting system as

$$\rho(\mathbf{r}) = \sum_i^n |\chi_i(\mathbf{x})|^2 \quad (2.24)$$

where the $\{\chi_k\}$ are the one-electron orbitals comprising the Slater determinant, as before.

Kohn and Sham⁶¹ reformulated the problem of determining the exact electron density by considering a system for which $T_s[\rho(\mathbf{r})]$ is the exact kinetic

energy. We rewrite $F[\rho(\mathbf{r})]$ as

$$F[\rho(\mathbf{r})] = T_s[\rho(\mathbf{r})] + J[\rho(\mathbf{r})] + E_{\text{xc}}[\rho(\mathbf{r})] \quad (2.25)$$

in which

$$E_{\text{xc}}[\rho(\mathbf{r})] \equiv T[\rho(\mathbf{r})] - T_s[\rho(\mathbf{r})] + V_{\text{ee}}[\rho(\mathbf{r})] - J[\rho(\mathbf{r})]. \quad (2.26)$$

The quantity $E_{\text{xc}}[\rho(\mathbf{r})]$ is denoted the exchange–correlation energy. Using this partitioning the Euler–Lagrange equation for the exact system is therefore

$$\mu = \frac{\delta T_s[\rho(\mathbf{r})]}{\delta \rho(\mathbf{r})} + v_{\text{eff}}(\mathbf{r}), \quad (2.27)$$

$$v_{\text{eff}}(\mathbf{r}) = v(\mathbf{r}) + \frac{\delta J[\rho(\mathbf{r})]}{\delta \rho(\mathbf{r})} + \frac{\delta E_{\text{xc}}[\rho(\mathbf{r})]}{\delta \rho(\mathbf{r})}, \quad (2.28)$$

which is identical to the conventional Euler–Lagrange equation [eq. (2.14)] for a non-interacting system (in which $T = T_s$ and $V_{\text{ee}} = 0$) evaluated with the external potential $v_{\text{eff}}(\mathbf{r})$. It follows that the density of the real system can be determined as the density of a non-interacting system moving in a potential $v_{\text{eff}}(\mathbf{r})$.

The Hamiltonian for this non-interacting system is given by

$$\hat{H} = -\frac{1}{2} \sum_i \nabla_i^2 + \sum_i v_{\text{eff}}(\mathbf{r}_i). \quad (2.29)$$

The exact density may therefore be obtained using eq. (2.24), using the orbitals which are the solutions to

$$\left(-\frac{1}{2} \nabla^2 + v_{\text{eff}}(\mathbf{r}) \right) \chi_i(\mathbf{r}, \sigma) = \epsilon_i \chi_i(\mathbf{r}, \sigma). \quad (2.30)$$

This method of solving the electronic structure problem is known as Kohn–Sham (KS) density functional theory (DFT). It allows several major contributions to the total energy to be computed exactly. All of the unknown contributions to the energy are confined in the term E_{xc} , the form of which is still unknown.

Practical considerations

The next section will detail the fundamental issue that we have still to address; the form of the exchange–correlation energy functional. However, before we

reach that point, consideration of a few practical issues is necessary. As in the case of the solution of the Hartree–Fock equations, a trial or guess density is required as eq. (2.30) must be solved iteratively for the orbitals giving rise to the density. We then evaluate the energy through eqs. (2.7) and (1.8).

As in Hartree–Fock theory, we expand each of the $\{\chi_k\}$ in terms of basis functions, and solve the SCF equations in the same way. The standard techniques applicable for the computation of molecular properties derived for Hartree–Fock theory are therefore also applicable here. The similarities between the forms of the KS DFT and Hartree–Fock equations demonstrates that the two methods have a similar computational cost, however KS DFT is formally exact.

One additional complication arises due to the non-analytic integrals arising in the representation of the exchange–correlation energy as a functional of the density; it is necessary to evaluate such integrals numerically. This is achieved by firstly partitioning a general molecular integral into components that are localised on a given atom.⁶² The components are then evaluated using standard numerical quadrature techniques.^{63,64}

2.3 EXCHANGE-CORRELATION FUNCTIONALS

At this stage it is apparent that whatever method we choose to attempt solution of the Schrödinger equation, something will need to be approximated. In DFT, we have a formally exact theory. However, the exact form of $F[\rho(\mathbf{r})]$ is unknown. For the KS partitioning the approximation is contained entirely within the E_{xc} term. The simplest approximation to E_{xc} of chemical relevance is obtained from a consideration of the homogeneous electron gas.

Now introduce the spin-polarised electron gas, with densities ρ_α and ρ_β associated with each spin. We define

$$\rho_\alpha(\mathbf{r}) = \sum_i^{n_\alpha} |\chi_i(\mathbf{r}, \alpha)|^2 \quad \rho_\beta(\mathbf{r}) = \sum_i^{n_\beta} |\chi_i(\mathbf{r}, \beta)|^2 \quad (2.31)$$

$$\rho(\mathbf{r}) = \rho_\alpha(\mathbf{r}) + \rho_\beta(\mathbf{r}) \quad (2.32)$$

with n_α and n_β respectively corresponding to the number of α -spin and β -spin electrons.

For closed shell systems we have that $\rho_\alpha = \rho_\beta = \rho/2$. For open-shell systems we may take the route described for Hartree–Fock theory regarding restricted or unrestricted spatial orbitals. It has been argued⁶⁵ that spin-unrestricted calculations are most appropriate in DFT. See chapter 3 for elaboration of this issue.

Local Spin Density Approximation

The introduction of spin-polarised densities allows the calculation of the exchange energy of the homogeneous electron gas as

$$E_x^{\text{LSDA}}[\rho_\alpha(\mathbf{r}), \rho_\beta(\mathbf{r})] = -\frac{3}{4}(3\pi)^{\frac{1}{3}}2^{\frac{1}{3}} \sum_\sigma \int d\mathbf{r} \rho_\sigma^{\frac{4}{3}}(\mathbf{r}), \quad (2.33)$$

in which σ is a spin co-ordinate taking values of α and β . This closed form expression is due to Slater,⁶⁶ who used this expression in the $X\alpha$ method in an attempt to simplify the computation of Hartree–Fock theory; it is the spin-polarised generalisation of Dirac’s eq. (2.22).

Whilst it is not possible to obtain a closed form expression of E_c^{LSDA} for the correlation energy of the homogeneous electron gas, it is possible to compute accurate values from quantum Monte-Carlo data.⁶⁷ Several parameterisations of this data have been proposed, most notably those of Vosko, Wilk and Nusair⁶⁸ (VWN) and Perdew and Wang⁶⁹ (PW91) both of which further partition the correlation energy into terms from the interaction of like-spin electrons and opposite-spin electrons. The LSDA approximation is obtained when we take the KS partitioning of F and represent E_{xc} as $E_x^{\text{LSDA}} + E_c^{\text{LSDA}}$ for non-homogeneous systems, where E_c^{LSDA} is one of the parameterisations mentioned above.

The LSDA has found widespread application in physics; it lends itself to metallic systems. In chemistry it is less successful; whilst for some properties it achieves similar accuracy to Hartree–Fock theory, it is known to significantly over-bind molecules. The failure of the LSDA to accurately model chemical systems is not surprising; molecules have inherently localised densities and so do not resemble the homogeneous gas. Also of relevance is that the various LSDA correlation approximations do not give a zero-valued correlation energy for one-electron systems. The LSDA may be thought of as the first term in

a Taylor series expansion for E_{xc} in the density. The obvious next step is therefore to express E_{xc} in terms of information about the density and its derivatives.

Generalised Gradient Approximations

The most natural way of including derivative information about the density is through the gradient expansion approximation⁷⁰ (GEA), which gives E_{xc} in terms of a Taylor series for a slowly varying density. Unfortunately this model is too simplistic; it performs no better than the LSDA, and in some cases is actually worse. This is due to the GEA failing to satisfy a number of exact conditions on the behaviour of the true E_{xc} that the LSDA does satisfy.

In order to make progress exchange-correlation functionals of the form

$$E_{xc}^{\text{GGA}}[\rho_{\alpha}(\mathbf{r}), \rho_{\beta}(\mathbf{r})] = \int d\mathbf{r} G[\rho_{\alpha}(\mathbf{r}), \rho_{\beta}(\mathbf{r}), \nabla\rho_{\alpha}(\mathbf{r}), \nabla\rho_{\beta}(\mathbf{r})] \quad (2.34)$$

are considered. When E_{xc} is approximated in this manner the resultant functionals are called generalised gradient approximations (GGAs). In general the exchange and correlation components are approximated separately. From a dimensional analysis it can be shown that a natural expansion term to use in a GGA is

$$x(\mathbf{r}) = \frac{\nabla\rho(\mathbf{r})}{\rho^{\frac{4}{3}}(\mathbf{r})}; \quad (2.35)$$

simple closed form expressions in terms of x form the basis of most GGA exchange functionals. There are two routes to determining forms for G : The first is to satisfy as many known conditions of the exact E_{xc} as possible with a functional form, leading to functionals such as Perdew–Wang^{69,71} 1991 (PW91) and Perdew–Burke–Ernzerhof⁷² (PBE). The alternative is to fit the parameters to reproduce known molecular properties. This second approach has met in general with more success in terms of the ability to readily achieve good quality results, but provides less physical insight. Equally, empirically derived functionals may suffer from a lack of transferability to systems that differ significantly from those used in their derivation. Examples of exchange functionals from this approach are the Becke 1986,⁷³ and Becke 1988⁷⁴ (B88) gradient correction functionals based on atomic energies, and Cohen and Handy's

OPTX.⁷⁵ Most notable of the correlation functionals is the Lee–Yang–Parr⁷⁶ (LYP) approximation, based on quantum Monte Carlo data for the helium atom.

The coupling⁷⁷ of Slater, B88 and LYP (to give the BLYP approximation) was responsible for the acceptance of DFT as a method suitable for chemical applications. Later functionals such as HCTH⁷⁸ have also proven popular. GGA approximations, despite offering improved performance in most areas over the LSDA, still fail to provide quantitative accuracy in many cases. This failure will be discussed in the context of several areas in later chapters; specifically those related to the incorrect asymptotic form of the exchange–correlation potential and self-interaction error which arise due to the difference between exchange evaluated using the Hartree–Fock expression [eq. (3.5)] evaluated with the KS orbitals (which we denote ‘exact’ orbital exchange, E_x^0 , in the DFT context) and local DFT exchange.

There are two approaches for improving exchange–correlation functionals over the GGA level, which are not mutually exclusive. The first involves inclusion of higher-order gradient information, giving meta-GGA functionals. The second involves incorporating some portion of exact exchange into a functional, giving so-called hybrid functionals.

Higher-order corrections

The inclusion of higher-order gradient corrections has been considered as a method of improving functional performance. This in general is accomplished through the kinetic energy density τ , defined as

$$\tau_\sigma(\mathbf{r}, \sigma) = \frac{1}{2} \sum_i |\nabla \chi_i(\mathbf{r}, \sigma)|^2. \quad (2.36)$$

Typically this approach is more numerically stable than those based on the Laplacian of the density. Meta-GGAs in general do not offer a significant improvement over GGA functionals; the second-order gradient correction usually has a less significant effect than the first-order one, but such functionals are able to satisfy an increased number of known exact conditions over GGAs. Examples are again obtained via the empirical or non-empirical routes taken in the construction of GGAs. The most notable meta-GGA is the non-

empirical Tao-Perdew-Staroverov-Scuseria^{79,80} (TPSS) exchange-correlation functional.

Hybrid functionals

The inclusion of some amount of exact exchange in an exchange-correlation functional can be justified through a consideration of the adiabatic connection⁸¹⁻⁸³ formalism (which will be discussed in detail in chapter 6).

Addition of DFT correlation to exact exchange is generally unsuccessful however as it effectively ‘misses’ the non-dynamic correlation. This is due to the important concept that local density-based exchange functionals approximately model wavefunction exchange and non-dynamic correlation. Density-based correlation functionals model only dynamic correlation; the partitioning into exchange and correlation in DFT is independent of the wavefunction definitions and is primarily based on the scaling relations of the resultant functionals. It should be noted that Becke and Johnson have recently considered functionals that can be added to exact exchange, which separately model dynamic and non-dynamic correlation.⁸⁴⁻⁸⁷

A generic hybrid functional takes the form of

$$E_{xc}^{\text{hybrid}} = (1 - c_x)E_x^{\text{DFT}} + E_c^{\text{DFT}} + c_x E_x^0 \quad (2.37)$$

where c_x is a mixing parameter taking values between 0 and 1. The first hybrid functional was the half-and-half functional of Becke,⁸⁸ in which $c_x = 0.5$. Such a value is in general not optimal (see chapter 3 for further discussion of this point). Becke’s later work⁸⁹ on hybrid functionals led to the extensively used Becke-3-Lee-Yang-Parr functional of Stephens⁹⁰ *et al.* and the PBE0^{91,92} functional, which have $c_x = 0.2$ and 0.25 respectively. Fractions of this size may be justified from a consideration of Møller-Plesset perturbation theory; see ref. 93. More recently functionals based on the Becke 1997⁹⁴ expansion, such as B97-1,⁷⁸ B97-2⁹⁵ and B97-3,⁹⁶ and hybrids of meta-GGA functionals, have been introduced. In general they offer some improvement over standard hybrid functionals, but there are a number of properties which are still poorly described, particularly those which require some formally exact behaviour that is only satisfied by the non-local E_x^0 ; the extent to which such properties are

well-described with hybrid functionals depends on the size of c_x . The next stage of functional development would be to include virtual orbital information.

Magnetic properties computed with hybrid functionals are particularly poor when compared to similar calculations using LSDAs or GGAs, due to the non-multiplicative exchange–correlation potential in standard implementations of hybrid functionals.

Optimised effective potentials

In the KS DFT approach, the exchange–correlation potential is defined as the functional derivative of E_{xc} with respect to the density [see eq. (2.28)]. In standard implementations of hybrid functionals the potential due to the non-local E_x^0 is evaluated as the derivative with respect to the orbitals, as in Hartree–Fock theory. This is formally inconsistent with the KS approach. In order to remedy this, the optimised effective potential (OEP) method is introduced. In the OEP method the energy for an arbitrary orbital-dependent functional is minimised subject to the constraint that the exchange–correlation potential be local and multiplicative. Solution of the self-consistent OEP equations is fraught with numerical difficulties. This will be discussed in more detail when the OEP method is used in the computation of magnetic response properties in chapter 5, where the Yang–Wu implementation⁹⁷ is considered. All other results presented are evaluated conventionally without recourse to OEPs, as most properties are unaffected by their use.

A related approach involves the computation of a multiplicative potential associated with a given density. The Wu–Yang⁹⁸ constrained search approach minimises the non-interacting kinetic energy subject to the constraint that the input density is reproduced from a multiplicative exchange–correlation potential. This method is also described in more detail at the point it is used in this thesis, in chapter 6.

Modern approaches to the exchange–correlation problem

It can easily be demonstrated that the optimal value of the mixing parameter c_x is different depending on the system and property under consideration.

There are two approaches to functional development which attempt to account for such variations. The first approach explicitly partitions the behaviour of the exchange functional into two separately treated parts, depending on how far the electrons are from each other—it introduces r_{12} -dependence. These functionals are introduced in chapter 3, and are later developed and discussed in significant detail. In chapter 4, these functionals are applied to the calculation of excitation energies in an extensive set of theoretically challenging molecules. Then in chapter 5, they are applied to other problems of interest including bond-length alternation and band gaps in polymeric systems, and the calculation of nuclear magnetic resonance parameters for main group and light transition metal systems.

The second approach involves returning to the theoretical basis for hybrid functionals—the adiabatic connection formalism.⁸¹⁻⁸³ Instead of the linear approximation used in the construction of hybrid functionals, more complicated approximations are considered. In order to assess the forms used to model the adiabatic connection, exact input data are constructed. This approach is described in detail in chapter 6.

Exchange-attenuation

As a prototypical example, the performance of the widely used B3LYP hybrid functional is assessed for a number of chemically relevant properties; successes and failures are highlighted. The practical difference between spin-restricted and spin-unrestricted treatments of open-shell systems is discussed. A possible means of improving upon the accuracy of hybrid functionals, the Coulomb-attenuated/ long-range corrected/ range-separated hybrid approach, is introduced with a discussion of recent developments. An exemplar attenuated functional, CAM-B3LYP, is assessed and the results compared with B3LYP. The parameter dependence of attenuated forms is considered, particularly with regard to the effect on atomisation energies and excited states. Several parameterisations are assessed over a wider range of properties.

Hybrid⁸⁹ exchange–correlation energy functionals have until relatively recently represented the state-of-the-art in KS DFT. Functionals such as B3LYP have been responsible for popularising DFT as a viable computational approach in the chemical community, providing a successful compromise between cost and accuracy. We begin by assessing the B3LYP functional for various properties of chemical relevance, with an emphasis on determining where it is successful and where it is less so. The failings of B3LYP, and other standard hybrid functionals, can for many properties be addressed from a consideration of the treatment of exchange in the functional.

3.1 ASSESSMENT OF A HYBRID FUNCTIONAL

As a representative hybrid functional we consider B3LYP. The B3LYP⁸⁹ functional is an empirically derived development of the half-and-half⁸⁸ functional of Becke, in which an approximate linear adiabatic connection form (see chapter 6) was used to justify the inclusion of exact exchange in an exchange–correlation functional. The form of the B3LYP functional was proposed by Becke, with later modification by Stephens⁹⁰ *et al.* In B3LYP, exchange is described^{60,74} by

$$E_x^{\text{B3LYP}} = 0.2E_x^0 + 0.8(E_x^{\text{LSDA}} + 0.9E_x^{\text{B88}}); \quad (3.1)$$

correlation is described^{68,76} by

$$E_c^{\text{B3LYP}} = 0.19E_c^{\text{VWN}} + 0.81E_c^{\text{LYP}}. \quad (3.2)$$

The parameters in B3LYP are empirically derived by fitting to a relatively simple set of thermochemical properties.

We determine the applicability of the B3LYP functional by considering its performance for the assessments in table 3.1,⁹⁹ which are subsets of those used for the B97-3⁹⁶ functional. For a complete discussion of the reference data and computational details see that reference, although an outline is provided below.

Atomisation energies (assessment 1) are a subset of the G2^{100,101} molecules. The ionisation potentials (assessment 2) are a subset of the G2-1¹⁰⁰ molecules. Each of these assessments are run at MP2/6-31G(d) geometries using the 6-311+(3df,2p) basis set following ref. 102, comparing with experimental data.

Classical reaction barriers (assessment 3) are a subset of the BH42/04 set,¹⁰³ consisting mainly of open-shell hydrogen transfer reactions. Single point energies are evaluated using the QCISD/6-311++G(3d2f,2df,2p) geometries of ref. 103, with the 6-311+(3df,2p) basis which gives results of similar quality to the basis set used in the earlier study. The reference values are estimated from a combination of experimental and theoretical kinetic data.

Geometry optimisations from three separate assessments are considered. The G2 bond lengths (assessment 4) are a subset of those considered in ref. 78 and the hydrogen-bonded dimer distances (assessment 5) are from ref. 104;

Table 3.1: The species included in the assessments set; see the text for original references.**1. G2 Atomisation energies**

Acetamide, acetic acid, acetone, acetyl chloride, acetyl fluoride, acrylonitrile, AlCl_3 , allene, aziridine, BCl_3 , BeH , benzene, BF_3 , bicyclobutane, C_2H_2 , C_2H_3 , C_2H_4 , C_2H_5 , C_2H_6 , CCH , CF_3CN , CF_4 , CH , $\text{CH}_2(^1A)$, CH_2CHF , CH_3 , $(\text{CH}_3)_2\text{CH}$, $\text{CH}_3\text{CH}_2\text{O}$, CH_3Cl , CH_3CO , CH_3O , CH_3OH , CH_4 , CHF_3 , Cl_2 , ClF , ClNO , CO , CO_2 , cyclobutene, cyclopropene, dimethylamine, dimethylether, ethanol, ethylchloride, F_2 , F_2O , formic acid, furan, H_2 , H_2CO , H_2COH , H_2O , H_2O_2 , HCl , HCO , HF , HOCl , isobutane, isopropanol, ketene, Li_2 , LiF , LiH , methyl cyanide, methyl ethylether, methyl formate, methyl nitrite, methylamine, methylene cyclopropane, N_2 , N_2O , Na_2 , NaCl , NF_3 , NH_3 , nitromethane, NO_2 , O_3 , OH , oxirane, propane, propylchloride, propyne, pyridine, pyrrole, *trans*-ethylamine, trimethylamine, 2-butyne, vinylchloride.

2. Ionisation potentials

Li , Be , B , C , N , O , F , Na , Mg , Al , CH_4 , NH_3 , H_2O , HF , HCl , C_2H_2 , C_2H_4 , CO , N_2 , Cl_2 , ClF .

3. Classical reaction barriers

$\text{CH}_3 + \text{H}_2 \rightarrow \text{CH}_4 + \text{H}$, $\text{OH} + \text{CH}_4 \rightarrow \text{CH}_3 + \text{H}_2\text{O}$,
 $\text{H} + \text{H}_2 \rightarrow \text{H}_2 + \text{H}$, $\text{OH} + \text{NH}_3 \rightarrow \text{H}_2\text{O} + \text{NH}_2$,
 $\text{HCl} + \text{CH}_3 \rightarrow \text{Cl} + \text{CH}_4$, $\text{OH} + \text{C}_2\text{H}_6 \rightarrow \text{H}_2\text{O} + \text{C}_2\text{H}_5$,
 $\text{F} + \text{H}_2 \rightarrow \text{HF} + \text{H}$, $\text{O} + \text{HCl} \rightarrow \text{OH} + \text{Cl}$,
 $\text{NH}_2 + \text{CH}_3 \rightarrow \text{CH}_4 + \text{NH}$, $\text{NH}_2 + \text{C}_2\text{H}_5 \rightarrow \text{C}_2\text{H}_6 + \text{NH}$,
 $\text{C}_2\text{H}_6 + \text{NH}_2 \rightarrow \text{NH}_3 + \text{C}_2\text{H}_5$, $\text{NH}_2 + \text{CH}_4 \rightarrow \text{CH}_3 + \text{NH}_3$,
 $\text{H}_2 + \text{Cl} \rightarrow \text{H} + \text{HCl}$, $\text{CH}_4 + \text{H} \rightarrow \text{CH}_3 + \text{H}_2$,
 $\text{H}_2\text{O} + \text{NH}_2 \rightarrow \text{OH} + \text{NH}_3$, $\text{Cl} + \text{CH}_4 \rightarrow \text{HCl} + \text{CH}_3$,
 $\text{H}_2\text{O} + \text{C}_2\text{H}_5 \rightarrow \text{OH} + \text{C}_2\text{H}_6$, $\text{OH} + \text{CH}_3 \rightarrow \text{O} + \text{CH}_4$,
 $\text{PH}_2 + \text{H}_2 \rightarrow \text{H} + \text{PH}_3$, $\text{H}_2 + \text{HS} \rightarrow \text{H} + \text{H}_2\text{S}$,
 $\text{OH} + \text{Cl} \rightarrow \text{O} + \text{HCl}$, $\text{NH}_3 + \text{C}_2\text{H}_5 \rightarrow \text{NH}_2 + \text{C}_2\text{H}_6$,
 $\text{CH}_3 + \text{NH}_3 \rightarrow \text{NH}_2 + \text{CH}_4$.

4. G2 bond lengths

H_2 , LiH , $\text{CH}_2(^1A)$, NH_3 , H_2O , HF , Li_2 , LiF , C_2H_2 , C_2H_4 , HCN , CO , H_2CO , N_2 , H_2O_2 , F_2 , CO_2 , HCl , Na_2 , Cl_2 , NaCl , SiO , CS , ClF .

5. Hydrogen-bonded dimer distances

$\text{HF} \cdots \text{FH}$, $\text{HCl} \cdots \text{ClH}$, $\text{H}_2\text{O} \cdots \text{H}_2\text{O}$, $\text{CO} \cdots \text{FH}$, $\text{OC} \cdots \text{FH}$.

6, 7. Diatomic bond lengths and harmonic vibrational wavenumbers

Li_2 , LiNa , LiK , Na_2 , NaK , K_2 , N_2 , NP , NAs , P_2 , PAs , As_2 , F_2 , FCl , Cl_2 , ClBr , Br_2 , LiF , LiCl , NaF , NaCl , NaBr , KF , KCl , BCl , BBr , AlF , AlCl , AlBr , CO , CS , CSe , SiO , SiS , SiSe , GeO , GeS .

8. Isotropic electronic polarisabilities

HF , F_2 , CO , N_2 , CH_4 , CO_2 , C_2H_4 , PH_3 , H_2O , H_2S , SO_2 , HCl , Cl_2 .

9. Small molecule vertical excitation energies

CO , N_2 , H_2CO , C_2H_4 .

the TZ2P basis set is used for both assessments. For the diatomics bond length and vibrational wavenumber assessments (assessments 6 and 7) we use a subset of those molecules considered in ref. 105, with bond lengths and wavenumbers determined using the 6-311+G(2df) basis set. Comparison is made with experimental values for the diatomics, and *ab initio* values for the polyatomics.

Isotropic electronic polarisabilities (assessment 8) are determined at near-experimental geometries following ref. 95, using the Sadlej^{106,107} basis set, comparing with *ab initio* values. The excitation energies (assessment 9) are compared with experimentally derived values, and were determined at experimental geometries using an augmented Sadlej basis set where additional diffuse basis functions are added following ref. 108; uncontracted functions with exponents of 0.0147 and 0.00448 on C, 0.0202 and 0.00608 on N, and 0.0270 and 0.00807 on O. All property calculations are performed with a development version of the DALTON¹⁰⁹ program. Energy calculations are also performed in DALTON, except for the unrestricted open-shell calculations, which use a development version of CADPAC.¹¹⁰

Table 3.2 highlights the errors associated with these assessments for the B3LYP functional. For assessments 1–3, which include open-shell species, results are presented in both unrestricted and restricted formalisms. In the unrestricted formalism, atomisation energies are reasonably described, although there is a tendency to underestimate. The ionisation potentials are good, but the reaction barriers are poor, with a severe underestimation; this underestimation is typical of standard functionals.^{111,112} It can be shown that more accurate reaction barriers may be obtained by increasing the amount of E_x^0 in a hybrid functional¹¹³ or through making the orbitals more Hartree–Fock-like.¹¹⁴

Bond lengths are also reasonably described while the associated harmonic wavenumbers are particularly accurate. The polarisabilities are poor however, which is primarily due to the description of the virtual orbitals. The excitation energies also appear poorly described, primarily due to the presence of excitations to Rydberg states. These failures arise due to the incorrect asymptotic nature of the exchange–correlation potential associated with standard local (and to a lesser extent) hybrid functionals.

Table 3.2: Mean error d and mean absolute error $|d|$, relative to reference values, for the assessments in table 3.1, with the B3LYP exchange–correlation functional in the unrestricted (UKS) and restricted open-shell (ROKS) formalisms.

	UKS	ROKS
1. Atomisation energies		
$d/\text{kcal mol}^{-1}$	−2.9	0.5
$ d /\text{kcal mol}^{-1}$	3.6	2.2
2. Ionisation potentials		
d/eV	0.00	0.03
$ d /\text{eV}$	0.17	0.15
3. Classical barriers		
$d/\text{kcal mol}^{-1}$	−3.7	−2.4
$ d /\text{kcal mol}^{-1}$	3.8	2.8
4, 5, 6. Bond lengths		
$d/\text{Å}$	0.009	
$ d /\text{Å}$	0.015	
7. Vib. wavenumbers		
d/cm^{-1}	6	
$ d /\text{cm}^{-1}$	22	
8. Polarisabilities		
$d/\text{a.u.}$	0.36	
$ d /\text{a.u.}$	0.45	
9. Excitation energies		
d/eV	−0.82	
$ d /\text{eV}$	0.84	

It has been argued in ref. 65 that the unrestricted formalism is most appropriate within KS DFT, since the electron density may locally be more β -spin polarised, which cannot occur in the restricted approach. The behaviour of B3LYP is significantly affected by the difference in the two approaches; smaller errors are actually obtained with spin-restricted calculations. This suggests that there is some error cancellation in this case; the underestimation typically associated with B3LYP with regard to atomisation energies and reaction barriers is lessened in the restricted formalism.

The failures of B3LYP highlighted thus far arise from either insufficient amounts of E_x^0 , or from the incorrect asymptotic behaviour of the potential. Note that the correct asymptotic behaviour is obtained from a local poten-

tial associated with E_x^0 (for instance obtained through the OEP procedure). Therefore the failings of B3LYP can in these cases be attributed to the treatment of exchange.

Of course B3LYP may fail in other cases due to the description of correlation; for instance it will not accurately describe binding in van der Waals complexes, or other dispersion-dominated systems. The local nature of the correlation in any standard DFT functional is insufficient to describe interactions when there is little or no orbital overlap. There are several approaches that attempt to model the dispersion interaction in DFT. Self-consistent functionals (see for example refs. 115 and 116) that attempt to introduce non-locality are one possible method, but these have met in general with limited use as they are computationally intensive and not widely implemented. Another approach, which involves the addition of a post-SCF correction, either in terms of directly adding an empirical dispersion term (such as in the DFT-D approach^{117,118} or the approach of Becke and Johnson¹¹⁹⁻¹²¹), or through adding a portion of the non-local MP2 correlation energy evaluated with the Kohn-Sham orbitals, as in the B2PLYP approach of Grimme,¹²²⁻¹²⁴ have been more widely applied due to their simplicity. These dispersion corrections may yield improved descriptions for a variety of properties, however the lack of a self-consistent density affords other problems. Equally they may be seen as simply increasing the flexibility in the functional—the corrections may improve the performance of the functional, but whether or not it can be attributed to their accurately modelling the dispersion interaction remains to be seen.

3.2 ATTENUATED EXCHANGE

Despite their improvement over GGA functionals, for some properties standard hybrid functionals remain insufficiently accurate. In some cases the deficiency may be traced to the treatment of exchange; the large amounts of density-based local exchange result in significantly larger errors for these properties than would be obtained from a treatment with a higher proportion of exact-exchange. Reaction barriers for instance tend to need a higher proportion of E_x^0 compared to atomisation energies. Certain types of excitation energy need the full amount of E_x^0 for an accurate description, due to

their long-range nature. Conventional hybrid functionals contain only a fixed amount of exact exchange for all occasions, and the size of that amount depends solely on what properties are considered most important at the time of derivation; the B3LYP functional contains 20% based on the thermochemical data it is optimised to reproduce. From the arguments here however it seems as though a more complicated mixing is required if we require a universally applicable exchange–correlation functional.

Attempts to introduce more complex mixings of exchange generally involve making the treatment of exchange dependent on the interelectron distance r_{12} . The expression for exact exchange involves non-local information from all of the occupied orbitals and the $1/r_{12}$ operator. DFT exchange contains only local information from the density and possibly its gradient at a point, and no explicit distance dependence.

Consider partitioning the $1/r_{12}$ operator¹²⁵ to allow the treatment of exchange to differ depending on the distance between electrons in a simple range-separated manner. For the applications that we consider we will achieve this by treating exchange at short-range primarily by DFT approximations, and at long-range primarily through exact exchange, with the expressions modified according to the partitioning we choose. If instead we were interested in removing the computational difficulty of evaluating exact exchange in periodic systems, we could reverse this treatment. Such an approach has recently been trialled by Scuseria and co-workers.^{126–130} We focus on the approach of long-range exact exchange however as this is the most relevant for improving the description of finite molecular systems.¹³¹ Note we do not partition any of the other terms in the total energy expression that involve the $1/r_{12}$ operator.

One computationally efficient method of partitioning the $1/r_{12}$ operator is through the identity¹²⁵

$$\frac{1}{r_{12}} \equiv \frac{\operatorname{erf}(\mu r_{12})}{r_{12}} + \frac{1 - \operatorname{erf}(\mu r_{12})}{r_{12}}, \quad (3.3)$$

where erf is the standard error function

$$\operatorname{erf}(r) \equiv \frac{2}{\sqrt{\pi}} \int_0^r dt \exp(-t^2). \quad (3.4)$$

The first term corresponds to a decreasing function going from $2/\sqrt{\pi}$ at $r_{12} = 0$ to 0 in the limit as $r_{12} \rightarrow \infty$, the rate of which is determined by the size of the parameter μ , which has units of a_0^{-1} and which takes values $0 \leq \mu a_0 < \infty$ (for brevity we write μa_0). It is more insightful to consider the behaviour of the numerator however, which is an increasing function taking values from 0 to 1 for positive μ . According to the prescription above, exact exchange is evaluated through

$$E_x^0 = -\frac{1}{2} \sum_{\sigma} \sum_{i,j} \iint d\mathbf{r}_1 d\mathbf{r}_2 \varphi_{i\sigma}(\mathbf{r}_1) \varphi_{j\sigma}(\mathbf{r}_1) \frac{1}{r_{12}} \varphi_{j\sigma}(\mathbf{r}_2) \varphi_{i\sigma}(\mathbf{r}_2), \quad (3.5)$$

with the $1/r_{12}$ operator replaced with the first term of eq. (3.3). The second term in eq. (3.3) is also a decreasing function, which approaches ∞ as $r_{12} \rightarrow 0$ and 0 as $r_{12} \rightarrow \infty$. Local DFT exchange is evaluated by making use of the one-particle density matrix expression for the exchange energy;

$$E_x = -\frac{1}{2} \sum_{\sigma} \iint d\mathbf{r}_1 d\mathbf{r}_2 \frac{P_{1\sigma}^2(\mathbf{r}_1, \mathbf{r}_2)}{r_{12}}, \quad (3.6)$$

by replacing the $1/r_{12}$ operator with the second term of eq. (3.3). It is again more intuitive to consider the behaviour of the numerator, which is a decreasing function going from 1 to 0 for positive μ . A closed form for eq. (3.6) may be obtained in terms of the density if we assume the LSDA. This is achieved by changing variables [to $\mathbf{r} = (\mathbf{r}_1 + \mathbf{r}_2)/2$, and $\mathbf{s} = \mathbf{r}_1 - \mathbf{r}_2$], and performing the \mathbf{s} integration analytically.¹²⁵ This gives an explicit expression for the exchange energy in terms of the one-particle density matrix for the uniform electron gas;

$$E_x^{\text{LSDA}} = -\frac{1}{2} \sum_{\sigma} \int d\mathbf{r} \rho_{\sigma}^{\frac{4}{3}}(\mathbf{r}) K_{\sigma}^{\text{LSDA}} \quad (3.7)$$

where K_{σ}^{LSDA} is a constant [$2^{\frac{1}{3}}(3/\pi)^{\frac{1}{3}}3/4$] which may be related to the Fermi momentum by

$$k_{\sigma}^{\text{LSDA}} = (9\pi/K_{\sigma}^{\text{LSDA}})^{\frac{1}{2}} \rho_{\sigma}^{\frac{1}{3}}(\mathbf{r}). \quad (3.8)$$

This approach whereby short-range exchange is treated by the LSDA approximation, and long-range exchange by exact exchange, was pioneered by Savin^{132,133} *et al.* Hirao and co-workers^{134,135} later modified the short-range

exchange expression for use with gradient corrected functionals. Since in general there is no corresponding closed-form expression for K_σ^{GGA} , this involves making the approximation that we may obtain the one-particle density matrix for a GGA by evaluating the LSDA matrix with the modified momentum

$$k_\sigma^{\text{GGA}} = (9\pi/K_\sigma^{\text{GGA}})^{\frac{1}{2}} \rho_\sigma^{\frac{1}{3}}(\mathbf{r}) \quad (3.9)$$

with K_σ^{GGA} giving the energy associated with a GGA exchange–correlation functional through an equation analogous to eq. (3.7). It has been demonstrated that in the case that the PBE exchange GGA is used, an expression for K_σ^{GGA} may be obtained since the exchange–correlation hole for that functional is known;¹³⁶ this has been developed into an alternative method of approximating K_σ^{GGA} for other functionals.¹³⁷

Whilst treating the short-range exchange via a GGA was found to give improved results over the LDA alternative, and the description of properties^{116,138,139} which required a large amount of exact exchange was improved over standard hybrid functionals, the resultant ‘long-range corrected’ (LC) functionals offer little improvement over conventional GGA results for properties such as atomisation energies. This may partially be understood from a consideration of the amount of exact exchange in the functional. The partitioning of eq. (3.3) gives for small r_{12} essentially no contribution from exact exchange; the functional behaves similarly to a conventional GGA. For large r_{12} , it behaves entirely as exact exchange. Properties like atomisation energies depend strongly on the short- to mid-range behaviour, and so in this formalism there is on average a smaller exact exchange contribution to the exchange–correlation energy than from a conventional hybrid. Yanai¹⁴⁰ *et al.* introduced the CAM-B3LYP functional to remedy this. The Coulomb-attenuating method (CAM) redefines the partitioning of the $1/r_{12}$ operator in order that it behave as a hybrid functional for small r_{12} , with increasing amounts of exact exchange as r_{12} increases;

$$\frac{1}{r_{12}} \equiv \frac{\alpha + \beta \operatorname{erf}(\mu r_{12})}{r_{12}} + \frac{1 - [\alpha + \beta \operatorname{erf}(\mu r_{12})]}{r_{12}}. \quad (3.10)$$

Additional flexibility is introduced through the unitless parameters α and β , which allow both the size of the short-range exact exchange contribution

(governed by α) and the asymptotic contribution (governed by $\alpha + \beta$) to vary. (Functionals of this form are perhaps more accurately described as exchange-attenuated functionals, as the $1/r_{12}$ operator is only partitioned in the exchange contribution to the total energy. For brevity we shall usually refer to these functionals as ‘attenuated functionals’.) The exact long-range behaviour may be obtained by enforcing

$$\alpha + \beta = 1. \quad (3.11)$$

As before, μ controls the rate of attenuation.

Short-range (SR) exchange is governed primarily by the second term of eq. (3.10); the approach of Hirao and co-workers is used to obtain K_σ^{GGA} . GGA exchange for CAM functionals is therefore evaluated with

$$E_x^{\text{SR}} = -\frac{1}{2} \sum_\sigma \int d\mathbf{r} \rho_\sigma^{\frac{4}{3}}(\mathbf{r}) K_\sigma^{\text{GGA}} \times \left[(1 - \alpha) - \beta \left(\frac{8}{3} a_\sigma \left[\sqrt{\pi} \operatorname{erf}\left(\frac{1}{2a_\sigma}\right) + 2a_\sigma(b_\sigma - c_\sigma) \right] \right) \right] \quad (3.12)$$

in which a_σ , b_σ and c_σ are defined as

$$a_\sigma = \frac{\mu}{2k_\sigma^{\text{GGA}}}, \quad (3.13)$$

$$b_\sigma = \exp\left(-\frac{1}{4a_\sigma^2}\right), \quad (3.14)$$

$$c_\sigma = 2a_\sigma^2 b_\sigma + \frac{1}{2}. \quad (3.15)$$

The CAM-B3LYP form defines K_σ^{GGA} in terms of K_σ^{LSDA} and the Becke 1988 gradient correction:

$$K_\sigma^{\text{GGA}} = K_\sigma^{\text{LSDA}} + \frac{2Bx_\sigma^2}{1 + 6Bx_\sigma \operatorname{arcsinh}(x_\sigma)} \quad (3.16)$$

in which $B = 0.0042$.

Long-range (LR) exchange is governed primarily by the first term of eq. (3.10), and is evaluated using a modified version of eq. (3.5);

$$E_x^{\text{LR}} = \alpha E_x^0 - \frac{\beta}{2} \sum_\sigma \sum_{i,j} \iint d\mathbf{r}_1 d\mathbf{r}_2 \varphi_{i\sigma}(\mathbf{r}_1) \varphi_{j\sigma}(\mathbf{r}_1) \frac{\operatorname{erf}(\mu r_{12})}{r_{12}} \varphi_{j\sigma}(\mathbf{r}_2) \varphi_{i\sigma}(\mathbf{r}_2). \quad (3.17)$$

Therefore the total exchange energy is given as the sum of eqs. (3.12) and (3.17). In the case of the CAM-B3LYP functional the correlation energy is given by eq. (3.2).

Yanai *et al.* determined values for the attenuation parameters α and β by fitting to (essentially) the G2-1 set of atomisation energies. The value of μ was held fixed following the previous work of Hirao and co-workers,^{134,135} at $\mu a_0 = 0.33$. If the exact constraint of eq. (3.11) is enforced, it is possible to improve on the error obtained with an LC functional on the G2-1¹⁰⁰ set of atomisation energies by a factor of two and a half; however the resultant error is still notably larger than that obtained for B3LYP. Relaxing this constraint, Yanai *et al.* found that the smallest error for the G2-1 set was obtained with values of $\alpha = 0.19$ and $\beta = 0.46$. These values of α , β and μ define the CAM-B3LYP functional.

Insight into the attenuation form of CAM-B3LYP can be garnered from a consideration of the limiting cases—how the functional behaves when the attenuation parameters are extremised. If $\alpha = 0$ and β or $\mu a_0 = 0$, the functional reduces to a standard GGA, where eq. (3.12) makes the sole contribution; if we neglect correlation it would reduce to Dirac (Slater) plus Becke 1988 exchange. Making α non-zero whilst β or $\mu a_0 = 0$ would then give a standard hybrid exchange functional. Despite using correlation of the form of eq. (3.2), the functional would not reduce to B3LYP in this case as the Becke 1988 gradient correction has a different prefactor in the two functionals. For non-zero β and μ attenuation is introduced. If $\beta = 1$ and $\alpha = 0$, a LC-type functional similar to those of Hirao and co-workers is obtained. The final limiting case is $\mu a_0 \rightarrow \infty$, in which case the exchange is entirely treated through eq. (3.5); eq. (3.17) becomes equivalent to eq. (3.5) and eq. (3.12) becomes trivially zero. We will consider the influence of the attenuation parameters on properties in a later section.

Recently there have been a number of developments of associated attenuated functionals. Gerber and Ángyán¹⁴¹ proposed a method based on LSDA exchange; Scuseria and co-workers¹³¹ treat short-range exchange via the PBE and TPSS exchange–correlation functionals; Chai and Head-Gordon^{142,143} recently introduced an attenuated functional based on the B97 gradient expansion. For other related approaches see refs. 144 and 145.

Table 3.3: Mean error d and mean absolute error $|d|$, relative to reference values, comparing B3LYP and CAM-B3LYP for the assessments of table 3.1. Open-shell calculations use the unrestricted formalism.

	B3LYP	CAM-B3LYP
1. Atomisation energies		
$d/\text{kcal mol}^{-1}$	-2.9	1.5
$ d /\text{kcal mol}^{-1}$	3.6	3.3
2. Ionisation potentials		
d/eV	0.00	0.11
$ d /\text{eV}$	0.17	0.17
3. Classical barriers		
$d/\text{kcal mol}^{-1}$	-3.7	-2.6
$ d /\text{kcal mol}^{-1}$	3.8	2.7
4, 5, 6. Bond lengths		
$d/\text{Å}$	0.009	-0.009
$ d /\text{Å}$	0.015	0.016
7. Vib. wavenumbers		
d/cm^{-1}	6	34
$ d /\text{cm}^{-1}$	22	37
8. Polarisabilities		
$d/\text{a.u.}$	0.36	0.15
$ d /\text{a.u.}$	0.45	0.30
9. Excitation energies		
d/eV	-0.82	-0.40
$ d /\text{eV}$	0.84	0.43

Performance of CAM-B3LYP

Taking the CAM-B3LYP functional with the parameters recommended by Yanai *et al.*, we now determine its performance for the assessments of table 3.1.^{99,146} For the open-shell species the unrestricted formalism is used. Errors are given in table 3.3, compared to B3LYP unrestricted values.

For the atomisation energies of assessment 1, CAM-B3LYP displays a similar performance to B3LYP; however it negates B3LYP's tendency to underestimate. Ionisation potentials are also similarly described between the two functionals, but in this case CAM-B3LYP tends to overestimate. Significantly improved are the classical reaction barriers of assessment 3; there is still a

tendency to underestimate, but the error is reduced by one kcal mol⁻¹. It is worth noting that if the restricted open-shell formalism is used, not only does the CAM-B3LYP error increase, but it becomes less accurate than B3LYP, for atomisation energies and ionisation potentials. Interestingly the performance with respect to classical reaction barriers improves in the restricted formalism.

Bond lengths in assessments 4, 5 and 6 are also comparable between B3LYP and CAM-B3LYP; bond lengths tend to be shorter with the latter functional, which is associated with the slight overestimation of vibrational wavenumbers observed for assessment 7. Of particular note is the improvement for polarisabilities and excitation energies in assessments 8 and 9; the reduced errors in excitation energies can be traced primarily to the description of Rydberg states, which are considerably more accurate than with B3LYP. This is due to the improved asymptotic behaviour of the functional. This issue will be discussed in greater detail in chapter 4.

3.3 PARAMETER DEPENDENCE OF ATTENUATED FUNCTIONALS

The parameters chosen by Yanai *et al.* for the attenuation of eq. (3.10) were not fully optimised and are inconsistent with the exact condition of eq. (3.11); however, on the assessment of table 3.1 it performs well. We now go on to perform¹⁴⁶ a systematic investigation of all of the attenuation parameters (Yanai *et al.* did not consider varying μ) with an emphasis on the effect on functional performance of imposing the exact long-range behaviour through eq. (3.11).

In order to gain insight into how the performance of attenuated functionals depends on the attenuation parameters, we apply a systematic approach. Initially we impose the condition of eq. (3.11) by setting $\beta = 1 - \alpha$, allowing α and μ to vary over a range of values. As is commonplace in functional development, we assess the quality of the functional for each set of parameters by considering the error in atomisation energies. This is achieved through using a representative subset of assessment 1 from table 3.1, with the computational details as for the larger set. Our subset consists of 14 molecules: C₂H₂, C₂H₄, CH₃NH₂, CH₃OH, CH₄, CO, CO₂, H₂O, H₂O₂, LiH, N₂, N₂O, NH₃, and NO₂.

To simplify the form of the functional, we remove the VWN correlation

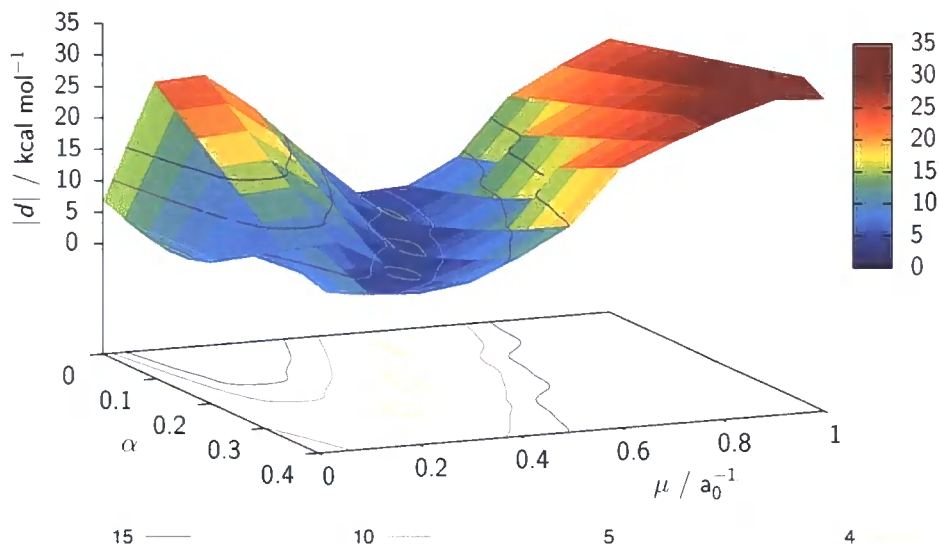


Figure 3.1: The mean absolute error $|d|$ for the subset atomisation energy assessment, as a function of the attenuation parameters α and μ , with $\beta = 1 - \alpha$.

term; correlation is therefore described by

$$E_c = E_c^{\text{LYP}}. \quad (3.18)$$

As noted by Yanai *et al.*, including a fraction of VWN correlation actually reduces atomisation energy quality, although we find that it does improve performance for total electronic energies. Treating correlation through eq. (3.18) instead of eq. (3.2) was found to have minimal influence on the accuracy of the functional in general. We do not consider treating the correlation through other correlation functionals, nor do we consider changing the form of the GGA exchange functional. It is worth noting that the optimal values of α and μ obtained from our investigation are consistent with the later work of Scuseria and co-workers^{131,147} with the ω -PBE and ω -TPSS functionals, and the work of Chai and Head-Gordon.^{142,143}

Figure 3.1 shows the variation of α and μ for $0 \leq \alpha \leq 0.4$ in intervals of 0.04, and $0 \leq \mu a_0 \leq 1$ in intervals of 0.1, for the case of $\beta = 1 - \alpha$. The figure highlights a strong dependence on μ . Along the $\alpha = 0$ path, the error rises steeply to $\mu a_0 = 0.1$, and then falls again as μ is increased further. The minimum for the $\alpha = 0$ path occurs near $\mu a_0 = 0.5$, consistent with the LSDA

results of Gerber and Ángyán.¹⁴¹ For this set of attenuation parameters the error for the atomisation energy subset is 4.8 kcal mol⁻¹, consistent with a larger error from functionals using the partitioning of eq. (3.3). As $\mu a_0 > 0.6$ the error increases monotonically as the functional becomes more Hartree–Fock like. For non-zero α , the error decreases over the $\alpha = 0$ case. There are three distinct minima, the lowest two of which have the same error (of 3.4 kcal mol⁻¹) on this subset. These correspond to $\alpha = 0.2$, $\beta = 0.8$ and $\mu a_0 = 0.4$, and $\alpha = 0.28$, $\beta = 0.72$ and $\mu a_0 = 0.3$; as figure 3.1 demonstrates, the optimal value of μ decreases as α increases. The corresponding error from the CAM-B3LYP functional for this subset is 2.2 kcal mol⁻¹.

We consider the performance of the first of these optimal functionals, corresponding to $\alpha = 0.2$, $\beta = 0.8$ and $\mu a_0 = 0.4$, for the extensive assessment of table 3.1. For convenience this parameterisation will be referred to as CAM(0.2, 0.8, 0.4). The overall performance of this functional is disappointing, as illustrated in table 3.4. Atomisation energies, bond lengths and vibrational wavenumbers are significantly less accurate than those obtained from the CAM-B3LYP and B3LYP functionals. Ionisation potentials and polarisabilities also degrade slightly. Classical reaction barriers notably improve however, consistent with the increased amount of exact exchange present in this functional.¹¹³ The excited states also improve significantly, due to the formally correct long-range behaviour observed with this functional. The optimal attenuation parameters are unaffected by the choice of treatment of the open-shell systems; the dependence when the restricted open-shell formalism is used essentially changes just the overall error of each point, but does not affect the shape of the surface. We do not present further assessment of the other low energy minima in figure 3.1, as the atomisation energy error for the full set is notably larger than for the case of CAM(0.2, 0.8, 0.4).

Consider the form of attenuation in the CAM(0.2, 0.8, 0.4) and CAM-B3LYP functionals, which are plotted in figure 3.2, together with the curve for B3LYP. The behaviour is different between the two attenuated functionals for all r_{12} . That CAM-B3LYP is generally more accurate may be closely related to it violating eq. (3.11); the form of attenuation in eq. (3.10) may be too restrictive to allow this condition to be satisfied without causing degradation in the description of some properties. With this in mind we now consider

Table 3.4: Mean error d and mean absolute error $|d|$, relative to reference values, comparing three optimised attenuated forms with CAM-B3LYP, for the assessments of table 3.1. Open-shell calculations use the unrestricted formalism.

	CAM- B3LYP	$\alpha = 0.2$ $\beta = 0.8$ $\mu a_0 = 0.4$	$\alpha = 0.16$ $\beta = 0.49$ $\mu a_0 = 0.4$	$\alpha = 0.16$ $\beta = 0.39$ $\mu a_0 = 0.4$
1. Atomisation energies				
$d/\text{kcal mol}^{-1}$	1.5	5.5	1.5	-0.3
$ d /\text{kcal mol}^{-1}$	3.3	7.5	3.2	2.4
2. Ionisation potentials				
d/eV	0.11	0.10	0.04	0.02
$ d /\text{eV}$	0.17	0.19	0.17	0.18
3. Classical barriers				
$d/\text{kcal mol}^{-1}$	-2.6	-1.3	-2.6	-2.8
$ d /\text{kcal mol}^{-1}$	2.7	1.7	2.7	2.9
4, 5, 6. Bond lengths				
$d/\text{\AA}$	-0.009	-0.027	-0.012	-0.007
$ d /\text{\AA}$	0.016	0.027	0.017	0.015
7. Vib. wavenumbers				
d/cm^{-1}	34	66	39	31
$ d /\text{cm}^{-1}$	37	66	41	34
8. Polarisabilities				
$d/\text{a.u.}$	0.15	-0.18	0.12	0.20
$ d /\text{a.u.}$	0.30	0.31	0.28	0.33
9. Excitation energies				
d/eV	-0.40	0.07	-0.34	-0.45
$ d /\text{eV}$	0.43	0.24	0.37	0.48

the parameter-dependence on α and μ as before, when the constraint of eq. (3.11) is relaxed. Given the performance of CAM-B3LYP, we initially set $\beta = 0.65 - \alpha$.

The resulting parameter surface is plotted in figure 3.3. The features of the surface are similar to those displayed for the case where $\beta = 1 - \alpha$ as plotted in figure 3.1, although the error of an individual point is in general lower. A non-zero α and μ are both beneficial in lowering the error. The minimum error (of $1.8 \text{ kcal mol}^{-1}$) obtained from $\alpha = 0.16$, $\beta = 0.49$ and $\mu a_0 = 0.4$ is *smaller* than the error from CAM-B3LYP, and half of the error

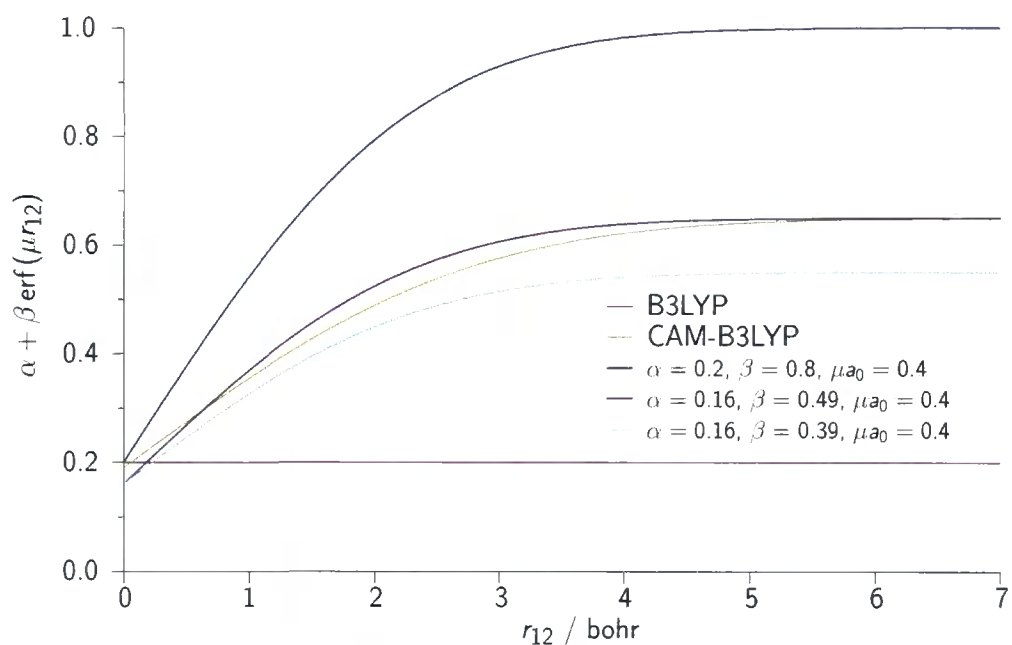


Figure 3.2: The shape of the attenuation curves for the exact exchange contribution to the exchange–correlation energy with different functionals.

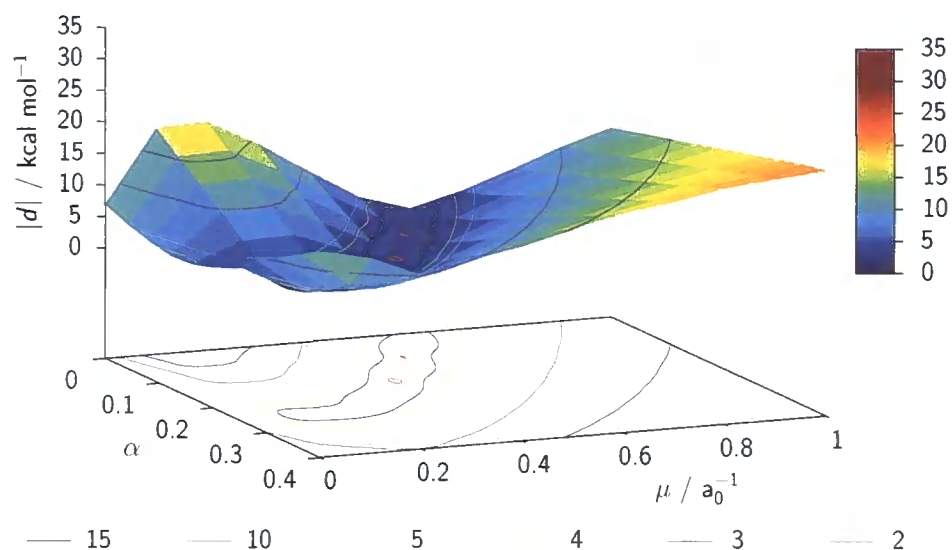


Figure 3.3: The mean absolute error $|d|$ for the subset atomisation energy assessment, as a function of the attenuation parameters α and μ , with $\beta = 0.65 - \alpha$.

associated with the CAM(0.2, 0.8, 0.4) functional. Note that if the restricted open-shell formalism is used, the optimal values of α and β change slightly (to $\alpha = 0.2$ and $\beta = 0.45$), although the overall error changes insignificantly between the two optimal functionals. The shape of the attenuation for the CAM(0.16, 0.49, 0.4) functional is plotted in figure 3.2; it is similar to that of the standard CAM-B3LYP functional.

When we consider the performance of this functional for the assessments of table 3.1, we find that most properties are similarly described to CAM-B3LYP. The results are presented in table 3.4, which shows that the performance is either similar to or an improvement over the CAM(0.2, 0.8, 0.4) functional, except for the excitation energies and reaction barriers. These observations highlight that the long-range behaviour of the exchange treatment is less important for most properties than the short- and mid-range behaviour. This is consistent with the recent observation of Chai and Head-Gordon,¹⁴⁸ and the work of Scuseria highlighting partitioning the $1/r_{12}$ operator into short-, mid- and long-range components.¹⁴⁹ In these other works the mid-range behaviour is shown to have the most significant impact on a property, except for cases such as Rydberg excitations.

At this stage we consider optimising the attenuation parameters to obtain as low an error as possible for the representative subset of atomisation energies. By removing all constraints, and varying the parameters over an appropriate range, we find that the lowest error (1.6 kcal mol⁻¹) is given by $\alpha = 0.16$, $\beta = 0.39$ and $\mu a_0 = 0.4$; the optimal value of μ remains unchanged. Again the use of the restricted open-shell formalism results in a (slightly) different optimal set of attenuation parameters. The attenuation form of the CAM(0.16, 0.39, 0.4) functional is shown in figure 3.2; the mid-range behaviour is again very similar to that obtained from the CAM-B3LYP and CAM(0.2, 0.49, 0.4) functionals. This functional is also assessed for the properties in table 3.1, the results of which are given in table 3.4. Atomisation energies are significantly improved over the other functionals considered in this study; reaction barriers and ionisation potentials are similar to CAM-B3LYP. This functional arguably has the best overall performance for the assessments of table 3.1 of those presented in this chapter, although the error for excitation energies is slightly larger than with CAM-B3LYP.

3.4 EXCITED STATES

We have succeeded in describing short-range properties accurately, albeit not necessarily from the same parameterisation, notably improving on conventional hybrid functionals. The real prospects of this approach lie in the potentially improved description of long-range dependent properties. Attenuated functionals offer the possibility of exact (or in the case of CAM-B3LYP, near-exact) long-range behaviour.

We have illustrated in table 3.4 that such significant improvements are observed in the description of excitation energies. Therefore we consider excitation energies in more detail. Particular attention is paid to the performance of the CAM(0.2, 0.8, 0.4) functional since it satisfies the condition of eq. (3.11) for the exact long-range behaviour, and also because of the high quality results it gave for assessment 9 of table 3.1. Also of interest is the performance of the CAM-B3LYP functional as our exemplar $\alpha + \beta = 0.65$ functional, and that of B3LYP, used to illustrate the performance of a conventional hybrid.

We begin by considering the excitation energies of assessment 9 in greater detail. Table 3.5 presents a more in depth error analysis, by grouping each excitation by type and molecule. The performance for valence excitations is essentially unchanged between the three functionals we consider; the description is marginally less accurate with CAM(0.2, 0.8, 0.4). The severe systematic underestimation of the Rydberg excitations with B3LYP is reduced with CAM-B3LYP, which is responsible for its improved overall performance. Imposing the exact long-range behaviour with CAM(0.2, 0.8, 0.4) affords a further significant increase in accuracy. It would however be possible to repair the quality of the B3LYP and CAM-B3LYP Rydberg excitations by application of a correction to the asymptotic region of the exchange–correlation potential (see for instance ref. 150). There is little variation in the size of error across the four molecules considered; the errors decrease as the amount of long-range exact exchange in the functional increases.

Next consider charge-transfer excitations, which are of considerable interest. It is with this class of excitation that attenuated functionals have the most to offer; the deficiencies of standard hybrid functionals that give rise to severely underestimated charge-transfer states cannot be repaired through

Table 3.5: Vertical excitation energy errors for CO, N₂, H₂CO, and C₂H₄, and combined errors for valence and Rydberg excitations, in eV.

	B3LYP	CAM- B3LYP	$\alpha = 0.2$ $\beta = 0.8$ $\mu a_0 = 0.4$
CO excitations			
d/eV	-0.77	-0.37	0.08
$ d /eV$	0.77	0.37	0.16
N₂ excitations			
d/eV	-0.86	-0.53	-0.13
$ d /eV$	0.86	0.54	0.30
H₂CO excitations			
d/eV	-0.66	-0.24	0.28
$ d /eV$	0.76	0.37	0.28
C₂H₄ excitations			
d/eV	-0.94	-0.40	0.12
$ d /eV$	0.94	0.40	0.22
Combined valence			
d/eV	-0.23	-0.20	-0.15
$ d /eV$	0.29	0.28	0.33
Combined rydberg			
d/eV	-1.14	-0.51	0.18
$ d /eV$	1.14	0.51	0.19
Combined total			
d/eV	-0.82	-0.40	0.07
$ d /eV$	0.84	0.43	0.24

simple procedures such as asymptotic corrections. To further assess the performance of attenuated functionals, we therefore consider two molecules which exhibit charge-transfer excitations. The first molecule is a model dipeptide (illustrated in figure 4.1) in which the severe failure of conventional functionals has previously been highlighted.¹⁵¹ Table 3.6 lists six vertical excitation energies computed with B3LYP, CAM-B3LYP and CAM(0.2, 0.8, 0.4), comparing with CASPT2 reference values from ref. 151. Following the notation of that reference, CT denotes charge-transfer; W and NV denote more localised excitations. In order to compare with the CASPT2 reference values, we use the BP86^{74,152} geometry obtained with the 6-31G(d) basis set. For the DFT excitation energy calculations we use the TZ2P^{153,154} basis set.

Table 3.6: Vertical excitation energies of the model dipeptide, in eV.

			B3LYP	CAM- B3LYP	$\alpha = 0.2$ $\beta = 0.8$ $\mu a_0 = 0.4$	CASPT2 ^a
¹ A''	$n_1 \rightarrow \pi_2^*$	CT	6.28	7.88	9.72	7.92
¹ A'	$\pi_1 \rightarrow \pi_2^*$	CT	6.07	6.94	7.56	6.92
¹ A'	$\pi_1 \rightarrow \pi_1^*$	NV	7.06	7.32	7.61	6.32
¹ A'	$\pi_2 \rightarrow \pi_2^*$	NV	7.11	7.53	8.36	6.29
¹ A''	$n_1 \rightarrow \pi_1^*$	W	5.54	5.65	5.81	5.61
¹ A''	$n_2 \rightarrow \pi_2^*$	W	5.74	5.88	6.04	5.82

^a ref. 151

One of the key observations of Yanai *et al.* was CAM-B3LYP's improved performance in the description of excitation energies for this model dipeptide. Table 3.6 shows the severe underestimation of the two CT states when B3LYP is employed. These excitations increase significantly when CAM-B3LYP is used, resulting in improved agreement with the CASPT2 reference values. The CAM(0.2, 0.8, 0.4) functional further increases the excitation energies of these CT states, giving rise to a large overestimation. For the W states, which most closely resemble the valence states of the molecules in assessment 9, there is a much smaller variation between the functionals. CAM-B3LYP is notably most accurate. Insight into the contrasting behaviour of the functionals for the CT and W type excitations is presented in chapter 4. The NV states however are poorly described by all three functionals; B3LYP overestimates the excitation energies for these states, and the attenuated functionals only amplify this overestimation.

Next consider 4-(*N,N*-dimethylamino)benzonitrile (DMABN), illustrated in figure 4.1, which has been extensively studied due to its dual fluorescence. Following the study of Serrano-Andrés⁴⁶ *et al.*, we use CASSCF structural parameters to define the geometry, in the planar configuration, with the amino wagging angle adjusted to 0°. For the DFT calculations we use the same ANO basis set as in ref. 46; we have confirmed that the calculated excitation energies are converged with respect to basis set size, and that using the planar geometry has minimal influence on the excitations under consideration.¹⁵⁵ For instance using the more extensive 6-311+G(2d,p) basis set as employed by Jamorski¹⁵⁶

Table 3.7: Vertical excitation energies of DMABN, in eV.

	B3LYP	CAM- B3LYP	$\alpha = 0.2$ $\beta = 0.8$ $\mu a_0 = 0.4$	CAS- PT2 ^a	STEOM- CCSD ^b	DFT/ CIS ^c	Expt. ^a
¹ B LE	4.37	4.66	4.93	4.05	4.15	4.09	4.25
¹ A CT	4.69	4.96	5.17	4.41	4.73	4.55	4.56

^a ref. 46; ^b ref. 157; ^c ref. 158

et al. changes the excitation energies by less than one tenth of an eV; replacing the geometry with an optimised non-planar B3LYP structure results in similar changes.

Table 3.7 lists vertical excitation energies computed with the B3LYP, CAM-B3LYP and CAM(0.2, 0.8, 0.4) functionals, comparing with the CASPT2 values of Serrano-Andrés⁴⁶ *et al.*, the similarity transformed equations of motion CCSD (STEOM-CCSD) values of Parusel¹⁵⁷ *et al.*, and the DFT/CIS values of Bulliard¹⁵⁸ *et al.* Also listed are experimental excitation energies from gas phase electron energy loss spectroscopy.¹⁵⁸ The experimental wagging angle is in the range of 12–15°;^{159,160} we have confirmed the insensitivity of the excitation energies considered to changes in this angle. Two states are of interest; a locally excited (LE) state corresponding to a transition dominated by HO→LU+1 (with HO referring to the highest occupied orbital and LU to the lowest unoccupied orbital), and a charge-transfer state (CT) corresponding to a HO→LU dominated transition.

For the LE state the B3LYP excitation energy at 4.37 eV lies above the range of reference values of 4.05–4.25 eV; B3LYP overestimates this excitation energy. In the case of the CT state the B3LYP value of 4.69 eV lies at the top end of the range of 4.41–4.73 eV. Both excitation energies increase in moving to CAM-B3LYP and then to CAM(0.2, 0.8, 0.4). A larger change is observed going from B3LYP to CAM-B3LYP for the locally excited state than was observed in the other molecules considered, resulting in the noticeable overestimation. The excitation energy of the CT state changes similarly. The observation of the overestimated CT state is contrary to the case in the dipeptide. We give insight into this observation in chapter 4.

A consideration of the μ -dependence of excitation energies computed with

attenuated functionals provides some insight into the behaviour of the functionals in describing excitation energies. For the functionals with $\alpha = 0.2$ and $\beta = 0.8$, we have determined excitation energies for a range of values of μ , and find that for each of the molecules in assessment 9, $\mu a_0 = 0.4$ is optimal. However, for the dipeptide a value of $\mu a_0 = 0.2$ is more appropriate (giving errors comparable to those from CAM-B3LYP), and for DMABN a value of $\mu a_0 = 0$ is best. The contrasting dependence on μ illustrates the complexities of finding a universally applicable functional and highlights the need for a more flexible attenuation form. A consideration of the μ -dependence of excitation energies also allows us to consider whether or not there is an advantage to partitioning the $1/r_{12}$ operator by eq. (3.10) as opposed to eq. (3.3). Yanai *et al.* introduced the α and β parameters to improve performance for short-range dependent properties such as atomisation energies. Examining excitations from the $\alpha = 0$ and $\beta = 1$ functionals, we find that as was observed above, a much smaller value of μ is required for an accurate description of the dipeptide and DMABN. In contrast however we find that the optimal value varies more between the molecules of assessment 9. A non-zero α therefore appears to be beneficial in this case.

In our investigation of the parameter dependence of eq. (3.10), which had not been considered previously for that attenuation form, we demonstrated the sensitivity of the atomisation energies to the rate of attenuation (controlled through μ) and the importance of a non-zero α . Perhaps surprisingly, CAM(0.16, 0.39, 0.4) was found to yield significantly higher quality atomisation energies than standard hybrid functionals. Imposing the exact condition of eq. (3.11) is detrimental to atomisation energies and many other properties, due to the notably different shape of the attenuation curve compared to CAM-B3LYP and other successful parameterisations. The success of the CAM-B3LYP functional is therefore attributed to the violation of eq. (3.11). The imposition of the exact condition is beneficial for long-range dependent properties such as Rydberg excitation energies, but notably no set of attenuation parameters is able to provide a simultaneously optimal description of all

of the classes of excitation considered. This suggests that the use of alternative attenuation schemes and partitionings is required to achieve a universally applicable functional. See refs. 161 and 162 for examples of where modifications have been employed. Avenues for developing different partitionings of the $1/r_{12}$ operator are described in ref. 163.

The results of this chapter highlight several deficiencies in the description of exchange with standard hybrid functionals. Through the theory of attenuated exchange–correlation functionals, we are able to at least partially correct for these deficiencies. In later chapters we go on to apply attenuated functionals to other properties that conventional hybrids struggle with. In chapter 4 a much broader range of excitation energies are considered in a systematic study, to determine the performance of CAM-B3LYP compared to conventional functionals. The proposition of an excitation energy error diagnostic test provides further insight into the seemingly conflicting results of the dipeptide and DMABN charge-transfer states. We explain the severe underestimation by standard hybrid functionals for the former molecule, and overestimation for the latter, in terms of the spatial overlap between the orbitals involved in the excitations. In chapter 5, CAM-B3LYP is applied to the bond length alternation and band gap of polyacetylene and polyynes oligomers, as example properties which are poorly described with conventional hybrids. We also consider the first application of attenuated functionals to the evaluation of magnetic properties with the optimised effective potential method, including a discussion of its performance for transition metal nuclear magnetic resonance response parameters.

Electronic excitations

The application of DFT to the excited states of molecules is considered, through linear response time-dependent (TD) DFT. The theory of TDDFT is introduced, and the successes and failures of standard functionals are elaborated. Attenuated functionals are applied to a wide variety of vertical excitation energies, and the results compared to those from standard functionals. The low-overlap failure of local functionals is explained, and a diagnostic quantity that is able to determine when standard functionals will fail due to lack of overlap is proposed.

Hohenberg and Kohn established for the time-independent Schrödinger equation the existence of a mapping between the ground state electron density and the external potential. The Runge–Gross¹⁶⁴ theorem establishes the equivalent mapping for the time-dependent case, where the external potential has a time-dependent contribution from a sum of time-dependent one-particle potentials. For many-body systems evolving from a fixed initial state, the time-dependent electron density determines the time-dependent external potential up to a spatially constant, time-dependent function, and consequently the time-dependent wavefunction up to a time-dependent phase factor. See refs. 165–167 for further details.

A variational principle may be established, analogous to the second theorem of Hohenberg and Kohn, through a consideration of the action integral and using the Runge–Gross theorem; it is not possible to determine a variational principle based on the total energy since in a time-dependent system it

is not a conserved quantity. A time-dependent Kohn–Sham formulation may therefore be obtained.

Whilst in principle the time-dependent Kohn–Sham formulation uses a time-dependent exchange–correlation action functional, as a first approximation we assume the adiabatic approximation, where it is taken that the density varies slowly with time; the exchange–correlation kernel may therefore be approximated via the functional derivative of the time-independent exchange–correlation potential v_{xc} evaluated with the time-dependent density. This allows exchange–correlation functionals derived for the ground state to be used in the computation of properties of excited states. For further details of this, see for instance refs. 166, 168 and 169. All of the calculations in this thesis use the adiabatic approximation.

4.1 LINEAR RESPONSE FORMULATION OF TDDFT

The most widely used method of calculating excited state properties is through the linear response formulation of time-dependent (TD) DFT, in the adiabatic approximation. In this section we shall demonstrate how excitation energies are obtained from the time-dependent linear response of the ground state electron density under the application of a time-dependent field. For a full consideration of the calculation of such quantities, see refs. 166 and 169–171.

Begin by reformulating the Kohn–Sham equation for the time-independent case. With some manipulation, it can be demonstrated that the equation

$$\left(-\frac{1}{2}\nabla^2 + v_{\text{eff}}(\mathbf{r})\right)\varphi_i(\mathbf{r}) = \varepsilon_i\varphi_i(\mathbf{r}) \quad (4.1)$$

may be written in terms of the Kohn–Sham Hamiltonian matrix \mathbf{F} and the density matrix \mathbf{P} , in the molecular orbital basis, as

$$\mathbf{FP} - \mathbf{PF} = 0, \quad (4.2)$$

for an idempotent density matrix \mathbf{P} .

We introduce the following notation: The elements (for the unperturbed ground state) of the time-independent Hamiltonian are denoted by $F_{pq}^{(0)}$ and

those of the associated density matrix by $P_{pq}^{(0)}$. These elements are given by

$$F_{pq}^{(0)} = \int d\mathbf{r}_1 \varphi_p^*(\mathbf{r}_1) \left(-\frac{1}{2} \nabla^2 - \sum_I \frac{Z_I}{r_{1I}} + \int d\mathbf{r}_2 \frac{\rho(\mathbf{r}_2)}{r_{12}} + \frac{\delta E_{xc}}{\delta \rho(\mathbf{r}_1)} \right) \varphi_q(\mathbf{r}_1) \quad (4.3)$$

$$P_{pq}^{(0)} = c_p c_q^* \quad (4.4)$$

where we no longer assume real-valued orbitals, and the labels p and q refer to any molecular orbital. Equation (4.2) is equivalent to the statement that the eigenfunctions of \mathbf{F} are also eigenfunctions of \mathbf{P} . If we work in the orthonormalised basis of unperturbed one-electron orbitals for the ground state, the matrices $F_{pq}^{(0)}$ and $P_{pq}^{(0)}$ are given by

$$F_{pq}^{(0)} = \delta_{pq} \varepsilon_p \quad (4.5)$$

$$P_{ij}^{(0)} = \delta_{ij} \quad (4.6)$$

$$P_{ia}^{(0)} = P_{ai}^{(0)} = P_{ab}^{(0)} = 0 \quad (4.7)$$

(with the i and j corresponding to occupied orbitals and the a and b corresponding to virtual orbitals) from which the commutation of the matrices immediately follows.

Equation (4.2) may be generalised to the time-dependent case (where we switch to component notation);

$$\sum_q (F_{pq} P_{qr} - P_{pq} F_{qr}) = i \frac{\partial}{\partial t} P_{pr} \quad (4.8)$$

in which the density matrix elements P_{pr} are related to the time-dependent electron density through

$$\rho(\mathbf{r}, t) = \sum_{p,q} c_p(t) c_q(t) \varphi_p(\mathbf{r}) \varphi_q(\mathbf{r}) \quad (4.9)$$

$$= \sum_{p,q} P_{pq}(t) \varphi_p(\mathbf{r}) \varphi_q(\mathbf{r}). \quad (4.10)$$

Now apply an oscillatory time-dependent field, and analyse the linear (first-order) response to the perturbation. In this case it is assumed that both the density and Kohn–Sham matrices become the sum of the unperturbed ground state matrix and a first-order time-dependent response;

$$P_{pq} = P_{pq}^{(0)} + P_{pq}^{(1)} \quad (4.11)$$

$$F_{pq} = F_{pq}^{(0)} + F_{pq}^{(1)}. \quad (4.12)$$

Through substitution of eqs. (4.11) and (4.12) into eq. (4.8), the following equation is obtained, by making use of the result of eq. (4.2);

$$\sum_q (F_{pq}^{(0)} P_{qr}^{(1)} - P_{pq}^{(1)} F_{qr}^{(0)} + F_{pq}^{(1)} P_{qr}^{(0)} - P_{pq}^{(0)} F_{qr}^{(1)}) = i \frac{\partial}{\partial t} P_{pr}. \quad (4.13)$$

We now step back to examine the first-order change of the Kohn–Sham Hamiltonian and density matrices to an applied perturbation. Two terms arise from the Kohn–Sham Hamiltonian matrix for the case that the perturbation is a time-dependent electromagnetic field; the first contribution is due to the time-dependent field itself. It is sufficient to consider a single Fourier transform component of the perturbation,¹⁷² which in matrix component notation is given by

$$g_{pq} = \frac{1}{2} [f_{pq} \exp(-i\omega t) + f_{qp}^* \exp(i\omega t)]. \quad (4.14)$$

The matrix \mathbf{f} is a one-electron operator which describes the applied perturbation. The second contribution to the Kohn–Sham Hamiltonian’s first-order response¹⁶⁸ is $\Delta F_{pq}^{(0)}$, which describes the two-electron operator response through its explicit dependence on the density matrix, and is given by

$$\Delta F_{pq}^{(0)} = \sum_{s,t} \frac{\partial F_{pq}^{(0)}}{\partial P_{st}} P_{st}^{(1)}. \quad (4.15)$$

It follows that the first-order change in the Kohn–Sham Hamiltonian is

$$F_{pq}^{(1)} = g_{pq} + \Delta F_{pq}^{(0)}. \quad (4.16)$$

Now consider the density matrix; to first-order the time-dependent change induced by the field perturbation is

$$P_{pq}^{(0)} = \frac{1}{2} [d_{pq} \exp(-i\omega t) + d_{qp}^* \exp(i\omega t)] \quad (4.17)$$

where \mathbf{d} represents the perturbation densities. By substitution of eqs. (4.16) and (4.17) into eq. (4.13), and by collecting terms that are multiplied by $\exp(-i\omega t)$, the following expression is obtained:

$$\sum_q \left[F_{pq}^{(0)} d_{qr} - d_{pq} F_{qr}^{(0)} + (f_{pq} + \sum_{s,t} \frac{\partial F_{pq}^{(0)}}{\partial P_{st}} d_{st}) P_{qr}^{(0)} - P_{pq}^{(0)} (f_{qr} + \sum_{s,t} \frac{\partial F_{qr}^{(0)}}{\partial P_{st}} d_{st}) \right] = \omega d_{pr}. \quad (4.18)$$

The terms multiplied by $\exp(i\omega t)$ yield the complex conjugate of eq. (4.18). From the idempotency condition on the first-order change in the density matrix, it is possible to put restrictions on the form of the matrix \mathbf{d} ; the occupied–occupied and virtual–virtual blocks d_{ii} and d_{aa} are zero-valued. Only the occupied–virtual (and virtual–occupied) blocks can contribute. Making use of the diagonal nature of the unperturbed Kohn–Sham Hamiltonian and density matrices, and of the conditions on \mathbf{d} , the following pair of equations can be obtained:

$$F_{aa}^{(0)} d_{ai} - d_{ai} F_{ii}^{(0)} + \left[f_{ai} + \sum_{b,j} \left(\frac{\partial F_{ai}}{\partial P_{bj}} d_{bj} + \frac{\partial F_{ai}}{\partial P_{jb}} d_{jb} \right) \right] P_{ii}^{(0)} = \omega d_{ai} \quad (4.19)$$

$$F_{ii}^{(0)} d_{ia} - d_{ia} F_{aa}^{(0)} - P_{ii}^{(0)} \left[f_{ia} + \sum_{b,j} \left(\frac{\partial F_{ia}}{\partial P_{bj}} d_{bj} + \frac{\partial F_{ia}}{\partial P_{jb}} d_{jb} \right) \right] = \omega d_{ia}. \quad (4.20)$$

At this point we set $d_{ai} = x_{ai}$ and $d_{ia} = y_{ai}$ to follow the conventional nomenclature. In the zero frequency limit (where $f_{ia} = f_{ai} = 0$ under the assumption that the perturbation is infinitesimal) we may make use of $F_{pp}^{(0)} = \epsilon_p$ and $P_{ii}^{(0)} = 1$ and rewrite eqs. (4.19) and (4.20) as a single non-Hermitian eigenvalue equation

$$\begin{pmatrix} \mathbf{A} & \mathbf{B} \\ \mathbf{B} & \mathbf{A} \end{pmatrix} \begin{pmatrix} \mathbf{X} \\ \mathbf{Y} \end{pmatrix} = \omega \begin{pmatrix} \mathbf{1} & \mathbf{0} \\ \mathbf{0} & -\mathbf{1} \end{pmatrix} \begin{pmatrix} \mathbf{X} \\ \mathbf{Y} \end{pmatrix}. \quad (4.21)$$

The elements of the matrices \mathbf{A} and \mathbf{B} for the case of a local density functional are given by

$$A_{ia,jb} = \delta_{ij} \delta_{ab} (\epsilon_a - \epsilon_i) + (ia|jb) + (ia|f_{xc}|jb), \quad (4.22)$$

$$B_{ia,jb} = (ia|bj) + (ia|f_{xc}|bj), \quad (4.23)$$

where in the adiabatic approximation the response of the exchange–correlation potential corresponds to the second functional derivative of E_{xc} :

$$(ia|f_{xc}|jb) = \iint d\mathbf{r}_1 d\mathbf{r}_2 \varphi_i(\mathbf{r}_1) \varphi_a(\mathbf{r}_1) \frac{\delta^2 E_{xc}}{\delta \rho(\mathbf{r}_1) \delta \rho(\mathbf{r}_2)} \varphi_j(\mathbf{r}_2) \varphi_b(\mathbf{r}_2). \quad (4.24)$$

Note that in the case of hybrid, or attenuated functionals, an additional term arises, in \mathbf{A} and \mathbf{B} ;

$$A_{ia,jb} = \delta_{ij} \delta_{ab} (\epsilon_a - \epsilon_i) + (ia|jb) + (ia|f_{xc}|jb) + (ia|K|jb), \quad (4.25)$$

$$B_{ia,jb} = (ia|bj) + (ia|f_{xc}|bj) + (ia|K|bj). \quad (4.26)$$

This additional term for the case of an attenuated functional of the form of CAM-B3LYP, is given by

$$(ia|K|jb) = \iint d\mathbf{r}_1 d\mathbf{r}_2 \varphi_i(\mathbf{r}_1) \varphi_a(\mathbf{r}_1) \frac{\alpha + \beta \operatorname{erf}(\mu r_{12})}{r_{12}} \varphi_j(\mathbf{r}_2) \varphi_b(\mathbf{r}_2). \quad (4.27)$$

For alternative derivations of the linear response equations see for instance refs. 150 and 173.

4.2 FAILINGS OF STANDARD FUNCTIONALS

If conventional GGA and hybrid functionals are used for the description of excited states, local excitations are well-described with average errors of the order of a few tenths of an eV (a few percent). Excitations to the more spatially diffuse Rydberg orbitals are significantly underestimated.¹⁰⁸

The failure of GGA functionals in describing excitations to Rydberg orbitals may be traced to the long-range behaviour of the exchange–correlation potential. Perdew¹⁷⁴ *et al.* demonstrated the exact exchange–correlation potential is discontinuous as the number of electrons passes through an integer; the potentials on the electron-deficient and electron-abundant sides are parallel, shifted from one another by a system-dependent amount¹⁷⁵ denoted Δ_{xc} . The potential on the electron-deficient side should vanish asymptotically whereas on the electron-abundant side it should approach a value of Δ_{xc} . Since GGA functionals do not exhibit any discontinuity in v_{xc} , they can at best average over it.¹⁷⁵ It has been demonstrated that in regions of significant electron density (the part of v_{xc} that describes occupied orbitals) GGA functionals do exhibit behaviour consistent with averaging over the discontinuity.¹⁷⁶ However, in the asymptotic regions where the electron density of the ground state is insignificant, the potential incorrectly tends to zero, adversely affecting the description of the virtual orbitals.

For an averaged potential, the potential should tend to $\Delta_{xc}/2$ asymptotically, which is well-represented by the sum of the ionisation potential and the HO orbital energy¹⁷⁶ ($I^0 + \varepsilon_{HO}$).^{174,177,178} The correct averaging behaviour

$$\lim_{r \rightarrow \infty} v_{xc}(\mathbf{r}) = -\frac{1}{r} + I^0 + \varepsilon_{HO} \quad (4.28)$$

may therefore be imposed upon a functional by forcing the v_{xc} of a GGA to satisfy this equation. This approach due to Tozer and Handy¹⁵⁰ is known as the asymptotic correction scheme, and improves both Rydberg excitation energies and other virtual orbital dependent properties such as static polarisabilities. Several variations of this method exist,^{179,180} including extensions to hybrid¹⁸¹ and attenuated¹⁸² functionals.

Charge-transfer failure of standard functionals

Many studies have also highlighted the significant underestimation of low-lying TDDFT excitation energies that are associated with significant charge-transfer (CT).^{151,183–192} Errors can be of the order of several eV, and importantly are not affected by an asymptotic correction. As we highlighted in chapter 3, the excitation energies from the model dipeptide were notably underestimated with B3LYP. For DMABN however, B3LYP only slightly overestimates the lowest CT excitation energy—standard functionals can provide an accurate description in some cases.^{156,193,194} It is therefore *difficult to determine in practice* when a CT excitation energy will be poorly described by TDDFT.

The origin of the CT error in TDDFT has been widely discussed; see for instance refs. 195–197. Of particular relevance to our work is the analysis of Dreuw¹⁹⁵ *et al.*, who considered the intermolecular CT excitation from an occupied orbital on one molecule to a virtual orbital on another molecule. At infinite intermolecular separation the spatial overlap between these two orbitals tends to zero. For local functionals such as GGAs, the elements of matrix **A** [in eq. (4.22)] reduce to orbital energy differences; the first term in that equation gives the orbital energy differences, the second and third terms do not contribute because of the absence of overlap between the orbitals. The same arguments apply to the terms of matrix **B**, consequently this is identically zero. The result is that the excitation of a CT state with no overlap between the donating and accepting orbitals is given simply by the orbital energy difference of the relevant orbitals whenever GGA functionals are employed. Following ref. 196, this failure can be understood from a consideration of the integer discontinuity. The exact vertical excitation energy for an excitation from the HO orbital of the donor D to the LU orbital of the acceptor

A at large internuclear separation R is given by

$$\omega^{\text{exact}} = I^{\text{D}} - A^{\text{A}} - \frac{1}{R} \quad (4.29)$$

where I^{D} is the exact vertical ionisation energy of D and A^{A} is the exact electron affinity of A. The $-1/R$ contribution arises due to the electrostatic interaction of the charged donor and acceptor upon the transfer of an electron. In the case a GGA functional is used, we have already demonstrated this quantity reduces to the orbital energy difference for these two orbitals when $R \rightarrow \infty$:

$$\omega^{\text{TDDFT}} = \varepsilon_{\text{LU}}^{\text{A}} - \varepsilon_{\text{HO}}^{\text{D}}. \quad (4.30)$$

Therefore the difference between the exact and TDDFT values for infinite separation is

$$\omega^{\text{TDDFT}} - \omega^{\text{exact}} = \varepsilon_{\text{LU}}^{\text{A}} - \varepsilon_{\text{HO}}^{\text{D}} - (I^{\text{D}} - A^{\text{A}}). \quad (4.31)$$

Note the relations from ref. 174: $\varepsilon_{\text{HO}}^- = -I^0$ and $\varepsilon_{\text{LU}}^+ = -A^0$. From the observed behaviour that GGA functionals typically average over the integer discontinuity for high-density regions, the equivalent orbital energies from a GGA functional will both be shifted relative to these. In the case of $\varepsilon_{\text{HO}}^{\text{D}}$ the eigenvalue is shifted upwards by approximately half of the discontinuity for the donor, and in the case of $\varepsilon_{\text{LU}}^{\text{A}}$ it is shifted down by approximately half of the discontinuity for the acceptor. Equation (4.31) therefore demonstrates that the experimental excitation energy will be underestimated by approximately the average of the integer discontinuities of the two molecules, which can be of the order of *several* eV.

When hybrid or attenuated functionals are used however, the additional terms (which resemble those arising in the ground state theory due to the classical Coulomb interaction J between electrons) contributing to the matrices **A** and **B** prevent the excitation energies from reducing to orbital energy differences in the case of zero overlap. It is also through these additional terms that the $-1/R$ dependence, required by eq. (4.29), is introduced. The accuracy of charge-transfer states for these extreme cases will therefore depend on the amount of exact exchange present in a functional for modelling this distance dependence; the standard hybrid functional B3LYP exhibits behaviour

as $-0.2/R$ since it contains 20% exact exchange. It has been demonstrated that⁹⁹ CAM-B3LYP's long-range behaviour significantly improves the distance dependence of CT excitations for intermolecular excitations, but since it still only contains 65% exact exchange at long-range, it does not exhibit the correct long-range behaviour. Forcing the attenuation parameters to satisfy $\alpha + \beta = 1$ does yield the correct behaviour however, but as has been demonstrated in chapter 3, this would yield significantly less accurate descriptions of other properties; it is insufficient to simply have the correct distance dependence.

Given the observed performance of CAM-B3LYP,^{138,140,182,198-201} and following the application of CAM-B3LYP to two examples of charge-transfer state^{99,146} in chapter 3 we now go on to consider a wider range of excitation energies. Firstly we provide an extensive assessment of the quality of TDDFT excitation energies from PBE, B3LYP and CAM-B3LYP, as prototypical GGA, hybrid and attenuated functionals. A wide range of vertical excitations in main group molecules are considered, comprising local, Rydberg and intramolecular CT types. Influenced by the above analysis highlighting GGA failure as the overlap tends to zero, we go on to consider the influence of the spatial overlap on a general excitation. Specifically we attempt to quantify the extent to which excitation energy errors correlate with the overlap between the occupied and virtual orbitals involved in an excitation. We then use this to explain the seemingly conflicting performance of functionals for CT in different molecules.

4.3 ASSESSMENT OF EXCHANGE-CORRELATION FUNCTIONALS

Molecules, excitations and computational details

Figure 4.1 lists the molecules considered in this study.²⁰² They were chosen to include a wide range of excitations of differing character, many of which have been demonstrated to represent a challenge for TDDFT. Table 4.1 lists the specific singlet vertical excitations of interest. We base our classification of the excitation energies on earlier studies; those assigned to be of Rydberg or charge-transfer character are labelled R and CT respectively. All other excitations are termed local, labelled L.

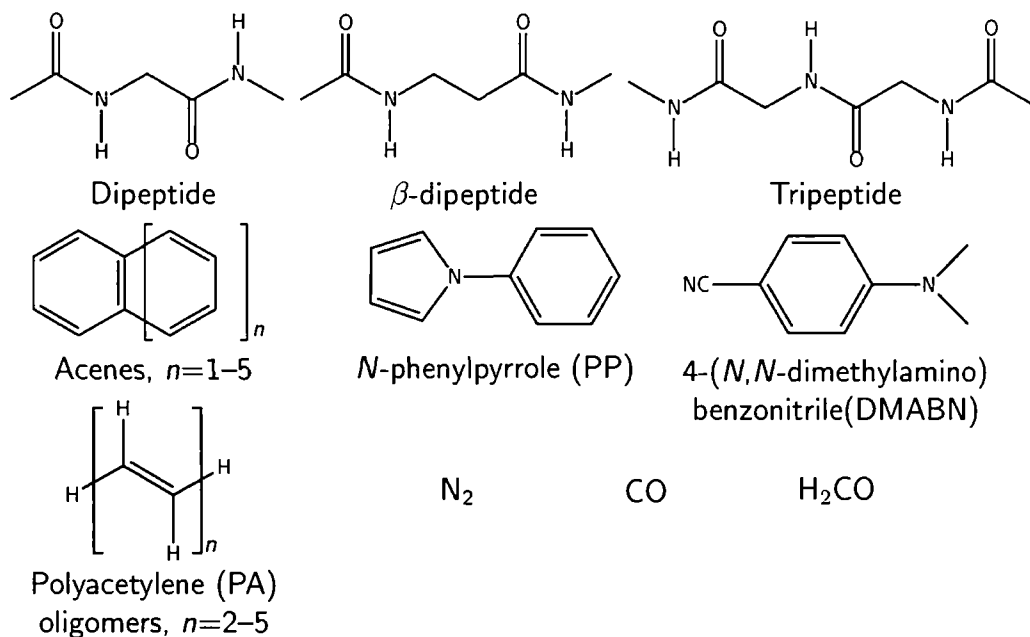


Figure 4.1: Schematic structures of the molecules for which excitation energies have been considered.

The first molecule we consider is the model dipeptide of ref. 203. This was one of the first highlighted cases¹⁵¹ where conventional functionals exhibit a large error associated with a CT state. The notations n_i , π_i and π_i^* in table 4.1 refer to the non-bonding, π and π^* orbitals approximately localised on carbonyl group i , with $i = 1, 2$. The $n_1 \rightarrow \pi_2^*$ and $\pi_1 \rightarrow \pi_2^*$ excitations therefore correspond to excitations from one carbonyl to another and are CT in character. The remaining $n_1 \rightarrow \pi_1^*$ and $n_2 \rightarrow \pi_2^*$ are local excitations since they only involve one carbonyl group. The next two molecules are a longer chain β -dipeptide and tripeptide, also from ref. 203, neither of which have previously been studied with TDDFT; the same notation is used to describe the excitations in these molecules. The larger distances between carbonyl groups in these molecules suggests that the CT errors from conventional functionals will be even more significant than in the dipeptide system.

Next is a series of linear condensed acenes, of increasing length, as considered in ref. 204. As noted in this earlier work, the ${}^1B_{2u}$ excitation is particularly problematic for TDDFT, and the state ordering for the ${}^1B_{2u}$ and ${}^1B_{3u}$ states

can be incorrect. The next two molecules are *N*-phenylpyrrole (PP), widely studied^{48,192} due to its photophysical properties, and DMABN, which is of significant interest due to its dual fluorescence. DMABN is an example of a system where conventional functionals give a good description of the lowest CT excitation. The next four molecules are polyacetylene (PA) oligomers, as recently investigated in ref. 205; see also chapter 5. We consider the lowest dipole-allowed transition. The final four molecules are N₂, CO, H₂CO (see ref. 150) and HCl (see ref. 206), the first three of which allow the accuracy of Rydberg excitations to be assessed.

All calculations were performed using a development version of the DALTON program. The TDDFT excitation energies were performed within the adiabatic approximation with three exchange-correlation functionals: the PBE GGA containing no exact exchange, the B3LYP hybrid containing a fixed amount of exact exchange, and the CAM-B3LYP attenuated functional with the parameters as defined by Yanai¹⁴⁰ *et al.*

Calculations on the acenes were performed at B3LYP/TVZP geometries to allow comparison with the CC2 reference values of Grimme and Parac.²⁰⁴ For the PA oligomers we use the CAM-B3LYP/6-31G* geometries (see chapter 5) due to their high quality bond-length alternation.^{205,207} For N₂ and CO the experimental geometries of ref. 208 are used. Calculations on all of the other molecules were performed at MP2/6-31G* geometries.

All of the excitation energies calculated in the present work are vertical values determined with the cc-pVTZ basis set,²⁰⁹ with the exception of N₂, CO and H₂CO, where the d-aug-cc-pVTZ²¹⁰ basis set is used due to the Rydberg character of some of the excitations; this point is discussed further in the next subsection. For the remaining molecules, we have confirmed where possible that the TDDFT results are relatively insensitive to the addition of diffuse functions to the basis—most excitation energies change by less than 0.1 eV in moving from cc-pVTZ to aug-cc-pVTZ.²¹¹

The accuracy of the TDDFT excitation energies is quantified through comparison with reference values. Where gas-phase experimental data are available, we use these as reference. For the model peptide systems, CASPT2 data is used. For the remaining molecules CC2 data is used. The CASPT2 and CC2 values were computed at the same geometries as the TDDFT val-

ues; all CC2 calculations performed for the present study use the cc-pVTZ basis set. Full details of the reference values are given in table 4.1. Note that the conclusions of this study are applicable outside of these chosen geometries, bases and reference values; analogous observations are made when the computational details of the earlier studies are instead used.

Functional performance

Table 4.1 compares TDDFT excitation energies with reference values. First consider the PBE functional. Excitations of CT character are significantly underestimated, with the exception of DMABN as highlighted in ref. 156 and chapter 3. As anticipated the performance is worst for the CT excitations in the tripeptide with errors up to 5 eV. The Rydberg excitations in N₂, CO and H₂CO exhibit the usual significant underestimation, with errors of up to several eV. These excitations have an unacceptable dependence on the diffuseness of the basis set; as an illustration we performed additional calculations using a triply augmented basis, obtained by adding an extra shell of diffuse functions for each angular momentum, with elements obtained from the geometric progression. All of the Rydberg excitation energies are reduced, by an average of 0.27 eV, whilst the local excitations are unaffected by the additional functions.

Consistent with ref. 204, the PBE ¹B_{2u} excitations in table 4.1 are much too low in the acenes, with the ¹B_{2u}/¹B_{3u} state ordering incorrect for the $n = 1$ case. The excitation energies of the local states in PP are notably underestimated, and the error for the PA oligomers increases as the chain lengthens. The remaining excitations are reasonably accurate. The poor overall performance of PBE is illustrated by the fact that of the 59 excitations we consider, 25 have an error larger than 1 eV and 35 have a percentage error greater than 10%.

Next consider the B3LYP functional, which introduces a fixed amount of exact exchange. The values of most excitation energies increase relative to PBE. Subsequently the CT excitations do improve, but in general still remain too low (the exception being DMABN). The Rydberg excitations also improve, but still have unacceptably large errors. Notably the basis set dependence of the Rydberg excitations is diminished; on average the excitation energies

Table 4.1: TDDFT excitation energies and reference values, in eV.

Molecule	Excitation	Type	PBE	B3LYP	CAM-B3LYP	Ref.
Dipeptide	$n_1 \rightarrow \pi_2^*$	CT	4.61	6.31	7.84	8.07 ^a
	$\pi_1 \rightarrow \pi_2^*$	CT	5.16	6.15	7.00	7.18 ^a
	$n_1 \rightarrow \pi_1^*$	L	5.35	5.55	5.68	5.62 ^a
	$n_2 \rightarrow \pi_2^*$	L	5.67	5.77	5.92	5.79 ^a
β -dipeptide	$n_1 \rightarrow \pi_2^*$	CT	4.78	7.26	8.38	9.13 ^a
	$\pi_1 \rightarrow \pi_2^*$	CT	5.32	7.20	8.01	7.99 ^a
	$n_1 \rightarrow \pi_1^*$	L	5.38	5.66	5.67	5.40 ^a
	$n_2 \rightarrow \pi_2^*$	L	5.41	5.56	5.76	5.10 ^a
Tripeptide	$\pi_1 \rightarrow \pi_2^*$	CT	5.18	6.27	6.98	7.01 ^a
	$\pi_2 \rightarrow \pi_3^*$	CT	5.51	6.60	7.69	7.39 ^a
	$\pi_1 \rightarrow \pi_3^*$	CT	4.76	6.06	8.51	8.74 ^a
	$n_1 \rightarrow \pi_3^*$	CT	4.26	6.12	8.67	9.30 ^a
	$n_2 \rightarrow \pi_3^*$	CT	5.16	6.83	8.25	8.33 ^a
	$n_1 \rightarrow \pi_2^*$	CT	4.61	6.33	7.78	8.12 ^a
	$n_1 \rightarrow \pi_1^*$	L	5.36	5.57	5.72	5.74 ^a
	$n_2 \rightarrow \pi_2^*$	L	5.58	5.74	5.93	5.61 ^a
	$n_3 \rightarrow \pi_3^*$	L	5.74	5.88	6.00	5.91 ^b
	Acene ($n=1$)	$^1B_{2u}$	L	4.11	4.38	4.67
$^1B_{3u}$		L	4.27	4.47	4.62	4.46 ^b
Acene ($n=2$)	$^1B_{2u}$	L	2.94	3.21	3.53	3.69 ^b
	$^1B_{3u}$	L	3.64	3.86	4.04	3.89 ^b
Acene ($n=3$)	$^1B_{2u}$	L	2.17	2.43	2.76	2.90 ^b
	$^1B_{3u}$	L	3.24	3.47	3.65	3.52 ^b
Acene ($n=4$)	$^1B_{2u}$	L	1.63	1.89	2.22	2.35 ^b
	$^1B_{3u}$	L	2.96	3.21	3.39	3.27 ^b
Acene ($n=5$)	$^1B_{2u}$	L	1.23	1.48	1.82	1.95 ^b
	$^1B_{3u}$	L	2.76	3.01	3.21	3.09 ^b
PP	1^1B_2	L	4.33	4.76	5.06	4.85 ^c
	2^1A_1	L	4.61	4.96	5.12	5.13 ^c
	2^1B_2	CT	3.98	4.58	5.27	5.47 ^c
	3^1A_1	CT	3.90	4.64	5.92	5.94 ^c
DMABN	1B	L	4.02	4.44	4.72	4.25 ^d
	1A	CT	4.30	4.64	4.91	4.56 ^d
PA Oligomer ($n=2$)	1^1B_u	L	5.74	5.88	6.04	5.92 ^e
PA Oligomer ($n=3$)	1^1B_u	L	4.63	4.81	5.03	4.95 ^f
PA Oligomer ($n=4$)	1^1B_u	L	3.93	4.13	4.39	4.41 ^g
PA Oligomer ($n=5$)	1^1B_u	L	3.44	3.66	3.94	4.27 ^c

Continued...

Table 4.1: Continuation of: TDDFT excitation energies and reference values, in eV.

Molecule	Excitation	Type	PBE	B3LYP	CAM-B3LYP	Ref.
N ₂	¹ Π _u	R	11.67	12.01	12.44	13.24 ^h
	¹ Σ _u ⁺	R	10.66	11.62	12.32	12.98 ^h
	¹ Π _u	R	10.76	11.65	12.27	12.90 ^h
	¹ Σ _g ⁺	R	10.41	11.24	11.80	12.20 ^h
	¹ Δ _u	L	10.08	9.72	9.68	10.27 ^h
	¹ Σ _u ⁻	L	9.68	9.33	9.21	9.92 ^h
	¹ Π _g	L	9.10	9.26	9.38	9.31 ^h
CO	<i>F</i> ¹ Σ ⁺	R	10.16	10.97	11.79	12.40 ⁱ
	<i>E</i> ¹ Π	R	9.45	10.19	10.90	11.53 ⁱ
	<i>C</i> ¹ Σ ⁺	R	9.40	10.13	10.80	11.40 ⁱ
	<i>B</i> ¹ Σ ⁺	R	9.09	9.80	10.37	10.78 ⁱ
	<i>D</i> ¹ Δ	L	10.18	10.03	10.08	10.23 ⁱ
	<i>I</i> ¹ Σ ⁻	L	9.86	9.72	9.71	9.88 ⁱ
	<i>A</i> ¹ Π	L	8.24	8.39	8.47	8.51 ⁱ
H ₂ CO	¹ A ₂	R	7.43	8.16	8.87	9.22 ^j
	¹ A ₂	R	6.61	7.34	7.94	8.38 ^j
	¹ B ₁	L	8.68	8.83	8.95	8.68 ^j
	¹ B ₂	R	6.50	7.16	7.62	8.12 ^j
	¹ A ₁	R	6.39	7.14	7.74	7.97 ^j
	¹ B ₂	R	5.78	6.43	6.89	7.09 ^j
	¹ A ₂	L	3.73	3.85	3.85	3.94 ^j
HCl	¹ Π	CT	7.55	7.65	7.79	8.23 ^c

^a CASPT2, ref. 203.^b CC2, ref. 204.^c CC2, this work.^d Gas phase expt., ref. 158.^e Gas phase expt., ref. 212.^f Gas phase expt., ref. 213.^g Gas phase expt., ref. 214.^h Gas phase expt., ref. 215.ⁱ Gas phase expt., refs. 208 and 216.^j Gas phase expt., refs. 217 and 218.

reduce by 0.1 eV when additional diffuse functions are added—one third of the reduction that occurred with PBE. Both the ${}^1B_{2u}$ and ${}^1B_{3u}$ states in the acenes become more accurate, although the state ordering is still incorrect for $n = 1$. The local excitations in PP improve significantly; the PA oligomer excitations also improve, however the error remains large for the longer chains. The remaining excitations are reasonably accurate. Overall 16 excitations have an error larger than 1 eV and 25 have a percentage error greater than 10%.

In moving to the attenuated CAM-B3LYP functional a further increase in most excitation energies is observed. For the CT excitations the tendency to underestimate is eliminated; only two errors are larger than 0.5 eV. The description of Rydberg excitations is also considerably improved compared to B3LYP; on average the error is halved. Further the basis set sensitivity is reduced again; the effect of additional diffuse functions is now to lower the excitation energies by less than 0.03 eV on average. The CAM-B3LYP error for the Rydberg excitations can still approach 1 eV however, which as noted in chapter 3 is due to the still-incorrect long-range behaviour of this functional. CAM-B3LYP provides a particularly good description of the acene excitations, with the state ordering *now correct* for all of the systems. It also performs well for PP and the PA oligomers, for which the error is now much less sensitive to chain length. Most of the remaining excitations are reasonably accurate, although large errors remain for the $n_2 \rightarrow \pi_2^*$ excitation in the β -dipeptide and the ${}^1\Sigma_u^-$ excitation in N_2 . None of the excitations have an error larger than 1 eV, and only two have a percentage error that is greater than 10%.

Table 4.2 lists the mean error d , mean absolute error $|d|$, standard deviation (SD) and maximum positive and negative deviations relative to reference values according to excitation category. The errors are defined as calculated minus reference. For local excitations B3LYP is a notable improvement over PBE. CAM-B3LYP provides a similar quality $|d|$ and SD to B3LYP, but is associated with slightly higher maximum errors. For both the Rydberg and CT excitations the improvement from PBE to B3LYP to CAM-B3LYP is significant.

Note that since the Rydberg and intermolecular CT excitations require 100% long-range exact exchange in the functional, the amount of long-range exchange in CAM-B3LYP is insufficient to provide a completely accurate de-

Table 4.2: Error analysis for the excitations considered in table 4.1 (mean error d , mean absolute error $|d|$, standard deviation (SD), and maximum positive and negative deviations) in eV.

	PBE	B3LYP	CAM-B3LYP
Local			
d	-0.31	-0.15	0.02
$ d $	0.33	0.22	0.20
SD	0.27	0.26	0.27
Max(+)	0.31	0.46	0.66
Max(-)	-0.83	-0.61	-0.71
Rydberg			
d	-1.84	-1.11	-0.50
$ d $	1.84	1.11	0.50
SD	0.30	0.23	0.18
Max(+)	None	None	None
Max(-)	-2.24	-1.43	-0.80
Charge-transfer			
d	-2.60	-1.35	-0.18
$ d $	2.60	1.36	0.27
SD	1.37	0.86	0.31
Max(+)	None	0.08	0.35
Max(-)	-5.04	-3.18	-0.75

scription of these properties. The influence of alternative parameterisations of CAM-B3LYP is not considered here due to the observations of chapter 3, where it was shown that many other excitations become poorly described when the nature of the attenuation is changed from the form in CAM-B3LYP. As previously highlighted, this suggests the need for designing different attenuation shapes to simultaneously describe all classes of excitation to the required accuracy.

4.4 CORRELATION BETWEEN ERROR AND ORBITAL OVERLAP

The excitation energy results described in the previous section highlight several important issues; all three functionals perform reasonably well for local excitations, but there is a marked variation in their performance for Ryd-

berg and CT states. As originally highlighted in ref. 195, the failure for some charge-transfer states seems to originate from the inappropriate collapse of the excitation energies to orbital energy differences when local functionals are employed. Whilst this can be repaired through the appropriate introduction of exact exchange into the functional, we consider whether it is possible to gain insight into the problem by explicitly determining a measure of the spatial overlap between the unperturbed occupied and virtual orbitals involved in an excitation, and the extent to which the error in a given excitation correlates with this overlap.²⁰²

For a given occupied orbital φ_i and virtual orbital φ_a , there are two natural measures of spatial overlap; the inner product of the moduli of the two orbitals

$$O_{ia}^M = \langle |\varphi_i| | |\varphi_a| \rangle = \int d\mathbf{r} |\varphi_i(\mathbf{r})| |\varphi_a(\mathbf{r})| \quad (4.32)$$

and the inner product of the square of the two orbitals

$$O_{ia}^S = \langle \varphi_i^2 | \varphi_a^2 \rangle = \int d\mathbf{r} \varphi_i^2(\mathbf{r}) \varphi_a^2(\mathbf{r}). \quad (4.33)$$

The latter of which has the advantage of maintaining the invariance to unitary transformations of the orbitals. It is necessary to ensure that the overlap uses only positive quantities to avoid sign cancellation; without the square or moduli, each of these quantities would be trivially zero. Either of these quantities can be easily evaluated, using the standard numerical quadrature schemes that are employed in the TDDFT calculations, to the necessary accuracy. In practice many occupied–virtual pairs contribute to a given excitation; the contribution from each pair can be measured by

$$\kappa_{ia} = X_{ia} + Y_{ia} \quad (4.34)$$

which correspond to the elements in eq. (4.21) of the matrices \mathbf{X} and \mathbf{Y} respectively. This quantity (to within a possible multiplicative constant normalisation factor) is commonly printed out in electronic structure programs for the purpose of aiding state assignment.

A measure of the spatial overlap for a given excitation may therefore be obtained by weighting each inner product O_{ia}^M or O_{ia}^S by some function $g(\kappa_{ia})$

and summing over all occupied–virtual pairs, suitably normalised;

$$\Lambda = \frac{\sum_{i,a} g(\kappa_{ia}) O_{ia}}{\sum_{i,a} g(\kappa_{ia})} \quad (4.35)$$

To again avoid cancellations due to sign changes, we consider both $g(\kappa_{ia}) = |\kappa_{ia}|$ and $g(\kappa_{ia}) = \kappa_{ia}^2$. This gives rise to four expressions for Λ , each of which satisfies $0 < \Lambda \leq 1$. We evaluated each of these overlap measures for all of the excitations given in table 4.1, with each of the three functionals. Figure 4.2 presents plots of the four overlap measures against excitation energy error for the PBE functional, with the points coded by colour and symbol for each excitation type; an individual point corresponds to a single excitation. Each of the four measures demonstrates some correlation between Λ and excitation energy error; however, we feel that expressions involving the moduli of the orbitals [eq. (4.32)] provide the most distinct correlation, with the error on average increasing as the overlap decreases. The case with $g(\kappa_{ia}) = \kappa_{ia}^2$ has values of Λ which cover more of the possible range, allowing excitations to be more readily distinguished. For the remainder of the study we therefore measure the spatial overlap in a given excitation by the quantity

$$\Lambda = \frac{\sum_{i,a} \kappa_{ia}^2 O_{ia}^M}{\sum_{i,a} \kappa_{ia}^2}. \quad (4.36)$$

A small value of Λ corresponds to a small overlap and a long-range excitation, whereas a large value signifies a short-range excitation corresponding to a high overlap. Figure 4.3 plots the error in each of the excitation energies of table 4.1 against the associated Λ values for the PBE, B3LYP and CAM-B3LYP exchange–correlation functionals. The Λ value for each individual excitation is given in table 4.3.

First consider the PBE results in figure 4.3. The three categories of excitation are readily distinguished. Local excitations have relatively large overlap, ranging from $0.45 \leq \Lambda \leq 0.89$, indicating that the occupied and virtual orbitals involved in these excitations occupy similar regions of space. This is consistent with the intuitive picture of a local excitation, and the associated small degree of charge redistribution. In contrast, the Rydberg excitations have much smaller overlap values, ranging from $0.08 \leq \Lambda \leq 0.27$, indicating

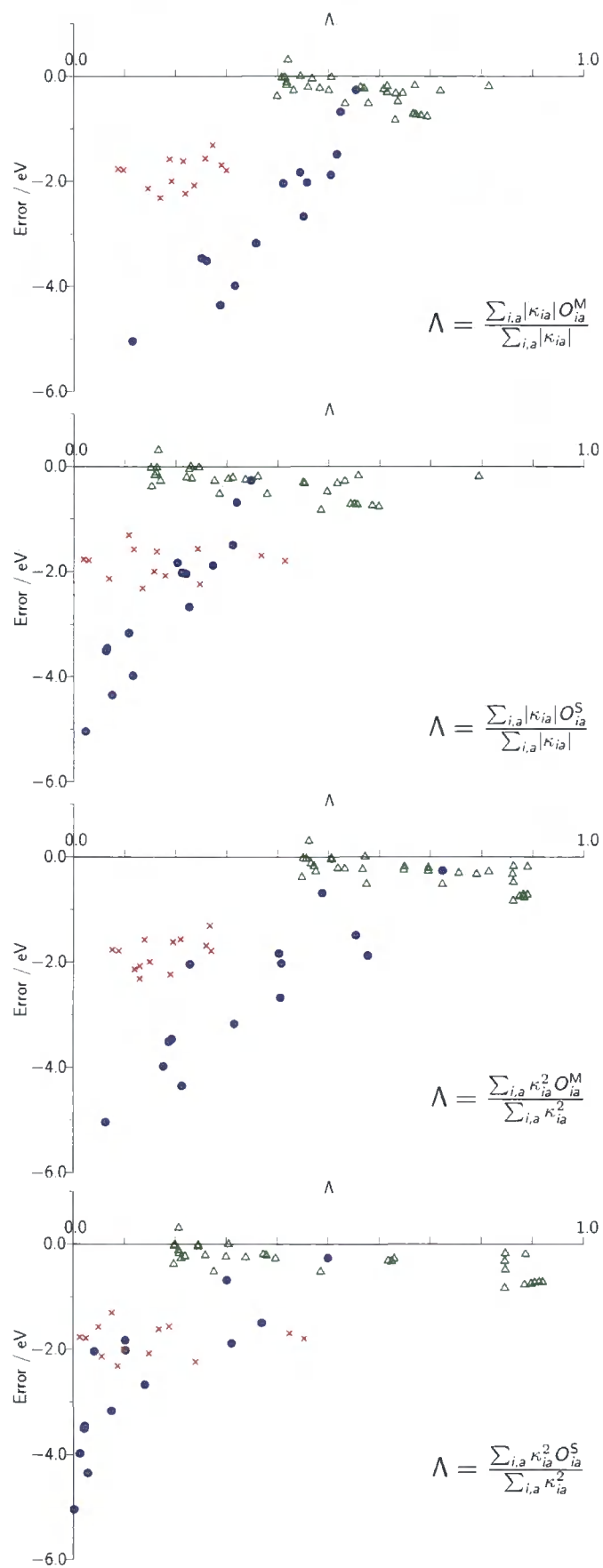


Figure 4.2: PBE excitation energy errors plotted against various definitions of Λ .

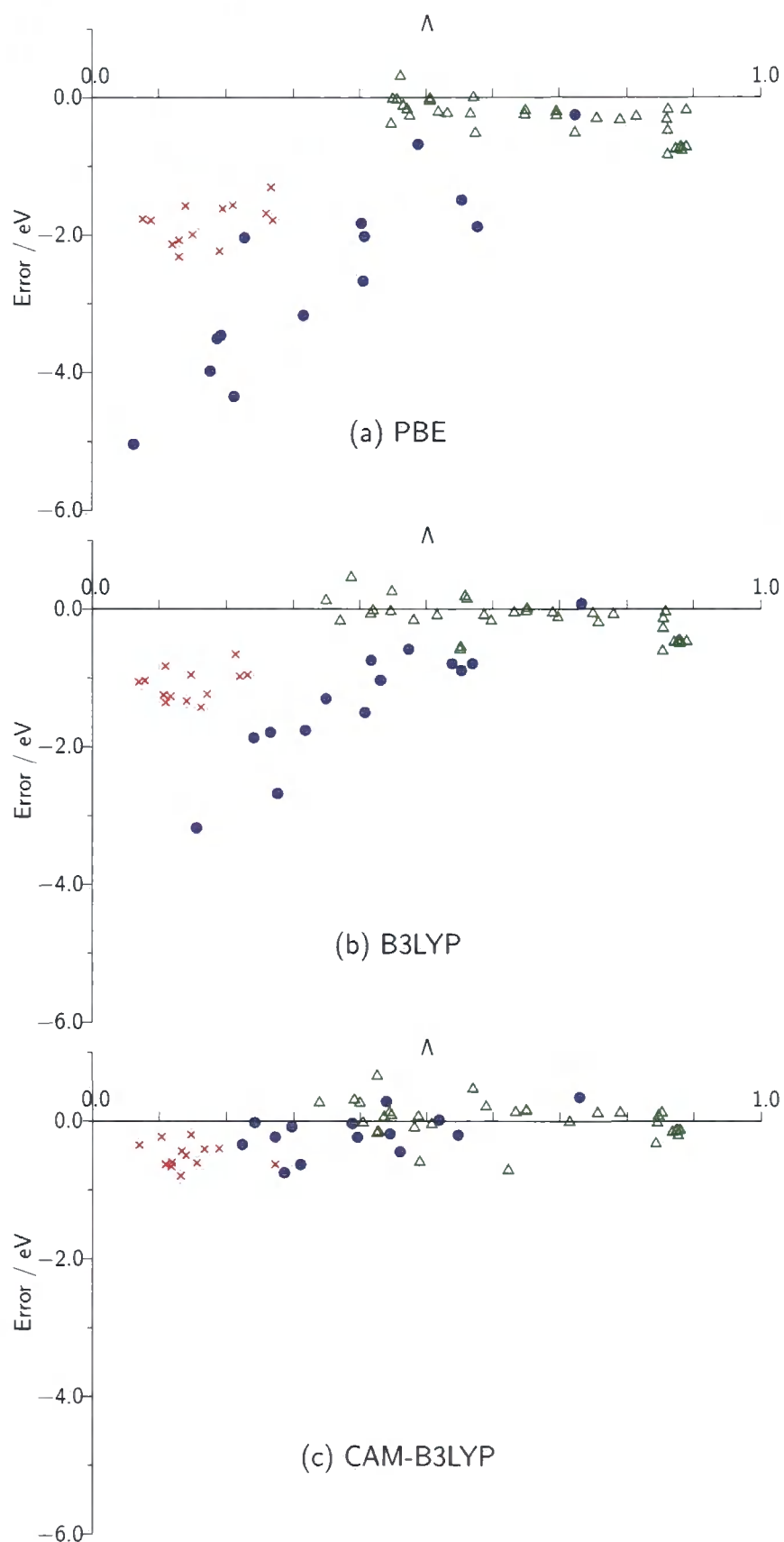


Figure 4.3: Excitation energy errors plotted against Λ [eq. (4.36)] using (a) PBE, (b) B3LYP, and (c) CAM-B3LYP, for local excitations (Δ), Rydberg excitations (\times), and CT excitations (\bullet).

only a minimal spatial overlap between the occupied and virtual orbitals involved in an excitation; this is equally consistent with the intuitive notion of an electron moving from a valence orbital to a diffuse virtual orbital. Unexpected is the behaviour of the Λ values associated with the CT excitations, which cover a *surprisingly wide range of overlaps*, from $\Lambda = 0.06$ in the tripeptide to $\Lambda = 0.72$ in DMABN. Figure 4.3 shows a clear correlation between the PBE excitation energy errors and Λ ; small errors are associated with large Λ and large errors are associated with small Λ . This correlation provides a simple explanation as to why the CT excitation in DMABN, unlike many CT excitations, is well described by PBE—the spatial overlap between the orbitals involved in the excitation is large. We highlight this by plotting the relevant orbitals in figure 4.4. In this sense the excitation more closely resembles a local excitation; the origin of the CT classification is from the large change in dipole moment associated with this electron transition. For comparison, the orbitals corresponding to the $n_1 \rightarrow \pi_3^*$ excitation in the tripeptide are also plotted in figure 4.4, corresponding to $\Lambda = 0.06$. The lack of overlap is particularly evident.

Note that we do not explicitly consider intermolecular CT excitations between infinitely separated molecules; for such systems, the error in the excitation energy is (as shown above) approximately the average of the integer discontinuities of the two molecules. The discontinuity may be approximated by twice the system-independent shift that must be introduced when semi-empirical functionals are determined from high-quality potentials. As such it is apparent that (consider for instance the data in table I of ref. 219) for typical pairs of molecules this error is well in excess of -5 eV and such data-points would fit well with the CT data in figure 4.3. We have confirmed from a number of sample calculations on $C_2H_4 \cdots C_2F_4$ complexes that for large intermolecular separation, we do obtain significant errors and essentially zero values of Λ .

In moving to B3LYP and CAM-B3LYP in figure 4.3, the excitation energy errors reduce according to the value of Λ . Those with large Λ values, such as the local excitations and the DMABN CT, do not change appreciably. With reducing Λ however, the error reduction becomes increasingly pronounced. For B3LYP, the correlation between excitation energy error and Λ is still present.

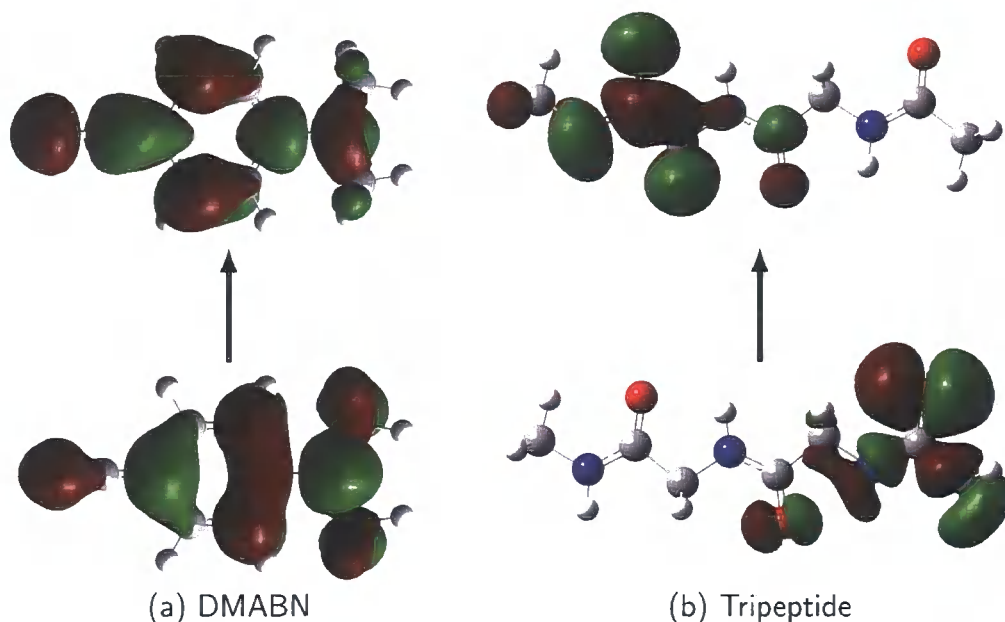


Figure 4.4: Charge-transfer dominant orbital transitions in DMABN and the model tripeptide, exemplifying large and small Λ , determined using the PBE GGA. All orbital plots in this work use a contour of 0.023 a.u.

It is notably less prominent than with PBE, indicating the partial success of the introduction of a fixed amount of exact exchange into a functional. For CAM-B3LYP there is essentially no correlation between the value of Λ and the associated error in an excitation energy, which is exactly what should be observed from a successful theoretical method. This removal of the correlation is due to the complicated mixing of exact orbital exchange in the functional. The overlap quantity Λ is now routinely evaluated in the DALTON program.

Of the three functionals considered, CAM-B3LYP provides by far the best overall description of the excitation energies considered, with essentially no observed correlation between the errors and spatial orbital overlap as measured by Λ . This functional is therefore recommended for general excitation energy calculations. For PBE and B3LYP, our observations lead us to propose a simple diagnostic test for judging the reliability of an excitation energy; following figure 4.3, a PBE excitation with $\Lambda < 0.4$ or a B3LYP excitation energy with $\Lambda < 0.3$ is likely to be in significant error. The quantity Λ is not unique, but it

provides a qualitative description of the failure of local functionals in describing excitation energies under certain circumstances. It captures the essential physics of the problem and may prove useful in practical calculations.

Table 4.3: Values of the overlap quantity Λ of eq. (4.36)

Molecule	Excitation	Type	PBE	B3LYP	CAM-B3LYP
Dipeptide	$n_1 \rightarrow \pi_2^*$	CT	0.19	0.32	0.27
	$\pi_1 \rightarrow \pi_2^*$	CT	0.41	0.43	0.45
	$n_1 \rightarrow \pi_1^*$	L	0.48	0.42	0.44
	$n_2 \rightarrow \pi_2^*$	L	0.47	0.42	0.44
β -dipeptide	$n_1 \rightarrow \pi_2^*$	CT	0.21	0.24	0.29
	$\pi_1 \rightarrow \pi_2^*$	CT	0.41	0.57	0.52
	$n_1 \rightarrow \pi_1^*$	L	0.45	0.45	0.40
	$n_2 \rightarrow \pi_2^*$	L	0.46	0.39	0.43
Tripeptide	$\pi_1 \rightarrow \pi_2^*$	CT	0.40	0.42	0.39
	$\pi_2 \rightarrow \pi_3^*$	CT	0.58	0.54	0.44
	$\pi_1 \rightarrow \pi_3^*$	CT	0.18	0.28	0.40
	$n_1 \rightarrow \pi_3^*$	CT	0.06	0.16	0.31
	$n_2 \rightarrow \pi_3^*$	CT	0.32	0.41	0.30
	$n_1 \rightarrow \pi_2^*$	CT	0.19	0.27	0.22
	$n_1 \rightarrow \pi_1^*$	L	0.45	0.37	0.40
	$n_2 \rightarrow \pi_2^*$	L	0.46	0.35	0.39
	$n_3 \rightarrow \pi_3^*$	L	0.47	0.45	0.45
	Acene ($n = 1$)	$^1B_{2u}$	L	0.88	0.88
$^1B_{3u}$		L	0.65	0.65	0.65
Acene ($n = 2$)	$^1B_{2u}$	L	0.87	0.87	0.87
	$^1B_{3u}$	L	0.65	0.65	0.65
Acene ($n = 3$)	$^1B_{2u}$	L	0.88	0.88	0.87
	$^1B_{3u}$	L	0.63	0.63	0.63
Acene ($n = 4$)	$^1B_{2u}$	L	0.88	0.88	0.88
	$^1B_{3u}$	L	0.62	0.62	0.62
Acene ($n = 5$)	$^1B_{2u}$	L	0.89	0.89	0.88
	$^1B_{3u}$	L	0.60	0.61	0.61
PP	1^1B_2	L	0.57	0.59	0.59
	2^1A_1	L	0.72	0.60	0.72
	2^1B_2	CT	0.55	0.55	0.55
	3^1A_1	CT	0.23	0.35	0.24
DMABN	1B	L	0.53	0.56	0.57
	1A	CT	0.72	0.73	0.73
PA Oligomer ($n = 2$)	1^1B_u	L	0.86	0.86	0.85
PA Oligomer ($n = 3$)	1^1B_u	L	0.86	0.85	0.85
PA Oligomer ($n = 4$)	1^1B_u	L	0.86	0.85	0.84
PA Oligomer ($n = 5$)	1^1B_u	L	0.86	0.85	0.84

Continued...

Table 4.3: Continuation of: Values of the overlap quantity Λ of eq. (4.36)

Molecule	Excitation	Type	PBE	B3LYP	CAM-B3LYP
N ₂	¹ Π _u	R	0.21	0.17	0.13
	¹ Σ _u ⁺	R	0.13	0.11	0.12
	¹ Π _u	R	0.12	0.11	0.11
	¹ Σ _g ⁺	R	0.27	0.23	0.19
	¹ Δ _u	L	0.89	0.55	0.49
	¹ Σ _u ⁻	L	0.57	0.55	0.62
	¹ Π _g	L	0.70	0.69	0.49
CO	<i>F</i> ¹ Σ ⁺	R	0.19	0.16	0.16
	<i>E</i> ¹ Π	R	0.13	0.14	0.27
	<i>C</i> ¹ Σ ⁺	R	0.15	0.12	0.12
	<i>B</i> ¹ Σ ⁺	R	0.26	0.22	0.17
	<i>D</i> ¹ Δ	L	0.51	0.76	0.43
	<i>I</i> ¹ Σ ⁻	L	0.51	0.48	0.43
	<i>A</i> ¹ Π	L	0.70	0.70	0.51
H ₂ CO	¹ A ₂	R	0.09	0.07	0.07
	¹ A ₂	R	0.08	0.08	0.13
	¹ B ₁	L	0.57	0.56	0.34
	¹ B ₂	R	0.20	0.15	0.14
	¹ A ₁	R	0.14	0.11	0.10
	¹ B ₂	R	0.27	0.21	0.14
	¹ A ₂	L	0.52	0.52	0.48
HCl	¹ Π	CT	0.49	0.47	0.46

4.5 APPLICATION OF TDDFT TO TRIAZENE CHROMOPHORES

Our calculations have demonstrated that for GGA and hybrid functionals there is a broad correlation between the error and the value of Λ associated with an excitation. Excitation energies are significantly underestimated when Λ is very small, whereas the errors tend to be smaller and more acceptable when Λ is large. This is an intuitive observation which reflects the fundamentally local nature of the description of exchange in approximate GGA functionals.

Recently Preat²²⁰ *et al.* considered a series of triazene chromophores^{221, 222} in dichloromethane. These authors demonstrated the PBE0 hybrid functional provides a theoretical absorption maximum in excellent agreement with experiment (recently determined by Khramov and Bielawski²²²), even for the molecules with strong ‘push–pull’ character. We now go on to apply the Λ diagnostic method to these triazenes, and discuss why the low- Λ breakdown was not observed in their work. We use the diagnostic to determine potentially problematic excitations, highlighting the use of the diagnostic in practice.

The assessment of CAM-B3LYP for a wide variety of excitation energies in the gas phase demonstrated the success of this functional in describing local, Rydberg and charge-transfer excitations. We therefore also consider the application of this functional to gas phase triazenes, through comparison with correlated wavefunction *ab initio* excitation energies.

Triazenes in solvent

We now apply the orbital overlap diagnostic to the four triazene chromophores illustrated in figure 4.5. Preat²²⁰ *et al.* determined PBE0/6-311G(d,p) geometries in the presence of a dichloromethane solvent, which was treated via the polarised continuum model²²³ (PCM) with cavity parameters defined by the united atom topological model²²⁴ applied to radii optimised for PBE0. They then calculated the lowest *five* singlet vertical excitation energies and associated oscillator strengths using PBE0/6-311+G(2d,p) with a non-equilibrium PCM treatment (with similarly defined cavity parameters). Theoretical absorption spectra were obtained by convolution of the oscillator strengths with

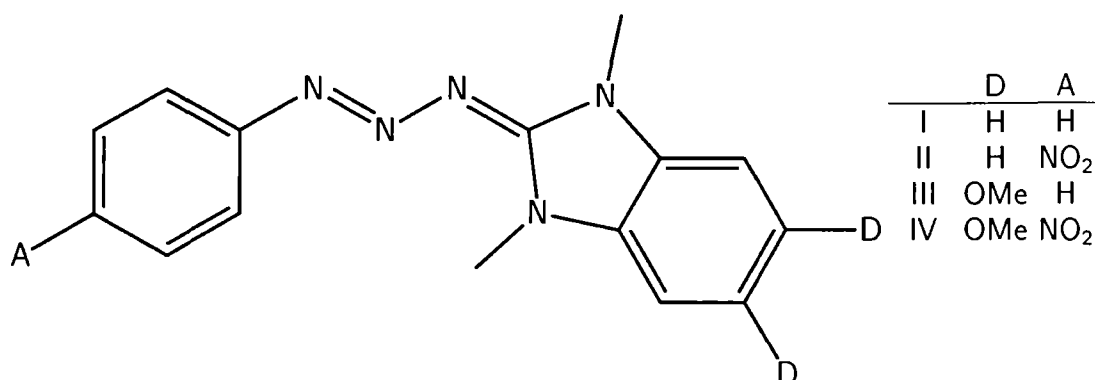


Figure 4.5: Schematic structures of the triazene molecules considered.

a Gaussian centred at the excitation energies. We repeated the calculations of Preat *et al.*, using the same computational approach, but with the PCM implementation in a development version of the DALTON program. Our PBE0 excitation energies and oscillator strengths are in excellent agreement with their published results. We have confirmed that the effect of changing to non-PBE0 based cavity parameters (for instance to the Hartree–Fock optimised parameters) changes excitation energies by less than 0.02 eV on average.

Preat *et al.* did not observe any catastrophic breakdown that we would attribute to low values of Λ , despite the potential in these molecules for charge-transfer type excitations. This can be understood from a consideration of the relationship between the oscillator strength and Λ . By construction, states which have a high oscillator strength must necessarily have a high Λ ; consistent with this, we find that our high oscillator strength excitations have Λ values in the range of 0.48–0.66 for the triazene molecules. Equally, states with low Λ necessarily have low oscillator strengths; we find that for the triazenes, the low Λ excitations have oscillator strengths in the range of 0.00–0.04. It follows that states with relatively high Λ will be seen preferentially in a theoretically determined absorption spectrum over those with relatively low Λ .

Importantly, the converse statements are not true; the oscillator strength *does not* contain the same information as Λ . For instance, several of our calculated states exhibit large values of Λ , but very small oscillator strengths.

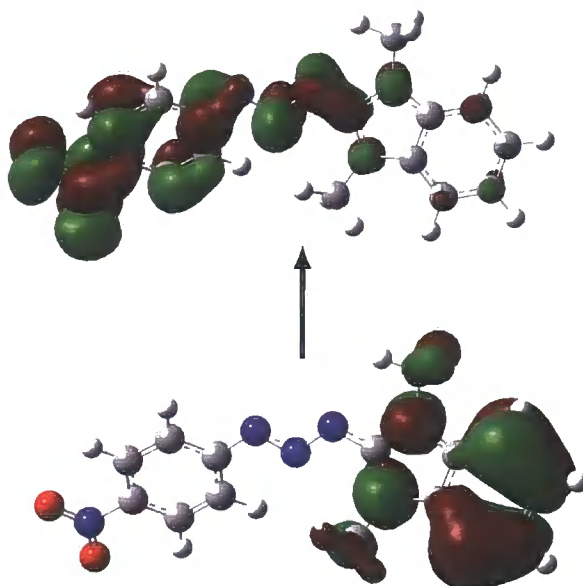


Figure 4.6: Dominant orbital transition for the predicted problematic excitation in triazene II, determined using the PBE GGA

We now consider whether there are any low- Λ problematic excitations amongst the lowest five transitions in each of the triazene molecules, determined with PBE0. The lowest five transitions in molecules I and III exhibit no small Λ values; the smallest values are 0.53 and 0.56 respectively. For molecules II and IV however, the smallest Λ we obtain are 0.28 and 0.31, consistent with the stronger ‘push–pull’ character of these two molecules. None of the Λ values lie significantly below the threshold of ~ 0.3 , and as such the diagnostic does not predict any significant breakdown with PBE0. We previously observed that the PBE GGA is more prone to failure due to small Λ than hybrid functionals. We therefore consider similar calculations with the PBE functional. For molecules I, III and IV, no excitations lie significantly below the threshold. However, molecule II does exhibit one particularly low- Λ excitation, with a value of just 0.27, which is significantly below the threshold of ~ 0.4 for PBE. The relevant orbitals are plotted in figure 4.6; the lack of overlap is evident.

The diagnostic test predicts that this excitation energy is likely to be significantly underestimated by PBE. Support for this is provided by the fact that the excitation is dominated by a single orbital transition and that the value of the excitation energy is within 0.05 eV of the corresponding orbital energy difference, consistent with a collapse of the TDDFT equations. The PBE excitation energy is more than one eV below the PBE0 value (which itself is approximately one eV below the equivalent CAM-B3LYP value); such variation with functional is indicative of a problematic excitation.

Triazenes in the gas phase

The value of Λ as a diagnostic quantity has previously only been demonstrated in the gas phase. Therefore it would be desirable to determine accurate excitation energies in a solvent, particularly for the potentially problematic excitation observed in molecule II, to allow the applicability of Λ in a solvent to be tested. Our current computational capabilities preclude the determination of accurate correlated *ab initio* excitation energies in a solvent. We therefore consider gas phase calculations where we can readily compare TDDFT excitation energies with correlated wavefunction values. For this analysis we consider molecule II since this exhibited the lowest Λ value in a solvent. The gas phase TDDFT calculations use the same basis set as in the solvent. For the reference correlated method, we use the resolution of the identity (RI-) formulation of CC2,^{38,51} as implemented in the TURBOMOLE 5.1 program.²²⁵⁻²²⁷ For these calculations we use the def-QZVPP²²⁸ basis set. All calculations were performed at the geometry of the previous subsection.

The RI-CC2 excitation energies were assigned in terms of their orbital rotations. These were used to identify (as far as possible) the equivalent excitations in the three DFT functionals. Figure 4.7 presents a schematic plot of selected excitation energies; specifically we consider the lowest five obtained with PBE, together with two additional excitations found to have particularly low Λ values. The excitations are colour-coded and labelled *i-vii*. For the three DFT functionals, the value on the left hand side of a TDDFT horizontal line gives the error relative to RI-CC2 and the value on the right hand side is the value of Λ associated with that excitation. The associated dominant PBE

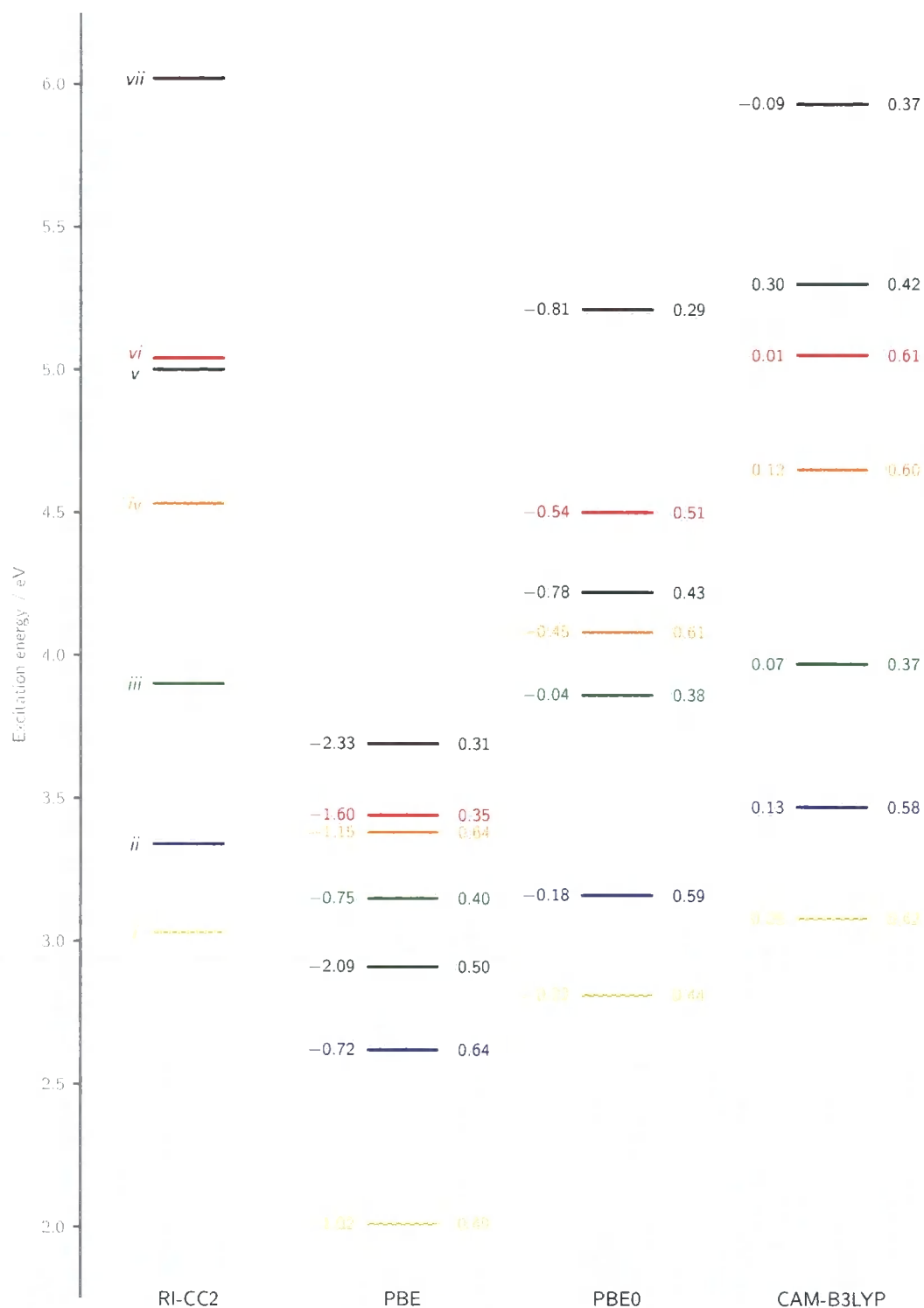


Figure 4.7: Gas phase excitation energies of triazene II. The value on the left hand side of each TDDFT level is the error in eV relative to RI-CC2. The value on the right hand side is λ .

orbital transitions are illustrated in figure 4.8.

First consider the PBE results; the diagnostic test states that excitations with $\Lambda < 0.4$ are likely to be significantly underestimated. There are two excitations (vi and vii) with Λ values below this threshold, at 0.35 and 0.31. They underestimate the RI-CC2 values by 1.60 and 2.33 eV respectively; the diagnostic test therefore successfully identifies these two excitations as problematic. Excitation vi corresponds to the excitation in figure 4.6, which had a small associated Λ value in the solvent calculations. However, the diagnostic test does not identify the other large PBE errors in figure 4.7. The largest of these failures is observed for excitation v , which underestimates RI-CC2 by 2.09 eV. This excitation has an associated Λ value of 0.5, which lies well above the threshold. This is not a failure of the test; the test states that a low value of Λ is likely to be associated with large errors. It *does not* preclude the possibility that excitations with large Λ values can be inaccurate. Indeed, close examination of figure 4.3 shows that analogous results were also present; notably with the PP molecule.

Insight into these observations is provided by figure 4.8, which presents the dominant PBE orbital transitions for the seven excitations. For excitations v , vi and vii an accurate TDDFT description requires non-local exchange, in the sense that $\varphi_i(\mathbf{r}_1)$ and $\varphi_a(\mathbf{r}_2)$ may both be significant when \mathbf{r}_1 and \mathbf{r}_2 are well-separated. All three excitations therefore fail for a local functional, giving excitation energies that are notably below the RI-CC2 values. The overlap-based diagnostic is not able to identify all three of these excitations as problematic because the failure of excitation v is not associated with a small overlap (and therefore Λ); it involves a localised orbital exciting to a spatially extended orbital. The results highlight the need for the development of more sophisticated diagnostic quantities that are able to identify both categories of failure.

Figure 4.7 also presents excitation energies determined using PBE0 and CAM-B3LYP. For PBE0, no excitations have Λ values significantly below the threshold. In general the PBE0 errors are smaller than those obtained with PBE, but results from this functional still notably underestimate RI-CC2 in some cases. In moving to CAM-B3LYP the agreement with RI-CC2 is dramatic; the mean absolute error is just 0.11 eV, with a maximum error of 0.3 eV.

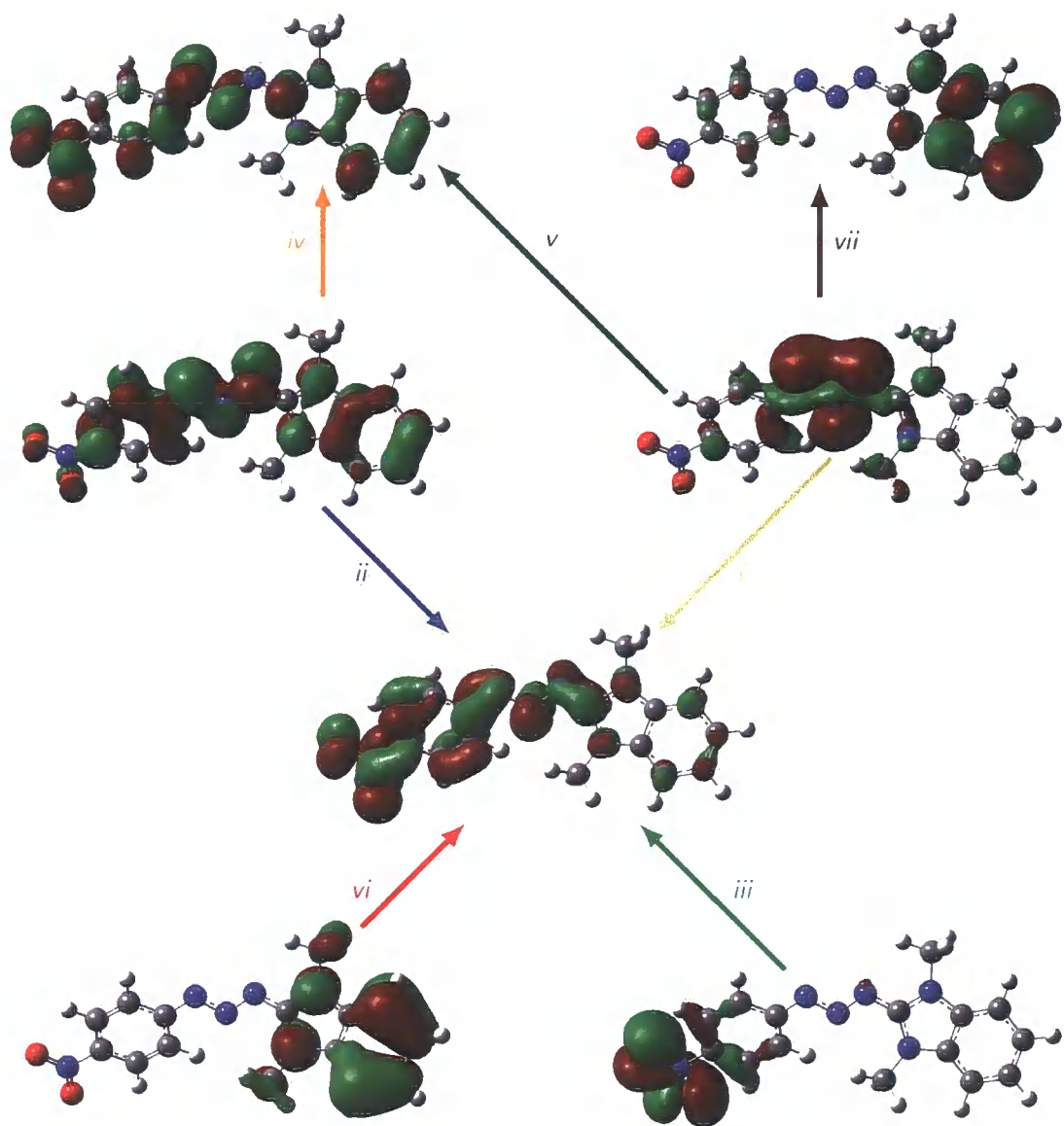


Figure 4.8: Gas phase dominant PBE orbital transitions for triazene II. Errors and Λ values are given in figure 4.7.

The associated mean absolute errors observed with PBE and PBE0 are much larger, taking values of 1.38 and 0.43 eV respectively. Notably CAM-B3LYP is able to repair the deficiencies observed with standard functionals. The general improvement from PBE to PBE0 to CAM-B3LYP is consistent with the extensive assessment of the previous section, and provides further evidence for the high quality TDDFT predictions from attenuated functionals. The use of sophisticated exchange–correlation functionals such as CAM-B3LYP effectively negates the need for diagnostic tests.

Formally exact TDDFT has been introduced, together with failings that occur in practice due to the use of approximate exchange–correlation functionals. An extensive assessment of the performance of PBE, B3LYP and CAM-B3LYP for the computation of excitation energies has been presented. A measure of the spatial overlap between orbitals involved in a given excitation (Λ) has been proposed, and subsequently used to demonstrate the notable differences between the quality of excitation energy obtained from each of these functionals. The significant variation in quality when the PBE functional is employed can in part be attributed to the failing of this functional when the overlap between the orbitals involved in an excitation drops too low. This is true to a lesser extent with hybrid functionals such as B3LYP. A diagnostic test based on Λ has been proposed to allow the reliability of an excitation to be judged. The diagnostic has been tested for the case of the triazene molecule II. Notably the diagnostic is able to predict the failure of two of the three particularly poorly described excitations in this molecule with PBE. However, it fails to predict the third of these poorly described excitations, which is associated predominantly with an excitation from a localised to a spatially extended orbital. This highlights the need for more sophisticated diagnostic quantities, which account for the spatial extent of an orbital as well as the overlap.

Through the use of the CAM-B3LYP functional, the highlighted deficiencies both of Rydberg and charge-transfer excitations can be repaired. The observed agreement with the high level correlated *ab initio* values for the triazene system is dramatic. CAM-B3LYP is recommended for general use in

the computation of excitation energies. Notably when this functional is employed the need for a diagnostic to test the reliability of an excitation energy is negated for local, Rydberg and CT excitations.

Finally, we also highlighted the ambiguous nature of the term ‘charge-transfer’. The CT excitations in figure 4.3 span a surprisingly wide range of Λ values, the smallest of which are associated with the extended peptide systems. The largest value is associated with DMABN. It is therefore inappropriate to state that local and hybrid functionals fail for CT excitations; the degree of CT—in the sense of how much the occupied and virtual orbitals overlap—must be quantified before judgement can be made.

Further applications of attenuated functionals

Following the introduction of attenuated exchange–correlation functionals in chapter 3, and the extensive discussion of excited states in chapter 4, both attenuated and conventional functionals are applied to other structural, electronic and magnetic properties of interest.

Through a consideration of *trans*-polyacetylene and polyynes, the ability of attenuated functionals to account for the bond-length alternation and band gap in polymeric chains is determined. The band gap is rigorously described through time-dependent DFT excitation energies from the highest occupied to the lowest unoccupied orbital, but is often approximated through the orbital energy gap. The assertion of the interchangeability of the two approaches is tested.

Nuclear magnetic resonance shieldings and chemical shifts are computed for both main-group and transition metal species. The optimised effective potential method is applied for the first time to attenuated functionals. Technical details of computing OEPs are discussed.

I. Polyacetylene and polyynes

5.1 BOND LENGTH ALTERNATION AND BAND GAP

The application of attenuated exchange functionals to chemically relevant problems has attracted a significant amount of interest. This is primarily

due to the improved description of long-range interactions that functionals such as CAM-B3LYP¹⁴⁰ afford, allowing consideration of systems and properties for which conventional exchange–correlation functionals fail due to their treatment of exchange. Functionals partitioning the treatment of exchange into a short-range component primarily described through DFT exchange, and a long-range component primarily described through exact orbital exchange, have been shown to offer improved performance for a variety of properties,^{99,131,145–147,229} such as excited states,^{135,138,146,182,198,199,201,230} electric-field-induced second harmonic generation,²³¹ non-linear optical properties,²³² optical rotation²³³ and reaction barriers.^{139,146} Our own work (see chapters 3 and 4) has highlighted the improved description of reaction barriers and excited states obtained from attenuated functionals, whilst they maintain competitive performance for other thermochemical and geometrical properties.

An area in which hybrid functional accuracy demonstrates a strong system and functional dependence is in the study of polymeric chains, which may include significantly delocalised orbitals, and thus may benefit from an attenuated exchange treatment. See for instance refs. 207 and 234–247 for recent relevant studies. In particular we highlight the work of Jacquemin²⁰⁷ *et al.*, and Yang and Kertesz.²⁴² Jacquemin *et al.* demonstrated the improved description of the bond length alternation (BLA) in short-chain oligomers of *trans*-polyacetylene (PA) afforded by CAM-B3LYP; however they considered neither the infinite limit nor any electronic properties. Yang and Kertesz considered infinite limit BLA and band gaps in PA, but did not consider attenuated functionals. The main focus of that work was polyynes (PY), although technical difficulties prevented infinite limit calculations in that case. Notably the band gaps were estimated through an orbital energy difference rather than as the appropriate TDDFT excitation energies. In this work we shall denote the band gap computed via the orbital energy difference as the highest occupied–lowest unoccupied (HO–LU) gap.

In the following sections we consider the BLA and electronic properties of PA and PY for both oligomers and the infinite limit. We consider explicitly the effect of exact exchange and an attenuated treatment of exchange, the convergence of the oligomer results to the infinite limit, and the validity of approximating TDDFT excitation energies as orbital energy differences for

the case of the HO–LU orbital transitions.

Computational Details

In order to quantify the effect of the treatment of exchange, we consider three exchange–correlation functionals in detail, with selected notable results from other functionals. The first of the functionals we consider is the ubiquitous standard hybrid functional B3LYP, which contains a fixed amount of exact exchange (20%). We also consider the BHHLYP functional,^{74,76,88} which is also a hybrid functional but it contains a fixed 50% of exact orbital exchange. As an attenuated functional we use CAM-B3LYP, although results from alternative parameterisations are discussed to give an indication of the parameter dependence of the properties of interest.

All calculations use the 6-31G(d) basis set, widely used in studies of BLA.^{207,241–245} We note that as the size of the system increases, basis set errors become less pronounced; an analysis of the PA results of refs. 241, 242 and 246 suggests that adding functions to the basis set would at most increase the BLA values by a few tenths of a picometre (a few percent), consistent with ref. 245. For excitation energies and band gaps, we have confirmed that for more than 10 carbon atoms, expanding the basis set to 6-31+G(d) or cc-pVTZ (for results from the latter basis see chapter 4) lowers the values by less than one tenth of an eV. Judging basis set effects in polyynes is more difficult due to the significant linear dependencies. Where comparison is possible with earlier studies, we have confirmed that our results are in excellent agreement with the earlier works,^{207,241,242} to aid in this comparison all B3LYP calculations use the VWN(III)⁶⁸ parameterisation.

Oligomer calculations were performed using a development version of the DALTON program. Geometries were fully optimised using analytic gradients. The effects due to chain termination (with H atoms) are minimised at the centre of the molecule; the measured BLA, defined as the difference between the longest multiple bond and the shortest single bond, therefore occurs at the molecule centre. HO–LU orbital energy gaps and TDDFT excitation energies were then determined at the optimised geometries. The excitation energies of interest are characterised by a transition of a single electron from the HO

orbital to the LU orbital, corresponding to the lowest dipole-allowed transition in each molecule: This is a ${}^1B_u \leftarrow {}^1A_g$ transition in PA, and a ${}^1\Sigma_u^+ \leftarrow {}^1\Sigma_g^+$ transition in PY.

Infinite chain calculations were performed through the use of periodic boundary conditions using a development version of DALTON. This code is based on the general approach of ref. 248. See ref. 205 for full details. Since analytic gradients were unavailable, the geometries were optimised by successive variation of a geometrical parameter and fitting a quadratic curve as a function of that parameter. This procedure was stopped when the energy was converged with respect to variation in all geometrical parameters. HO-LU gaps (band gaps) were again determined at the optimised geometries; TDDFT excitation energies are not presently available for periodic systems.

5.2 POLYACETYLENE (PA)

Figure 5.1 presents the BLA values for PA oligomers containing $4 \leq N \leq 40$ carbon atoms as a function of $1/N$, where N is the number of carbon atoms. Values of BLA from the BHHLYP and CAM-B3LYP functionals are very similar, and notably larger than those obtained from B3LYP. The results highlight the increase in BLA associated with an increase in the amount of exact exchange in a functional; in one case this is through an increase in the exchange mixing factor (BHHLYP) and the other through the use of attenuated exchange. As was argued in ref. 241, CAM-B3LYP yields a very good estimate of the BLA in PA oligomers, since the results are bracketed by MP2 and CCSD values, which are considered (respectively) to be lower and upper bounds on the actual BLA values. Figure 5.1 also presents a value of the BLA for the infinite chain case, (at $1/N = 0$), determined using periodic boundary conditions. For B3LYP it appears likely that there is a minimum in the curve for longer chain lengths; calculations on a 48 carbon chain yield a BLA value marginally below the infinite chain value, supporting the presence of a minimum. Extrapolation to the infinite limit based on short-chain oligomers would therefore be difficult with B3LYP, as evident from the discrepancy between extrapolated and periodic BLA values from refs. 242 and 244. Note our B3LYP oligomer results are in good agreement with those of ref. 241 and our infinite chain

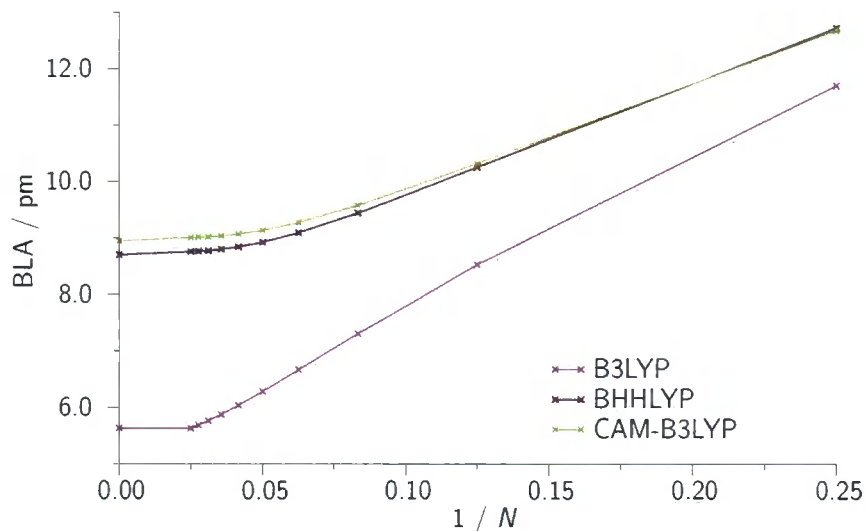


Figure 5.1: BLA in polyacetylene oligomers, as a function of $1/N$.

result is in good agreement with the values in refs. 242 and 244. The convergence from oligomers to infinite chain appears to be monotonic however for BHHLYP and CAM-B3LYP. Compared to the solid state experimental BLA of 7–9 pm,^{249–251} the B3LYP value of 5.6 pm is too short. In contrast the BHHLYP and CAM-B3LYP values, of 8.7 and 8.9 pm respectively, do lie within the experimental range.

Table 5.1 lists excitation energies and HO–LU gaps for PA, as functions of N . Experimental excitations are also presented for chain lengths $4 \leq N \leq 10$. In the case of B3LYP, the TDDFT vertical excitation energies for the transition from the HO orbital to the LU orbital are rather close to the corresponding HO–LU gaps; the agreement improves with increasing chain length. This is consistent with the observations of Ma²⁵² *et al.*, demonstrating the validity of approximating the PA excitation energy via the HO–LU gap with B3LYP. For both BHHLYP and CAM-B3LYP however, the values are dissimilar even for the longest chains, indicating that the approximation is invalid.

Also presented in table 5.1 is the HO–LU gap from infinite chain calculations. The convergence of the gaps from oligomers to the infinite case is shown in figure 5.2. Given the aforementioned similarity between B3LYP HO–LU gaps and the corresponding excitation energies, the infinite chain B3LYP HO–

Table 5.1: TDDFT excitation energies and HO-LU gaps (in eV) in polyacetylene oligomers, as a function of the number of carbon atoms, N .

N	B3LYP	BHhLYP	CAM-B3LYP	Expt. ^a
Excitation energy				
4	6.04	6.36	6.29	5.92
6	4.87	5.26	5.19	4.95
8	4.14	4.56	4.51	4.41
10	3.63	4.08	4.04	4.02
12	3.25	3.73	3.71	
16	2.72	3.26	3.25	
20	2.37	2.96	2.97	
24	2.12	2.75	2.78	
28	1.93	2.61	2.65	
32	1.78	2.51	2.55	
36	1.67	2.43	2.48	
40	1.58	2.37	2.42	
HO-LU gap				
4	5.62	8.18	8.56	
6	4.49	6.84	7.24	
8	3.79	6.02	6.43	
10	3.32	5.46	5.88	
12	2.98	5.07	5.49	
16	2.52	4.54	4.97	
20	2.23	4.22	4.66	
24	2.02	4.01	4.45	
28	1.88	3.86	4.31	
32	1.77	3.75	4.20	
36	1.68	3.67	4.13	
40	1.61	3.61	4.07	
∞	1.19	3.24	3.71	

^a ref. 212–214, 253

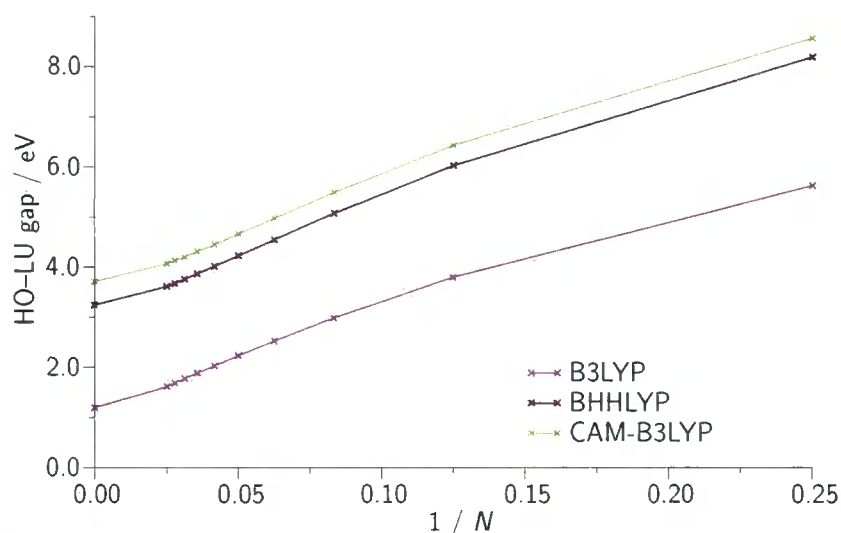


Figure 5.2: HO–LU gap in polyacetylene oligomers, as a function of $1/N$.

LU gap may be taken to be a reasonable estimate of the B3LYP excitation energy in the infinite chain. The value obtained (1.2 eV) is below the experimental optical gap of 1.5–1.8 eV,^{254,255} consistent with the underestimated BLA; experimentally the band gap may be related²⁴² to the degree of bond length alternation. The infinite chain HO–LU gaps are much larger with the BHHLYP and CAM-B3LYP functionals, at 3.2 and 3.7 eV respectively; however, as noted above, these will not resemble the associated excitation energies.

One approach for approximating the excitation energy for the infinite chain is to consider the relationship between excitation energies and HO–LU gaps for the oligomers, and extrapolate based on the value of the infinite chain HO–LU gap. Investigation of extrapolated values obtained from a variety of polynomial fits to the oligomer quantities highlights the relative insensitivity to the choice of fitting function, and to whether all oligomer results are included or just those pertaining to the longer oligomers. For simplicity we therefore choose to extrapolate to the infinite chain excitation energy based on fitting a quadratic curve to each data set. This is illustrated in figure 5.3 for CAM-B3LYP. The infinite chain excitation energies obtained from this procedure are 1.1, 2.0 and 2.1 eV for B3LYP, BHHLYP and CAM-B3LYP, respectively. For B3LYP, this value is close to the value estimated above,



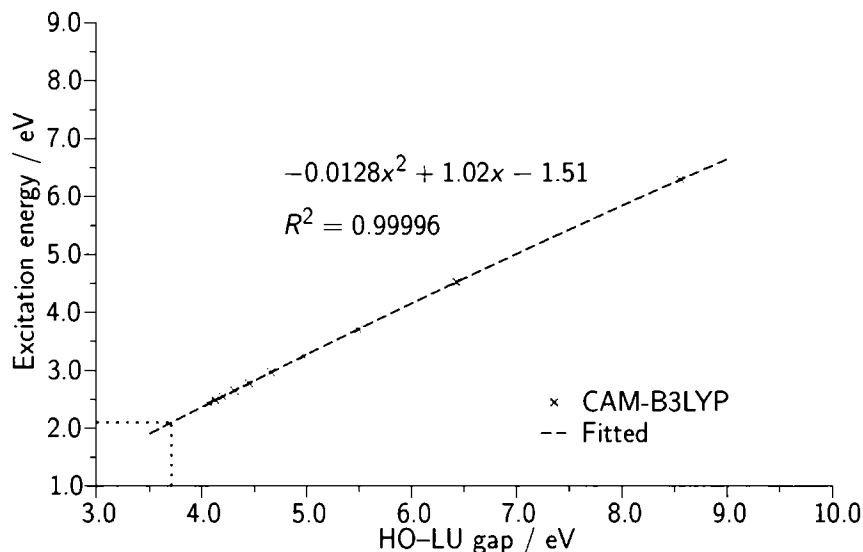


Figure 5.3: CAM-B3LYP extrapolation of TDDFT excitation energy for polyacetylene.

consistent with the argument that for this system B3LYP HO-LU gaps and excitation energies are very similar to one another. The BHHLYP and CAM-B3LYP values are noticeably larger than the corresponding B3LYP excitation energy, and slightly overestimate the experimental range of 1.5–1.8 eV.

Figure 5.4 presents the evolution of oligomer excitation energies for the three functionals we consider, together with the estimated infinite chain results from above (at $1/N = 0$). A simple linear extrapolation to the infinite chain case would clearly underestimate the value obtained from our extrapolation procedure, and in the case of B3LYP this would severely underestimate the observed band gap, consistent with the results of ref. 256.

The CAM-B3LYP functional has 65% exact orbital exchange at long-range. We consider the performance of the CAM(0.2, 0.8, 0.4) and CAM(0.0, 1.0, 0.4) functionals as examples of functionals which exhibit the correct long-range behaviour. The behaviour of these functionals at short-range does not resemble CAM-B3LYP or the other recommended parameterisations of chapter 3. Consistent with our previous observations regarding the geometry performance of functionals satisfying the formally correct long-range behaviour, the BLA results from these two methods are poor, converging rapidly with N

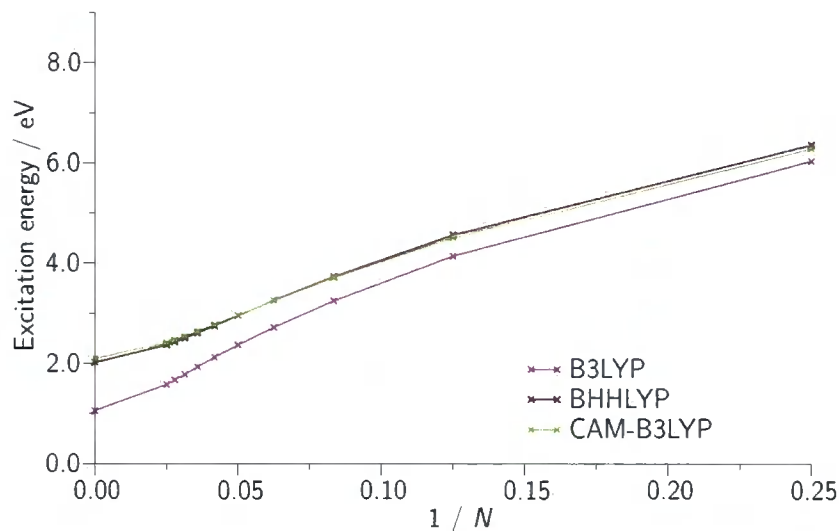


Figure 5.4: TDDFT excitation energy in polyacetylene oligomers, as a function of $1/N$.

to values of 10.9 and 10.7 pm respectively, which are significantly too large. The use of these functionals cannot be recommended for the properties under consideration here.

5.3 POLYNYNE (PY)

Figure 5.5 presents the BLA values of PY oligomers containing N carbon atoms as a function of $1/N$, for $4 \leq N \leq 24$. Results for longer chains are not presented due to convergence difficulties. Again BHHLYP and CAM-B3LYP yield similar BLA values, although the ordering is reversed compared to PA. The BLA values from these functionals are noticeably larger than from B3LYP. Convergence to the infinite chain values for BHHLYP and CAM-B3LYP resembles that observed for PA. For B3LYP the behaviour is different to that observed with PA; however this may simply reflect the shorter maximum chain length reached by the oligomers in this case. The infinite chain BLA values obtained with BHHLYP and CAM-B3LYP are 13.3 and 13.1 pm respectively, which are both close to the estimated value of 13 pm from ref. 242. As in the case of PA, the B3LYP BLA value of 8.8 pm is much smaller.

Table 5.2 gives excitation energies and HO-LU gaps in PY, as functions of

Table 5.2: TDDFT excitation energies and HO-LU gaps (in eV) in polyne oligomers, as a function of the number of carbon atoms, N .

N	B3LYP	BHLYP	CAM-B3LYP	Expt. ^a
Excitation energy				
4	8.51	8.98	8.79	7.54
6	6.87	7.42	7.25	6.77
8	5.83	6.43	6.29	5.98
10	5.10	5.74	5.62	5.33
12	4.56	5.24	5.13	4.99
14	4.13	4.86	4.76	4.67
16	3.79	4.56	4.48	4.41
18	3.52	4.33	4.25	4.19
20	3.29	4.14	4.07	4.02
22	3.09	3.99	3.92	3.87
24	2.93	3.86	3.80	3.74
HO-LU gap				
4	6.46	9.21	9.48	
6	5.14	7.71	8.00	
8	4.36	6.81	7.10	
10	3.83	6.22	6.52	
12	3.45	5.80	6.10	
14	3.17	5.50	5.80	
16	2.95	5.27	5.57	
18	2.78	5.09	5.39	
20	2.64	4.95	5.25	
22	2.52	4.83	5.13	
24	2.43	4.74	5.04	
∞	1.59	4.04	4.33	

^a refs. 257–259

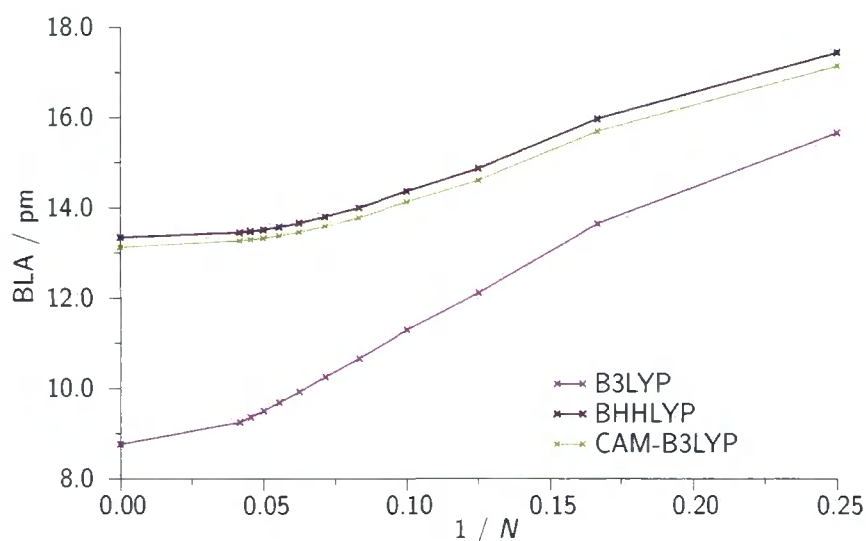


Figure 5.5: BLA in polyacetylene oligomers, as a function of $1/N$.

N , together with reference experimental values. For the larger chain lengths where basis set deficiencies are less pronounced, the BHHLYP and CAM-B3LYP excitation energies are in improved agreement with experiment over those obtained from B3LYP. Contrasting with the results of PA, the HO–LU gap is a poor approximation to the excitation energy for all three functionals. Also shown in table 5.2 is the HO–LU gap from the infinite chain calculations. Convergence of this quantity from oligomer to infinite chain is shown in figure 5.6. The behaviour of the gaps exhibits a similar trend to the PA case, with values of 1.6, 4.0 and 4.3 eV obtained from B3LYP, BHHLYP and CAM-B3LYP respectively.

Application of the same quadratic extrapolation procedure, as in the previous section, to the infinite chain yields estimated excitation energies of 1.6, 2.9 and 2.9 eV for B3LYP, BHHLYP and CAM-B3LYP. An example of the extrapolation is presented for CAM-B3LYP in figure 5.7. The convergence of the excitation energies to the extrapolated infinite values is shown in figure 5.8. Of interest is the similarity between the B3LYP extrapolated excitation energy and the infinite chain HO–LU gap, suggesting that this approximation is more reasonable in the limit for PY. As with PA, the B3LYP value is significantly below the experimental optical gap, which is estimated to be

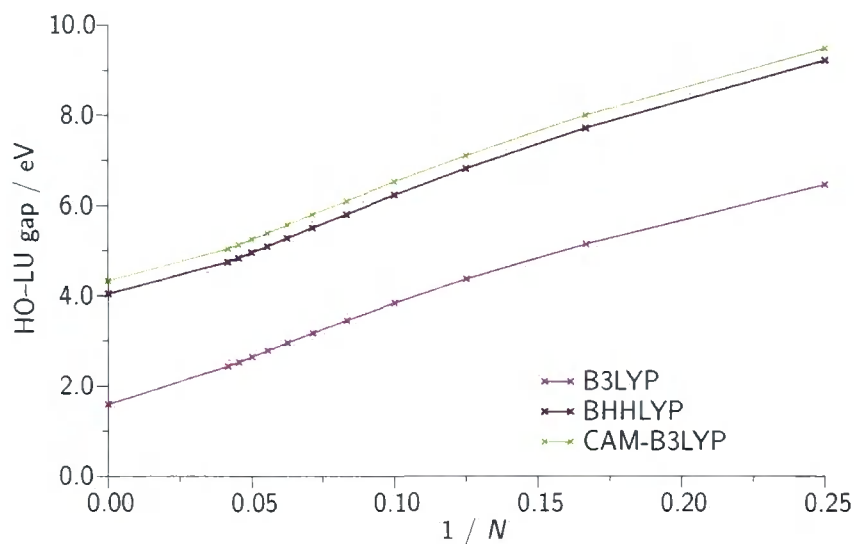


Figure 5.6: HO-LU gap in polyacetylene oligomers, as a function of $1/N$.

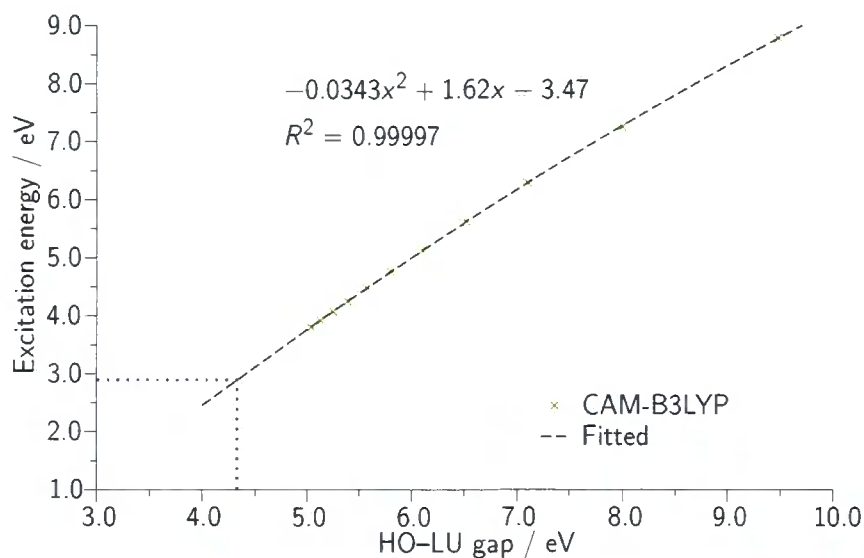


Figure 5.7: CAM-B3LYP extrapolation of TDDFT excitation energy for polyene.

2.3–2.4 eV in ref. 242 by using a linear extrapolation of experimental oligomer optical absorption results. The BHHLYP and CAM-B3LYP values are higher than this estimate, but note the above comment (that was also made in ref. 256) regarding the validity of the linear extrapolation used to determine this estimate.

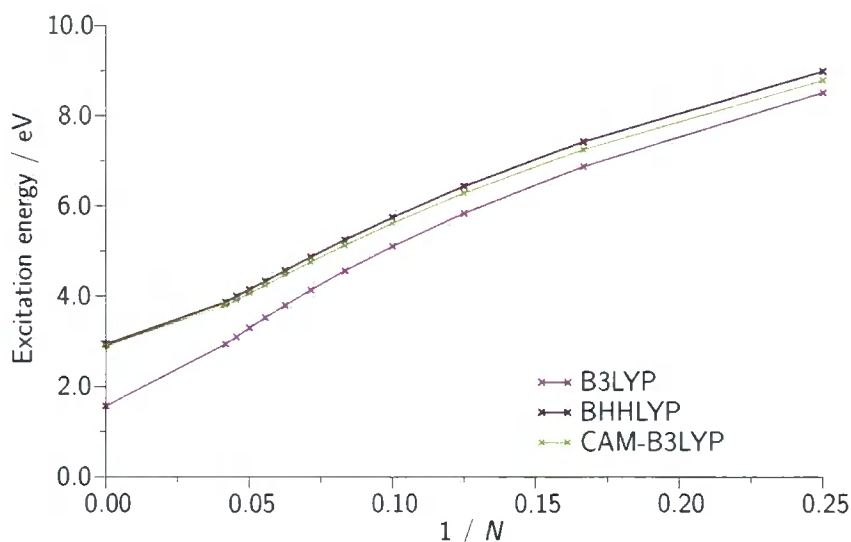


Figure 5.8: TDDFT excitation energy in polyacetylene oligomers, as a function of $1/N$.

Whilst the HO–LU gap varies significantly as the amount of exact exchange in the functional varies, the associated excitation energy is relatively insensitive. The gap and excitation energy are similar for long-chain PA and infinite limit PY when B3LYP is used, but are notably different for BHHLYP and CAM-B3LYP where the amount of exact exchange in the functional is larger; the HO–LU gap is then larger than the associated excitation energy. Conversely we have confirmed that the HO–LU gap is smaller than the excitation energy in the case of using a GGA functional with no exact exchange. These observations are consistent with the finding of Yang and Kertesz²⁴² that the BHHLYP HO–LU gap, despite being evaluated at the good quality BHHLYP geometry, overestimates the experimental optical gap, whereas the B3LYP HO–LU gap, evaluated at the BHHLYP geometry, is more accurate. Such behaviour would not be observed if the experimental optical gap were computed through the rigorous excitation energy calculation, as undertaken above. The need to combine two functionals to obtain results in line with experiment can be avoided by using either BHHLYP or CAM-B3LYP at their respective geometries, providing the optical gap is computed in the theoretically rigorous manner.

II. Nuclear magnetic resonance

5.4 EVALUATING MAGNETIC RESPONSE

Attenuated functionals have primarily been applied to time-dependent response properties. There have been *virtually no applications* of attenuated functionals to the calculation of static magnetic response properties, despite the considerable interest in obtaining accurate results for such properties. The aim of this brief section is to determine the performance of CAM-B3LYP when applied to NMR shielding constants and chemical shifts.

A key observation²⁶⁰ is that for such properties the performance of orbital-dependent exchange–correlation functionals is often poor, except when these properties are evaluated from a multiplicative exchange–correlation potential. GGA functionals will therefore often yield more accurate results than orbital-dependent functionals in the evaluation of shielding constants and chemical shifts. This unusual observation may be understood by considering the differences in the computation of second-order magnetic response parameters between GGA and orbital-dependent functionals.

For GGA functionals the magnetic Hessian, which determines the imaginary component of the orbital response to a static magnetic perturbation, is diagonal and consequently the response parameters are determined in an uncoupled manner using the Kohn–Sham molecular orbitals and orbital energies (see for instance the discussion in ref. 260). Standard implementations of orbital-dependent functionals have contributions to the orbital equations that are derived from a minimisation with respect to the orbitals (as in Hartree–Fock theory) rather than with respect to the density, resulting in a non-diagonal magnetic Hessian. If however a multiplicative potential is derived by minimising all of the contributions with respect to the density, the magnetic Hessian will be diagonal as in the GGA case, allowing the evaluation of the response through the same uncoupled equations.

Wilson and Tozer²⁶⁰ used the Zhao–Morrison–Parr²⁶¹ method to determine multiplicative potentials associated with hybrid functionals for a series of small, highly correlated molecules containing main-group atoms. For these systems the resulting shieldings were two to three times more accurate than

those calculated in the conventional manner.

A multiplicative potential may also be obtained by applying the optimised effective potential (OEP) method as introduced in chapter 1. Cohen²⁶² *et al.* have demonstrated that when using the OEP method, essentially identical results to those of Wilson and Tozer are observed. Other notable improvements have been observed in the calculation of chemical shifts,²⁶³ magnetisabilities²⁶⁴ and rotational g-tensors²⁶⁵ when multiplicative potentials are used. The OEP method has also been applied to transition metal shielding constants and chemical shifts.²⁶⁶

Computational approach

The optimised effective potential method involves the determination of a potential, which is the same for each electron, and with respect to which the energy is stationary. The approach we use, due to Yang and Wu,⁹⁷ rewrites the Kohn–Sham potential $v_s(\mathbf{r})$ as

$$v_s(\mathbf{r}) = v(\mathbf{r}) + v_{\text{Ref}}(\mathbf{r}) + \sum_t b_t g_t(\mathbf{r}), \quad (5.1)$$

the sum of the external potential, a fixed reference potential and an expansion in a Gaussian basis set $\{g_t(\mathbf{r})\}$. The unknown parameters \mathbf{b} are determined by directly minimising the total electronic energy with respect to these parameters, using an approximate Newton scheme²⁶⁷ that requires the inverse of the Hessian matrix of this minimisation. In order to obtain the most reliable approximation to the inverse Hessian, some regularisation is necessary in order to filter out near-singular contributions that can lead to numerical instabilities. We use the truncated singular value decomposition (TSVD) approach, which removes terms in the Hessian whose magnitude lies below a cut-off. For our OEP calculations we use a cut-off of 1×10^{-8} .

There is equally an issue that unphysical, oscillatory potentials may be found if the minimisation is pushed too far, with the energy corresponding to highly oscillatory potentials collapsing to that obtained through evaluation with a non-local potential.^{268,269} We have confirmed that the potentials obtained in our calculations do not exhibit unphysical structure.

Following ref. 266 the reference potential we use is given by

$$v_{\text{Ref}}(\mathbf{r}_1) = \left(1 - \frac{\alpha - \beta}{n}\right) \int d\mathbf{r}_2 \frac{\rho(\mathbf{r}_2)}{|\mathbf{r}_1 - \mathbf{r}_2|} + (1 - \alpha - \beta)(3\pi)^{\frac{1}{3}} \rho^{\frac{1}{3}}(\mathbf{r}_1). \quad (5.2)$$

It corresponds to a combination of the Fermi–Amaldi potential²⁷⁰ and the potential associated with LSDA exchange, and is designed to give the correct long-range behaviour of the potential for a given functional. This is evaluated using the density obtained from a conventional DFT calculation for the respective functional under consideration.

We consider three applications. The 21 small, highly correlated molecules of ref. 260 are examined to assess the performance for main-group systems. Applicability to first-row transition metal complexes is assessed using the molecules in ref. 266. The hydrogen-bonded formaldehyde systems of ref. 271 are also considered as an interesting application. A suitable basis set is required for the expansion of both the orbitals and the potential (corresponding to the $\{g_t(\mathbf{r})\}$). To provide a balanced description we use the same basis set for the expansion of the potential as used for the orbitals. For the shielding constants in the 21 main-group molecules, we use the Huzinaga IGLO-IV basis set,^{272,273} near-experimental geometries are used following ref. 260. The shielding constants and chemical shifts in the hydrogen-bonded formaldehyde systems are computed using the aug-cc-pVTZ basis set on all of the atoms; we have confirmed that the results are unaffected (to within 1 ppm) by the use of this basis over the mixed basis set used in the earlier study. To allow comparison with the *ab initio* reference values of ref. 271 the CCSD geometries of that reference are used for all of the structures. Further the transition metal systems of ref. 266 are considered using the cc-pVTZ basis set on both the metal and the ligands; again we use the geometries of that reference. We use an extensive numerical integration grid for all systems, and gauge-invariant atomic orbitals.^{274–276} All calculations are performed with a development version of the DALTON program.

Three functionals are applied to these systems. The KT2²⁷⁷ GGA functional is applied as it was specifically designed for the calculation of accurate shielding constants and chemical shifts. Also considered is the widely used B3LYP hybrid functional, with the results computed both conventionally and through the Yang–Wu OEP method. As a first application of an attenuated

functional to magnetic properties, CAM-B3LYP results are considered, again computed both conventionally and through the OEP method.

One method for judging the accuracy of the OEP calculations is to apply the OEP procedure to a GGA functional. Since the response equations are already uncoupled with GGA functionals, an exact OEP calculation should yield identical results. Any discrepancy between the conventional and OEP-GGA results can therefore be attributed to inaccuracies introduced in the practical OEP calculation. We examine this dependence for the KT2 functional for all of the molecules considered.

5.5 FUNCTIONAL PERFORMANCE

We denote results obtained from the OEP method by an O- prefix; for instance the KT2 results obtained within the OEP formalism are denoted O-KT2. Table 5.3 presents isotropic shielding constants for 21 main-group molecules. The KT2 results are in good agreement with the O-KT2 results, which indicates that the reference potential and the basis set for the expansion of the potential are sufficient for an accurate description of the optimised effective potential. Notably the errors from KT2 are significantly smaller than the associated errors from B3LYP and CAM-B3LYP, highlighting the poor performance of hybrid and attenuated functionals when there is no rigorous associated potential. Applying the OEP method to B3LYP yields significantly improved results over the non-OEP values. Interestingly there are large changes for molecules such as O_3 , but very small changes for molecules such as H_2O . A similar observation is made for CAM-B3LYP. The O-B3LYP and O-CAM-B3LYP results are quite similar, although the mean absolute error from the latter is marginally smaller. Neither approach yields errors comparable with those from KT2 however.

The exchange–correlation potential for N_2 obtained with O-CAM-B3LYP is plotted in figure 5.9. There is no unphysical structure observed in the potential. Similar, physically sensible potentials are obtained for the other functionals and molecules considered.

The CCSD(T) reference results of table 5.4 show the effect of hydrogen bonding on a system consisting of a formaldehyde molecule complexed with

Table 5.3: NMR isotropic shielding constants (in ppm) for main-group molecules compared to experimental values.

		KT2	O-KT2	B3LYP	O-B3LYP	CAM-B3LYP	O-CAM-B3LYP	Expt. ^a
HF	F	411.5	411.4	411.1	413.7	414.0	416.2	419.7
H ₂ O	O	329.5	329.5	327.7	329.9	331.3	332.9	357.6
CH ₄	C	195.1	194.9	188.7	188.3	191.8	190.0	198.4
CO	C	6.8	5.7	-19.0	-8.5	-20.2	-7.7	2.8
	O	-57.1	-57.9	-81.1	-53.0	-79.8	-48.4	-36.7
N ₂	N	-60.4	-61.5	-92.3	-71.1	-92.8	-69.1	-59.6
F ₂	F	-209.1	-218.2	-250.4	-222.2	-238.4	-216.4	-192.8
O ₃	O	-1279.6	-1294.1	-1693.3	-1245.5	-1761.6	-1188.1	-1290.0
	O'	-810.6	-817.1	-1129.1	-828.1	-1231.5	-822.1	-724.0
PN	P	52.9	48.9	-50.1	18.3	-66.0	32.6	53.0
	N	-365.9	-367.4	-431.7	-365.7	-433.1	-347.6	-349.0
H ₂ S	S	735.0	734.1	700.5	703.8	706.8	710.4	752.0
NH ₃	N	264.7	264.7	259.9	260.7	263.0	263.0	273.3
HCN	C	85.7	85.1	69.1	74.5	68.0	74.6	82.1
	N	-19.7	-20.8	-49.5	-31.0	-49.9	-28.0	-20.4
C ₂ H ₂	C	120.1	119.6	106.9	109.9	106.4	109.7	117.2
C ₂ H ₄	C	63.0	62.4	47.2	51.4	47.4	51.7	64.5
H ₂ CO	C	-5.0	-5.9	-24.4	-20.3	-25.6	-22.0	-4.4
	O	-379.6	-382.9	-452.4	-378.7	-461.0	-367.8	-375.0
N ₂ O	N	102.0	101.4	81.9	96.0	80.9	97.7	99.5
	N'	11.5	10.9	-11.4	2.2	-14.7	2.2	11.3
	O	177.2	176.8	173.1	189.3	179.3	196.1	200.5
CO ₂	C	62.7	62.3	48.9	53.0	48.2	53.0	58.8
	O	221.3	220.9	213.5	224.0	217.6	227.8	243.4
OF ₂	O	-533.7	-542.2	-583.1	-552.1	-561.0	-541.7	-473.1
H ₂ CN ₂	C	167.1	167.0	160.0	161.5	162.2	162.7	164.5
	N	-42.1	-42.9	-60.1	-52.8	-54.3	-51.1	-43.4
	N'	-138.9	-140.7	-192.7	-148.4	-206.9	-139.1	-149.0
HCl	Cl	750.7	751.8	711.7	719.1	709.7	712.9	952.0
SO ₂	S	-148.5	-154.2	-262.5	-203.0	-279.7	-199.7	-126.0
	O	-251.5	-253.9	-283.5	-225.4	-276.6	-208.3	-205.0
PH ₃	P	598.5	597.3	561.8	562.6	567.6	568.2	599.9
<i>d</i>		-17.1	-19.3	-69.0	-26.6	-73.8	-20.5	
<i>d</i>		19.8	20.8	69.0	29.4	73.8	28.1	

^a ref. 260 and references therein.

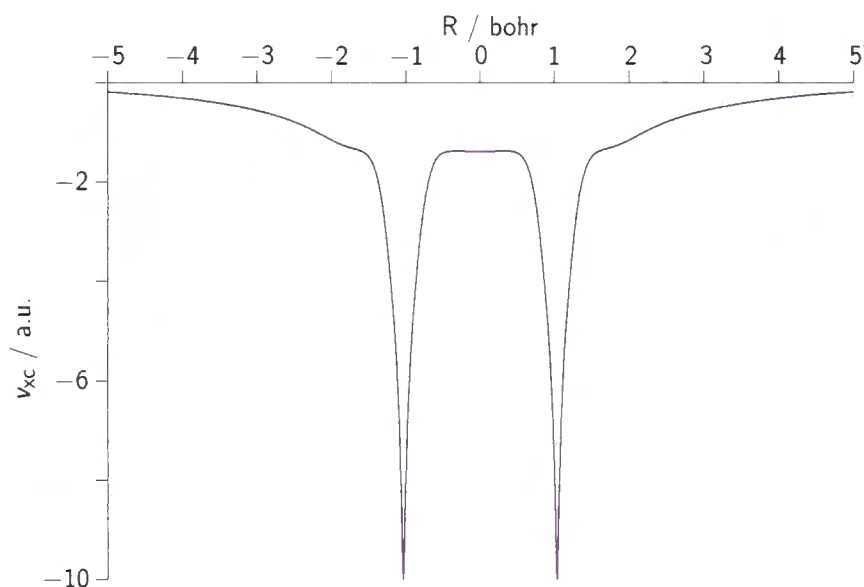


Figure 5.9: The N_2 exchange–correlation potential v_{xc} obtained from an O-CAM-B3LYP calculation, with the nuclei at ± 1.0375 bohr.

Table 5.4: NMR isotropic shielding constants and chemical shifts (in ppm) of complexed formaldehyde and formaldehyde compared with reference CCSD(T) values

		KT2	O-KT2	B3LYP	O-B3LYP	CAM-B3LYP	O-CAM-B3LYP	CCSD(T) ^a
Shielding constants								
H ₂ CO	O	-300.8	-309.5	-362.1	-299.5	-365.2	-288.9	-298.7
+2H ₂ O	C	-6.0	-9.8	-28.6	-23.3	-30.0	-24.9	0.8
H ₂ CO	O	-353.1	-362.7	-426.2	-352.4	-434.3	-342.1	-350.6
	C	6.3	2.8	-15.0	-10.4	-16.0	-12.2	13.0
Chemical shifts								
	O	52.3	53.2	64.0	52.9	69.2	53.2	52.0
	C	-12.3	-12.5	-13.7	-12.9	-14.0	-12.6	-12.2

^a ref. 271.

two water molecules, by comparison with values for an isolated formaldehyde molecule. The values for the isolated molecule are considered at the formaldehyde structure from the complex (we have confirmed that the effect due to relaxation of the structure is small compared to the effect of the hydrogen bonding). In table 5.4 the chemical shifts refer to the difference between the complexed environment and the isolated environment.

The KT2 results demonstrate excellent agreement for the oxygen shielding constants compared to CCSD(T). Whilst the absolute values of the carbon shieldings are less accurately reproduced, the behaviour of the shifts is very similar to the CCSD(T) values. We again have good agreement between the KT2 and O-KT2 values, suggesting there is sufficient flexibility in the basis set used for the expansion of the potential.

Both the conventional B3LYP and CAM-B3LYP results agree less well with the CCSD(T) values; the shifts are also less well represented. By applying the OEP method, the results for both functionals improve significantly, with both more accurate shieldings and shifts obtained. The O-CAM-B3LYP shieldings are slightly less accurate than the O-B3LYP results, but the shifts are comparable.

For main-group applications, the use of the OEP method yields results from hybrid and attenuated functionals that are closer to accurate reference values; importantly O-CAM-B3LYP provides results of a similar quality to O-B3LYP, despite their different behaviour for other properties.

Obtaining agreement between the KT2 and O-KT2 shielding constants for the transition metal systems (see table 5.5) is more difficult than in the main-group systems. However, with the cc-pVTZ basis set used the discrepancy is in all cases less than 30 ppm, which represents a small percentage error. The exchange–correlation potential obtained from an O-CAM-B3LYP calculation on CrO_4^{2-} is plotted in figure 5.10 to illustrate that smooth, physically sensible potentials are obtained.

There is for all functionals a large discrepancy with respect to the experimental chemical shifts; this may in part be due to the difficulties of comparing with experimental data. Both conventional B3LYP and CAM-B3LYP perform less well than KT2. All the functionals yield significant errors for the manganese-containing systems. The use of OEPs does improve

Table 5.5: Transition metal NMR isotropic shielding constants and chemical shifts δ (in ppm) compared with experimental chemical shifts $\delta_{\text{Expt.}}$

	KT2	O-KT2	B3LYP	O-B3LYP	CAM-B3LYP	O-CAM-B3LYP	$\delta_{\text{Expt.}}^a$
TiCl ₄	-947.8	-955.7	-1000.0	-833.6	-975.8	-731.6	
TiCl ₃ Me	-1397.1	-1422.6	-1479.1	-1237.8	-1478.3	-1123.1	
δ	449.3	466.8	479.0	404.1	502.5	391.4	613
Cr(CO) ₆	-644.4	-670.0	-1058.5	-571.0	-1160.1	-506.8	
CrO ₄ ²⁻	-2587.1	-2596.5	-3141.1	-2479.2	-3203.5	-2424.7	
δ	1942.8	1926.5	2082.6	1908.3	2043.4	1918.0	1795
MnO ₄ ⁻	-3817.5	-3822.1	-4995.8	-3724.9	-5191.6	-3696.3	
Mn(CO) ₆	-1808.0	-1841.9	-2713.2	-1639.9	-2946.0	-1531.3	
δ	-2009.5	-1980.2	-2282.5	-2084.9	-2245.6	-2165.0	-1445
VOCl ₃	-1901.8	-1905.6	-2257.2	-1784.7	-2311.3	-1695.7	
VF ₅	-1174.7	-1174.0	-1245.2	-1032.0	-1197.6	-963.3	
δ	-727.1	-731.5	-1012.0	-752.7	-1113.8	-732.5	-895
VOF ₃	-1205.4	-1206.4	-1375.6	-1088.1	-1383.6	-1032.5	
δ	-696.5	-699.2	-881.6	-696.6	-927.8	-663.3	-757
$ d $	221	207	300	233	310	264	

^a ref. 266 and references therein.

the mean absolute error for O-B3LYP and O-CAM-B3LYP, however for the titanium-containing systems the chemical shift becomes significantly less accurate. Overall the performance of O-B3LYP is similar to that of KT2; O-CAM-B3LYP performs less well, but still represents an improvement over the conventional CAM-B3LYP results. The effect of using OEPs is large for all of the transition metal shielding constants. Importantly, the application of OEPs to attenuated functionals yields similar trends to those observed with conventional hybrids, with in many cases the performance of O-CAM-B3LYP improving over the conventional approach.

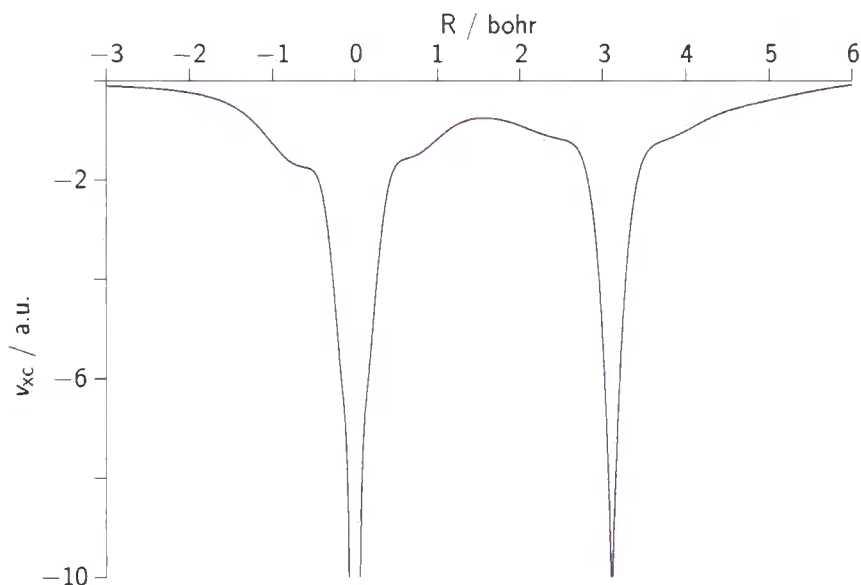


Figure 5.10: The CrO_4^{2-} exchange–correlation potential v_{xc} obtained from an O-CAM-B3LYP calculation, plotted along a Cr–O bond with the Cr nucleus at the origin and the O nucleus at 3.118 bohr.

Summary

This chapter has applied attenuated functionals to bond length alternation, further excitation energies and static magnetic properties. BLA values and HO–LU gaps have been determined using both finite oligomer and infinite chain calculations (using periodic boundary conditions), for three representative exchange–correlation functionals. TDDFT excitation energies have been determined for the oligomers, and have been extrapolated to the infinite case through a consideration of their relationship to the HO–LU gaps. Both CAM-B3LYP and BHLYP give BLA values and excitation energies that are larger and more accurate than those obtained from B3LYP. The approach of the infinite chain values of both the BLA and band gap has been discussed, highlighting the differing conclusions that would in some cases be drawn depending on the extrapolation used. The extent to which the band gap (computed via the associated excitation energy) may be approximated by HO–LU gaps has been considered; in general this approximation is poor, particularly for func-

tionals containing large amounts of exact exchange. Our previous work has established CAM-B3LYP as a good quality, all round functional that exhibits improved long-range behaviour over conventional approximations. This study of PA and PY supports this observation.

In the first application of the OEP method to attenuated functionals, we have considered the performance of CAM-B3LYP for a number of NMR shielding constants and chemical shifts. In order to justify the use of OEP, rather than conventional evaluation of NMR parameters for attenuated functionals, the effect of the OEP on general orbital-dependent functionals has been discussed. We consider the computation of NMR isotropic shielding constants and chemical shifts in main-group and transition metal systems. For the 21 small main-group molecules considered, results using O-CAM-B3LYP are comparable with existing approaches, and yield significantly improved results over the conventional evaluation of NMR parameters.

Equally the application to the model formaldehyde systems shows that both hybrid and attenuated functionals can give GGA quality results when the OEP method is used; conventional results are notably less accurate. For the transition metal systems however, none of the functionals considered can give rise to accurate chemical shifts, although the OEP results are in better agreement with experiment than the conventional results.

The results highlight that the behaviour of O-CAM-B3LYP is similar to that of standard hybrid functionals such as O-B3LYP when evaluated through the OEP procedure, despite the significantly differing performance observed for other response properties. Since O-CAM-B3LYP performs similarly to hybrid functionals such as O-B3LYP, there remains significant room for improvement. The further development of attenuated functionals should consider the rigorous computation of NMR through the OEP method.

Adiabatic connection

The Hellmann–Feynman theorem provides a formally exact expression for the exchange–correlation energy, as an integral over a functional W_λ , which serves to connect the energies of a fictitious non-interacting system ($\lambda = 0$) with the physical, interacting system ($\lambda = 1$). Several approximate exchange–correlation functionals, such as BHHLYP and more recently the MCY functionals, have been derived by approximating W_λ using simple mathematical forms with (possibly) approximate input data. To enable the accuracy of an approximate W_λ form to be judged, essentially exact data is determined from FCI calculations, corresponding to the value and gradient of W_λ when $\lambda = 0$, and the value when $\lambda = 1$. When this data is used as input to approximate W_λ forms, the only approximation is due to the form itself.

This procedure is applied to a number of approximate forms, considering two challenging problems for conventional DFT. First the singlet ground state potential energy curve of the H_2 molecule in a restricted formalism is considered, which is the famous and challenging example of non-dynamic electron correlation. Second the helium isoelectronic series from H^- – Ne^{8+} is considered.

Following the success of some of the forms in describing these problems, we consider whether it is possible to achieve similar accuracy from more easily obtainable input data, and the applicability to a many-electron system.

The Hellmann–Feynman theorem states that for some parameter λ in a Hamiltonian,

$$\frac{\partial E_\lambda}{\partial \lambda} = \langle \psi_\lambda | \frac{\partial \hat{H}_\lambda}{\partial \lambda} | \psi_\lambda \rangle, \quad (6.1)$$

providing the other parameters that determine the wavefunction are either independent of λ or are variationally optimised with respect to λ . This may for instance be used to calculate molecular forces in origin-independent basis sets, or the response of a system to an applied field.

In order to derive the adiabatic connection formalism,^{81–83,93,278–281} consider the n -electron Hamiltonians defined by

$$\hat{H}_\lambda = \hat{T} + \lambda \hat{V}_{ee} + \sum_i v_\lambda(\mathbf{r}_i) \quad (6.2)$$

where λ is a coupling strength parameter which scales the electron–electron interaction

$$\hat{V}_{ee} = \sum_{i,j>i} \frac{1}{r_{ij}}; \quad (6.3)$$

the case with $\lambda = 0$ corresponds to the fictitious non-interacting Kohn–Sham reference system, and the case with $\lambda = 1$ corresponds to the physical interacting system. The final term is the (λ -dependent) external potential, through which the density is held fixed at the density of the interacting system.⁸³ If we apply the Hellmann–Feynman theorem to this Hamiltonian, we obtain

$$\frac{\partial}{\partial \lambda} \langle \psi_\lambda | \hat{H}_\lambda | \psi_\lambda \rangle = \langle \psi_\lambda | \frac{\partial}{\partial \lambda} \left(\sum_i v_\lambda(\mathbf{r}_i) \right) + \hat{V}_{ee} | \psi_\lambda \rangle, \quad (6.4)$$

where ψ_λ is the wavefunction associated with the system with Hamiltonian \hat{H}_λ . Next assume that the electron–electron interaction is turned on smoothly by varying λ from 0 to 1, which corresponds to transforming the non-interacting

reference system into the physical system:

$$\int_0^1 d\lambda \frac{\partial}{\partial \lambda} \langle \psi_\lambda | \hat{H}_\lambda | \psi_\lambda \rangle = \int_0^1 d\lambda \langle \psi_\lambda | \frac{\partial}{\partial \lambda} \left(\sum_i v_\lambda(\mathbf{r}_i) \right) + \hat{V}_{ee} | \psi_\lambda \rangle \quad (6.5)$$

$$\begin{aligned} \langle \psi_1 | \hat{H}_1 | \psi_1 \rangle - \langle \psi_0 | \hat{H}_0 | \psi_0 \rangle &= \langle \psi_1 | \left(\sum_i v_1(\mathbf{r}_i) \right) | \psi_1 \rangle - \langle \psi_0 | \left(\sum_i v_0(\mathbf{r}_i) \right) | \psi_0 \rangle \\ &\quad + \int_0^1 d\lambda \langle \psi_\lambda | \hat{V}_{ee} | \psi_\lambda \rangle \end{aligned} \quad (6.6)$$

$$E_1 - E_0 = \int d\mathbf{r} \rho(\mathbf{r}) v_1(\mathbf{r}) - \int d\mathbf{r} \rho(\mathbf{r}) v_0(\mathbf{r}) + \int_0^1 d\lambda \langle \psi_\lambda | \hat{V}_{ee} | \psi_\lambda \rangle, \quad (6.7)$$

which holds under the assumption that the density is held fixed for all values of λ .⁸³ When $\lambda = 0$, the wavefunction is the exact non-interacting Kohn–Sham single Slater determinant ψ_0 . Since for $\lambda = 0$

$$E_0 = \langle \psi_0 | \hat{T} | \psi_0 \rangle + \int d\mathbf{r} \rho(\mathbf{r}) v_0(\mathbf{r}) \quad (6.8)$$

$$= T_s + \int d\mathbf{r} \rho(\mathbf{r}) v_0(\mathbf{r}), \quad (6.9)$$

we may use eq. (6.6) to express E_1 as

$$E_1 = \langle \psi_0 | \hat{T} | \psi_0 \rangle + \int d\mathbf{r} \rho(\mathbf{r}) v_1(\mathbf{r}) + \int_0^1 d\lambda \langle \psi_\lambda | \hat{V}_{ee} | \psi_\lambda \rangle \quad (6.10)$$

$$= T_s + V_{ne} + \int_0^1 d\lambda \langle \psi_\lambda | \hat{V}_{ee} | \psi_\lambda \rangle \quad (6.11)$$

$$= T_s + V_{ne} + J + \int_0^1 d\lambda \langle \psi_\lambda | \hat{V}_{ee} | \psi_\lambda \rangle - J, \quad (6.12)$$

from which it is possible to identify the exact exchange–correlation energy as

$$E_{xc} = \int_0^1 d\lambda \langle \psi_\lambda | \hat{V}_{ee} | \psi_\lambda \rangle - J. \quad (6.13)$$

We define W_λ such that

$$W_\lambda = \langle \psi_\lambda | \hat{V}_{ee} | \psi_\lambda \rangle - J. \quad (6.14)$$

When $\lambda = 0$, eq. (6.14) becomes

$$W_0 = \langle \psi_0 | \hat{V}_{ee} | \psi_0 \rangle - J = J + E_x - J = E_x. \quad (6.15)$$

in which E_x is the exact value of the orbital exchange energy. When $\lambda = 1$, the wavefunction corresponds to the exact wavefunction of the interacting physical system, ψ_1 , so

$$W_1 = \langle \psi_1 | \hat{V}_{ee} | \psi_1 \rangle - J = V_{ee} - J, \quad (6.16)$$

in which V_{ee} and J are the exact values of the electron–electron interaction and the Coulomb energies for the interacting physical system. It follows that the correlation kinetic energy, which is defined by $T_c = E_{xc} - (V_{ee} - J)$, is given by $T_c = E_{xc} - W_1$. As illustrated in figure 6.1, E_{xc} and T_c have a simple geometrical interpretation in terms of the adiabatic connection. Given the known property that the adiabatic connection curve is monotonically decreasing, it follows that $|T_c| \leq |E_c|$. The exact gradient of W_λ when $\lambda = 0$ is given by the second-order correlation energy from Görling–Levy^{282,283} perturbation theory (GL2)

$$\left. \frac{\partial W_\lambda}{\partial \lambda} \right|_{\lambda=0} = 2E_c^{\text{GL2}} = -\frac{1}{2} \sum_{i,j,\alpha,\beta} \frac{|(\alpha i | \beta j) - (\alpha j | \beta i)|^2}{\varepsilon_\alpha + \varepsilon_\beta - \varepsilon_i - \varepsilon_j} - 2 \sum_{i,\alpha} \frac{\langle \phi_i | v_x - v_x^{\text{NL}} | \phi_\alpha \rangle^2}{\varepsilon_\alpha - \varepsilon_i}. \quad (6.17)$$

Here the first term is twice the conventional second-order Møller–Plesset correlation energy expression which involves two-electron integrals of exact occupied (i,j) and virtual (α,β) Kohn–Sham orbitals and their associated orbital energies ε . The second term involves the difference between the exact multiplicative exchange potential v_x and the non-multiplicative, non-local (NL) exchange v_x^{NL} .

For practical calculations, W_λ can be approximated using simple mathematical forms that model—to various extents—the known behaviour of the exact adiabatic connection. The parameters in an approximate adiabatic connection form are then defined to reproduce known properties of the adiabatic

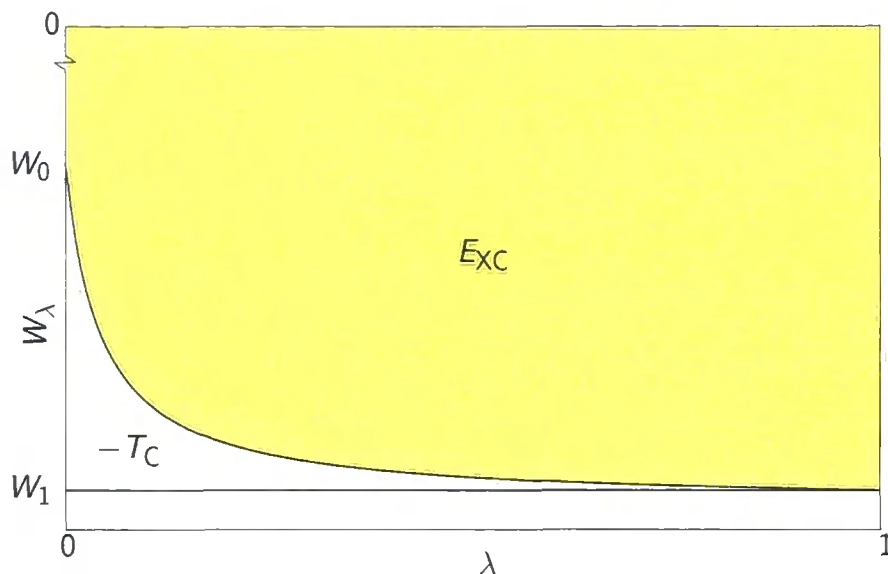


Figure 6.1: Schematic representation of the adiabatic connection; E_{xc} and $-T_c$ are given by the integrals as indicated.

connection, either exactly or approximately. Therefore the accuracy of a calculation, within a given basis set, is governed both by the chosen mathematical form and the accuracy of the input data used to determine any parameters. There have been a number of attempts to develop exchange–correlation functionals through explicit approximation of W_λ ; the energy of such approximations is then evaluated through

$$E_{xc} = \int_0^1 d\lambda W_\lambda^{\text{Approx}}, \quad (6.18)$$

where $W_\lambda^{\text{Approx}}$ refers to an approximation to the exact W_λ form. Examples of such approximations are the half-and-half functional of Becke⁸⁸ which uses a linear adiabatic connection form; the [1,1]-Padé based form of Ernzerhof;²⁸⁴ the two-legged representation of Burke²⁸⁵ *et al.*; and the interaction strength interpolation of Seidl²⁸⁶ *et al.* Mori-Sánchez, Cohen and Yang²⁸⁷ (MCY) recently proposed two functionals based on the same form considered by Ernzerhof,²⁸⁴

$$W_\lambda^{\text{MCY}} = a + \frac{b\lambda}{1 + c\lambda}, \quad (6.19)$$

but with alternative definitions of the three parameters.

It is trivial to show that the quantities a and b in eq. (6.19) respectively define the value and the gradient of W_λ^{MCY} at $\lambda = 0$. In order that the approximate form satisfy eq. (6.15), Mori-Sánchez *et al.* defined the parameter a to be the orbital exchange energy E_x . For evaluation of the parameter b they used a value of a modified TPSS gradient, with an additional scaling factor of 4.0 to optimise the thermochemical performance. The parameter c was chosen so that the value of eq. (6.19) for $\lambda = 0.63$ was equal to W_λ^{BLYP} evaluated with the same value of λ ; this value was again chosen to optimise the performance of the functional. W_λ^{BLYP} is the adiabatic connection form associated with the BLYP exchange–correlation functional; as illustrated by Mori-Sánchez *et al.*, it can be obtained for any local functional through coordinate scaling relations.²⁸⁸ This functional was denoted MCY1. A second functional, denoted MCY2, involves an additional parameter introduced to improve atomic energies.

One of the justifications for choosing the form of W_λ^{MCY} and the subsequent definition of the parameters is that the resultant functionals are one-electron self-interaction free. This means that the exchange–correlation energy exactly cancels the Coulomb energy for any density containing up to one electron; by definition this requires that the exchange–correlation energy for such a density reduces to $E_{\text{xc}} = E_x = -J$. This occurs in the case of the MCY functionals because as defined the gradient b is zero for a one-electron system and the exchange–correlation energy therefore trivially reduces to E_x as required. They are not however many-electron self-interaction free.^{289–291} Self-interaction error is extended to many-electron systems as the requirement that the total electronic energy be piecewise linear as a function of electron number n ; for non-integer numbers of electrons $n < m < n + 1$, the exact total electronic energy is expressible as a linear combination of the exact total electronic energies at the surrounding integers,¹⁷⁴

$$E(m) = (m - n)E(n) + (n + 1 - m)E(n + 1). \quad (6.20)$$

A similar relation may also be obtained for the densities of the m -electron system. In general GGA functionals and Hartree–Fock theory deviate significantly from this linear behaviour, in opposite directions. It has recently

been demonstrated that attenuated functionals, such as those considered in the previous chapters (with appropriately modified attenuation parameters), can exhibit near-linear behaviour as a function of electron number. Cohen¹⁴⁵ *et al.* have subsequently introduced the MCY3 functional which is designed specifically to be close to many-electron self-interaction free.

The quality of the MCY1 and MCY2 functionals is encouraging, with the performance providing a simultaneously good description of thermochemistry and kinetics.²⁸⁷ Recently several other $W_\lambda^{\text{Approx}}$ were proposed by Cohen²⁹² *et al.*; they concluded that when input data determined in a similar manner to that of MCY1 and MCY2 were used—where only the value of W_0 was determined using an exact expression—there was little to differentiate between the quality of the forms.

The accuracy of results from adiabatic connection-based functionals is dependent on both the mathematical form of $W_\lambda^{\text{Approx}}$ and the procedure used to obtain any of the parameters contained within a $W_\lambda^{\text{Approx}}$. It is therefore difficult to isolate the cause of the success (or failure) of these functionals. The first aim of the work in this chapter is to use correlated *ab initio* calculations to investigate the performance of various $W_\lambda^{\text{Approx}}$ when *all of the parameters are determined such that they reproduce accurate properties of the exact adiabatic connection*. This will establish how well a given $W_\lambda^{\text{Approx}}$ can represent the exact W_λ .

To test the $W_\lambda^{\text{Approx}}$, we consider the singlet ground state potential energy curve of the H_2 molecule, which is the famous and challenging example of non-dynamic correlation. The small size of this system allows essentially exact *ab initio* calculations to be performed and the two-electron nature affords several welcome simplifications. This work is particularly relevant in light of the study by Fuchs²⁹³ *et al.*, who considered the dissociation of H_2 using the random phase approximation;^{81,83} see ref. 293 for a detailed discussion of H_2 dissociation within density functional theory. Given the simplifications that arise in the computation of accurate W_λ data for two-electron systems, we then extend the study to consider how well the AC forms can describe the electronic energies of the helium isoelectronic series, from H^- to Ne^{8+} ; the accurate calculation of these energies, particularly as the atomic number Z increases, poses a further significant challenge for approximate exchange–

correlation functionals.^{279, 280, 294–297}

6.1 COMPUTATIONAL APPROACH

All calculations in this chapter are performed using a development version of the DALTON program, and are treated in the appropriate ground state singlet spin-restricted formalism throughout. The basis sets used are discussed in detail at the point of use; for H₂ and the helium isoelectronic series doubly augmented sextuple- ζ quality bases are used. FCI calculations are performed using these extensive basis sets; we calculate both the total electronic energy and the total electron density (which are exact within the basis set used).

Our first task is to compute accurate properties of W_λ . In principle an accurate W_λ curve may be determined by evaluating eq. (6.14) using wavefunctions from FCI calculations; this is non-trivial for arbitrary λ , but when λ is 0 or 1, it is straightforward. For $\lambda = 0$, evaluation of eq. (6.15) using FCI data gives the exchange energy, determined using the Kohn–Sham orbitals associated with the FCI density. For a two-electron system, the exchange energy is the negative of one half of the Coulomb energy, so we may evaluate

$$W_0^{\text{FCI}} = -\frac{1}{2}J^{\text{FCI}} \quad (6.21)$$

where the FCI label denotes evaluation with FCI-derived quantities; in this case we evaluate the Coulomb energy J with the FCI density. For $\lambda = 1$, evaluation of eq. (6.16) using FCI data gives

$$W_1^{\text{FCI}} = V_{\text{ee}}^{\text{FCI}} - J^{\text{FCI}} \quad (6.22)$$

in which $V_{\text{ee}}^{\text{FCI}}$ is the FCI electron–electron repulsion energy, obtained by subtracting the nuclear–nuclear repulsion and one-electron energies determined using the FCI density matrix, from the FCI total electronic energy. Equations (6.21) and (6.22) represent exact values of W_λ^{FCI} , which may easily be determined from an FCI calculation; the FCI labels are used to differentiate between the true exact adiabatic connection W_λ and that determined within a finite basis set, W_λ^{FCI} .

The gradient at $\lambda = 0$ is twice the GL2 correlation energy, given in eq. (6.17), evaluated with the Kohn–Sham orbitals and orbital energies associated

with the FCI density. For two-electron systems v_x in the second term of eq. (6.17) is the negative of one half of the Coulomb potential, since the potential is the functional derivative of the corresponding energy. Since there is only one occupied orbital ϕ_1 , from a consideration of the explicit orbital pair contributions it follows that

$$\langle \phi_1 | v_x | \phi_\alpha \rangle = \langle \phi_1 | v_x^{\text{NL}} | \phi_\alpha \rangle, \quad (6.23)$$

for all virtual orbitals ϕ_α . Hence the latter term in eq. (6.17) is identically zero, and

$$W_0^{\text{FCI}} = \left. \frac{\partial W_\lambda^{\text{FCI}}}{\partial \lambda} \right|_{\lambda=0} = -\frac{1}{2} \sum_{i,j,\alpha,\beta} \frac{|(\alpha i | \beta j) - (\alpha j | \beta i)|^2}{\varepsilon_\alpha + \varepsilon_\beta - \varepsilon_i - \varepsilon_j}. \quad (6.24)$$

In order to evaluate this expression we require the Kohn–Sham orbitals and orbital energies associated with the FCI density. The accuracy of these quantities will depend on the method used to obtain them. The Wu–Yang⁹⁸ (WY) implementation of the constrained search formalism^{54,56} is one possibility, which minimises the non-interacting kinetic energy under the constraint that the FCI density is recovered. In general the method allows the construction of the potential associated with a given ground state density $\rho(\mathbf{r})$. The potential, in a similar manner to the Yang–Wu optimised effective potential⁹⁷ method, is expanded in terms of contributions from a known reference potential which is ‘corrected’ by a basis set expansion in terms of Gaussian functions \mathbf{g} to account for any deviations of the actual potential $v_s(\mathbf{r})$ from the reference potential $v(\mathbf{r}) + v_{\text{Ref}}(\mathbf{r})$;

$$v_s(\mathbf{r}) = v(\mathbf{r}) + v_{\text{Ref}}(\mathbf{r}) + \sum_t b_t g_t(\mathbf{r}). \quad (6.25)$$

The problem therefore reduces to the determination of the appropriate basis set expansion coefficients \mathbf{b} that minimise the non-interacting kinetic energy over all possible potentials $v_s(\mathbf{r})$ that reproduce the input density.

As with the Yang–Wu optimised effective potential procedure, a well-balanced description of the orbitals and potential is important.^{266,298} In our WY calculations we therefore use the same extensive sextuple- ζ basis set for the expansion of the potential and the orbitals; the extensive and largely

uncontracted nature of these basis sets is sufficient to provide an accurate representation of both the potential and the orbitals. For the reference potential we use a Fermi–Amaldi²⁷⁰ potential; we have confirmed that essentially identical results are obtained if a Slater reference potential⁶⁶ is instead used. As a cut-off in the truncated singular value decomposition we use a value of 1×10^{-6} , which provides essentially identical results to those obtained using a cut-off of 1×10^{-8} ; any further reduction in the cut-off is numerically undesirable. Since by construction the density of the occupied Kohn–Sham orbital should equal the FCI density, the accuracy of the calculation may be judged by a comparison of the Coulomb energies associated with the two densities; for the H_2 and helium isoelectronic series, the energies from the two densities differ by at most 7×10^{-4} %.

Schipper²⁹⁹ *et al.* have demonstrated that the exchange–correlation potential that exactly corresponds to a density obtained from a finite Gaussian basis set may exhibit unphysical oscillatory structure. At large H_2 internuclear separations, our WY-obtained exchange–correlation potentials do exhibit minor undulations. In order to force the potentials to give a smoother, more physically sensible structure, we have performed additional calculations using the procedure of Heaton-Burgess²⁹⁸ *et al.*, which introduces a smoothing norm into the minimisation. The resultant potentials are very smooth; however, the potential energy curves we obtain (see later) are essentially indistinguishable from those obtained without the smoothing norm procedure. The FCI density however is less well reproduced because the procedure necessarily limits the extent to which the solution point can be reached.

For two-electron systems there is an alternative possibility for obtaining the exchange–correlation potential that yields the finite basis set FCI density; it may be obtained directly from inverting the Kohn–Sham equation.²⁹⁴ See ref. 300 for a related study on the H_2 molecule. We have performed such a direct inversion, and find, consistent with Schipper²⁹⁹ *et al.*, that the potential is oscillatory in the vicinity of the nuclei. It is possible to obtain orbitals and orbital energies by solving the finite basis set Kohn–Sham problem with this potential; again the potential energy curves are essentially indistinguishable from those above, although the FCI density is again less well reproduced compared to the WY procedure, due to the use of a finite basis set. Throughout

the remainder of this study we therefore obtain orbitals and orbital energies through the use of the WY procedure applied to the FCI densities.

We determine accurate W_λ^{FCI} data using eqs. (6.21), (6.22) and (6.24), which we then use to define the parameters in approximate adiabatic connection forms. These forms will exactly reproduce the FCI values (or a subset of them). The exchange–correlation energies associated with an approximate adiabatic connection form will then differ from the exact exchange–correlation energy (within that basis set) *solely* due to the failure of the form in representing the exact AC curve at points other than those used as input—any error in the exchange–correlation energy is attributable to the failure of the approximate form in representing the exact W_λ^{FCI} .

In practical calculations it is often more intuitive to consider total electronic energies and their related properties, rather than exchange–correlation energies. The nuclear–electron and Coulomb components of the total energy are always explicit functionals of the density and so can be evaluated exactly using the FCI density. For two-electron systems the occupied Kohn–Sham orbital is the square root of one half of the electron density; the non-interacting kinetic energy, generally a functional of the orbitals, then becomes an explicit functional of the density given by the von Weizsäcker expression:⁵⁹

$$T_s = T_W = \frac{1}{8} \int d\mathbf{r} \frac{|\nabla\rho(\mathbf{r})|^2}{\rho(\mathbf{r})}. \quad (6.26)$$

Therefore the non-interacting kinetic energy may also be evaluated exactly from the FCI density; the only other component is the nuclear–nuclear repulsion, which is trivial to determine. We therefore evaluate the total DFT energy E through

$$E = T_W^{\text{FCI}} + V_{\text{ne}}^{\text{FCI}} + J^{\text{FCI}} + V_{\text{nn}} + E_{\text{xc}}^{\text{AC}} \quad (6.27)$$

in which T_W^{FCI} and $V_{\text{ne}}^{\text{FCI}}$ are the von Weizsäcker kinetic and nuclear–electron energies evaluated with the FCI density, and $E_{\text{xc}}^{\text{AC}}$ is the exchange–correlation energy [evaluated through eq. (6.18)] associated with an approximate adiabatic connection (AC) form. The first four terms are exact and the error in the final term arises entirely from the use of an approximate AC form. Comparison of E with the FCI total electronic energy will allow the accuracy of the AC form to be quantified.

As a first application we consider the AC form used by Mori-Sánchez *et al.*,

$$W_{\lambda}^{\text{AC1}} = a + \frac{b\lambda}{1+c\lambda}. \quad (6.28)$$

We introduce the notation AC1 to refer to this form. The exchange–correlation energy associated with eq. (6.28) is given by

$$E_{\text{xc}}^{\text{AC1}} = a + \frac{b}{c} \left(1 - \frac{\log_e(1+c)}{c} \right). \quad (6.29)$$

As discussed above, we define the parameters a , b and c by requiring that the value and gradient of W_{λ}^{AC1} at $\lambda = 0$, together with the value at $\lambda = 1$, equal the corresponding FCI values;

$$W_0^{\text{AC1}} = a = W_0^{\text{FCI}}, \quad (6.30)$$

$$\left. \frac{\partial W_{\lambda}^{\text{AC1}}}{\partial \lambda} \right|_{\lambda=0} = b = \left. \frac{\partial W_{\lambda}^{\text{FCI}}}{\partial \lambda} \right|_{\lambda=0}, \quad (6.31)$$

$$W_1^{\text{AC1}} = a + \frac{b}{1+c} = W_1^{\text{FCI}}. \quad (6.32)$$

Through eqs. (6.21), (6.22) and (6.24) we obtain the following values for the parameters;

$$a = -\frac{1}{2} J^{\text{FCI}}, \quad (6.33)$$

$$b = -\frac{1}{2} \sum_{i,j,\alpha,\beta} \frac{[(\alpha i|\beta j) - (\alpha j|\beta i)]^2}{\varepsilon_{\alpha} + \varepsilon_{\beta} - \varepsilon_i - \varepsilon_j}, \quad (6.34)$$

evaluated with the Kohn–Sham quantities obtained from the WY calculation. The equation for the final parameter is obtained by solving for c with a and b defined as above;

$$W_1 = a + \frac{b}{1+c} = V_{\text{ee}}^{\text{FCI}} - J^{\text{FCI}} \quad (6.35)$$

$$\Rightarrow c = \frac{b}{V_{\text{ee}}^{\text{FCI}} - J^{\text{FCI}} - a} - 1. \quad (6.36)$$

For each required AC1 total energy, an FCI calculation was performed and the quantities a , b and c evaluated according to eqs. (6.33), (6.34) and (6.36); this data was then combined with the other FCI-derived energy components in eq. (6.27). Results from this procedure are denoted AC1.^{301,302}

Table 6.1: H₂ FCI total electronic and exchange–correlation energies (in Hartree) as a function of bond distance R (in bohr), compared to reference total electronic energies.

R	Ref. ^a	FCI	E_{xc}^{FCI}
1	−1.124540	−1.124394	−0.78581
1.4	−1.174476	−1.174361	−0.70251
2	−1.138133	−1.138042	−0.61751
3	−1.057326	−1.057268	−0.55436
4	−1.016390	−1.016364	−0.56412
5	−1.003786	−1.003776	−0.59403
6	−1.000836	−1.000832	−0.61181
7	−1.000198	−1.000196	−0.61960
8	−1.000056	−1.000054	−0.62280
9	−1.000020	−1.000018	−0.62410
10	−1.000009	−1.000007	−0.62463

^a refs. 303 and 304.

6.2 GROUND STATE H₂ POTENTIAL ENERGY CURVES

We commence by considering the singlet ground state potential energy curves of H₂ determined using standard methods, reiterating that all calculations in this study use the appropriate spin-restricted formalism. For all calculations in this section we use the d-aug-cc-pV6Z basis set. The FCI total electronic energies obtained with this basis set are compared with accurate reference values in table 6.1, as a function of the bond distance R . The agreement with the reference data reflects the extensive basis set used. Also presented are the exchange–correlation energies associated with the FCI calculations. Figure 6.2 compares self-consistent Hartree–Fock (HF) and B3LYP curves with the FCI reference curve, for $0.7 \leq R \leq 10$ bohr. The HF curve is very poor, reflecting the failure of a single determinant in describing the wavefunction, particularly at dissociation where non-dynamic correlation is significant—there are unphysical ionic contributions to the wavefunction. The B3LYP curve is an improvement, particularly at equilibrium, although significant error remains at larger bond distances. Also shown is the self-consistent MCY1 curve, which is similar to the MCY2 curve (not shown). MCY1 provides similar performance to B3LYP whilst removing the one-electron self-interaction error.

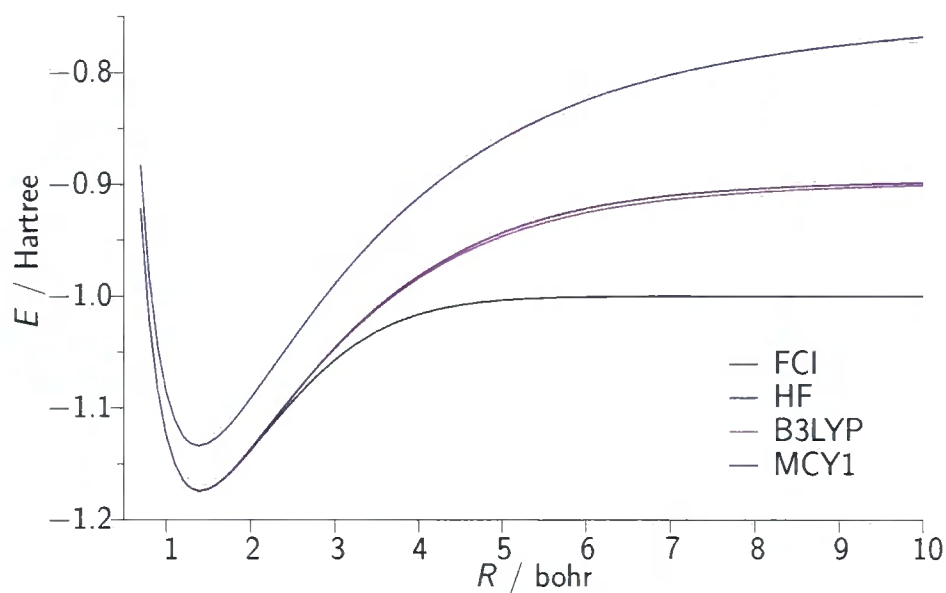


Figure 6.2: Potential energy curve of H_2 determined using FCI, compared with those from self-consistent HF, MCY1 and B3LYP.

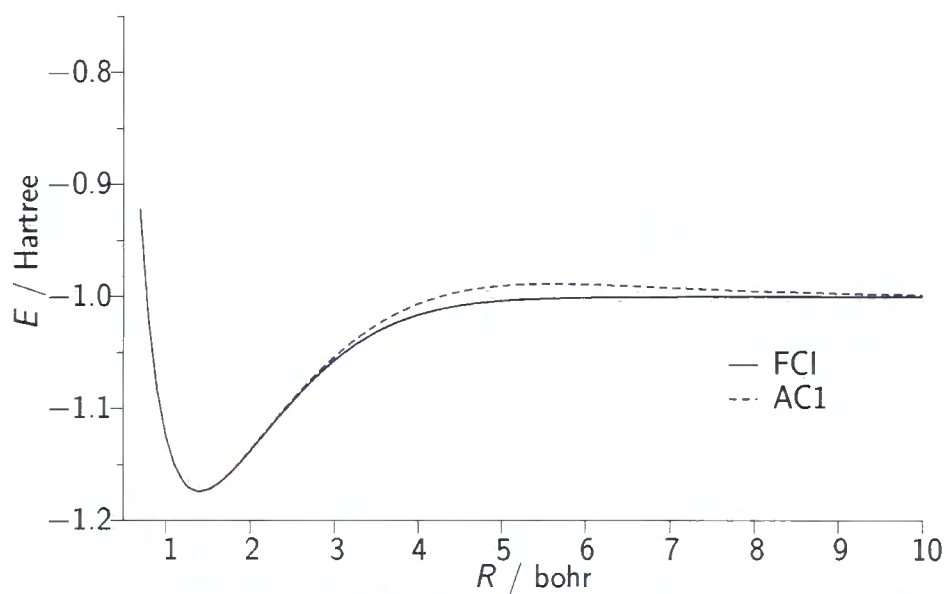


Figure 6.3: Potential energy curve of H_2 determined using FCI, compared with the AC1 curve.

Figure 6.3 compares the AC1 potential energy curve with the FCI reference curve, on the same scale as figure 6.2. It is a significant improvement over the results from the other approximate methods. It is important to note that this improvement is not simply a consequence of using accurate Kohn–Sham orbitals; we have performed MCY1 calculations using the WY orbitals obtained from the FCI density, and find that the shape of the potential energy curve is essentially unchanged compared to the MCY1 curve in figure 6.2, other than by an upward shift due to the non-self-consistent nature of such calculations.

AC1 provides a good description of the potential energy curve in the vicinity of the minimum; MCY1 and B3LYP are also accurate in this region, but HF is poor. One measure of the accuracy is the optimised bond length R_e obtained for each method; table 6.2 presents values of R_e for each of the methods considered, comparing with the FCI value, which agrees with experiment to the precision quoted. Both AC1 and MCY1 give bond lengths in agreement with the FCI value; B3LYP overestimates by just 0.001 bohr. The bond length is notably underestimated with HF however. The potential energy curves have also been used to determine vibrational energy levels, using the LEVEL 7.5 code of Le Roy.³⁰⁵ The potential energy curves used as input consisted of points ranging from $R = 0.7$ bohr to $R = 3.5$ bohr with a spacing of 0.01 bohr (0.001 bohr in the region of the minimum). Convergence of the calculated levels was set to $1 \times 10^{-2} \text{ cm}^{-1}$ and ten point piecewise polynomial interpolation was used. Zero-point, fundamental and first overtone wavenumbers ($J = 0$) are presented in table 6.2 comparing with our FCI values (which agree with experiment to within 1 cm^{-1}). AC1 provides a significant improvement over the conventional methods, with errors relative to FCI of just 6, 14 and 33 cm^{-1} respectively for the zero-point, fundamental and first overtone; the corresponding percentage errors are 0.3%, 0.3% and 0.4%. Of the conventional methods the next best results are obtained from the B3LYP functional, where the errors are 6, 26 and 75 cm^{-1} . The MCY1 errors are comparable to B3LYP, at 11, 35 and 94 cm^{-1} . All three approaches provide an accurate zero-point wavenumber, but the differences between the methods become increasingly pronounced for the higher levels, with MCY1 and (to a lesser extent) B3LYP degrading. The Hartree–Fock errors are all significantly larger, consistent with

Table 6.2: Equilibrium bond lengths R_e in bohr, and zero point (ZP), fundamental ($v=0 \rightarrow v=1$) and first overtone ($v=0 \rightarrow v=2$) vibrational wavenumbers in cm^{-1} , compared to reference total electronic energies.

	HF	B3LYP	MCY1	AC1	AC3	AC5
R_e	1.386	1.402	1.401	1.401	1.403	1.399
ZP	2274	2186	2191	2186	2179	2260
$v = 0 \rightarrow v = 1$	4373	4188	4197	4176	4153	4123
$v = 0 \rightarrow v = 2$	8546	8163	8182	8121	8068	8081
	AC6	AC7	AC8	AC9	FCI	Expt.
R_e	1.401	1.399	1.403	1.401	1.401	1.401 ^a
ZP	2186	2191	2173	2184	2180	2179 ^b
$v = 0 \rightarrow v = 1$	4170	4182	4140	4166	4162	4161 ^b
$v = 0 \rightarrow v = 2$	8107	8135	8040	8096	8088	8087 ^b

^a ref. 208.

^b Determined using the Dunham coefficients in ref. 208 with the Kaiser correction (ref. 306).

the poor overall description of the curve.

The curves in figure 6.3 also demonstrate that at large R , AC1 recovers a large amount of the necessary non-dynamic correlation, resulting in a significant improvement over B3LYP and the other conventional approaches. In fact the dissociation limit is obtained exactly; as $R \rightarrow \infty$ the quantity $b \rightarrow -\infty$ due to the orbital energy degeneracy in the denominator of eq. (6.34). It follows that the associated exchange–correlation energy in eq. (6.29) approaches the value W_1^{AC1} , which by construction [eq. (6.36)] equals W_1^{FCI} in eq. (6.16). In this limit there is no electron–electron repulsion, so W_1^{FCI} is just the negative of the FCI Coulomb energy; the exchange–correlation energy exactly cancels the Coulomb energy and the total energy of eq. (6.27) reduces to the sum of the one-electron contributions as required. This is also evident from a consideration of the derivative of eq. (6.28),

$$\frac{\partial W_\lambda^{\text{AC1}}}{\partial \lambda} = \frac{b}{(1 + c\lambda)^2}, \quad (6.37)$$

as $R \rightarrow \infty$. Equation (6.37) exhibits the correct behaviour (as described in ref. 293); when $\lambda = 0$ the gradient equals b , which is $-\infty$ in the limit. For

any non-zero λ however, the gradient is zero due to the quadratic divergence present in the denominator. As $R \rightarrow \infty$, W_λ^{AC1} therefore drops from its initial value of $W_0^{\text{AC1}} = a = -J^{\text{FCI}}/2$ with an infinite slope, acquiring the constant value $W_1^{\text{AC1}} = 2a = -J^{\text{FCI}}$ for all non-zero λ . It follows (consider for instance figure 6.1, figure 2 of ref. 293 and the discussion of figure 6.4) that T_c is exactly zero, which is appropriate for the case of two isolated one-electron systems. Of note is the fact that this lack of λ -dependence in W_λ^{AC1} will occur whenever $b \rightarrow -\infty$, for example in the dissociation of a general homonuclear diatomic molecule. In cases with many-electron fragments, it is incorrect to have $T_c = 0$. Mori-Sánchez²⁸⁷ *et al.* discuss the related example of the homogeneous electron gas.

Next consider intermediate bond lengths in figure 6.3. The AC1 curve resembles that obtained by Fuchs²⁹³ *et al.*, using the RPA. There is an unphysical barrier to dissociation, which is the first significant discrepancy compared to FCI. We reiterate that this feature is unaffected by smoothing the potential in the WY procedure, the use of the direct-inversion alternative, or to changes in the basis set used either for the orbitals or the expansion of the potential. This does not imply that the choice of orbitals and orbital energies are unimportant; replacing the FCI-based WY quantities with those obtained from the PBE GGA functional more than doubles the size of the barrier; using Hartree-Fock orbitals and orbital energies results in a further significant degradation. See ref. 307 for a discussion of the orbital dependence of this feature within the RPA. Our interpretation of this barrier to dissociation is that it is a failure of the form of eq. (6.28). We note that Fuchs *et al.* used a similar form to represent their near-exact adiabatic connection near equilibrium, but had to introduce additional flexibility into their model form at intermediate R .

It is instructive to consider the shape of the W_λ^{AC1} curves at three geometries; 1.4 bohr, 5 bohr and 10 bohr, corresponding to two different regions where W_λ^{AC1} provides an accurate description, and one where it is less accurate. We present these curves along with the self-consistent MCY curves for comparison in figure 6.4. Note that although both methods define W_0 to equal the orbital exchange energy, the values differ in practice due to the different data used in their evaluation. At 1.4 bohr, corresponding to the equilibrium bond length, the two curves have different shapes but the integrals that

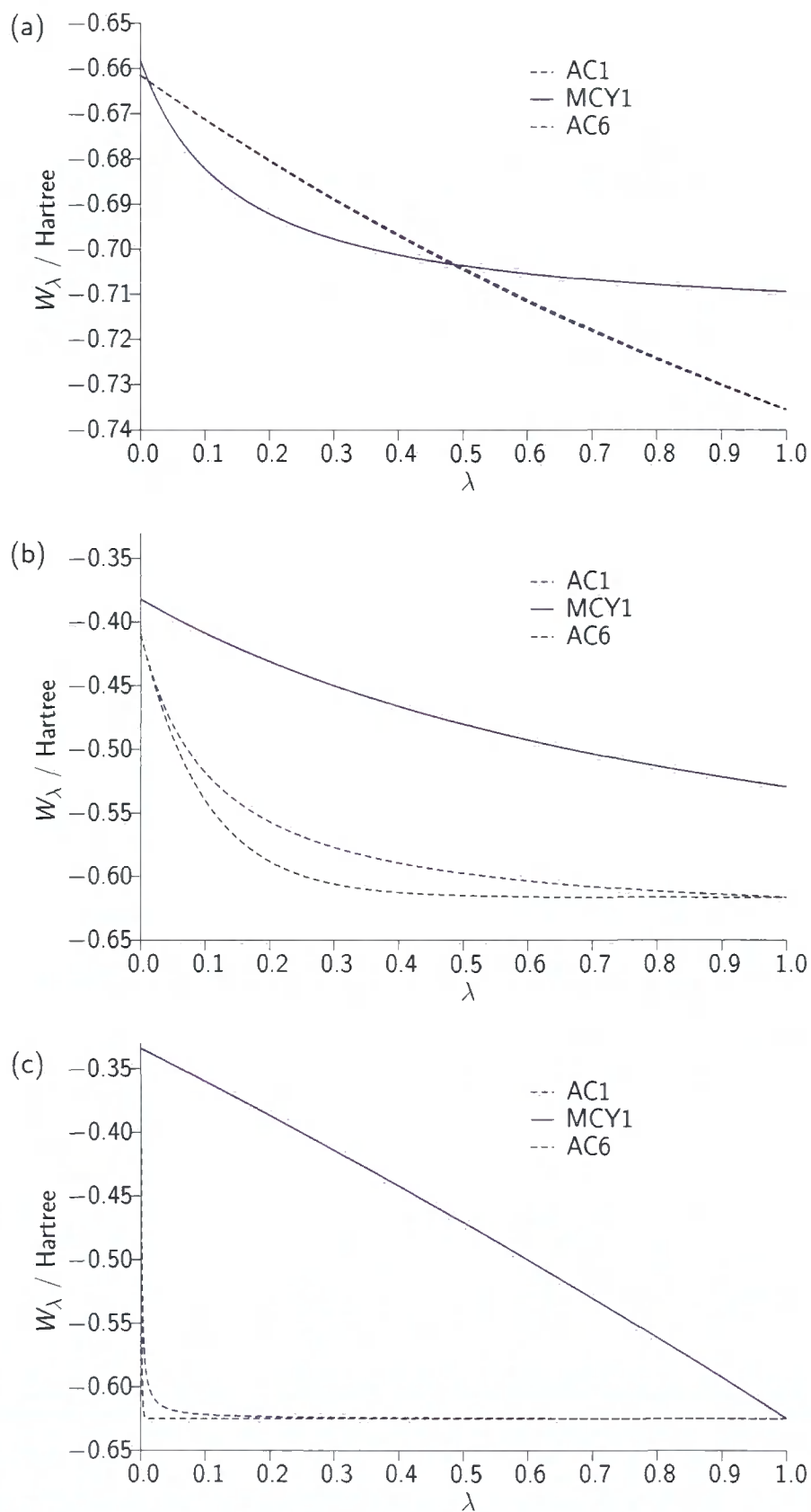


Figure 6.4: Comparison of W_λ from MCY1, AC1 and AC6, evaluated at internuclear separations of (a) 1.4 bohr, (b) 5 bohr, and (c) 10 bohr.

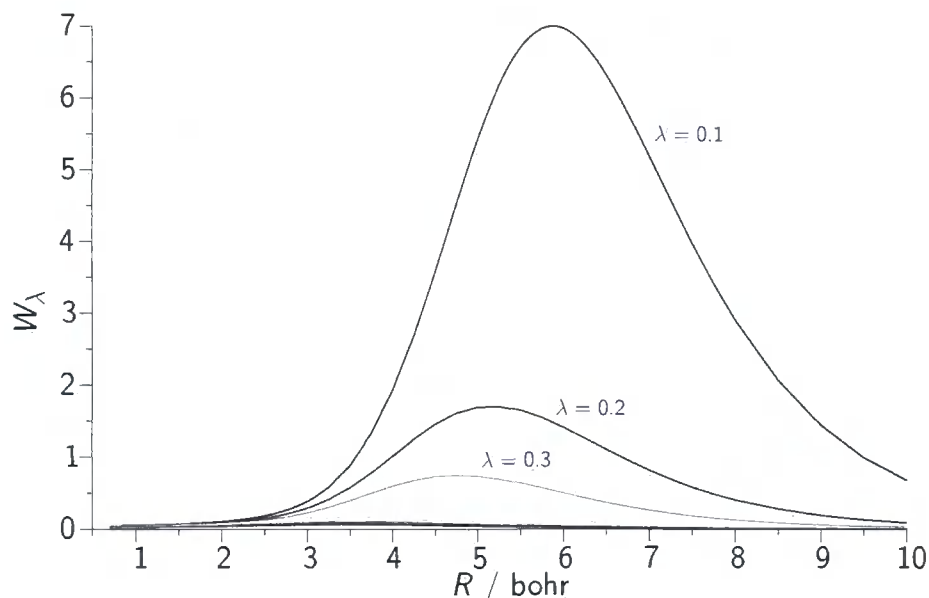


Figure 6.5: $\partial^2 W_\lambda / \partial \lambda^2$, as a function of R for various values of λ .

determine E_{xc} through eq. (6.18) are similar, resulting in the corresponding similarities observed in the potential energy curves near equilibrium. The AC1 curve closely resembles the ‘exact’ curve of Fuchs²⁹³ *et al.* As R increases, the MCY1 integral becomes increasingly less negative compared to that of AC1, which is again reflected in the behaviour of the potential energy curves. At $R = 10$ bohr the AC1 curve is essentially flat; it will become completely flat as $R \rightarrow \infty$, as discussed above. Interestingly the curves from AC1 and MCY1 have similar values at $\lambda = 1$, implying that the failure can be attributed to the TPSS gradient failing to diverge as the exact gradient does; this highlights the importance of virtual orbital energies in recovering non-dynamic correlation. We have again confirmed that the W_λ^{MCY} curves do not improve if they are evaluated with the WY orbitals and orbital energies.

Also of interest is the behaviour of the second derivative of W_λ^{AC1} with respect to λ ; this is plotted as a function of R for various values of λ in figure 6.5. For all of the λ values shown, the curvature is small near equilibrium, increasing to a maximum for intermediate R (in the region of 5–6 bohr), but then decreasing again as dissociation is approached. The observation that the potential energy curve is accurate near equilibrium and near dissociation,

but relatively poor in intermediate regions, indicates that the form of eq. (6.28) works preferentially when the curvature is small. The high curvature of W_λ^{AC1} for intermediate R and the associated failure of the exchange–correlation energy in this region may reflect the rapidly changing nature of the exact wavefunction, as evidenced by rapid changes in the occupation numbers of the σ_g and σ_u natural orbitals in this region. The inclusion of higher order terms in the expansion appears desirable, but would require additional input data. We therefore take an alternative approach, whereby alternative forms that continue to make use of the available input data are trialled.

Calculations that use the exchange–correlation energy obtained from eq. (6.29), with the parameters defined either to reproduce exact values of the adiabatic connection (as in the AC1 form) or as in the MCY functionals of ref. 287, are not in general size-extensive. For the case of H₂ discussed above the size-extensivity condition does hold; however it fails for a heteronuclear system due to the form of the energy expression. In general the size-extensivity condition will only hold if the contributions from the energy associated with a given $W_\lambda^{\text{Approx}}$ are linear in any parameters a , b and c . We therefore next consider polynomial AC forms, which provide fully size-extensive models.³⁰¹

For simplicity we continue to define $W_\lambda^{\text{Approx}}$ models in terms of parameters a , b and c , although their definitions may differ from the case of AC1. Firstly we consider the two parameter linear AC2 and three parameter quadratic AC3 forms of table 6.3. The associated exchange–correlation energies are trivially computed; see appendix A for the expressions for $E_{\text{xc}}^{\text{AC}}$, a , b and c for the W_λ forms considered.

For AC2, we can require that the value and slope of W_λ^{AC2} at $\lambda = 0$ equal the appropriate FCI-derived values;

$$W_0^{\text{AC2}} = a = W_0^{\text{FCI}}, \quad (6.38)$$

$$\left. \frac{\partial W_\lambda^{\text{AC2}}}{\partial \lambda} \right|_{\lambda=0} = b = \left. \frac{\partial W_\lambda^{\text{FCI}}}{\partial \lambda} \right|_{\lambda=0} \quad (6.39)$$

and so a and b are evaluated using eqs. (6.21) and (6.24). The potential energy curve obtained in this manner is denoted AC2 in figure 6.6. It is in poor agreement with FCI near equilibrium, diverging rapidly as R increases due to the divergence of b . It should be noted that the AC2 form is an exact repre-

Table 6.3: Approximate AC forms considered in this study. For the definitions of a , b and c , see appendix A.

$$\begin{aligned}
 W_{\lambda}^{\text{AC1}} &= a + \frac{b\lambda}{1 + c\lambda} \\
 W_{\lambda}^{\text{AC2}} &= a + b\lambda \\
 W_{\lambda}^{\text{AC3}} &= a + b\lambda + c\lambda^2 \\
 W_{\lambda}^{\text{AC4}} &= a + b \left(\frac{\lambda}{1 + \lambda} \right) \\
 W_{\lambda}^{\text{AC5}} &= a + b \left(\frac{\lambda}{1 + \lambda} \right) + c \left(\frac{\lambda}{1 + \lambda} \right)^2 \\
 W_{\lambda}^{\text{AC6}} &= a + b \exp(-c\lambda) \\
 W_{\lambda}^{\text{AC7}} &= a + b \log(1 + c\lambda) \\
 W_{\lambda}^{\text{AC8}} &= a + b \tanh(-c\lambda) \\
 W_{\lambda}^{\text{AC9}} &= a + b\lambda \exp(-c\lambda)
 \end{aligned}$$

sensation of GL2 theory, which is equivalent to MP2 theory (evaluated with a Kohn–Sham reference as opposed to the standard Hartree–Fock reference) for two-electron systems. The difference in the reference, and the typical reduction in the orbital energy gaps, accounts for the faster divergence over the equivalent MP2 curve.

In light of the half-and-half approximation of W_{λ} due to Becke, which also uses the linear interpolation of the AC2 form, we may alternatively require the parameters of W_{λ}^{AC2} equal the FCI values for $\lambda = 0$ and $\lambda = 1$; this can be regarded as an exact representation of the half-and-half functional. In this case, eq. (6.39) is replaced with

$$W_1^{\text{AC2}} = a + b = W_1^{\text{FCI}} \quad (6.40)$$

which is then evaluated using eq. (6.22). We denote results from this method as AC2(H&H). The potential energy curve is shown in figure 6.7; it is in poor agreement with FCI near equilibrium, however there is no divergence at large R due to the absence of the divergent gradient.

The AC3 form contains three parameters, which are defined to equal the

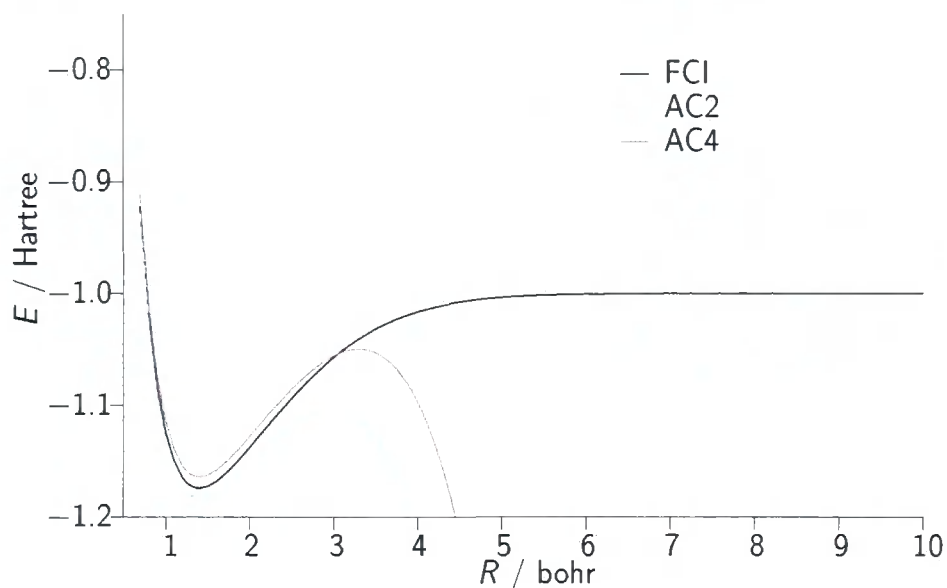


Figure 6.6: Potential energy curve of H_2 determined using FCI, compared with those from AC2 and AC4.

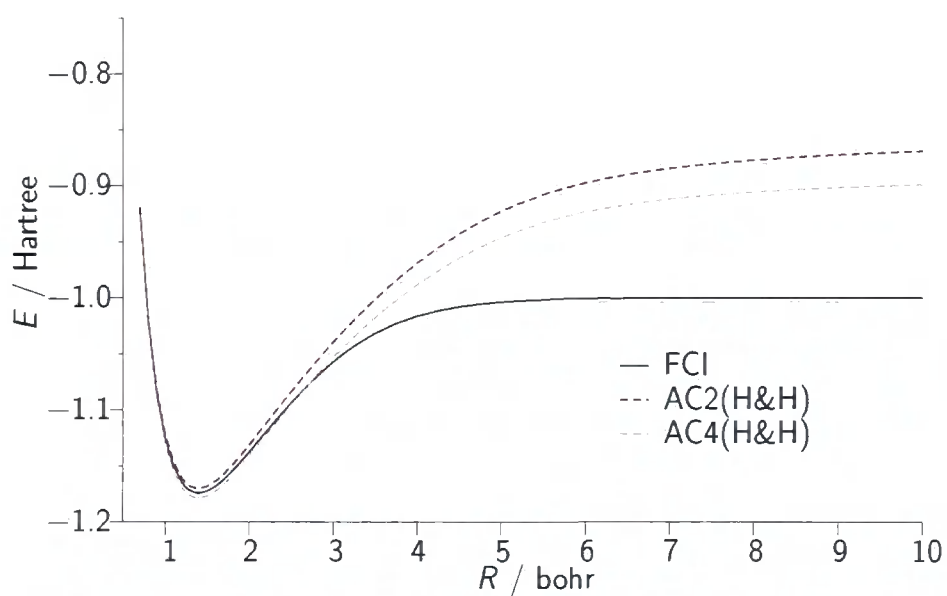


Figure 6.7: Potential energy curve of H_2 determined using FCI, compared with those from AC2(H&H) and AC4(H&H).

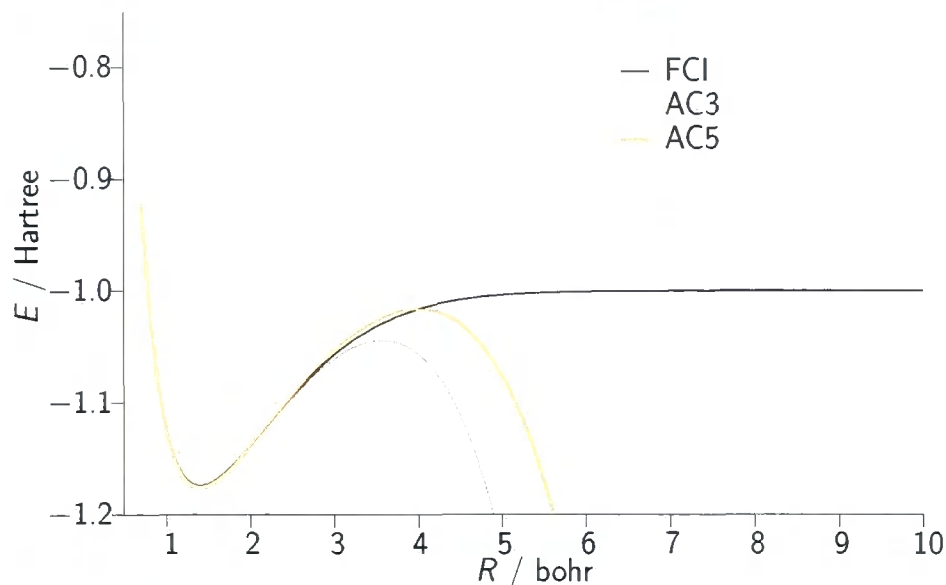


Figure 6.8: Potential energy curve of H_2 determined using FCI, compared with those from AC3 and AC5.

three appropriate values derived from FCI. The potential energy curve so determined is shown in figure 6.8. The agreement with FCI near equilibrium is now significantly improved. The bond length of 1.403 bohr is in good agreement with the FCI bond length, and the zero-point, fundamental and first overtone vibrational wavenumbers are underestimated by just 1, 9 and 20 cm^{-1} respectively. However the curve still diverges at large R , albeit more slowly than in the case of AC2. This again suggests that the inclusion of higher order terms in λ would be desirable, particularly as the bond is stretched.

Whilst AC2 and AC3 $W_\lambda^{\text{Approx}}$ give energies that are size-extensive and one-electron self-interaction free when a , b and c are defined as above, they fail to scale to a constant in the strong interaction limit ($\lambda \rightarrow \infty$) whenever b and c are non-zero. This leads us to consider the alternative AC4 and AC5 forms in table 6.3, which modify AC2 and AC3 respectively such that they scale to a constant for finite non-zero values of b and c . Using exactly the same approach as with AC2 and AC3 but with appropriately amended definitions of b and c , we determined potential energy curves for the AC4, AC4(H&H) and AC5 models. These results are presented in figures 6.6, 6.7 and 6.8 respectively. The behaviour at large R is improved compared to the corresponding AC2,

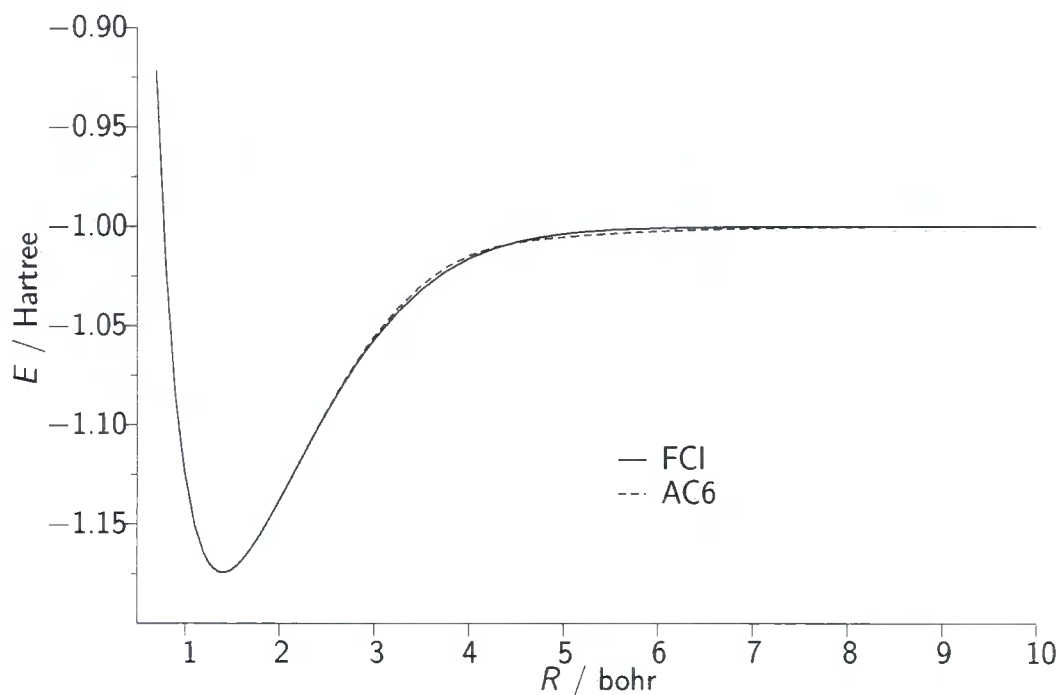


Figure 6.9: Potential energy curve of H_2 determined using FCI, compared with that obtained from AC6.

AC2(H&H) and AC3 results. As illustrated in table 6.2, the curvature of the AC5 potential energy curve is higher than the corresponding AC3 curve, resulting in notably different vibrational wavenumbers.

For the case of H_2 , the size-extensivity of the energy expression for a general molecule appears irrelevant given the best results thus far have been obtained with the non size-extensive AC1 form. With this in mind, we consider the AC6–AC9 forms of table 6.3, which were first considered by Cohen²⁹² *et al.* with approximate input data. These forms remain one-electron self-interaction free, but like AC1, are not in general size-extensive.

The key observation from the consideration of these alternative forms is the high quality description obtained with the exponential-based AC6 form as illustrated in the potential energy curve of figure 6.9. The potential energy curve is virtually indistinguishable from the FCI curve and the unphysical barrier associated with AC1 is completely eliminated. The accurate bond length and high quality vibrational wavenumbers associated with this method

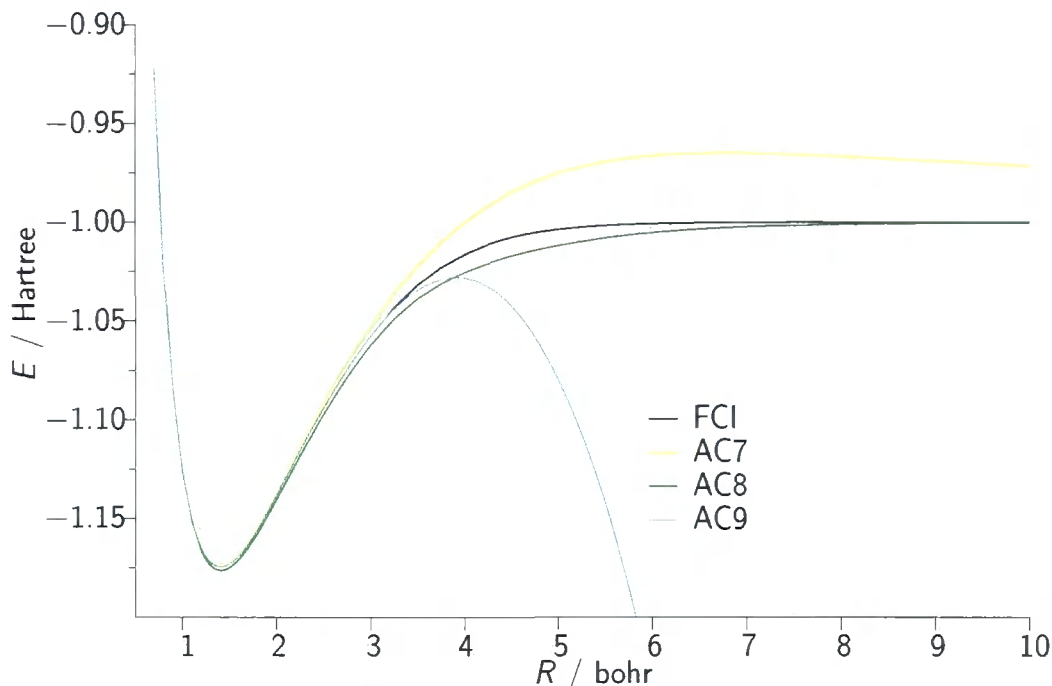


Figure 6.10: Potential energy curve of H_2 determined using FCI, compared with those obtained from AC7, AC8 and AC9

are given in table 6.2. These high quality results for the AC6 form highlight what can be achieved for two-electron systems using simple AC forms when accurate input data is used. One means of understanding the difference in behaviour between the AC1 and AC6 forms is through a consideration of W_{λ}^{AC6} as a function of λ , plotted in figure 6.4. At equilibrium, the W_{λ}^{AC6} curve is essentially indistinguishable from the AC1 curve. However, at 5 bohr (where AC1 exhibits its maximum discrepancy with FCI) there is a marked difference between the two curves; the AC6 curve is everywhere below that of AC1, consistent with the larger (more negative) exchange–correlation energy from AC6. At 10 bohr, the AC6 curve is much sharper than the AC1 curve, indicating that the dissociation limit is reached faster with AC6.

As illustrated in figure 6.10 and table 6.2, AC7 is reasonably accurate near equilibrium, but suffers from a large, wide barrier to dissociation; we have confirmed that the correct dissociation is eventually reached at very large R . AC8 (also shown in figure 6.10) everywhere overestimates the magnitude of

the exchange–correlation energy, but does provide a reasonable description of the dissociation. Figure 6.10 also presents the AC9 curve, which is divergent at large R . However, it has an accurate bond length and the most accurate fundamental and first overtone vibrational frequencies obtained in this study. The observations for H₂ are summarised in figure 6.11, where the error in the total electronic energy relative to FCI is plotted for each of the AC forms considered.

The accurate dissociation that is observed with the AC6, AC7 and AC8 curves can be understood in a similar manner to the AC1 curve,³⁰² from a consideration of the exact W_λ curve as $R \rightarrow \infty$. In this limit the exact curve drops with an infinite slope due to the divergence of the GL2 correlation energy resulting from the orbital degeneracy; the W_λ^{AC6} curve observed in figure 6.4 demonstrates similar behaviour at 10 bohr. It is again worth noting that as in the AC1 case, these forms will not exhibit the correct dissociation behaviour for other homonuclear diatomics where T_c is non-zero, and equally will fail to dissociate a general heteronuclear diatomic due to the size-extensivity failure.

We have identified a number of forms which show promise in the approximation of the exact W_λ , at least when essentially exact input data is used, for the description of the ground state potential energy curve of H₂. We now move on to consider further two-electron systems, specifically the helium iso-electronic series.

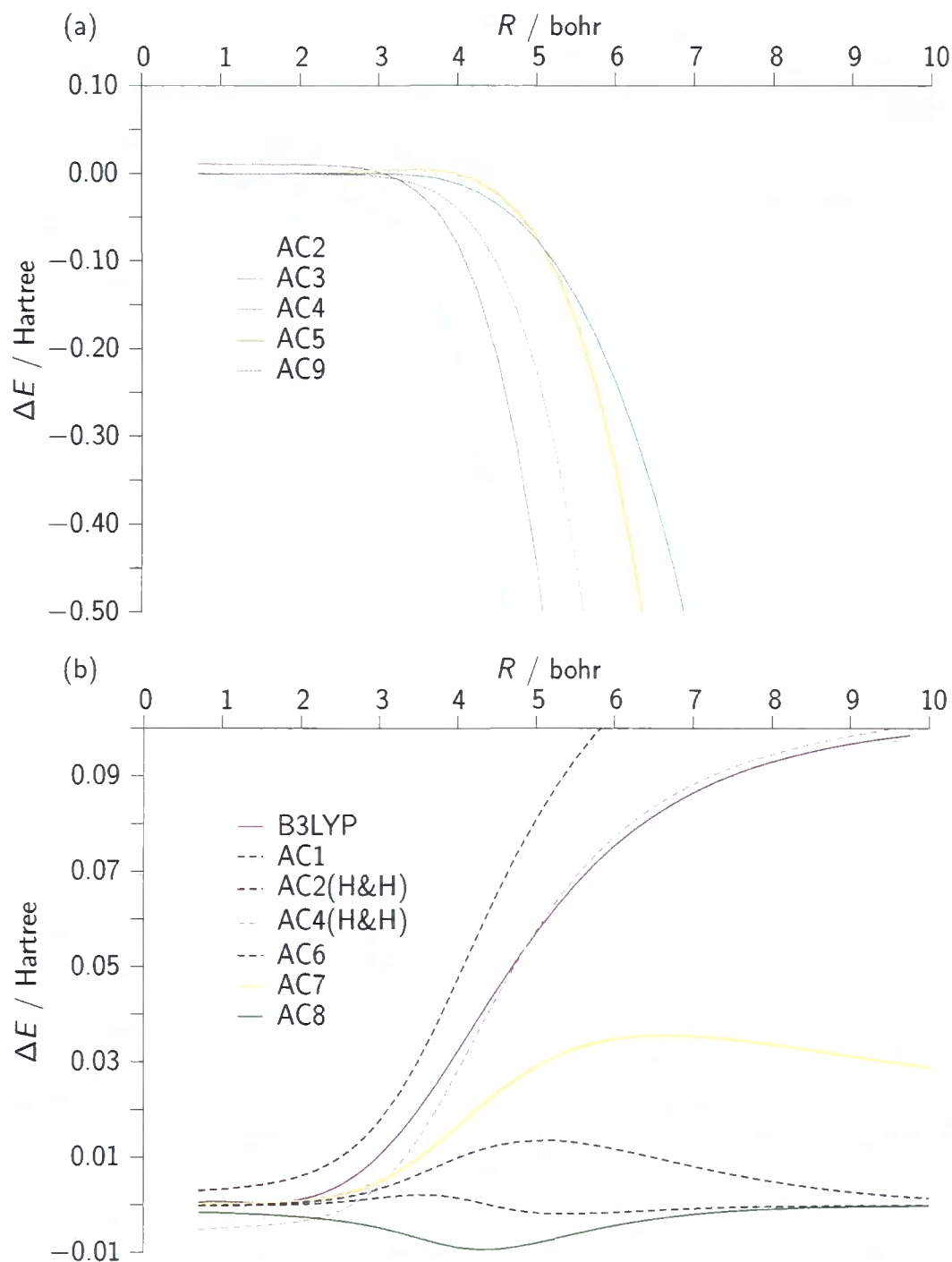


Figure 6.11: The error in total electronic energy $\Delta E = E - E^{\text{FCI}}$ for self-consistent B3LYP and the AC approximations of table 6.3 for the H₂ molecule as a function of R . The shaded area of part (a) denotes the scale of part (b).

6.3 HELIUM ISOELECTRONIC SERIES

We now consider applying the procedure of section 6.1 and the approximate AC forms of table 6.3 to the helium isoelectronic series from H^- to Ne^{8+} . Our preliminary calculations used the standard d-aug-cc-pV6Z basis set for H^- and He, the d-aug-cc-pVQZ basis sets for Li^+ and Be^{2+} (the largest available) and the d-aug-cc-pCV6Z basis sets for B^{3+} – Ne^{8+} . We subsequently performed extensive basis set investigations in order to provide a more uniform description across all of the considered Z . First we took the helium d-aug-cc-pV6Z basis set and applied the same Z -dependent scaling to each exponent, chosen to minimise the Hartree–Fock energy of each system. The FCI results using the scaled basis sets were then compared to those from our preliminary calculations; we found that using the scaled helium basis set was beneficial for H^- to B^{3+} in lowering the FCI energy compared to the standard basis sets. We next applied the same scaling procedure to the boron d-aug-cc-pCV6Z basis set and found that for B^{3+} to Ne^{8+} the FCI energies obtained were lowered compared to both the unscaled d-aug-cc-pCV6Z basis sets and the scaled helium basis. Finally we repeated the procedure with the neon d-aug-cc-pCV6Z basis set, but found that this did not improve upon our best FCI energies for any of the systems.³⁰²

The results presented here therefore use the combination of basis sets that yield the lowest FCI energies; this corresponds to using the scaled helium basis set for H^- to Be^{2+} and the scaled boron basis set for B^{3+} to Ne^{8+} . The optimal basis set scaling factors used in this work are given in table 6.4. We have confirmed that the results of this study are barely affected by the difference in the highest level of angular momenta between the two basis sets, and also whether the unmodified standard basis sets or our modified scaled basis sets are employed.

Table 6.5 compares our FCI total electronic energies with accurate reference values;^{308,309} the agreement again reflects the extensive basis set used in this study. Also presented are the exchange–correlation energies associated with the FCI calculations. We have also confirmed that our individual energy components determined from the FCI data are in excellent agreement with the values presented in ref. 310. Figure 6.12 presents errors in the total

Table 6.4: Helium isoelectronic series basis set scaling factors.

	scaling factor
d-aug-cc-pV6Z(He)	
H ⁻	0.25
He	1.37
Li ⁺	4.10
B ²⁺	8.40
d-aug-cc-pCV6Z(B)	
B ³⁺	1.093
C ⁴⁺	1.627
N ⁵⁺	2.267
O ⁶⁺	3.015
F ⁷⁺	3.869
Ne ⁸⁺	4.830

Table 6.5: Helium isoelectronic series FCI and exchange–correlation energies (in Hartree) compared to reference values

	Ref. ^a	FCI	E_{xc}^{FCI}
H ⁻	-0.527751	-0.527677	-0.42267
He	-2.903724	-2.903488	-1.06637
Li ⁺	-7.279913	-7.279603	-1.69424
Be ²⁺	-13.655566	-13.655202	-2.32054
B ³⁺	-22.030972	-22.030568	-2.94625
C ⁴⁺	-32.406247	-32.405823	-3.57174
N ⁵⁺	-44.781445	-44.781006	-4.19709
O ⁶⁺	-59.156595	-59.156144	-4.82235
F ⁷⁺	-75.531712	-75.531251	-5.44755
Ne ⁸⁺	-93.906807	-93.906336	-6.07271

^a refs. 308 and 309

electronic energy relative to FCI as a function of Z for self-consistent B3LYP calculations, and for the AC forms determined using the procedure outlined previously.

As highlighted in ref. 295, the B3LYP error increases significantly with Z . First consider the two-parameter forms: AC4 and AC4(H&H) are accurate for H⁻ but degrade as Z increases. In contrast the errors associated with AC2 and AC2(H&H) decrease as Z increases. Of the three-parameter forms, AC5 provides an excellent description of H⁻, but degrades with increasing

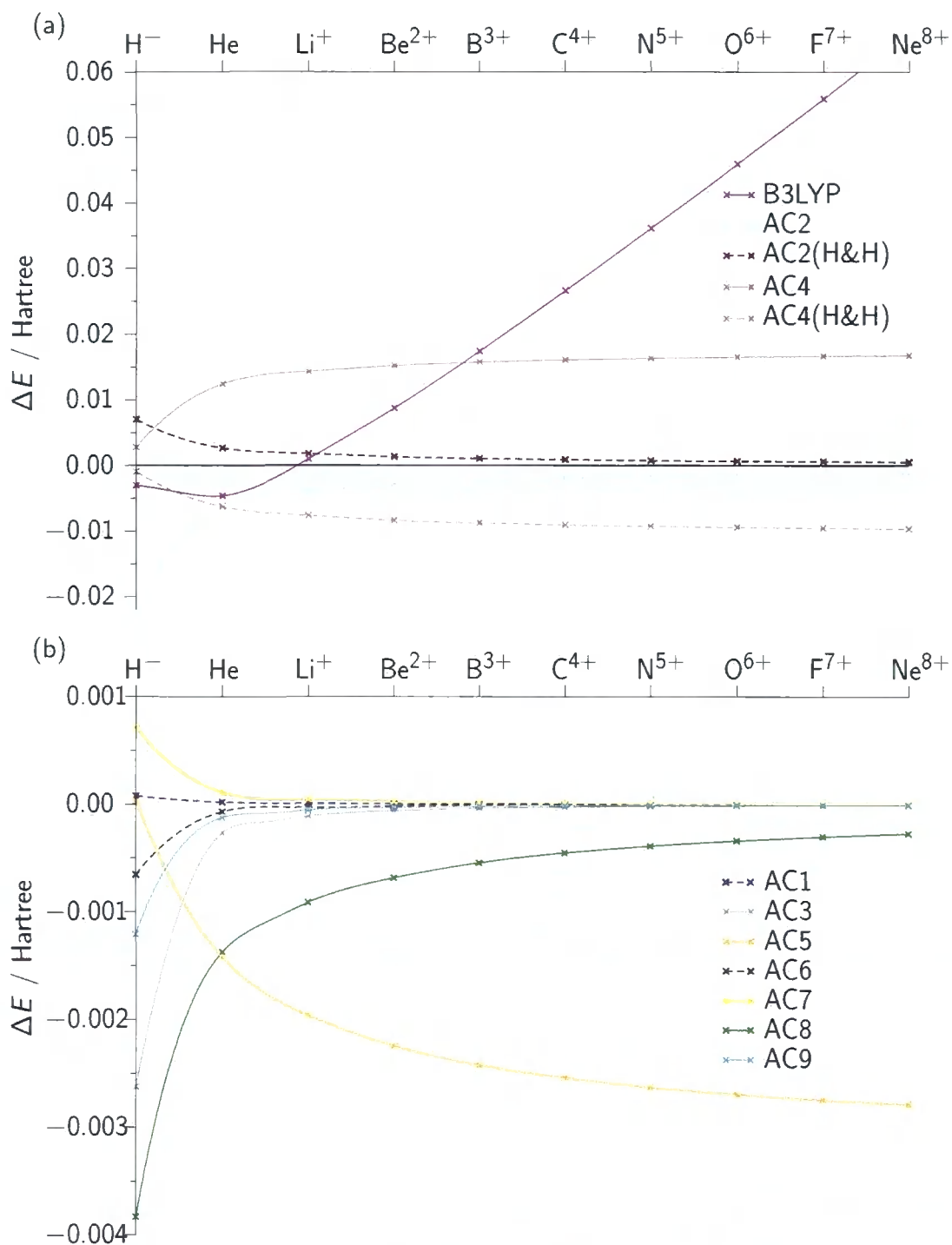


Figure 6.12: The error in total electronic energy $\Delta E = E - E^{FCI}$ for self-consistent B3LYP and the AC approximations of table 6.3 for the helium isoelectronic series as a function of Z . The shaded area of part (a) denotes the scale of part (b).

Z . For all of the other three-parameter forms, the error decreases as Z increases. For AC1, AC3, AC6, AC7, and AC9 the errors are barely visible for $Z > 5$, despite the very small scale of the figure. AC1 provides the best overall description of the series, followed by AC6. The results are a dramatic improvement over those obtained with B3LYP, illustrating the high quality results that may be obtained for two-electron systems from simple AC forms. For these single-centre systems, the lack of size-extensivity of many of these approximate forms is irrelevant; for instance the AC1 error for Ne^{8+} is nearly five orders of magnitude smaller than that obtained from B3LYP.

The majority of the AC forms therefore become more accurate as Z increases, with the exception of AC4, AC4(H&H) and AC5. This may be understood from a consideration of the behaviour of the exact W_λ . In the $Z \rightarrow \infty$ limit, the electron–electron interaction can be treated as a small perturbation and so the exact W_λ becomes linear^{282–284,286,310–312} in λ ;

$$W_\lambda = E_x + 2E_{c,\text{GL2}}\lambda, \quad (6.41)$$

for which the associated exchange–correlation energy is simply given as the sum of the exchange and GL2 correlation energies. When evaluated with the data derived from FCI, this equation becomes $E_x^{\text{FCI}} + 2E_{c,\text{GL2}}^{\text{FCI}}\lambda$. An analysis of the behaviour of a , b and c for each of the forms that improve with Z shows that each of them behaves as eq. (6.41) as $Z \rightarrow \infty$. The improvement with increasing Z observed for most of the AC forms simply reflects the approach of this exact, limiting situation. As a specific illustration, consider the AC1 form in this limit. From eq. (6.28) and using the values determined according to eqs. (6.21) and (6.24),

$$W_\lambda^{\text{AC1}} = E_x^{\text{FCI}} + \frac{2E_{c,\text{GL2}}\lambda}{1 + c\lambda}. \quad (6.42)$$

Through eq. (6.22) the value of W_λ^{AC1} evaluated at $\lambda = 1$ is constrained to equal the exact W_1 ; when $Z \rightarrow \infty$ W_1 may alternatively be evaluated through eq. (6.41). By equating these two values for W_1 , it follows that $c = 0$ in this limit, so W_λ^{AC1} reduces to the required form for all λ . It therefore yields the correct exchange–correlation energy in the limit as $Z \rightarrow \infty$. This analysis highlights the importance of using information about virtual orbitals and

orbital energies in exchange–correlation functionals; without these quantities (from the GL2 expression) the non-linear forms would not yield the correct limiting behaviour.

As previously alluded to, the W_λ^{AC2} form exactly equals the linear expression of eq. (6.41) for all systems. It follows that the AC2 errors in figure 6.12 arise due to the lack of higher order terms in λ ; these errors provide an indication of the deviation from linearity of the exact AC with Z . The curvature of the exact W_λ reduces as Z increases, but as indicated by the size of the AC2 error, it is not insignificant even for Ne^{8+} . In order to provide an accurate description of the helium isoelectronic series as a whole, it is therefore necessary for a $W_\lambda^{\text{Approx}}$ to reproduce the evolution of the non-linearity with Z . For the forms we consider this is best achieved with AC1, followed by AC6. The reduction in curvature from H^- to Ne^{8+} is illustrated in figure 6.13, which plots $(W_\lambda^{\text{AC1}} - W_0^{\text{AC1}})$ as a function of λ for the ten systems. The diffuse-density H^- system stands out, consistent with figure 6.12. Note that the corresponding plot for AC6 is essentially the same, with the only discernible difference for H^- as reflected in the different total energies.

Also of interest is the similar accuracy obtained for AC1 and AC5 for the H^- system. This can be understood from the behaviour of the parameters in the two forms (see table 6.3). For H^- , c is near zero (-0.024) in W_λ^{AC5} but near unity (0.829) in W_λ^{AC1} . The values of a and b are identical in both; it follows that the two curves are very similar, yielding almost the same exchange–correlation energies. The breakdown in the agreement between the two methods as Z increases reflects the differing evolution of c between the two approaches. For AC1, as described above, $c \rightarrow 0$ in the limit as $Z \rightarrow \infty$; however, c becomes increasingly negative with AC5. A similar analysis can also explain the performance of AC4 and AC4(H&H) for this system.

The study has illustrated the high-quality description afforded by simple AC forms in the description of two-electron systems when near-exact input data is used. However, the scheme is impractical for an arbitrary molecular system. We now go on to consider the possibility of using alternative input data and

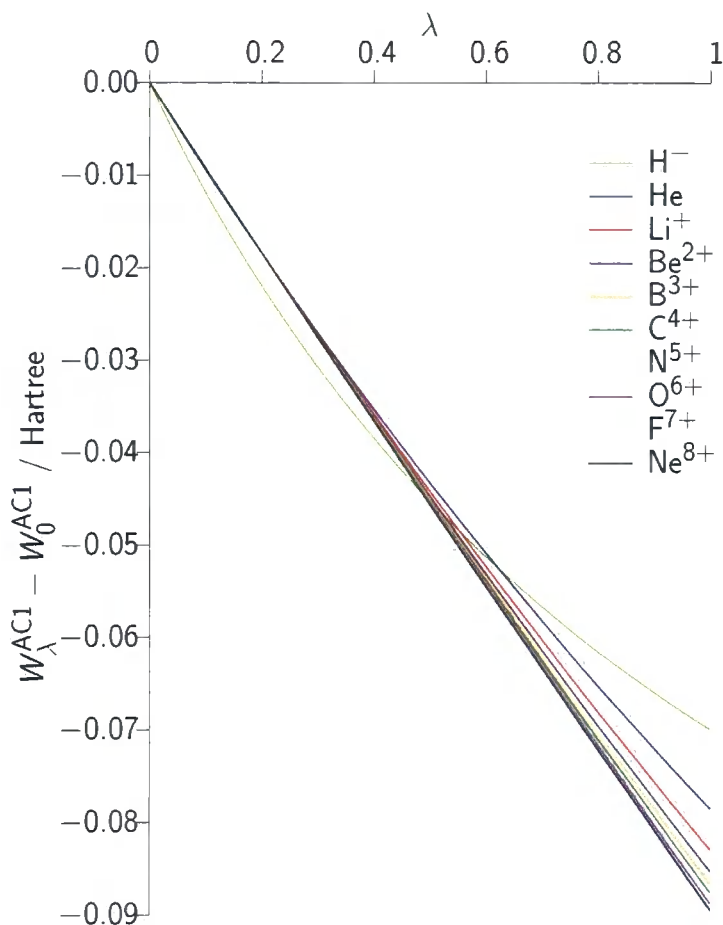


Figure 6.13: W_λ^{AC1} curves for the helium isoelectronic series.

its effect on the performance of the forms, and also the effect of moving to a many-electron system.

6.4 TOWARD A PRACTICAL FUNCTIONAL

We now consider if it is possible to move towards a practical exchange–correlation functional by considering additional or alternative input data. The value of a is easily obtained in practical calculations for self-consistent orbitals since $W_0 = a = E_x$. The practicality of b and c evaluated as in the previous sections however is severely limited; it is in principle possible, albeit computationally intensive, to construct self-consistent orbitals associated with the two-electron W'_0 given by eq. (6.24). There is no method of obtaining an

accurate value of W_1 except from large basis set FCI calculations. It is therefore beneficial to consider evaluation of an approximate W_λ^{AC} form without at least one of the quantities W'_0 or W_1 . Given that the most successful forms for two-electron systems use all three of these quantities, and the two-parameter forms considered were significantly less accurate, we need alternatives to these computationally difficult terms.

In the interaction strength interpolation model of Seidl *et al.*, the value of W_λ when $\lambda \rightarrow \infty$ (which we denote W_∞) is approximated and used as part of the functional construction. For infinite electron–electron repulsion corresponding to this limit of λ , the system may be described by the concept of strictly correlated electrons.³¹³ Consider a two-electron system in which the electron–electron repulsion is infinite; the position of one electron will be solely dependent on the position of the other electron at a given point in time. For spherical two-electron systems, it is possible to solve this problem exactly. For general many-electron systems, the strictly correlated electron result may be approximated by the point-charge plus continuum (PC) model gradient expansion approximation,^{313,314}

$$W_\infty^{\text{PC}}[\rho(\mathbf{r})] = \int d\mathbf{r} \left(-\frac{9}{10} \left(\frac{4\pi}{3}\right)^{\frac{1}{3}} \rho^{\frac{4}{3}}(\mathbf{r}) + \frac{3}{350} \left(\frac{3}{4\pi}\right)^{\frac{1}{3}} \frac{|\nabla\rho(\mathbf{r})|^2}{\rho^{\frac{4}{3}}(\mathbf{r})} \right). \quad (6.43)$$

Seidl^{286,313–315} and co-workers have demonstrated that this is a good approximation to the value obtained from the strictly correlated electrons approach; for our purposes it importantly depends only on the electron density. To compute values of W_∞^{PC} associated with a FCI density, we construct the quantities $|\nabla\rho(\mathbf{r})|^2$ and $\rho^{\frac{4}{3}}(\mathbf{r})$ on a very large quadrature grid, allowing simple evaluation of $W_\infty^{\text{PC,FCI}}$. When coupled with the exact conditions of the previous sections, we have in principle four pieces of input data from which we can determine input parameters for the approximate AC forms; W_0^{FCI} , W_1^{FCI} , W_0^{FCI} and $W_\infty^{\text{PC,FCI}}$.

As a starting point for the use of this additional input data, we consider the AC1 form of table 6.3. The use of this form may be justified, not just on the success observed in previous sections of its description of two-electron systems, but also from a consideration of the value of W_λ^{AC1} as $\lambda \rightarrow \infty$. In

this limit the AC1 form,

$$W_{\lambda}^{\text{AC1}} = a + \frac{b\lambda}{1 + c\lambda}, \quad (6.44)$$

takes the value of

$$W_{\infty}^{\text{AC1}} = a + \frac{b}{c}. \quad (6.45)$$

By comparing the value of $W_{\infty}^{\text{PC,FCI}}$ for H_2 (as a function of R) and $\text{H}^{-}\text{-Ne}^{8+}$ (as a function of Z) with the value obtained from the large- λ limit of the various W_{λ}^{AC} with their respective definitions of a , b and c , it is apparent that the best agreement is observed with the AC1 form. As the value of W_{∞}^{AC1} obtained using our procedure from the previous sections yields a value for the two-electron systems that is very close to the value obtained from W_{∞}^{PC} evaluated using the FCI density, this suggests that for this form it may be possible to obtain similar quality results regardless of the choice from our selection of input data.

From the four pieces of input data we may sensibly choose three pieces in the following ways: We can choose the original three pieces (W_0^{FCI} , $W_0^{\prime\text{FCI}}$ and W_1^{FCI}) to give the AC1 approach, or we may obtain two alternative definitions based on the AC1 form; AC1-2 which uses W_0^{FCI} , W_1^{FCI} and $W_{\infty}^{\text{PC,FCI}}$, and AC1-3 which uses W_0^{FCI} , $W_0^{\prime\text{FCI}}$ and $W_{\infty}^{\text{PC,FCI}}$. We do not consider the fourth combination as this would not fix the value of the curve when $\lambda = 0$. Values of b and c for AC1-2 are defined by

$$b = (W_{\infty}^{\text{PC,FCI}} - W_0^{\text{FCI}})c \quad (6.46)$$

$$c = \frac{W_1^{\text{FCI}} - W_0^{\text{FCI}}}{W_{\infty}^{\text{PC,FCI}} - W_1^{\text{FCI}}} \quad (6.47)$$

and the equivalent definitions for AC1-3 are

$$b = W_0^{\prime\text{FCI}} \quad (6.48)$$

$$c = \frac{W_0^{\prime\text{FCI}}}{W_{\infty}^{\text{PC,FCI}} - W_0^{\prime\text{FCI}}}. \quad (6.49)$$

Applying the AC1-2 and AC1-3 approaches to the ground state potential energy curve of H_2 , as illustrated in figure 6.14, we find that there is little to

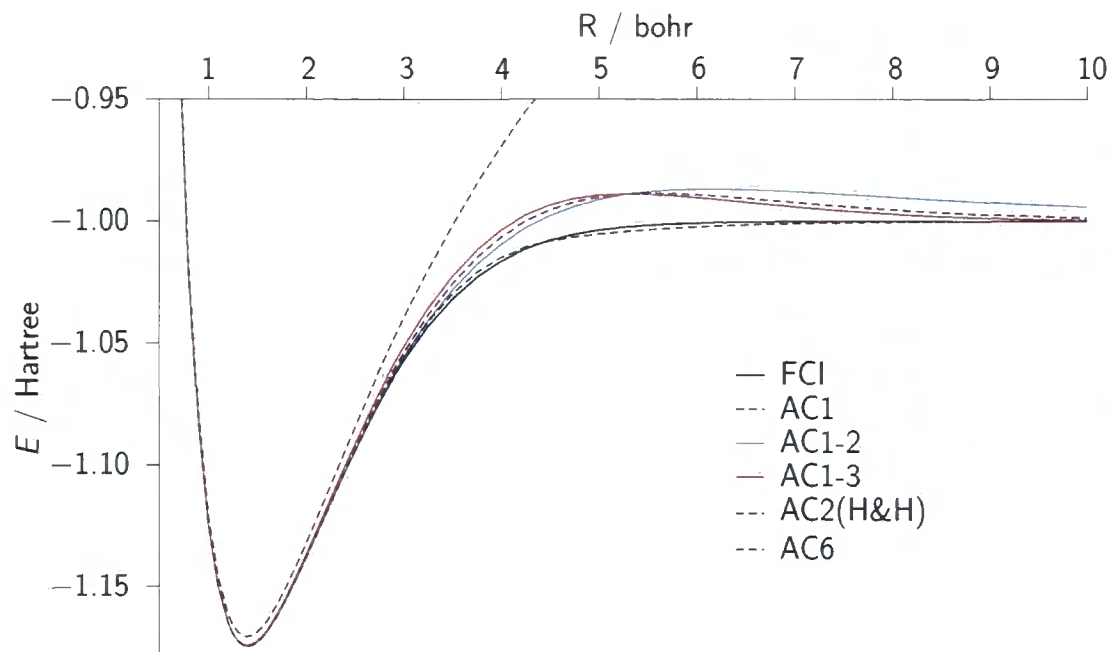


Figure 6.14: The H_2 potential energy curve obtained with standard adiabatic connection approaches and with those that use the additional $W_{\infty}^{\text{PC,FCI}}$ as input.

differentiate between those definitions that involve evaluation with $W_{\infty}^{\text{PC,FCI}}$ and the original AC1 curve. Also presented for comparison are the AC6 and AC2(H&H) curves. Equally figure 6.15 demonstrates that for the helium isoelectronic series, the error relative to FCI is essentially unchanged, particularly as Z increases.

The observation that for two-electron systems it is possible to obtain results that are significantly better than those from conventional functionals is encouraging, particularly for AC1-3, which involves evaluation with known orbital- or density-dependent expressions. With this in mind we go on to apply the AC1, AC1-2, AC1-3, AC2(H&H) and AC6 forms to a many-electron system, CO.

Carbon Monoxide

From the discussion of the AC forms applied to H_2 in this chapter, it is clear that the application of some of the approximate AC forms to many-electron

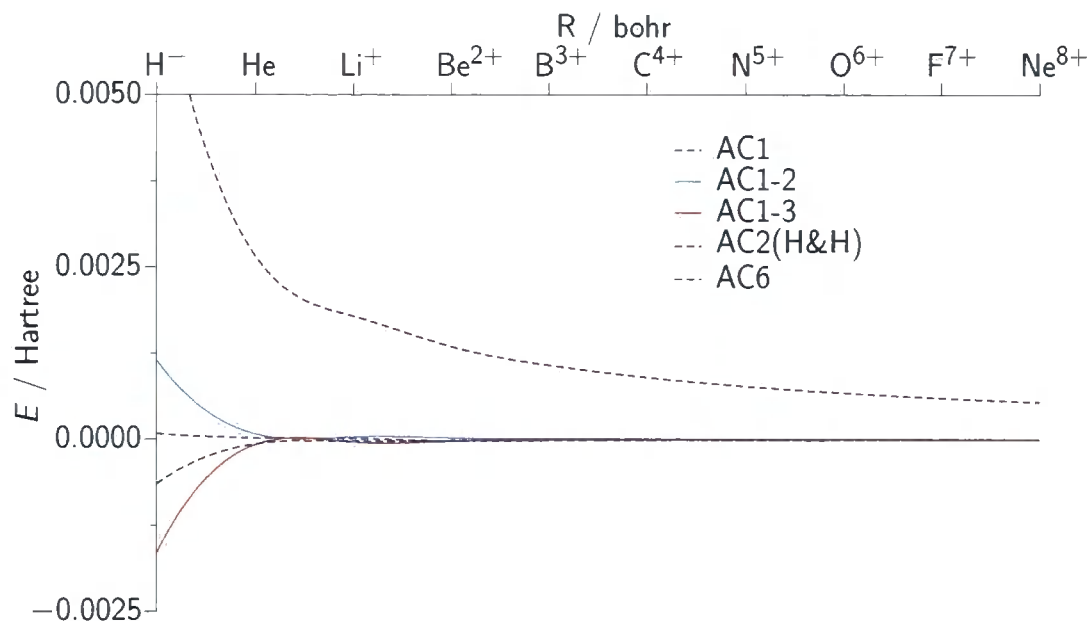


Figure 6.15: The error in total electronic energy $\Delta E = E - E^{\text{FCI}}$, as obtained with standard adiabatic connection approaches and with those that use the additional $W_{\infty}^{\text{PC,FCI}}$ as input.

systems may prove problematic. The size-extensivity failure is one issue, although it is difficult to judge in advance how significant a problem this is, particularly if we limit ourselves to near-equilibrium geometries. Perhaps more significant is the failure upon dissociation of a general homonuclear molecule due to the divergence of the gradient of W_{λ} resulting in a zero-valued T_c .

We now generalise the procedure of section 6.1 to systems with more than two electrons. The simplifications that arise for two-electron systems in the evaluation of the exact adiabatic connection data are of course no longer valid when we consider many-electron systems. For simplicity we assume that the singles contribution to the GL2 correlation energy is negligible, and as such we continue to evaluate it through eq. (6.24).

As the von Weizsäcker kinetic energy is not exact for systems with more than two electrons, we use the T_s obtained from the WY procedure; for the case of H_2 the value from the WY procedure agreed to six significant figures with T_W evaluated using eq. (6.26). FCI calculations in a large basis set are prohibitively expensive for systems with so many electrons. We have therefore

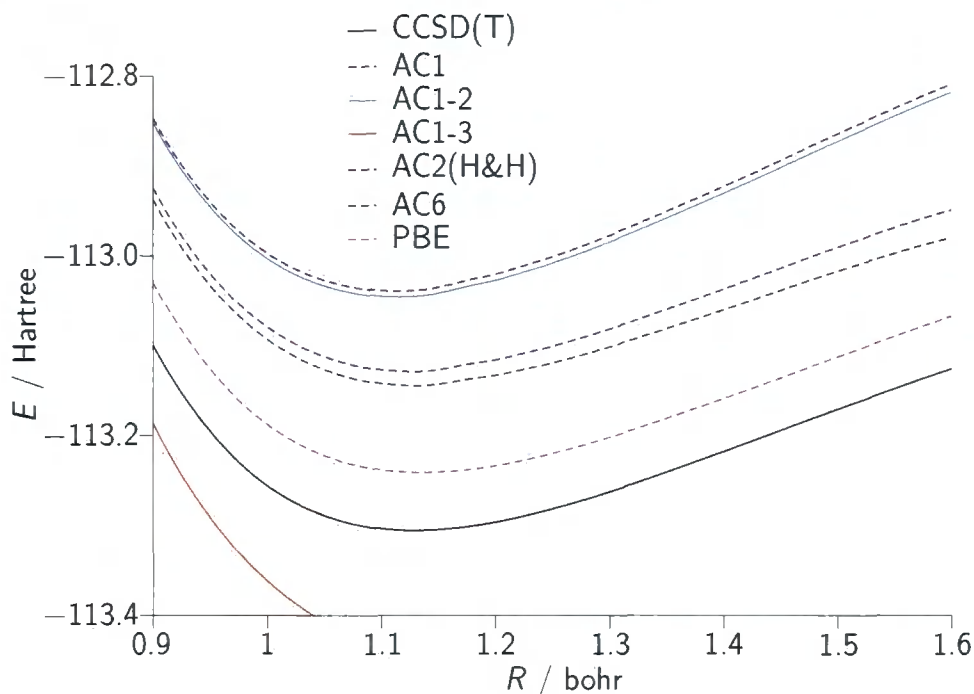


Figure 6.16: Potential energy curve of CO determined using CCSD(T), compared with those from various AC approximations.

evaluated CCSD(T) total electronic energies and densities at a series of bond lengths from 0.9 to 1.6 bohr. In order to determine the basis set dependence of the results, this was undertaken with the *cc-pVDZ*, *cc-pVTZ*, *cc-pCVTZ*, uncontracted *cc-pCVTZ*, *cc-pVQZ*, and *cc-pCVQZ* basis sets. The results presented in figure 6.16 are with the largest of these basis sets, *cc-pCVQZ*. This basis was chosen for its ability to describe both the orbitals and the potential in the WY procedure, as well as being large enough to provide accurate CCSD(T) energies and densities.

In our basis set investigations the presence of core functions proved of vital importance. The values obtained both for the CCSD(T) energies and the derived energy components and input data were essentially unchanged between *cc-pCVTZ*, uncontracted *cc-pCVTZ* and *cc-pCVQZ*; the conclusions of this work would remain unchanged if any of these basis sets were used.

As illustrated in figure 6.16, the agreement between CCSD(T) and the AC1 and AC6 forms is inconsistent with the observations for the two-electron

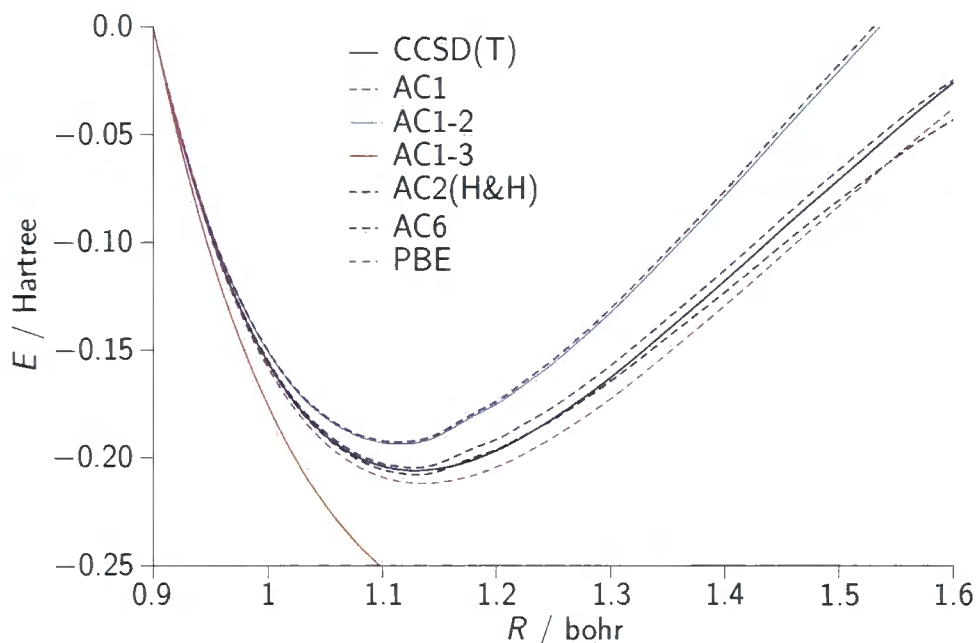


Figure 6.17: Potential energy curve of CO determined using CCSD(T) compared with curves, shifted to a common reference at 0.9 bohr, from various AC approximations.

systems. This is not a consequence of neglecting the (small) singles term in the evaluation of W_0^{FCI} ; scaling the value of this derivative by 10% has no discernible effect on either of these curves. Equally scaling the value of W_1 by 10% has only a small effect. The curve obtained from the AC1-2 approach is very similar to that obtained from AC2(H&H). The AC1-3 curve is completely unphysical, and does not bind CO. This is a disappointing observation given that the input parameters for AC1-3 are all expressed in terms of known quantities.

If the curves are shifted to a common reference point (so that each curve is aligned with the CCSD(T) energy at 0.9 bohr) as in figure 6.17, it is apparent that AC1 and AC6 behave in a similar way to the case of H_2 as the bond lengthens. AC1 appears to dissociate from above, and AC6 from below the CCSD(T) curve. Results are also presented from self-consistent PBE calculations using the same basis set. The results from these calculations appear to be no better or worse than those from any of the AC forms considered;

no significant improvement over standard functionals is observed for CO. Importantly the observation that the AC1-2 and AC1-3 approaches represented viable alternatives to AC1 is negated in the case of CO.

Whilst it must be stressed that these are only preliminary results, it does appear that the dramatic improvements observed when AC1 and AC6 are used for two-electron systems are not carried over into the many-electron case. The input data used in the case of CO, whilst necessarily less accurate than the FCI results obtained for two-electron systems, nevertheless represent high-quality data compared to what would be obtained from for instance PBE-derived quantities. We have in fact confirmed that the evaluation with PBE-derived data gives rise to similar conclusions as those evaluated with CCSD(T)-derived data. Further investigation of the applicability of approximate adiabatic connection forms to many-electron systems is required, particularly with respect to the effects of size-extensivity failure and the incorrect description of T_c on bond dissociation for the AC1 and AC6 forms.

We have used FCI data to quantify the accuracy of approximate AC forms in describing both the ground state potential energy curve of H_2 , and the helium isoelectronic series from H^- – Ne^{8+} , within spin-restricted density functional theory. To achieve this, essentially exact adiabatic connection data has been determined using FCI calculations; the approximate AC forms considered are then forced to reproduce this data by appropriately defining their parameters. This removes any error in the exchange–correlation component of the total energy except that due to the approximate AC form. Initially we focused on the AC1 form, demonstrating that it can provide a significant improvement over conventional functionals in the description of the ground state potential energy curve of H_2 . Importantly this form allows the correct dissociation of H_2 . Several other forms considered also correctly dissociate this molecule; notably the AC6 form which provides an excellent description of the exchange–correlation energy for all bond distances.

In our analysis of the helium isoelectronic series, the AC1 and AC6 forms again perform best. The minimal variation with approximate form observed

by Cohen²⁹² *et al.* for the case of approximate input data is not observed when accurate input data is used, although it should be stressed that their study was over a variety of molecules and properties—it is unclear if they would observe similar features for a study on a single molecule.

The observations for CO however suggest the need for more sophisticated approximate adiabatic connection forms if generally applicable functionals are to be obtained, particularly if approximate input data is used. The present study highlights the importance of using virtual orbitals and orbital energies,^{293,316,317} although the inclusion of this information appears to necessarily require sophisticated model forms if it is to be of practical use.

Conclusions

Computationally intensive accurate wavefunction methods generally remain within the purview of the small molecule and the quantum chemist. Kohn–Sham density functional theory (DFT) is applicable to much larger systems due to its relative computational simplicity, resulting in its extensive use. This significant use of DFT in chemical applications has fuelled functional development. In many cases existing exchange–correlation functionals are successfully applied, yet there remains a number of significant areas where they may fail, in some cases catastrophically. This thesis has focused on situations where standard functionals are known to fail, and approaches to address these deficiencies.

Exchange-attenuation was discussed in chapter 3 as a means to repair some of the failings of standard hybrid functionals. The prototypical CAM-B3LYP functional was examined in detail, comparing with the B3LYP hybrid functional. It was demonstrated that the CAM-B3LYP approach allows a roughly comparable description to B3LYP where that functional performs acceptably, but importantly for classical reaction barriers, polarisabilities and excitation energies it offers a notable improvement. To provide insight into the performance of attenuated functionals, errors in atomisation and excitation energies were considered as functions of the attenuation parameters. It was concluded that the form of attenuation used in CAM-B3LYP is insufficiently flexible to allow the satisfaction of a known long-range exact condition, which is necessary for the correct behaviour of, for instance, Rydberg excitation energies,

without degrading the description of other properties to an unacceptable extent. The need for more flexible attenuation forms was further highlighted by the observation that optimised attenuation parameters can vary significantly with both the property and species under consideration. However, the notably improved description of excitation energies with CAM-B3LYP indicates that the approach is introducing some of the physics required.

Following the successful application of attenuated functionals to excitation energies, the CAM-B3LYP functional was applied to an extensive set of excitation energies from a number of theoretically challenging molecules, in chapter 4. The use of conventional functionals (PBE and B3LYP) in many cases results in unacceptably large errors, particularly for the extended model peptide systems. CAM-B3LYP's successful description of these systems highlights the need for non-local information in an approximate exchange–correlation functional. Following a detailed discussion of the origin of the failings of conventional functionals, particularly for charge-transfer excitations where it can be attributed to a lack of occupied–virtual orbital overlap, a measure of the orbital overlap (Λ) was proposed. Both PBE and (to a lesser extent) B3LYP show correlation between the error in an excitation energy and the overlap between orbitals involved in that excitation, to the extent that it may be used to help judge the reliability of a calculation. When the overlap as defined by Λ falls below a given threshold, it is likely that the excitation energy will be in significant error if evaluated with a conventional functional. CAM-B3LYP exhibits no correlation with Λ ; the error does not become unacceptably large as the overlap drops. The application of the diagnostic test and CAM-B3LYP to a series of triazene chromophores further highlights the success of CAM-B3LYP as a theoretical method for the computation of excited states. However, it illustrates that with conventional functionals, unacceptably large errors may still be obtained even when Λ is large—in spatially extended systems non-locality is important regardless of occupied–virtual orbital overlap.

In order to further assess the geometrical and optical properties of attenuated functionals, the bond length alternation (BLA) and band gap of polyacetylene and polyyne oligomers were considered in chapter 5. Both the BLA and highest occupied–lowest unoccupied (HO–LU) gaps were determined for oligomers and the infinite chain (through the use of periodic boundary condi-

tions). Excitation energies were obtained for the oligomers and extrapolated to the infinite limit. Both CAM-B3LYP and BHLYP give BLA values and excitation energies that are larger and more accurate than those obtained from B3LYP. It was also illustrated that, in general, approximating the band gap as the HO–LU orbital energy gap yields results that are significantly different from the corresponding excitation energy.

Also considered in chapter 5 was the first application of CAM-B3LYP to shielding constants and chemical shifts in main-group, hydrogen-bonded and first-row transition metal-containing molecules. The results highlight the importance of using the theoretically rigorous OEP method to obtain a local, multiplicative potential, when the computation of NMR parameters is considered with hybrid and attenuated functionals. Importantly, when this approach is used, the performance of CAM-B3LYP is similar to that of standard hybrid functionals.

An alternative approach to the development of exchange–correlation functionals was discussed in chapter 6. The adiabatic connection (AC) was introduced as a rigorous approach for representing the exchange–correlation functional, by connecting a non-interacting system (corresponding to $\lambda = 0$) to the physical system (corresponding to $\lambda = 1$).

In general, functional construction uses both approximate input data and approximate forms to model the exact adiabatic connection. The ability of approximate forms to model the exact AC was investigated through the use of large basis set FCI calculations, which were used to derive essentially exact input data corresponding to the value and slope of the adiabatic connection in the non-interacting system and its value for the physical system. Two challenging problems were considered—the singlet ground state potential energy curve of H_2 within a restricted formalism and the total energies of the helium isoelectronic series from H^- – Ne^{8+} . For these systems it was found that exponential- and Padé-based forms performed best (AC6 and AC1), which enable the correct dissociation limit of H_2 and the correct evolution of the energies of the helium isoelectronic series with nuclear charge. Several other forms provided the correct limiting behaviour for both problems, but provide overall less accurate descriptions. These successes are in spite of the lack of size-extensivity of the forms. The correct limiting behaviour is a direct consequence of the

inclusion of information about virtual orbitals and their associated energies, highlighting the need for such quantities in exchange–correlation functionals.

Through the use of data determined for the large- λ limit, approximated through the point-charge plus continuum model, it is possible when using the AC1 form to obtain essentially identical results for H_2 and the helium isoelectronic series without the need for the generally unknown value of the AC for the physical system, or alternatively the gradient for the non-interacting system, which would make the approach more practicable for functional development. Preliminary calculations applying the approximate AC forms to CO were also undertaken. The AC offers an attractive approach for functional development, but requires both more accurate approximate forms and input data if it is to prove successful.

The ongoing development of new exchange–correlation functionals, particularly ones that are able to repair the deficiencies of existing approximations, is of vital importance to the chemistry community; this work contributes to this development.

Supplementary information for chapter 6

The definitions of the parameters a , b and c for the approximate AC forms of chapter 6 are given, along with the corresponding exchange–correlation energy expressions.

AC1:

$$W_{\lambda}^{\text{AC1}} = a + \frac{b\lambda}{1 + c\lambda} \quad (\text{A.1})$$

$$a = W_0^{\text{FCI}} \quad (\text{A.2})$$

$$b = W_0^{\prime\text{FCI}} \quad (\text{A.3})$$

$$c = \frac{b}{W_1^{\text{FCI}} - W_0^{\text{FCI}}} - 1 \quad (\text{A.4})$$

$$E_{\text{xc}}^{\text{AC1}} = a + \frac{b}{c} \left(1 - \frac{\log_e(1 + c)}{c} \right) \quad (\text{A.5})$$

AC2:

$$W_{\lambda}^{\text{AC2}} = a + b\lambda \quad (\text{A.6})$$

$$a = W_0^{\text{FCI}} \quad (\text{A.7})$$

$$b = W_0^{\prime\text{FCI}} \quad (\text{A.8})$$

$$E_{\text{xc}}^{\text{AC2}} = a + \frac{b}{2} \quad (\text{A.9})$$

AC2(H&H):

$$a = W_0^{\text{FCI}} \quad (\text{A.10})$$

$$b = W_1^{\text{FCI}} - W_0^{\text{FCI}} \quad (\text{A.11})$$

AC3:

$$W_{\lambda}^{\text{AC2}} = a + b\lambda + c\lambda^2 \quad (\text{A.12})$$

$$a = W_0^{\text{FCI}} \quad (\text{A.13})$$

$$b = W_0^{\prime\text{FCI}} \quad (\text{A.14})$$

$$c = W_1^{\text{FCI}} - W_0^{\text{FCI}} - W_0^{\prime\text{FCI}} \quad (\text{A.15})$$

$$E_{\text{xc}}^{\text{AC3}} = a + \frac{b}{2} + \frac{c}{3} \quad (\text{A.16})$$

AC4:

$$W_{\lambda}^{\text{AC4}} = a + b\left(\frac{\lambda}{1 + \lambda}\right) \quad (\text{A.17})$$

$$a = W_0^{\text{FCI}} \quad (\text{A.18})$$

$$b = W_0^{\prime\text{FCI}} \quad (\text{A.19})$$

$$E_{\text{xc}}^{\text{AC4}} = a + b(1 - \log_e(2)) \quad (\text{A.20})$$

AC4(H&H):

$$a = W_0^{\text{FCI}} \quad (\text{A.21})$$

$$b = 2(W_1^{\text{FCI}} - W_0^{\text{FCI}}) \quad (\text{A.22})$$

AC5:

$$W_{\lambda}^{\text{AC5}} = a + b\left(\frac{\lambda}{1 + \lambda}\right) + c\left(\frac{\lambda}{1 + \lambda}\right)^2 \quad (\text{A.23})$$

$$a = W_0^{\text{FCI}} \quad (\text{A.24})$$

$$b = W_0^{\prime\text{FCI}} \quad (\text{A.25})$$

$$c = 4\left(W_1^{\text{FCI}} - W_0^{\text{FCI}} - \frac{W_0^{\prime\text{FCI}}}{2}\right) \quad (\text{A.26})$$

$$E_{\text{xc}}^{\text{AC5}} = a + b(1 - \log_e(2)) + c\left(\frac{3}{2} - 2\log_e(2)\right) \quad (\text{A.27})$$

AC6:

$$W_{\lambda}^{\text{AC6}} = a + b\exp(-c\lambda) \quad (\text{A.28})$$

$$a = W_0^{\text{FCI}} - b \quad (\text{A.29})$$

$$b(1 - \exp(W_0^{\prime\text{FCI}}/b)) = W_0^{\text{FCI}} - W_1^{\text{FCI}} \quad (\text{A.30})$$

$$c = -\frac{W_0^{\prime\text{FCI}}}{b} \quad (\text{A.31})$$

$$E_{\text{xc}}^{\text{AC6}} = a + \frac{b}{c}(1 - \exp(-c)) \quad (\text{A.32})$$

AC7:

$$W_\lambda^{\text{AC7}} = a + b \log(1 + c\lambda) \quad (\text{A.33})$$

$$a = W_0^{\text{FCI}} \quad (\text{A.34})$$

$$b \log_e(1 + W_0^{\text{FCI}}/b) = W_1^{\text{FCI}} - W_0^{\text{FCI}} \quad (\text{A.35})$$

$$c = \frac{W_0^{\text{FCI}}}{b} \quad (\text{A.36})$$

$$E_{\text{xc}}^{\text{AC7}} = a - b + \frac{b}{c}((1 + c) \log_e(1 + c)) \quad (\text{A.37})$$

AC8:

$$W_\lambda^{\text{AC8}} = a + b \tanh(-c\lambda) \quad (\text{A.38})$$

$$a = W_0^{\text{FCI}} \quad (\text{A.39})$$

$$b \tanh(W_0^{\text{FCI}}/b) = W_1^{\text{FCI}} - W_0^{\text{FCI}} \quad (\text{A.40})$$

$$c = -\frac{W_0^{\text{FCI}}}{b} \quad (\text{A.41})$$

$$E_{\text{xc}}^{\text{AC8}} = a - \frac{b}{c} \log_e(\cosh(c)) \quad (\text{A.42})$$

AC9:

$$W_\lambda^{\text{AC9}} = a + b\lambda \exp(-c\lambda) \quad (\text{A.43})$$

$$a = W_0^{\text{FCI}} \quad (\text{A.44})$$

$$b = W_0^{\text{FCI}} \quad (\text{A.45})$$

$$c = \log_e(W_0^{\text{FCI}}) - \log_e(W_1^{\text{FCI}} - W_0^{\text{FCI}}) \quad (\text{A.46})$$

$$E_{\text{xc}}^{\text{AC9}} = a + \frac{b}{c^2}(1 - (1 + c) \exp(-c)) \quad (\text{A.47})$$

Publications

A significant portion of the work presented in this thesis has been published in peer-reviewed journals.

1. *Assessment of a Coulomb-attenuated exchange–correlation functional*
M. J. G. Peach, T. Helgaker, P. Sałek, T. W. Keal, O. B. Lutnæs, D. J. Tozer and N. C. Handy,
Phys. Chem. Chem. Phys., 2006, **8** 558–562.
2. *Influence of Coulomb-attenuation on exchange–correlation functional quality*
M. J. G. Peach, A. J. Cohen and D. J. Tozer,
Phys. Chem. Chem. Phys., 2006, **8** 4543–4549.
3. *An electrostatic gauche effect in β -fluoro and β -hydroxy *N*-ethylpyridinium cations*
N. E. J. Gooseman, D. O’Hagan, M. J. G. Peach, A. M. Z. Slawin, D. J. Tozer and R. J. Young,
Angew. Chem. Int. Ed., 2007, **46** 5904–5908.
4. *Modelling the adiabatic connection in H_2*
M. J. G. Peach, A. M. Teale and D. J. Tozer,
J. Chem. Phys., 2007, **126** 244104 (1–9).

5. *Structural and Electronic Properties of Polyacetylene and Polyynes from Hybrid and Coulomb-Attenuated Density Functionals*

M. J. G. Peach, E. I. Tellgren, P. Salek, T. Helgaker and D. J. Tozer,
J. Phys. Chem. A, **111** 11930–11935.

6. *Excitation energies in DFT: An evaluation and a diagnostic test*

M. J. G. Peach, P. Benfield, T. Helgaker and D. J. Tozer,
J. Chem. Phys., 2008, **128** 044118 (1–8).

7. *Adiabatic connection forms in density functional theory: H_2 and the He isoelectronic series*

M. J. G. Peach, A. M. Miller, A. M. Teale and D. J. Tozer,
J. Chem. Phys., 2008, **129** 064105 (1–7).

8. *TDDFT diagnostic testing and functional assessment for triazine chromophores*

M. J. G. Peach, C. R. Le Sueur, K. Ruud, M. Guillaume and D. J. Tozer,
Phys. Chem. Chem. Phys., Accepted.

Conferences attended

1. *Mathematical Challenges in Quantum Chemistry Problems*, Warwick, July 2007
2. *12th International Conference on the Applications of Density Functional Theory in Chemistry and Physics*, Amsterdam, August 2007 (Poster presented)
3. *Computational Molecular Science*, Cirencester, June 2008 (Poster presented).

References

1. M. Planck, *Ann. Phys.*, 1901, **4**, 553–563.
2. A. Einstein, *Ann. Phys.*, 1905, **17**, 132–148.
3. N. Bohr, *Phil. Mag.*, 1913, **6**, 1–25.
4. L. de Broglie, *Annales de Physique*, 1925, **3**, 22–128.
5. W. Heisenberg, *Z. Phys.*, 1925, **33**, 879–893.
6. R. P. Feynman, *Ann. Phys.*, 1944, **20**, 367–387.
7. E. Schrödinger, *Ann. Phys.*, 1926, **79**, 361–376.
8. E. Schrödinger, *Ann. Phys.*, 1926, **79**, 489–527.
9. E. Schrödinger, *Die Naturwissenschaften*, 1926, **28**, 664–666.
10. E. Schrödinger, *Ann. Phys.*, 1926, **79**, 734–756.
11. E. Schrödinger, *Ann. Phys.*, 1926, **80**, 437–490.
12. E. Schrödinger, *Ann. Phys.*, 1926, **81**, 109–139.
13. P. A. M. Dirac, *The Principles of Quantum Mechanics*, Oxford University Press, 4th edn., 1958.
14. T. Helgaker, P. Jørgensen and J. Olsen, *Molecular Electronic-Structure Theory*, John Wiley & Sons, Ltd, 1st edn., 2000.
15. P. A. M. Dirac, *Proc. Roy. Soc.*, 1927, **A117**, 610–624.
16. P. A. M. Dirac, *Proc. Roy. Soc.*, 1928, **A118**, 351–61.

17. W. Kutzelnigg, *Phys. Scr.*, 1987, **36**, 416–431.
18. M. Born, *Z. Phys.*, 1926, **38**, 803–827.
19. M. Born and J. R. Oppenheimer, *Ann. Phys.*, 1927, **84**, 457–484.
20. M. J. Feinberg, K. Rudenberg and E. L. Mehler, *Adv. Quantum Chem.*, 1970, **5**, 27–98.
21. D. R. Hartree, *Proc. Camb. Phil. Soc.*, 1928, **24**, 89–110.
22. D. R. Hartree, *Proc. Camb. Phil. Soc.*, 1928, **24**, 111–132.
23. D. R. Hartree, *Proc. Camb. Phil. Soc.*, 1928, **24**, 426–37.
24. W. Pauli, *Z. Phys.*, 1927, **43**, 601–623.
25. J. C. Slater, *Phys. Rev.*, 1929, **34**, 1293–1322.
26. J. C. Slater, *Phys. Rev.*, 1930, **35**, 509–529.
27. V. Fock, *Z. Phys.*, 1930, **61**, 126–148.
28. V. Fock, *Z. Phys.*, 1930, **62**, 795–805.
29. S. F. Boys, *Proc. Roy. Soc.*, 1950, **A200**, 542–554.
30. C. C. J. Roothaan, *Rev. Mod. Phys.*, 1951, **23**, 69–89.
31. G. G. Hall, *Proc. Roy. Soc.*, 1951, **A205**, 541–552.
32. S. R. Langhoff and E. R. Davidson, *Int. J. Quantum Chem.*, 1974, **8**, 61–72.
33. J. Čížek, *J. Chem. Phys.*, 1966, **45**, 4256–4266.
34. J. Čížek and J. Paldus, *Int. J. Quantum Chem.*, 1971, **5**, 359–379.
35. J. Čížek, *Theor. Chim. Acta.*, 1991, **80**, 91–94.
36. E. Merzbacher, *Quantum Mechanics*, Wiley, New York, 2nd edn., 1970.
37. J. Noga and R. J. Bartlett, *J. Chem. Phys.*, 1987, **86**, 7041–7050.

38. O. Christiansen, H. Koch and P. Jørgensen, *Chem. Phys. Lett.*, 1995, **243**, 409–418.
39. O. Christiansen, *Theor. Chem. Acc.*, 2006, **116**, 106–123.
40. O. Christiansen, H. Koch and P. Jørgensen, *J. Chem. Phys.*, 1995, **103**, 7429–7441.
41. H. Koch, O. Christiansen, P. Jørgensen, A. M. Sanchez de Meras and T. Helgaker, *J. Chem. Phys.*, 1997, **106**, 1808–1818.
42. J. A. Pople, M. Head-Gordon and K. Raghavachari, *J. Chem. Phys.*, 1987, **87**, 5968–5975.
43. J. Paldus, J. Čížek and B. Jeziorski, *J. Chem. Phys.*, 1989, **90**, 4356–4362.
44. J. A. Pople, M. Head-Gordon and K. Raghavachari, *J. Chem. Phys.*, 1989, **90**, 4635–4636.
45. C. Møller and M. S. Plesset, *Phys. Rev.*, 1934, **46**, 618–622.
46. L. Serrano-Andrés, M. Merchán, B. O. Roos and R. Lindh, *J. Am. Chem. Soc.*, 1995, **117**, 3189–3204.
47. J. Finley, P.-Å. Malmqvist, B. O. Roos and L. Serrano-Andrés, *Chem. Phys. Lett.*, 1998, **288**, 299–306.
48. B. Proppe, M. Merchán and L. Serrano-Andrés, *J. Phys. Chem. A*, 2000, **104**, 1608–1616.
49. K. Raghavachari, G. W. Trucks, J. A. Pople and M. Head-Gordon, *Chem. Phys. Lett.*, 1989, **157**, 479–483.
50. O. Vahtras, J. Almlöf and M. W. Feyereisen, *Chem. Phys. Lett.*, 1993, **213**, 514–518.
51. C. Hättig and F. Weigend, *J. Chem. Phys.*, 2000, **113**, 5154–5161.
52. M. Schutz and F. R. Manby, *Phys. Chem. Chem. Phys.*, 2003, **5**, 3349–3358.

-
53. P. Hohenberg and W. Kohn, *Phys. Rev.*, 1964, **136**, B864–B871.
 54. M. Levy, *Phys. Rev. A*, 1982, **26**, 1200–1208.
 55. E. H. Lieb, *Int. J. Quantum Chem.*, 1983, **24**, 243–277.
 56. M. Levy, *Proc. Natl. Acad. Sci. USA*, 1979, **76**, 6062–6065.
 57. L. H. Thomas, *Proc. Camb. Phil. Soc.*, 1927, **23**, 542–548.
 58. E. Fermi, *Z. Phys.*, 1928, **48**, 73–79.
 59. C. F. von Weizsäcker, *Z. Physik*, 1935, **96**, 431–458.
 60. P. A. M. Dirac, *Proc. Cam. Phil. Soc.*, 1930, **26**, 376–385.
 61. W. Kohn and L. J. Sham, *Phys. Rev.*, 1965, **140**, A1133–A1138.
 62. A. D. Becke, *J. Chem. Phys.*, 1988, **88**, 2547–2553.
 63. C. W. Murray, G. J. Laming, N. C. Handy and R. D. Amos, *Chem. Phys. Lett.*, 1992, **199**, 551–556.
 64. C. W. Murray, N. C. Handy and G. J. Laming, *Mol. Phys.*, 1993, **78**, 997–1014.
 65. J. A. Pople, P. M. W. Gill and N. C. Handy, *Int. J. Quantum Chem.*, 1995, **56**, 303–305.
 66. J. C. Slater, *Phys. Rev.*, 1951, **81**, 385–390.
 67. D. M. Ceperley and B. J. Alder, *Phys. Rev. Lett.*, 1980, **45**, 566–569.
 68. S. H. Vosko, L. Wilk and M. Nusair, *Can. J. Phys.*, 1980, **58**, 1200–1211.
 69. J. P. Perdew and Y. Wang, *Phys. Rev. B*, 1992, **45**, 13244–13249.
 70. J. P. Perdew, *Phys. Rev. Lett.*, 1985, **55**, 1665–1668.
 71. J. P. Perdew and W. Yue, *Phys. Rev. B*, 1986, **33**, 8800–8802.
 72. J. P. Perdew, K. Burke and M. Ernzerhof, *Phys. Rev. Lett.*, 1996, **77**, 3865–3868.

-
73. A. D. Becke, *J. Chem. Phys.*, 1986, **84**, 4524–4529.
 74. A. D. Becke, *Phys. Rev. A*, 1988, **38**, 3098–3100.
 75. A. J. Cohen and N. C. Handy, *Mol. Phys.*, 2001, **99**, 403–412.
 76. C. Lee, W. Yang and R. G. Parr, *Phys. Rev. B*, 1988, **37**, 785–789.
 77. A. D. Becke, *J. Chem. Phys.*, 1992, **97**, 9173–9177.
 78. F. A. Hamprecht, A. J. Cohen, D. J. Tozer and N. C. Handy, *J. Chem. Phys.*, 1998, **109**, 6264–6271.
 79. J. Tao, J. P. Perdew, V. N. Staroverov and G. E. Scuseria, *Phys. Rev. Lett.*, 2003, **91**, 146401 (1–4).
 80. J. P. Perdew, J. Tao, V. N. Staroverov and G. E. Scuseria, *J. Chem. Phys.*, 2004, **120**, 6898–6911.
 81. D. C. Langreth and J. P. Perdew, *Solid State Commun.*, 1975, **17**, 1425–1429.
 82. O. Gunnarsson and B. I. Lundqvist, *Phys. Rev. B*, 1976, **13**, 4274–4298.
 83. D. C. Langreth and J. P. Perdew, *Phys. Rev. B*, 1977, **15**, 2884–2901.
 84. E. R. Johnson and A. D. Becke, *J. Chem. Phys.*, 2005, **123**, 024101 (1–7).
 85. E. R. Johnson and A. D. Becke, *J. Chem. Phys.*, 2006, **124**, 174104 (1–9).
 86. A. D. Becke and E. R. Johnson, *J. Chem. Phys.*, 2007, **127**, 124108 (1–8).
 87. E. R. Johnson and A. D. Becke, *J. Chem. Phys.*, 2008, **128**, 124105 (1–3).
 88. A. D. Becke, *J. Chem. Phys.*, 1993, **98**, 1372–1377.
 89. A. D. Becke, *J. Chem. Phys.*, 1993, **98**, 5648–5652.
 90. P. J. Stephens, F. J. Devlin, C. F. Chabalowski and M. J. Frisch, *J. Phys. Chem.*, 1994, **98**, 11623–11627.
 91. M. Ernzerhof and G. E. Scuseria, *J. Chem. Phys.*, 1999, **110**, 5029–5036.

92. C. Adamo and V. Barone, *J. Chem. Phys.*, 1999, **110**, 6158–6170.
93. J. P. Perdew, M. Ernzerhof and K. Burke, *J. Chem. Phys.*, 1996, **105**, 9982–9985.
94. A. D. Becke, *J. Chem. Phys.*, 1997, **107**, 8554–8560.
95. P. J. Wilson, T. J. Bradley and D. J. Tozer, *J. Chem. Phys.*, 2001, **115**, 9233–9242.
96. T. W. Keal and D. J. Tozer, *J. Chem. Phys.*, 2005, **123**, 121103 (1–4).
97. W. Yang and Q. Wu, *Phys. Rev. Lett.*, 2002, **89**, 143002 (1–4).
98. Q. Wu and W. Yang, *J. Chem. Phys.*, 2003, **118**, 2498–2509.
99. M. J. G. Peach, T. Helgaker, P. Salek, T. W. Keal, O. B. Lutnæs, D. J. Tozer and N. C. Handy, *Phys. Chem. Chem. Phys.*, 2006, **8**, 558–562.
100. L. A. Curtiss, K. Raghavachari, G. W. Trucks and J. A. Pople, *J. Chem. Phys.*, 1991, **94**, 7221–7230.
101. L. A. Curtiss, K. Raghavachari, P. C. Redfern and J. A. Pople, *J. Chem. Phys.*, 1997, **106**, 1063–1079.
102. C. Adamo, M. Ernzerhof and G. E. Scuseria, *J. Chem. Phys.*, 2000, **112**, 2643–2649.
103. Y. Zhao, B. J. Lynch and D. G. Truhlar, *J. Phys. Chem. A*, 2004, **108**, 2715–2719.
104. T. W. Keal and D. J. Tozer, *J. Chem. Phys.*, 2004, **121**, 5654–5660.
105. G. Menconi and D. J. Tozer, *Chem. Phys. Lett.*, 2002, **360**, 38–46.
106. A. J. Sadlej, *Collect. Czech. Chem. Commun.*, 1988, **53**, 1995–2016.
107. A. J. Sadlej, *Theor. Chim. Acta.*, 1991, **79**, 123–140.
108. M. E. Casida, C. Jamorski, K. C. Casida and D. R. Salahub, *J. Chem. Phys.*, 1998, **108**, 4439–4449.

-
109. DALTON, *a molecular electronic structure program, Release 2.0*, 2005, see <http://www.kjemi.uio.no/software/dalton/dalton.html>.
110. R. D. Amos, I. L. Alberts, J. S. Andrews, A. J. Cohen, S. M. Colwell, N. C. Handy, D. Jayatilaka, P. J. Knowles, R. Kobayashi, G. J. Laming, A. M. Lee, P. E. Maslen, C. W. Murray, P. Palmieri, J. E. Rice, E. D. Simandiras, A. J. Stone, M.-D. Su and D. J. Tozer, *CADPAC 6.5, The Cambridge Analytic Derivatives Package*, 1998, Cambridge, England.
111. S. Skokov and R. A. Wheeler, *Chem. Phys. Lett.*, 1997, **271**, 251–258.
112. M. Filatov and W. Thiel, *Chem. Phys. Lett.*, 1998, **295**, 467–474.
113. B. J. Lynch, P. L. Fast, M. Harris and D. G. Truhlar, *J. Phys. Chem. A*, 2000, **104**, 4811–4815.
114. B. G. Janesko and G. E. Scuseria, *J. Chem. Phys.*, 2008, **128**, 244112 (1–4).
115. Y. Andersson, D. C. Langreth and B. I. Lundqvist, *Phys. Rev. Lett.*, 1996, **76**, 102–105.
116. T. Sato, T. Tsuneda and K. Hirao, *J. Chem. Phys.*, 2007, **126**, 234114 (1–12).
117. J. Antony and S. Grimme, *Phys. Chem. Chem. Phys.*, 2006, **8**, 5287–5293.
118. S. Grimme, *J. Comput. Chem.*, 2006, **27**, 1787–1799.
119. A. D. Becke and E. R. Johnson, *J. Chem. Phys.*, 2005, **123**, 154101 (1–9).
120. A. D. Becke and E. R. Johnson, *J. Chem. Phys.*, 2006, **124**, 014104 (1–6).
121. A. D. Becke and E. R. Johnson, *J. Chem. Phys.*, 2007, **127**, 154108 (1–6).
122. S. Grimme, *J. Chem. Phys.*, 2006, **124**, 034108 (1–16).
123. F. Neese, T. Schwabe and S. Grimme, *J. Chem. Phys.*, 2007, **126**, 124115 (1–15).

-
124. T. Schwabe and S. Grimme, *Phys. Chem. Chem. Phys.*, 2006, **8**, 4398–4401.
 125. P. M. W. Gill, R. D. Adamson and J. A. Pople, *Mol. Phys.*, 1996, **88**, 1005–1010.
 126. J. Heyd, G. E. Scuseria and M. Ernzerhof, *J. Chem. Phys.*, 2003, **118**, 8207–8215.
 127. J. Heyd and G. E. Scuseria, *J. Chem. Phys.*, 2004, **120**, 7274–7280.
 128. J. Heyd and G. E. Scuseria, *J. Chem. Phys.*, 2004, **121**, 1187–1192.
 129. J. Heyd, J. E. Peralta, G. E. Scuseria and R. L. Martin, *J. Chem. Phys.*, 2005, **123**, 174101 (1–8).
 130. E. N. Brothers, A. F. Izmaylov, J. O. Normand, V. Barone and G. E. Scuseria, *J. Chem. Phys.*, 2008, **129**, 011102 (1–4).
 131. O. A. Vydrov, J. Heyd, A. V. Krukau and G. E. Scuseria, *J. Chem. Phys.*, 2006, **125**, 074106 (1–9).
 132. A. Savin, in *Recent Developments and Applications of Modern Density Functional Theory*, ed. J. M. Seminario, Elsevier, Amsterdam, 1996, pp. 327–357.
 133. T. Leininger, H. Stoll, H.-J. Werner and A. Savin, *Chem. Phys. Lett.*, 1997, **275**, 151–160.
 134. H. Iikura, T. Tsuneda, T. Yanai and K. Hirao, *J. Chem. Phys.*, 2001, **115**, 3540–3544.
 135. Y. Tawada, T. Tsuneda, S. Yanagisawa, T. Yanai and K. Hirao, *J. Chem. Phys.*, 2004, **120**, 8425–8433.
 136. M. Ernzerhof and J. P. Perdew, *J. Chem. Phys.*, 1998, **109**, 3313–3320.
 137. T. M. Henderson, B. G. Janesko and G. E. Scuseria, *J. Chem. Phys.*, 2008, **128**, 194105 (1–9).

-
138. M. Chiba, T. Tsuneda and K. Hirao, *J. Chem. Phys.*, 2006, **124**, 144106 (1–11).
139. J.-W. Song, T. Hirose, T. Tsuneda and K. Hirao, *J. Chem. Phys.*, 2007, **126**, 154105 (1–7).
140. T. Yanai, D. P. Tew and N. C. Handy, *Chem. Phys. Lett.*, 2004, **393**, 51–57.
141. I. C. Gerber and J. G. Ángyán, *Chem. Phys. Lett.*, 2005, **415**, 100–105.
142. J.-D. Chai and M. Head-Gordon, *J. Chem. Phys.*, 2008, **128**, 084106 (1–15).
143. J.-D. Chai and M. Head-Gordon, *Phys. Chem. Chem. Phys.*, 2008, **10**, 6615–6620.
144. R. Baer and D. Neuhauser, *Phys. Rev. Lett.*, 2005, **94**, 043002 (1–4).
145. A. J. Cohen, P. Mori-Sanchez and W. Yang, *J. Chem. Phys.*, 2007, **126**, 191109 (1–5).
146. M. J. G. Peach, A. J. Cohen and D. J. Tozer, *Phys. Chem. Chem. Phys.*, 2006, **8**, 4543–4549.
147. O. A. Vydrov and G. E. Scuseria, *J. Chem. Phys.*, 2006, **125**, 234109 (1–9).
148. J.-D. Chai and M. Head-Gordon, *Chem. Phys. Lett.*, 2008, **467**, 176–178.
149. T. M. Henderson, A. F. Izmaylov, G. E. Scuseria and A. Savin, *J. Chem. Phys.*, 2007, **127**, 221103 (1–4).
150. D. J. Tozer and N. C. Handy, *J. Chem. Phys.*, 1998, **109**, 10180–10189.
151. D. J. Tozer, R. D. Amos, N. C. Handy, B. O. Roos and L. Serrano-Andrés, *Mol. Phys.*, 1999, **97**, 859–868.
152. J. P. Perdew, *Phys. Rev. B*, 1986, **33**, 8822–8824.
153. T. H. Dunning Jr., *J. Chem. Phys.*, 1971, **55**, 716–723.

154. S. Huzinaga, *J. Chem. Phys.*, 1965, **42**, 1293–1302.
155. A. B. J. Parusel, G. Kohler and S. Grimme, *J. Phys. Chem. A*, 1998, **102**, 6297–6306.
156. C. Jamorski, J. B. Foresman, C. Thilgen and H.-P. Lüthi, *J. Chem. Phys.*, 2002, **116**, 8761–8771.
157. A. B. J. Parusel, G. Kohler and M. Nooijen, *J. Phys. Chem. A*, 1999, **103**, 4056–4064.
158. C. Bulliard, M. Allan, G. Wirtz, E. Haselbach, K. Zachariasse, N. Detzer and S. Grimme, *J. Phys. Chem. A*, 1999, **103**, 7766–7772.
159. A. Heine, R. Herbst-Irmer, D. Stalke, W. Kühnle and K. A. Zachariasse, *Acta Crystallogr. Sect. B*, 1994, **50**, 363–373.
160. O. Kajimoto, H. Yokoyama, Y. Ooshima and Y. Endo, *Chem. Phys. Lett.*, 1991, **179**, 455–459.
161. J.-W. Song, S. Tokura, T. Sato, M. A. Watson and K. Hirao, *J. Chem. Phys.*, 2007, **127**, 154109 (1–6).
162. A. V. Krukau, G. E. Scuseria, J. P. Perdew and A. Savin, *J. Chem. Phys.*, 2008, **129**, 124103 (1–7).
163. S. A. Varganov, A. T. B. Gilbert, E. Deplazes and P. M. W. Gill, *J. Chem. Phys.*, 2008, **128**, 201104 (1–4).
164. E. Runge and E. K. U. Gross, *Phys. Rev. Lett.*, 1984, **52**, 997–1000.
165. E. K. U. Gross and W. Kohn, in *Density Functional Theory of Many-Fermion Systems*, ed. P.-O. Löwdin, Academic Press, 1990, vol. 21, pp. 255–291.
166. M. E. Casida, in *Recent Advances in Density Functional Methods, Part I*, ed. D. P. Chong, Singapore, World Scientific, 1995, pp. 155–192.
167. R. van Leeuwen, *Phys. Rev. Lett.*, 1998, **80**, 1280–1283.
168. A. Dreuw and M. Head-Gordon, *Chem. Rev.*, 2005, **105**, 4009–4037.

-
169. E. K. U. Gross, C. A. Ullrich and U. J. Gossmann, in *Density Functional Theory*, ed. E. K. U. Gross and R. M. Dreizler, Plenum, New York, 1994, pp. 149–171.
170. M. A. L. Marques and E. K. U. Gross, *Annu. Rev. Phys. Chem.*, 2004, **55**, 427–455.
171. M. A. L. Marques and E. K. U. Gross, *A Primer in Density Functional Theory*, 2003, 144–184.
172. R. McWeeny and B. T. Sutcliffe, *Methods of Molecular Quantum Mechanics*, Academic Press, London, 1969.
173. R. Bauernschmitt and R. Ahlrichs, *Chem. Phys. Lett.*, 1996, **256**, 454–464.
174. J. P. Perdew, R. G. Parr, M. Levy and J. L. Balduz, *Phys. Rev. Lett.*, 1982, **49**, 1691–1694.
175. J. P. Perdew and M. Levy, *Phys. Rev. Lett.*, 1983, **51**, 1884–1887.
176. A. M. Teale, F. De Proft and D. J. Tozer, *J. Chem. Phys.*, 2008, **129**, 044110 (1–12).
177. J. P. Perdew and K. Burke, *Int. J. Quantum Chem.*, 1996, **57**, 309–319.
178. D. J. Tozer and N. C. Handy, *J. Chem. Phys.*, 1998, **108**, 2545–2555.
179. M. E. Casida, K. C. Casida and D. R. Salahub, *Int. J. Quantum Chem.*, 1998, **70**, 933–941.
180. M. Grüning, O. V. Gritsenko, S. J. A. van Gisbergen and E. J. Baerends, *J. Chem. Phys.*, 2001, **114**, 652–660.
181. M. J. Allen and D. J. Tozer, *J. Chem. Phys.*, 2000, **113**, 5185–5192.
182. T. Yanai, R. J. Harrison and N. C. Handy, *Mol. Phys.*, 2005, **103**, 413–424.
183. J. Fabian, *Theor. Chem. Acc.*, 2001, **106**, 199–217.

-
184. A. Dreuw, G. R. Fleming and M. Head-Gordon, *J. Phys. Chem. B*, 2003, **107**, 6500–6503.
185. A. Dreuw, G. R. Fleming and M. Head-Gordon, *Phys. Chem. Chem. Phys.*, 2003, **5**, 3247–3256.
186. M.-S. Liao, Y. Lu and S. Scheiner, *J. Comput. Chem.*, 2003, **24**, 623–631.
187. A. L. Sobolewski and W. Domcke, *Chem. Phys.*, 2003, **294**, 73–83.
188. A. Dreuw and M. Head-Gordon, *J. Am. Chem. Soc.*, 2004, **126**, 4007–4016.
189. S. Anand and H. B. Schlegel, *Mol. Phys.*, 2006, **104**, 933–941.
190. E. Fabiano, F. DellaSala, G. Barbarella, S. Lattante, M. Anni, G. Sotgiu, C. Hättig, R. Cingolani and G. Gigli, *J. Phys. Chem. B*, 2006, **110**, 18651–18660.
191. E. A. Perpète, J. Preat, J.-M. Andre and D. Jacquemin, *J. Phys. Chem. A*, 2006, **110**, 5629–5635.
192. X. Xu, Z. Cao and Q. Zhang, *J. Phys. Chem. A*, 2006, **110**, 1740–1748.
193. D. Rappoport and F. Furche, *J. Am. Chem. Soc.*, 2004, **126**, 1277–1284.
194. D. Jacquemin, M. Bouhy and E. A. Perpète, *J. Chem. Phys.*, 2006, **124**, 204321 (1–9).
195. A. Dreuw, J. L. Weisman and M. Head-Gordon, *J. Chem. Phys.*, 2003, **119**, 2943–2946.
196. D. J. Tozer, *J. Chem. Phys.*, 2003, **119**, 12697–12699.
197. O. Gritsenko and E. J. Baerends, *J. Chem. Phys.*, 2004, **121**, 655–660.
198. R. Kobayashi and R. D. Amos, *Chem. Phys. Lett.*, 2006, **420**, 106–109.
199. P. N. Day, K. A. Nguyen and R. Pachter, *J. Chem. Phys.*, 2006, **125**, 094103 (1–13).

-
200. D. Jacquemin, E. A. Perpète, O. A. Vydrov, G. E. Scuseria and C. Adamo, *J. Chem. Phys.*, 2007, **127**, 094102 (1–6).
201. K. A. Nguyen, P. N. Day and R. Pachter, *J. Chem. Phys.*, 2007, **126**, 094303 (1–9).
202. M. J. G. Peach, P. Benfield, T. Helgaker and D. J. Tozer, *J. Chem. Phys.*, 2008, **128**, 044118 (1–8).
203. L. Serrano-Andrés and M. P. Fülscher, *J. Am. Chem. Soc.*, 1998, **120**, 10912–10920.
204. S. Grimme and M. Parac, *ChemPhysChem*, 2003, **4**, 292–295.
205. M. J. G. Peach, E. I. Tellgren, P. Salek, T. Helgaker and D. J. Tozer, *J. Phys. Chem. A*, 2007, **111**, 11930–11935.
206. C. Hu, O. Sugino and Y. Miyamoto, *Phys. Rev. A*, 2006, **74**, 032508 (1–7).
207. D. Jacquemin, E. A. Perpète, G. Scalmani, M. J. Frisch, R. Kobayashi and C. Adamo, *J. Chem. Phys.*, 2007, **126**, 144105 (1–12).
208. K. P. Huber and G. Herzberg, *Molecular spectra and molecular structure. 4, Constants of diatomic molecules.*, Van Nostrand, New York, 1979.
209. T. H. Dunning Jr., *J. Chem. Phys.*, 1989, **90**, 1007–1023.
210. D. E. Woon and T. H. Dunning Jr., *J. Chem. Phys.*, 1994, **100**, 2975–2988.
211. R. A. Kendall, T. H. Dunning Jr. and R. J. Harrison, *J. Chem. Phys.*, 1992, **96**, 6796–6806.
212. R. McDiarmid, *J. Chem. Phys.*, 1976, **64**, 514–521.
213. W. M. Flicker, O. A. Mosher and A. Kuppermann, *Chem. Phys. Lett.*, 1977, **45**, 492–497.
214. D. G. Leopold, R. D. Pendley, J. L. Roebber, R. J. Hemley and V. Vaida, *J. Chem. Phys.*, 1984, **81**, 4218–4229.

-
215. S. B. Ben-Shlomo and U. Kaldor, *J. Chem. Phys.*, 1990, **92**, 3680–3682.
216. E. S. Nielsen, P. Jørgensen and J. Oddershede, *J. Chem. Phys.*, 1980, **73**, 6238–6246.
217. D. J. Clouthier and D. A. Ramsay, *Annu. Rev. Phys. Chem.*, 1983, **34**, 31–58.
218. S. Taylor, D. G. Wilden and J. Comer, *Chem. Phys.*, 1982, **70**, 291–298.
219. D. J. Tozer and N. C. Handy, *Mol. Phys.*, 2003, **101**, 2669–2675.
220. J. Preat, C. Michaux, A. Lewalle, E. A. Perpète and D. Jacquemin, *Chem. Phys. Lett.*, 2008, **451**, 37–42.
221. D. M. Khramov and C. W. Bielawski, *Chem. Commun.*, 2005, **39**, 4958–4960.
222. D. M. Khramov and C. W. Bielawski, *J. Org. Chem.*, 2007, **72**, 9407–9417.
223. J. Tomasi, B. Mennucci and R. Cammi, *Chem. Rev.*, 2005, **105**, 2999–3094.
224. V. Barone, M. Cossi and J. Tomasi, *J. Chem. Phys.*, 1997, **107**, 3210–3221.
225. R. Ahlrichs, M. Bär, M. Häser, H. Horn and C. Kölmel, *Chem. Phys. Lett.*, 1989, **162**, 165–169.
226. C. Hättig, A. Hellweg and A. Köhn, *Phys. Chem. Chem. Phys.*, 2006, **8**, 1159–1169.
227. C. Hättig and A. Köhn, *J. Chem. Phys.*, 2002, **117**, 6939–6951.
228. C. Hättig, *Phys. Chem. Chem. Phys.*, 2005, **7**, 59–66.
229. A. V. Krukau, O. A. Vydrov, A. F. Izmaylov and G. E. Scuseria, *J. Chem. Phys.*, 2006, **125**, 224106 (1–5).

-
230. Z.-L. Cai, M. Crossley, J. Reimers, R. Kobayashi and R. Amos, *J. Phys. Chem. B*, 2006, **110**, 15624–15632.
231. L. Ferrighi, L. Frediani, C. Cappelli, P. Salek, H. Ågren, T. Helgaker and K. Ruud, *Chem. Phys. Lett.*, 2006, **425**, 267–272.
232. A. Baev, P. Norman, J. Henriksson and H. Ågren, *J. Phys. Chem. B*, 2006, **110**, 20912–20916.
233. M. Pecul, *Chem. Phys. Lett.*, 2006, **418**, 1–10.
234. H. Katagiri, Y. Shimoi and S. Abe, *Chem. Phys.*, 2004, **306**, 191–200.
235. M. Weimer, W. Hieringer, F. D. Sala and A. Görling, *Chem. Phys.*, 2005, **309**, 77–87.
236. S. Yang, P. Olishovski and M. Kertesz, *Synth. Met.*, 2004, **141**, 171–177.
237. D. Jacquemin, J.-M. Andre and E. A. Perpète, *J. Chem. Phys.*, 2004, **121**, 4389–4396.
238. T. D. Poulsen, K. V. Mikkelsen, J. G. Fripiat, D. Jacquemin and B. Champagne, *J. Chem. Phys.*, 2001, **114**, 5917–5922.
239. G. R. Hutchison, Y.-J. Zhao, B. Delley, A. J. Freeman, M. A. Ratner and T. J. Marks, *Phys. Rev. B*, 2003, **68**, 035204 (1–13).
240. D. Jacquemin, A. Femenias, H. Chermette, J.-M. Andre and E. A. Perpète, *J. Phys. Chem. A*, 2005, **109**, 5734–5741.
241. D. Jacquemin, A. Femenias, H. Chermette, I. Ciofini, C. Adamo, J.-M. Andre and E. A. Perpète, *J. Phys. Chem. A*, 2006, **110**, 5952–5959.
242. S. Yang and M. Kertesz, *J. Phys. Chem. A*, 2006, **110**, 9771–9774.
243. D. Jacquemin, E. A. Perpète, I. Ciofini and C. Adamo, *Chem. Phys. Lett.*, 2005, **405**, 376–381.
244. S. Hirata and S. Iwata, *J. Chem. Phys.*, 1997, **107**, 10075–10084.

-
245. C. H. Choi, M. Kertesz and A. Karpfen, *J. Chem. Phys.*, 1997, **107**, 6712–6721.
246. R. Pino and G. E. Scuseria, *J. Chem. Phys.*, 2004, **121**, 8113–8119.
247. K. N. Kudin and G. E. Scuseria, *Phys. Rev. B*, 2000, **61**, 16440–16453.
248. *Quantum-Mechanical Ab-initio Calculation of the Properties of Crystalline Materials*, ed. C. Pisani, Springer, Berlin, 1996.
249. C. S. Yannoni and T. C. Clarke, *Phys. Rev. Lett.*, 1983, **51**, 1191–1193.
250. M. J. Duijvestijn, A. Manenschijn, J. Smidt and R. A. Wind, *J. Mag. Resonance*, 1985, **64**, 461–469.
251. H. Kahlert, O. Leitner and G. Leising, *Synth. Met.*, 1987, **17**, 467–472.
252. J. Ma, S. Li and Y. Jiang, *Macromolecules*, 2002, **35**, 1109–1115.
253. K. L. D'Amico, C. Manos and R. L. Christensen, *J. Am. Chem. Soc.*, 1980, **102**, 1777–1782.
254. T. Tani, P. M. Grant, W. D. Gill, G. B. Street and T. C. Clarke, *Solid State Commun.*, 1980, **33**, 499–503.
255. C. R. Fincher, C. E. Chen, A. J. Heeger, A. G. MacDiarmid and J. B. Hastings, *Phys. Rev. Lett.*, 1982, **48**, 100–104.
256. J. Gierschner, J. Cornil and H.-J. Egelhaaf, *Adv. Mat.*, 2007, **19**, 173–191.
257. T. Pino, H. Ding, F. Guthe and J. P. Maier, *J. Chem. Phys.*, 2001, **114**, 2208–2212.
258. E. Kloster-Jensen, H.-J. Haink and H. Christen, *Helv. Chim. Acta*, 1974, **57**, 1731–1744.
259. M. Grutter, M. Wyss, J. Fulara and J. Maier, *J. Phys. Chem. A*, 1998, **102**, 9785–9790.
260. P. J. Wilson and D. J. Tozer, *Chem. Phys. Lett.*, 2001, **337**, 341–348.

-
261. Q. Zhao, R. C. Morrison and R. G. Parr, *Phys. Rev. A*, 1994, **50**, 2138–2142.
262. A. J. Cohen, Q. Wu and W. Yang, *Chem. Phys. Lett.*, 2004, **399**, 84–88.
263. M. J. Allen, T. W. Keal and D. J. Tozer, *Chem. Phys. Lett.*, 2003, **380**, 70–77.
264. P. J. Wilson and D. J. Tozer, *J. Mol. Struct.*, 2002, **602–603**, 191–197.
265. O. B. Lutnæs, A. M. Teale, T. Helgaker and D. J. Tozer, *J. Chem. Theory Comput.*, 2006, **2**, 827–834.
266. A. M. Teale, A. J. Cohen and D. J. Tozer, *J. Chem. Phys.*, 2007, **126**, 074101 (1–7).
267. Q. Wu and W. Yang, *J. Theor. Comput. Chem.*, 2003, **2**, 627–638.
268. V. N. Staroverov, G. E. Scuseria and E. R. Davidson, *J. Chem. Phys.*, 2006, **124**, 141103 (1–4).
269. V. N. Staroverov, G. E. Scuseria and E. R. Davidson, *J. Chem. Phys.*, 2006, **125**, 081104 (1–4).
270. E. Fermi and E. Amaldi, *Mem. classe sci. fis. mat. nat. accad. Italia*, 1934, **6**, 117–149.
271. J. Kongsted, K. Aidas, K. V. Mikkelsen and S. P. A. Sauer, *J. Chem. Theory Comput.*, 2008, **4**, 267–277.
272. S. Huzinaga, *Approximate Atomic Functions*, University of Alberta, Edmonton, 1971.
273. W. Kutzelnigg, U. Fleischer and M. Schlindler, *NMR—Basic Principles and Progress*, Springer, Heidelberg, 1990, vol. 23.
274. F. London, *J. Phys. Radium*, 1937, **8**, 397–409.
275. H. F. Hameka, *Mol. Phys.*, 1958, **1**, 203–215.
276. J. A. Pople, *Mol. Phys.*, 1958, **1**, 175–180.

-
277. T. W. Keal and D. J. Tozer, *J. Chem. Phys.*, 2003, **119**, 3015–3024.
278. M. Levy, *Phys. Rev. A*, 1991, **43**, 4637–4646.
279. D. P. Joubert and G. P. Srivastava, *J. Chem. Phys.*, 1998, **109**, 5212–5220.
280. F. Colonna and A. Savin, *J. Chem. Phys.*, 1999, **110**, 2828–2835.
281. D. Frydel, W. M. Terilla and K. Burke, *J. Chem. Phys.*, 2000, **112**, 5292–5297.
282. A. Görling and M. Levy, *Phys. Rev. B*, 1993, **47**, 13105–13113.
283. A. Görling and M. Levy, *Phys. Rev. A*, 1994, **50**, 196–204.
284. M. Ernzerhof, *Chem. Phys. Lett.*, 1996, **263**, 499–506.
285. K. Burke, M. Ernzerhof and J. P. Perdew, *Chem. Phys. Lett.*, 1997, **265**, 115–120.
286. M. Seidl, J. P. Perdew and S. Kurth, *Phys. Rev. Lett.*, 2000, **84**, 5070–5073.
287. P. Mori-Sánchez, A. J. Cohen and W. Yang, *J. Chem. Phys.*, 2006, **124**, 091102 (1–4).
288. M. Levy and J. P. Perdew, *Phys. Rev. A*, 1985, **32**, 2010–2021.
289. P. Mori-Sánchez, A. J. Cohen and W. Yang, *J. Chem. Phys.*, 2006, **125**, 201102 (1–4).
290. A. Ruzsinszky, J. P. Perdew, G. I. Csonka, O. A. Vydrov and G. E. Scuseria, *J. Chem. Phys.*, 2007, **126**, 104102 (1–8).
291. A. J. Cohen, P. Mori-Sánchez and W. Yang, *J. Chem. Phys.*, 2008, **129**, 121104 (1–4).
292. A. J. Cohen, P. Mori-Sánchez and W. Yang, *J. Chem. Phys.*, 2007, **127**, 034101 (1–14).

-
293. M. Fuchs, Y.-M. Niquet, X. Gonze and K. Burke, *J. Chem. Phys.*, 2005, **122**, 094116 (1–13).
294. C. J. Umrigar and X. Gonze, *Phys. Rev. A*, 1994, **50**, 3827–3837.
295. A. A. Jarzecki and E. R. Davidson, *Phys. Rev. A*, 1998, **58**, 1902–1909.
296. P. M. W. Gill, D. L. Crittenden, D. P. O’Neill and N. A. Besley, *Phys. Chem. Chem. Phys.*, 2006, **8**, 15–25.
297. J. Katriel, S. Roy and M. Springborg, *J. Chem. Phys.*, 2005, **123**, 104104 (1–6).
298. T. Heaton-Burgess, F. A. Bulat and W. Yang, *Phys. Rev. Lett.*, 2007, **98**, 256401 (1–4).
299. P. R. T. Schipper, O. V. Gritsenko and E. J. Baerends, *Theor. Chim. Acta.*, 1997, **98**, 16–24.
300. M. A. Buijse, E. J. Baerends and J. G. Snijders, *Phys. Rev. A*, 1989, **40**, 4190–4202.
301. M. J. G. Peach, A. M. Teale and D. J. Tozer, *J. Chem. Phys.*, 2007, **126**, 244104 (1–9).
302. M. J. G. Peach, A. M. Miller, A. M. Teale and D. J. Tozer, *J. Chem. Phys.*, 2008, **129**, 064105 (1–7).
303. W. Kołos, K. Szalewicz and H. J. Monkhorst, *J. Chem. Phys.*, 1986, **84**, 3278–3283.
304. W. Kołos and J. Rychlewski, *J. Chem. Phys.*, 1993, **98**, 3960–3967.
305. R. J. Le Roy, *LEVEL 7.5: A Computer Program for Solving the Radial Schrödinger Equation for Bound and Quasibound Levels*, 2002, see the “Computer Programs” link at <http://leroy.uwaterloo.ca>.
306. E. W. Kaiser, *J. Chem. Phys.*, 1970, **53**, 1686–1703.
307. N. E. Dahlen, R. van Leeuwen and U. von Barth, *Phys. Rev. A*, 2006, **73**, 012511 (1–13).

-
308. H. Cox, S. J. Smith and B. T. Sutcliffe, *Phys. Rev. A*, 1994, **49**, 4533–4539.
309. E. R. Davidson, S. A. Hagstrom, S. J. Chakravorty, V. M. Umar and C. F. Fischer, *Phys. Rev. A*, 1991, **44**, 7071–7083.
310. C.-J. Huang and C. J. Umrigar, *Phys. Rev. A*, 1997, **56**, 290–296.
311. T. K. Whittingham and K. Burke, *J. Chem. Phys.*, 2005, **122**, 134108 (1–7).
312. J. P. Perdew, E. R. McMullen and A. Zunger, *Phys. Rev. A*, 1981, **23**, 2785–2789.
313. M. Seidl, J. P. Perdew and M. Levy, *Phys. Rev. A*, 1999, **59**, 51–54.
314. M. Seidl, *Phys. Rev. A*, 1999, **60**, 4387–4395.
315. M. Seidl, J. P. Perdew and S. Kurth, *Phys. Rev. A*, 2000, **62**, 012502 (1–15).
316. E. J. Baerends, *Phys. Rev. Lett.*, 2001, **87**, 133004 (1–4).
317. M. Grüning, O. V. Gritsenko and E. J. Baerends, *J. Chem. Phys.*, 2003, **118**, 7183–7192.

Index

- Adiabatic connection, 38, 119–124
 - AC1, 129, 132–134, 136, 142, 148, 149, 152, 155
 - AC1-2, 153, 156
 - AC1-3, 153, 156
 - AC2, 137, 149
 - AC2(H&H), 138
 - AC3, 137, 138, 148
 - AC4, 140, 148
 - AC4(H&H), 140, 148
 - AC5, 140, 148, 149
 - AC6, 141, 142, 148, 149, 155
 - AC7, 142, 148
 - AC8, 142
 - AC9, 143, 148
- Attenuated exchange
 - Definition, 42
 - Attenuated functionals, 47
 - CAM-B3LYP, *see* CAM-B3LYP
 - Parameter dependence, 49–54, 76, 102
- B3LYP, 34, 38
 - Assessment, 40–42, 98, 101, 103, 111, 114, 130, 132, 133, 146
 - Definition, 38
 - Excited states, 57, 58, 68, 72–75, 81, 102, 106
- Born–Oppenheimer Approximation, 5, 6, 18
- CAM(0.16, 0.39, 0.4), 54
- CAM(0.16, 0.49, 0.4), 54
- CAM(0.2, 0.8, 0.4)
 - Assessment, 54, 102
 - Attenuation form, 51
 - Definition, 51
 - Excited states, 55, 58
- CAM-B3LYP
 - Assessment, 48–49, 96, 98, 99, 101, 103, 111, 114
 - Definition, 45–47
 - Excited states, 57, 58, 75, 81, 82, 91, 102, 106
- CO, 71, 72, 153
- Configuration interaction, 14–15
 - CIS, 14
 - CISD, 15, 17
- Constrained search
 - Levy, 26–27
 - Wu–Yang implementation, 35, 126–127, 154

- Correlation functional
 LYP, 33, 38, 50
 VWN, 31, 38, 50
- Coulomb energy J , 28, 125, 128
- Coupled cluster, 15–18
 CC2, 17, 71, 89
 CC3, 17
 CCSD, 16, 17, 19, 20, 98
 CCSD(T), 19, 111, 155
 CCSDT, 16, 19
- Diagnostic test, 76–83, 86, 91, 93
 Relation to oscillator strength,
 87
- Dipeptide, 57, 70
- DMABN, 57, 67, 71, 72, 81
- Exchange functional
 LSDA, 28, 31
- Exchange–correlation functional
 Attenuated, *see* Attenuated ex-
 change
 Definition, 29
 GGA, 32–33
 Hybrid, 34–35
 Assessment, 40–42
 B97- n , 34, 38, 47
 half-and-half, 34, 98, 101, 103,
 107, 122
 LSDA, 31–32
 meta-GGA, 33–34
 TPSS, 34, 47, 123, 136
- H₂, 13, 15, 17, 19, 130–143, 152
- Hartree–Fock, 8–13, 20, 87
 Assessment, 130, 132, 133
 Relation to Møller–Plesset PT,
 18
- Helium isoelectronic series, 145–150,
 153
- Hohenberg–Kohn Theorems, 23–26
- Kohn–Sham Theory, 28–29
- Møller–Plesset perturbation theory,
 34
 MP2, 19, 20, 98, 121, 126, 138
- Open-shell formalism, 12–13, 31, 40,
 41, 51, 54
- Optimised effective potential, 35, 109–
 110
- PBE, 32, 45, 47
 Assessment, 156
 Excited states, 72, 78, 81, 91
 PBE0, 34
 Excited states, 86–88, 91
- Polyacetylene, 71, 72, 96, 98–103
- Polyne, 96, 103–106
- Self-interaction, 140
 Definition, 123
 Many-electron generalisation, 123
- Size-extensivity, 15, 17, 137, 140,
 154
- Triazene chromophores, 86, 87, 91
- Tripeptide, 70, 72, 81
- Weizsäcker kinetic energy, 27, 128,
 154

